



ISSN 2686-7575 (Online)

ТОНКИЕ ХИМИЧЕСКИЕ ТЕХНОЛОГИИ

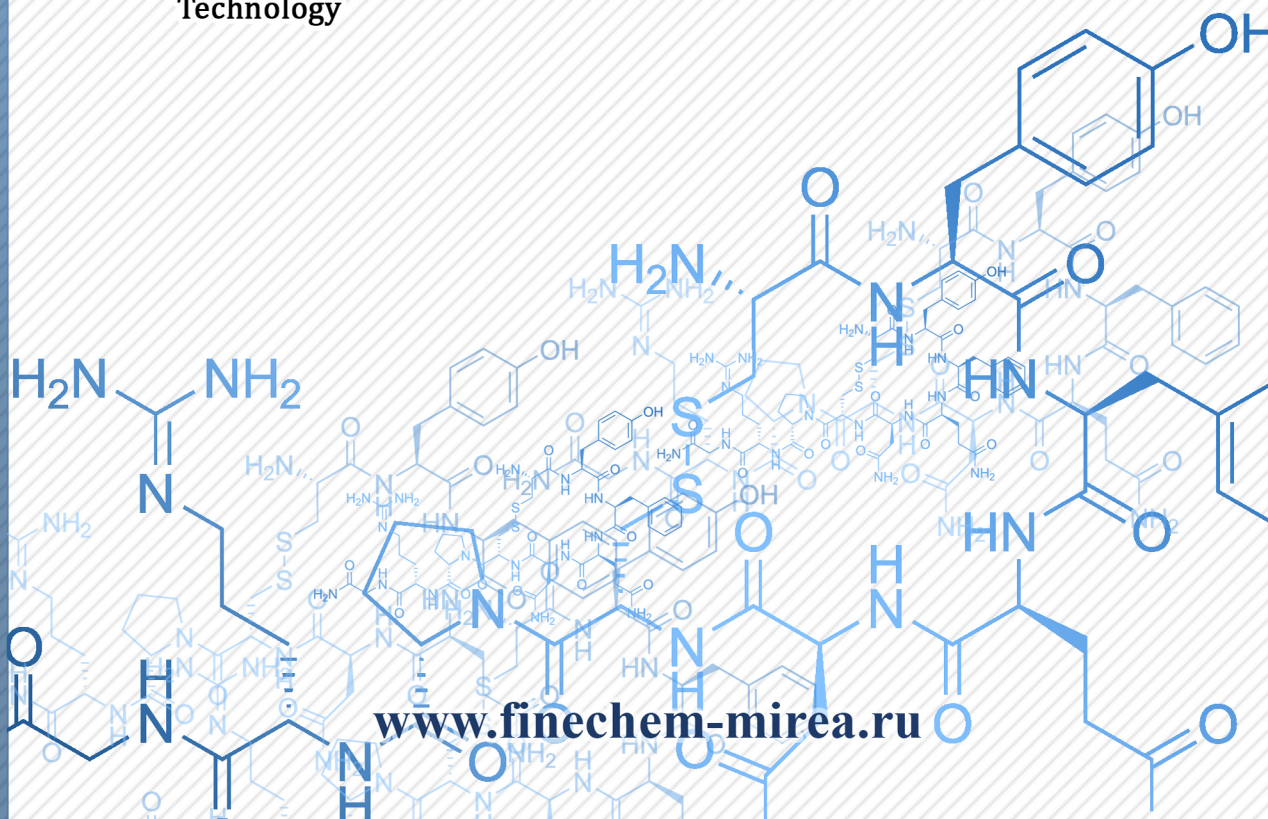
Fine Chemical Technologies

- | Theoretical Basis of Chemical Technology
- | Chemistry and Technology of Organic Substances
- | Chemistry and Technology of Medicinal Compounds and Biologically Active Substances
- | Biochemistry and Biotechnology
- | Synthesis and Processing of Polymers and Polymeric Composites
- | Chemistry and Technology of Inorganic Materials
- | Analytical Methods in Chemistry and Chemical Technology
- | Mathematical Methods and Information Systems in Chemical Technology

20(2)

2025

www.finechem-mirea.ru





ТОНКИЕ ХИМИЧЕСКИЕ ТЕХНОЛОГИИ

Fine Chemical Technologies

- | Theoretical Basis of Chemical Technology
- | Chemistry and Technology of Organic Substances
- | Chemistry and Technology of Medicinal Compounds and Biologically Active Substances
- | Biochemistry and Biotechnology
- | Synthesis and Processing of Polymers and Polymeric Composites
- | Chemistry and Technology of Inorganic Materials
- | Analytical Methods in Chemistry and Chemical Technology
- | Mathematical Methods and Information Systems in Chemical Technology

Tonkie Khimicheskie Tekhnologii =
Fine Chemical Technologies.
Vol. 20, No. 2, 2025

Тонкие химические технологии =
Fine Chemical Technologies.
Том 20, № 2, 2025

<https://doi.org/10.32362/2410-6593-2025-20-2>

www.finechem-mirea.ru

**Tonkie Khimicheskie Tekhnologii =
Fine Chemical Technologies
2025, Vol. 20, No. 2**

The peer-reviewed scientific and technical journal Fine Chemical Technologies highlights the modern achievements of fundamental and applied research in the field of fine chemical technologies, including the theoretical basis of chemical technology, chemistry and technology of medicinal compounds and biologically active substances, organic substances and inorganic materials, biochemistry and biotechnology, synthesis and processing of polymers and polymeric composites, analytical and mathematical methods and information systems in chemistry and chemical technology.

Founder and Publisher

Federal State Budget
Educational Institution of Higher Education
“MIREA – Russian Technological University”
78, Vernadskogo pr., Moscow, 119454, Russian Federation.
Publication frequency: bimonthly.
The journal was founded in 2006. The name was Vestnik MITHT until 2015 (ISSN 1819-1487).

The journal is included into the List of peer-reviewed science press of the State Commission for Academic Degrees and Titles of the Russian Federation.

The journal is indexed: SCOPUS, DOAJ, Chemical Abstracts, Science Index, RSCI, Ulrich’s International Periodicals Directory

Editor-in-Chief:

Andrey V. Timoshenko – Dr. Sci. (Eng.), Cand. Sci. (Chem.), Professor, MIREA – Russian Technological University, Moscow, Russian Federation. Scopus Author ID 56576076700, ResearcherID Y-8709-2018, <https://orcid.org/0000-0002-6511-7440>, timoshenko@mirea.ru

Deputy Editor-in-Chief:

Valery V. Fomichev – Dr. Sci. (Chem.), Professor, MIREA – Russian Technological University, Moscow, Russian Federation. Scopus Author ID 57196028937, <http://orcid.org/0000-0003-4840-0655>, fomichev@mirea.ru

Editorial staff:

| | |
|--------------------|--|
| Managing Editor | Cand. Sci. (Eng.) Galina D. Seredina |
| Editor | Sofya M. Mazina |
| Executive Editor | Elizaveta I. Kuricheva |
| Science editors | Dr. Sci. (Chem.), Prof. Tatyana M. Buslaeva Dr. Sci. (Chem.), Prof. Anatolii A. Ischenko Dr. Sci. (Eng.), Prof. Anatolii V. Markov Dr. Sci. (Chem.), Prof. Vladimir A. Tverskoy |
| Desktop publishing | Sergey V. Trofimov |

86, Vernadskogo pr., Moscow, 119571, Russian Federation.
Phone: +7 (499) 600-80-80 (#31288)
E-mail: seredina@mirea.ru

The registration number ПИ № ФС 77-74580 was issued in December 14, 2018 by the Federal Service for Supervision of Communications, Information Technology, and Mass Media of Russia

The subscription index of *Pressa Rossii*: **36924**

The Editorial Board’s viewpoint may not coincide with the viewpoint of the authors of the articles published in the journal.

**Тонкие химические технологии =
Fine Chemical Technologies
2025, том 20, № 2**

Научно-технический рецензируемый журнал «Тонкие химические технологии» освещает современные достижения фундаментальных и прикладных исследований в области тонких химических технологий, включая теоретические основы химической технологии, химию и технологию лекарственных препаратов и биологически активных соединений, органических веществ и неорганических материалов, биохимию и биотехнологию, синтез и переработку полимеров и композитов на их основе, аналитические и математические методы и информационные системы в химии и химической технологии.

Учредитель и издатель

федеральное государственное бюджетное образовательное учреждение высшего образования «МИРЭА – Российский технологический университет» 119454, РФ, Москва, пр-т Вернадского, д. 78.
Периодичность: один раз в два месяца.
Журнал основан в 2006 году. До 2015 года издавался под названием «Вестник МИТХТ» (ISSN 1819-1487).

Журнал входит в Перечень ведущих рецензируемых научных журналов ВАК РФ.

Индексируется: SCOPUS, DOAJ, Chemical Abstracts, РИНЦ (Science Index), RSCI, Ulrich’s International Periodicals Directory

Главный редактор:

Тимошенко Андрей Всеволодович – д.т.н., к.х.н., профессор, МИРЭА – Российский технологический университет, Москва, Российская Федерация. Scopus Author ID 56576076700, ResearcherID Y-8709-2018, <https://orcid.org/0000-0002-6511-7440>, timoshenko@mirea.ru

Заместитель главного редактора:

Фомичёв Валерий Вячеславович – д.х.н., профессор, МИРЭА – Российский технологический университет, Москва, Российская Федерация. Scopus Author ID 57196028937, <http://orcid.org/0000-0003-4840-0655>, fomichev@mirea.ru

Редакция:

| | |
|----------------------|--|
| Зав. редакцией | к.т.н. Г.Д. Середина |
| Редактор | С.М. Мазина |
| Выпускающий редактор | Е.И. Куричева |
| Научные редакторы | д.х.н., проф. Т.М. Буслаева д.х.н., проф. А.А. Ищенко д.т.н., проф. А.В. Марков д.х.н., проф. В.А. Тверской |
| Компьютерная верстка | С.В. Трофимов |

РФ, 119571, Москва, пр. Вернадского, 86, оф. Р-108.
Тел.: +7 (499) 600-80-80 (#31288)
E-mail: seredina@mirea.ru

Регистрационный номер и дата принятия решения о регистрации СМИ: ПИ № ФС 77-74580 от 14.12.2018 г. СМИ зарегистрировано Федеральной службой по надзору в сфере связи, информационных технологий и массовых коммуникаций (Роскомнадзор)

Индекс по Объединенному каталогу «Пресса России»: **36924**

Мнение редакции может не совпадать с мнением авторов публикуемых в журнале статей.

EDITORIAL BOARD

Andrey V. Blokhin – Dr. Sci. (Chem.), Professor, Belarusian State University, Minsk, Belarus.
Scopus Author ID 7101971167,
ResearcherID AAF-8122-2019,
<https://orcid.org/0000-0003-4778-5872>,
blokhin@bsu.by.

Sergey P. Verevkin – Dr. Sci. (Eng.), Professor, University of Rostock, Rostock, Germany.
Scopus Author ID 7006607848, ResearcherID G-3243-2011,
<https://orcid.org/0000-0002-0957-5594>,
Sergey.verevkin@uni-rostock.de.

Konstantin Yu. Zhizhin – Corresponding Member of the Russian Academy of Sciences (RAS), Dr. Sci. (Chem.), Professor, N.S. Kurnakov Institute of General and Inorganic Chemistry of the RAS, Moscow, Russian Federation.
Scopus Author ID 6701495620, ResearcherID C-5681-2013,
<http://orcid.org/0000-0002-4475-124X>,
kyuzhizhin@igic.ras.ru.

Igor V. Ivanov – Dr. Sci. (Chem.), Professor, MIREA – Russian Technological University, Moscow, Russian Federation.
Scopus Author ID 34770109800, ResearcherID I-5606-2016,
<http://orcid.org/0000-0003-0543-2067>,
ivanov_i@mirea.ru.

Carlos A. Cardona – PhD (Eng.), Professor, National University of Columbia, Manizales, Colombia.
Scopus Author ID 7004278560,
<http://orcid.org/0000-0002-0237-2313>,
ccardonaal@unal.edu.co.

Elvira T. Krut'ko – Dr. Sci. (Eng.), Professor, Belarusian State Technological University, Minsk, Belarus.
Scopus Author ID 6602297257,
ela_krutko@mail.ru.

Anatolii I. Miroshnikov – Academician at the RAS, Dr. Sci. (Chem.), Professor, M.M. Shemyakin and Yu.A. Ovchinnikov Institute of Bioorganic Chemistry of the RAS, Member of the Presidium of the RAS, Chairman of the Presidium of the RAS Pushchino Research Center, Moscow, Russian Federation.
Scopus Author ID 7006592304, ResearcherID G-5017-2017,
aiv@ibch.ru.

Aziz M. Muzafarov – Academician at the RAS, Dr. Sci. (Chem.), Professor, A.N. Nesmeyanov Institute of Organoelement Compounds of the RAS, Moscow, Russian Federation.
Scopus Author ID 7004472780, ResearcherID G-1644-2011,
<https://orcid.org/0000-0002-3050-3253>,
aziz@ineos.ac.ru.

РЕДАКЦИОННАЯ КОЛЛЕГИЯ

Блохин Андрей Викторович – д.х.н., профессор Белорусского государственного университета, Минск, Беларусь.
Scopus Author ID 7101971167, ResearcherID AAF-8122-2019,
<https://orcid.org/0000-0003-4778-5872>,
blokhin@bsu.by.

Верёвкин Сергей Петрович – д.т.н., профессор Университета г. Росток, Росток, Германия.
Scopus Author ID 7006607848, ResearcherID G-3243-2011,
<https://orcid.org/0000-0002-0957-5594>,
Sergey.verevkin@uni-rostock.de.

Жижин Константин Юрьевич – член-корр. Российской академии наук (РАН), д.х.н., профессор, Институт общей и неорганической химии им. Н.С. Курнакова РАН, Москва, Российская Федерация.
Scopus Author ID 6701495620, ResearcherID C-5681-2013,
<http://orcid.org/0000-0002-4475-124X>,
kyuzhizhin@igic.ras.ru.

Иванов Игорь Владимирович – д.х.н., профессор, МИРЭА – Российский технологический университет, Москва, Российская Федерация.
Scopus Author ID 34770109800, ResearcherID I-5606-2016,
<http://orcid.org/0000-0003-0543-2067>,
ivanov_i@mirea.ru.

Кардона Карлос Ариэль – PhD, профессор Национального университета Колумбии, Манизалес, Колумбия.
Scopus Author ID 7004278560,
<http://orcid.org/0000-0002-0237-2313>,
ccardonaal@unal.edu.co.

Крутько Эльвира Тихоновна – д.т.н., профессор Белорусского государственного технологического университета, Минск, Беларусь.
Scopus Author ID 6602297257,
ela_krutko@mail.ru.

Мирошников Анатолий Иванович – академик РАН, д.х.н., профессор, Институт биоорганической химии им. академиков М.М. Шемякина и Ю.А. Овчинникова РАН, член Президиума РАН, председатель Президиума Пушкинского научного центра РАН, Москва, Российская Федерация.
Scopus Author ID 7006592304, ResearcherID G-5017-2017,
aiv@ibch.ru.

Музафаров Азиз Мансурович – академик РАН, д.х.н., профессор, Институт элементоорганических соединений им. А.Н. Несмеянова РАН, Москва, Российская Федерация.
Scopus Author ID 7004472780, ResearcherID G-1644-2011,
<https://orcid.org/0000-0002-3050-3253>,
aziz@ineos.ac.ru.

Ivan A. Novakov – Academician at the RAS, Dr. Sci. (Chem.), Professor, President of the Volgograd State Technical University, Volgograd, Russian Federation.
Scopus Author ID 7003436556, ResearcherID I-4668-2015, <http://orcid.org/0000-0002-0980-6591>, president@vstu.ru.

Alexander N. Ozerin – Corresponding Member of the RAS, Dr. Sci. (Chem.), Professor, Enikolopov Institute of Synthetic Polymeric Materials of the RAS, Moscow, Russian Federation.
Scopus Author ID 7006188944, ResearcherID J-1866-2018, <https://orcid.org/0000-0001-7505-6090>, ozerin@ispm.ru.

Tapani A. Pakkanen – PhD, Professor, Department of Chemistry, University of Eastern Finland, Joensuu, Finland.
Scopus Author ID 7102310323, tapani.pakkanen@uef.fi.

Armando J.L. Pombeiro – Academician at the Academy of Sciences of Lisbon, PhD, Professor, President of the Center for Structural Chemistry of the Higher Technical Institute of the University of Lisbon, Lisbon, Portugal.
Scopus Author ID 7006067269, ResearcherID I-5945-2012, <https://orcid.org/0000-0001-8323-888X>, pombeiro@ist.utl.pt.

Dmitrii V. Pyshnyi – Corresponding Member of the RAS, Dr. Sci. (Chem.), Professor, Institute of Chemical Biology and Fundamental Medicine, Siberian Branch of the RAS, Novosibirsk, Russian Federation.
Scopus Author ID 7006677629, ResearcherID F-4729-2013, <https://orcid.org/0000-0002-2587-3719>, pyshnyi@niboch.nsc.ru.

Alexander S. Sigov – Academician at the RAS, Dr. Sci. (Phys. and Math.), Professor, President of MIREA – Russian Technological University, Moscow, Russian Federation.
Scopus Author ID 35557510600, ResearcherID L-4103-2017, sigov@mirea.ru.

Alexander M. Toikka – Dr. Sci. (Chem.), Professor, Institute of Chemistry, Saint Petersburg State University, St. Petersburg, Russian Federation.
Scopus Author ID 6603464176, ResearcherID A-5698-2010, <http://orcid.org/0000-0002-1863-5528>, a.toikka@spbu.ru.

Andrzej W. Trochimczuk – Dr. Sci. (Chem.), Professor, Faculty of Chemistry, Wrocław University of Science and Technology, Wrocław, Poland.
Scopus Author ID 7003604847, andrzej.trochimczuk@pwr.edu.pl.

Aslan Yu. Tsvadze – Academician at the RAS, Dr. Sci. (Chem.), Professor, A.N. Frumkin Institute of Physical Chemistry and Electrochemistry of the RAS, Moscow, Russian Federation.
Scopus Author ID 7004245066, ResearcherID G-7422-2014, tsiv@phyche.ac.ru.

Новаков Иван Александрович – академик РАН, д.х.н., профессор, президент Волгоградского государственного технического университета, Волгоград, Российская Федерация.
Scopus Author ID 7003436556, ResearcherID I-4668-2015, <http://orcid.org/0000-0002-0980-6591>, president@vstu.ru.

Озерин Александр Никифорович – член-корр. РАН, д.х.н., профессор, Институт синтетических полимерных материалов им. Н.С. Ениколопова РАН, Москва, Российская Федерация.
Scopus Author ID 7006188944, ResearcherID J-1866-2018, <https://orcid.org/0000-0001-7505-6090>, ozerin@ispm.ru.

Пакканен Тапани – PhD, профессор, Департамент химии, Университет Восточной Финляндии, Йоенсуу, Финляндия.
Scopus Author ID 7102310323, tapani.pakkanen@uef.fi.

Помбейро Армандо – академик Академии наук Лиссабона, PhD, профессор, президент Центра структурной химии Высшего технического института Университета Лиссабона, Португалия.
Scopus Author ID 7006067269, ResearcherID I-5945-2012, <https://orcid.org/0000-0001-8323-888X>, pombeiro@ist.utl.pt.

Пышный Дмитрий Владимирович – член-корр. РАН, д.х.н., профессор, Институт химической биологии и фундаментальной медицины Сибирского отделения РАН, Новосибирск, Российская Федерация.
Scopus Author ID 7006677629, ResearcherID F-4729-2013, <https://orcid.org/0000-0002-2587-3719>, pyshnyi@niboch.nsc.ru.

Сигов Александр Сергеевич – академик РАН, д.ф.-м.н., профессор, президент МИРЭА – Российского технологического университета, Москва, Российская Федерация.
Scopus Author ID 35557510600, ResearcherID L-4103-2017, sigov@mirea.ru.

Тойкка Александр Матвеевич – д.х.н., профессор, Институт химии, Санкт-Петербургский государственный университет, Санкт-Петербург, Российская Федерация.
Scopus Author ID 6603464176, ResearcherID A-5698-2010, <http://orcid.org/0000-0002-1863-5528>, a.toikka@spbu.ru.

Трохимчук Анджей – д.х.н., профессор, Химический факультет Вроцлавского политехнического университета, Вроцлав, Польша.
Scopus Author ID 7003604847, andrzej.trochimczuk@pwr.edu.pl.

Цивадзе Аслан Юсупович – академик РАН, д.х.н., профессор, Институт физической химии и электрохимии им. А.Н. Фрумкина РАН, Москва, Российская Федерация.
Scopus Author ID 7004245066, ResearcherID G-7422-2014, tsiv@phyche.ac.ru.

Contents

THEORETICAL BASIS OF CHEMICAL TECHNOLOGY

- 95** *Danila G. Rudakov, Sergey M. Kharlamov, Pavel S. Klauzner, Elena A. Anokhina, Andrey V. Timoshenko*
Extractive distillation of tetrahydrofuran–ethyl acetate–water mixture in schemes including columns with side sections and side draws

BIOCHEMISTRY AND BIOTECHNOLOGY

- 107** *Elena D. Avdonina, Kristina A. Pervoykina, Ludmila V. Verkhovskaya, Dmitriy N. Shcherbinin, Natalia Yu. Viskova, Irina S. Kruzhkova, Maria A. Ilina, Larisa V. Kudriavtseva, Lyudmila V. Kolobukhina, Maksim M. Shmarov, Natalya A. Antipyat, Alexander L. Gintsburg, Igor N. Tyurin*
Production of the recombinant hemagglutinin protein of the swine influenza virus A/H1N1 and analysis of its physicochemical and antigenic properties
- 119** *Alexandrina M. Sulman, Vladimir P. Molchanov, Daria V. Balakshina, Olga V. Grebennikova, Valentina G. Matveeva*
New nanostructured carriers for cellulase immobilization

CHEMISTRY AND TECHNOLOGY OF INORGANIC MATERIALS

- 137** *Nina V. Sidorenko, Marat A. Vaniev, Iurii M. Mkrtchyan, Nikita A. Salykin, Andrey A. Vernigora, Ivan A. Novakov*
N-[(1RS)-camphane-2-ylidene]aniline: A novel efficient liquid UV absorber for 3D printing
- 146** *Pavel G. Shelenkov, Petr V. Pantyukhov, Anatoly A. Olkhov, Anatoly A. Popov*
Gas permeability of films based on low-density polyethylene–ethylene-vinyl acetate blends with cellulosic fillers

CHEMISTRY AND TECHNOLOGY OF INORGANIC MATERIALS

- 156** *Yuliya S. Elkina, Vitaly A. Vlasov, Elena N. Lysenko, Anatoly P. Surzhikov*
The influence of lanthanum content in the $\text{Fe}_2\text{O}_3\text{--Li}_2\text{O--La(OH)}_3$ system on phase formation and properties of composite material
- 167** *Olga V. Slatinskaia, German O. Stepanov, Olga V. Fartushnaya, Evgenii V. Zubkov, Anastasia D. Zatykina, Olesya M. Gizitdinova, Nikita S. Karpov, Alexey V. Smirnov, Vladimir S. Boriskin, Natalia N. Rodionova, Anastasia O. Petrova*
Post-vibration activity of electrochemically activated water

ERRATUM

- 185** *Igor G. Solomonik, Vladimir Z. Mordkovich, Andrei S. Gorshkov*
Erratum to the article “Study into optimizing the temperature regime for the reduction of Fischer–Tropsch synthesis catalysts”

СОДЕРЖАНИЕ

ТЕОРЕТИЧЕСКИЕ ОСНОВЫ ХИМИЧЕСКОЙ ТЕХНОЛОГИИ

95

Д.Г. Рудаков, С.М. Харламов, П.С. Клаузнер, Е.А. Анохина, А.В. Тимошенко
Экстрактивная ректификация смеси тетрагидрофуран–этилацетат–вода в схемах, включающих колонны с боковыми секциями и отборами

БИОХИМИЯ И БИОТЕХНОЛОГИЯ

107

Е.Д. Авдонина, К.А. Первойкина, Л.В. Верховская, Д.Н. Щербинин, Н.Ю. Вискова, И.С. Кружкова, М.А. Ильина, Л.В. Кудрявцева, Л.В. Колобухина, М.М. Шмаров, Н.А. Антипят, А.Л. Гинцбург, И.Н. Тюрин
Получение и анализ физико-химических и антигенных свойств рекомбинантного белка геммаглобулина вируса свиного гриппа А/Н1N1

119

А.М. Сульман, В.П. Молчанов, Д.В. Балакишина, О.В. Гребенникова, В.Г. Матвеева
Новые наноструктурированные носители для иммобилизации целлюлаз

СИНТЕЗ И ПЕРЕРАБОТКА ПОЛИМЕРОВ И КОМПОЗИТОВ НА ИХ ОСНОВЕ

137

Н.В. Сидоренко, М.А. Ваниев, Ю.М. Мкртчян, Н.А. Салыкин, А.А. Вернигора, И.А. Новаков
N-[(1RS)-камфан-2-илиден]анилин — новый эффективный жидкий УФ-абсорбер для 3D-печати в условиях фотохимического инициирования

146

П.Г. Шеленков, П.В. Пантюхов, А.А. Ольхов, А.А. Попов
Газопроницаемость пленок на основе смесей полиэтиленов низкой плотности – сэвиленов с целлюлозосодержащими наполнителями

ХИМИЯ И ТЕХНОЛОГИЯ НЕОРГАНИЧЕСКИХ МАТЕРИАЛОВ

156

Ю.С. Елькина, В.А. Власов, Е.Н. Лысенко, А.П. Суржиков
Влияние содержания лантана в системе $\text{Fe}_2\text{O}_3\text{-Li}_2\text{O-La(OH)}_3$ на фазообразование и свойства композиционного материала

167

О.В. Слатинская, Г.О. Степанов, О.В. Фартушина, Е.В. Зубков, А.Д. Затыкина, О.М. Гизитдинова, Н.С. Карпов, А.В. Смирнов, В.С. Борискин, Н.Н. Родионова, А.О. Петрова
Поствибрационная активность электрохимически активированной воды

ИСПРАВЛЕНИЯ

185

Igor G. Solomonik, Vladimir Z. Mordkovich, Andrei S. Gorshkov
Исправления к статье «Study into optimizing the temperature regime for the reduction of Fischer–Tropsch synthesis catalysts»

Theoretical basis of chemical technology
Теоретические основы химической технологии

UDC 660:51.001.57+66

<https://doi.org/10.32362/2410-6593-2025-20-2-95-106>

EDN XRBSSO



RESEARCH ARTICLE

Extractive distillation of tetrahydrofuran–ethyl acetate–water mixture in schemes including columns with side sections and side draws

Danila G. Rudakov, Sergey M. Kharlamov, Pavel S. Klauzner✉, Elena A. Anokhina, Andrey V. Timoshenko

MIREA – Russian Technological University (M.V. Lomonosov Institute of Fine Chemical Technologies), Moscow, 119454 Russia

✉ Corresponding author; e-mail: klauzner@mirea.ru

Abstract

Objectives. The work set out to evaluate the energy efficiency of using schemes including columns with side sections and side draws in the extractive distillation of tetrahydrofuran–ethyl acetate–water mixture with dimethyl sulfoxide as an entrainer.

Methods. The main research method consisted of a computational experiment with the Aspen Plus v. 12 software package. The local composition UNIQUAC equation model was used for describing vapor–liquid equilibrium. Parametric optimization of initial scheme and schemes, including columns with side sections and side draws, was carried out according to the criterion of energy consumptions in distillation columns reboilers.

Results. Two variants of schemes including partially thermally coupled distillation columns and two variants of schemes including columns with side draws were synthesized on the basis of the conventional scheme of double extractive distillation consisting of two-withdrawal columns using the graph method. The optimal operating parameters of the conventional scheme and all schemes obtained on its basis were determined. The schemes, including columns with side draw, were modeled in two variants, namely, in the vapor phase with side draw, and in the liquid phase. The energy efficiency of the proposed schemes was evaluated in comparison with the conventional scheme.

Conclusions. The phase state of the side draw is shown to have little effect on the total energy consumption in column reboilers, the amount of liquid-phase side draw being 1.4–5.2 times greater than that of vapor-phase draw. Among the schemes including complex columns with a side section, the maximum reduction of energy consumption by 5.9% in relation to the scheme of two-withdrawal columns is provided by the scheme according to which the thermal coupling between the second extractive column and the regeneration column of the entrainer is realized. Thermal coupling of extractive columns provides a significantly lower energy saving (1.36%). Among the schemes including complex columns with side draw, the greatest energy efficiency (5.9%) is characterized by the scheme in which the draw in the vapor phase is taken from the second extractive column to the regeneration column.

Keywords

extractive distillation, side draws, side sections, tetrahydrofuran, ethyl acetate, water, energy saving

Submitted: 16.10.2024

Revised: 19.12.2024

Accepted: 21.02.2025

For citation

Rudakov D.G., Kharlamov S.M., Klauzner P.S., Anokhina E.A., Timoshenko A.V. Extractive distillation of tetrahydrofuran–ethyl acetate–water mixture in schemes including columns with side sections and side draws. *Tonk. Khim. Tekhnol. = Fine Chem. Technol.* 2025;20(2):95–106. <https://doi.org/10.32362/2410-6593-2025-20-2-95-106>

НАУЧНАЯ СТАТЬЯ

Экстрактивная ректификация смеси тетрагидрофуран–этилацетат–вода в схемах, включающих колонны с боковыми секциями и отборами

Д.Г. Рудаков, С.М. Харламов, П.С. Клаузнер✉, Е.А. Анохина, А.В. Тимошенко

МИРЭА – Российский технологический университет (Институт тонких химических технологий им. М. В. Ломоносова), Москва, 119454 Россия

✉ Автор для переписки, e-mail: klauzner@mirea.ru

Аннотация

Цели. Провести оценку энергетической эффективности применения схем, включающих колонны с боковыми секциями и отборами, в процессе экстрактивной ректификации смеси тетрагидрофуран–этилацетат–вода с диметилсульфоксидом в качестве разделяющего агента.

Методы. Основным методом исследования являлся вычислительный эксперимент, реализуемый с применением программного комплекса Aspen Plus v. 12. Для моделирования парожидкостного равновесия было использовано уравнение локальных составов UNIQUAC. Параметрическая оптимизация всех рассмотренных в работе схем экстрактивной ректификации выполнялась по критерию суммарных энергетических затрат в кипятильниках колонн.

Результаты. С применением метода графов на основе базовой схемы двухступенчатой экстрактивной ректификации, состоящей из двухотборных колонн, синтезировано два варианта схем, включающих комплексы с частично связанными тепловыми и материальными потоками, и два варианта схем, включающих колонны с боковым отбором. Определены оптимальные рабочие параметры базовой схемы, а также всех полученных на ее основе схем. Схемы, включающие колонны с боковыми отборами, смоделированы в двух вариантах, а именно: с отбором бокового потока в паровой и в жидкой фазах. Проведена оценка энергоэффективности предложенных схем по сравнению с базовой схемой.

Выводы. Выявлено, что фазовое состояние бокового отбора мало влияет на суммарные энергозатраты в кипятильниках колонн, при этом количество жидкофазного бокового потока в 1.4–5.2 раза больше, чем парофазного. Установлено, что среди схем, включающих сложные колонны с боковой секцией, максимальное снижение энергозатрат на 5.9% относительно схемы из двухотборных колонн обеспечивает схема, в которой реализуется термическая связь между второй экстрактивной колонной и колонной регенерации разделяющего агента. Термическое связывание экстрактивных колонн дает существенно меньшую экономию энергозатрат (1.36%). Среди схем, включающих сложные колонны с боковым отбором, наибольшей энергоэффективностью (5.9%) характеризуется схема, в которой осуществляется отбор потока в паровой фазе из второй экстрактивной колонны в колонну регенерации.

Ключевые слова

экстрактивная ректификация, боковые отборы, боковые секции, тетрагидрофуран, этилацетат, вода, энергосбережение

Поступила: 16.10.2024

Доработана: 19.12.2024

Принята в печать: 21.02.2025

Для цитирования

Рудаков Д.Г., Харламов С.М., Клаузнер П.С., Анохина Е.А., Тимошенко А.В. Экстрактивная ректификация смеси тетрагидрофуран – этилацетат – вода в схемах, включающих колонны с боковыми секциями и отборами. *Тонкие химические технологии*. 2025;20(2):95–106. <https://doi.org/10.32362/2410-6593-2025-20-2-95-106>

INTRODUCTION

Tetrahydrofuran (THF) and ethyl acetate (EAc) are widely used as solvents in the pharmaceutical industry. As a result of the technological process used to obtain these solvents, some pollutants get into wastewater [1]. Separation of THF–EAc–water mixture into pure components is difficult due to the presence of two binary azeotropes THF–water and EAc–water [2]. This mixture can be used to separated using extractive distillation (ED), which is the most widely used method for separating azeotropic mixtures and mixtures of components having relative volatility close to unity. However, like conventional distillation, ED has low thermodynamic efficiency, leading to high thermal energy consumption for its realization. This set of circumstances determines the relevance of searching for ways to improve the energy efficiency of the process [3–5].

One of the approaches to reduce energy consumption involves the transfer of heat removed from the strengthening section of the column to the distillation section of the same or another column, which is realized in schemes using heat pumps [6–8] and nonadiabatic distillation [9–11]. The same concept forms the basis for schemes using internal heat integration [11, 12] referred to as a heat integrated distillation column (HIDiC) system. However, despite their high energy efficiency, heat pump schemes are significant disadvantaged by the need to use expensive hot compressors.

Another approach is based on approximating the distillation process to a hypothetical thermodynamically reversible process using complexes with partially coupled heat and material flows, which are realized in practice in the form of complex columns with side sections [3, 13]. Another promising approach for reducing energy consumption involves the use of schemes including columns with side draws [14, 15]. The above-described methods can also be used in combination.

The authors [16] propose the use of complex columns with side draws to improve the energy efficiency of the scheme of two-stage ED of THF–EAc–water mixture with dimethyl sulfoxide (DMSO) as an entrainer (Fig. 1). Three schemes with side draws were considered: (1) a scheme with a side draw of the flow from the first extractive column (EC1) to the second; (2) with a side draw from the second extractive column (EC2) to the regeneration column (RC); (3) a scheme combining both previous options. In addition to this, a combination of schemes with side extraction and heat pump was studied. However, it should be noted that the authors considered all schemes with side flow draw exclusively in the liquid phase. Despite the block diagram of the optimization algorithm given in [16], it remains unclear according to what principle the transformation of the basic scheme into schemes with

side draws was carried out, as well as on what basis the selection of initial conditions (number of the side draw plate and its number) in the optimization was made. The authors [16] also failed to take into account that DMSO begins to decompose at temperatures above 150°C [17] when selecting the working pressure in the columns. The top pressure of the DMSO RC was chosen to be 50 kPa at a temperature in the reboilers of 169°C. Thus, the results obtained by the authors of [16] require clarification and correction. Another interesting task consists in studying the energy efficiency of schemes with side flow draws in the vapor phase and comparing them with complexes having partially thermally coupled distillation columns (PTCDC).

Thus, the aim of the present study is to evaluate the energy efficiency of schemes including columns with side sections and columns with side flow draws in both vapor and liquid phases.

CALCULATIONS

Methods

Mathematical modeling and computational experiment were used as the main research method. In accordance with the recommendations of the authors [16], the UNIQUAC (UNIversal QUAsiChemical) equation was chosen as a model for describing the vapor–liquid equilibrium in the THF–EAc–water–DMSO system. For all binary components except for the THF–EAc pair, we used the equation parameters from the Aspen Properties v. 12.1 database integrated into the software package, while the parameters for the THF–EAc system were taken from the supplementary materials of the published work [16]. An analysis of the quality of description of experimental data on phase equilibrium [18–22] by UNIQUAC, NRTL (Non-Random Two Liquid) and UNIFAC (UNIQUAC Functional-group Activity Coefficients) models showed that the vapor phase composition and boiling point (or pressure in the case of isothermal data) of binary systems is described with the lowest error using the UNIQUAC model with the above parameters. The average relative errors in the description of vapor phase composition and boiling point (pressure in the case of isothermal data) do not exceed 3.0% and 0.5%, respectively.

The initial (basic) scheme of two-stage ED of THF–EAc–water mixture with DMSO as the entrainer is presented in Fig. 1 (Scheme A).

Calculations were carried out for 5900 kg/h of the initial mixture of the following composition: THF, 40.33 wt %; EAc, 49.28 wt %; water, 10.38 wt %. The feed flow was supplied at a temperature of 40°C and a pressure of 50 kPa. The concentrations of product flows were kept constant and equal for THF, 98.8 wt %; EAc, 99.5 wt %; water, 99.6 wt %; regenerated DMSO, 99.99 wt % [16].

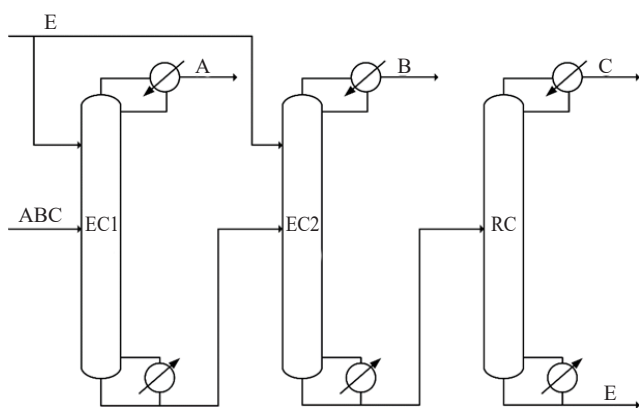


Fig. 1. Scheme of two-stage ED (Scheme A). EC1 and EC2 are extractive columns; RC is the entrainer regeneration column. Hereinafter: A is tetrahydrofuran, B is ethyl acetate, C is water, E is dimethyl sulfoxide

The pressure in the columns was chosen such that the temperature in the column bottoms did not exceed 150°C, since it is at this temperature that the decomposition of DMSO begins [17]. Thus, the pressure in columns EC1 and EC2 was set equal to 50 kPa, in RC—25 kPa. The optimized parameters were the number of theoretical plates in columns (N_{total}), temperature (T_E) and flow rate (F_E) of entrainer, position of feed plates (N_F) and entrainer (N_E) in columns. The total heat duty in the column reboilers was used as an optimization criterion ($\sum Q_{reb}$). The constraint on optimization consisted in the need to keep constant the concentrations of components in the product flow of the columns.

At the first stage, the influence of entrainer flow rate on the reflux ratio R in columns EC1 and EC2 at

a fixed entrainer feed temperature (T_E) equal to 50°C was investigated. Based on the obtained dependence, the DMSO flow rate in EC1 equal to 4500 kg/h and in EC2 equal to 1150 kg/h was taken as an initial approximation. Then, the total number of plates (N_{total}) in the columns was determined at a fixed flow rate and entrainer temperature. After selecting N_{total} , the effect of T_E on the energy consumption in the ED column bottoms was investigated at a fixed total number of plates in the columns. This influence was found to be practically absent. Based on the top temperatures of columns EC1 and EC2, $T_E = 50^\circ\text{C}$ was chosen. At the next stage, the boundaries of variation of entrainer flow rates in each EC were determined (i.e., the values of the optimum and minimum flow rates). The final stage of optimization consisted in selecting the optimal amount of entrainer for the entire scheme. The optimization procedure was as follows:

- 1) setting values of N_E and N_F for EC1 and determining optimal values of entrainer flow rate for the entire scheme for all sets of N_E and N_F for EC2;
- 2) setting new values of N_E and N_F for EC1 and repeating step 1;
- 3) repeating steps 1–2 until reaching the minimum value of $\sum Q_{reb}$.

Optimal operating parameters of Scheme A are given in Table 1.

Synthesis of schemes including columns with side sections and side draws

The transformation of the graph of the basic two-stage ED scheme (Scheme A) into schemes including columns with side sections and side draws is shown in Fig. 2.

Table 1. Optimal operating parameters of Scheme A

| Column | N_{total} | N_E | N_F | $T_E, ^\circ\text{C}$ | $F_E, \text{kg/h}$ | R | Q_{reb}, kW | $\sum Q_{reb}, \text{kW}$ |
|--------|-------------|-------|-------|-----------------------|--------------------|------|----------------------|---------------------------|
| EC1 | 46 | 10 | 16 | 50 | 6614 | 6.40 | 2417 | 3831 |
| EC2 | 19 | 5 | 14 | 50 | 988 | 0.30 | 656 | |
| RC | 13 | – | 5 | – | – | 0.75 | 758 | |

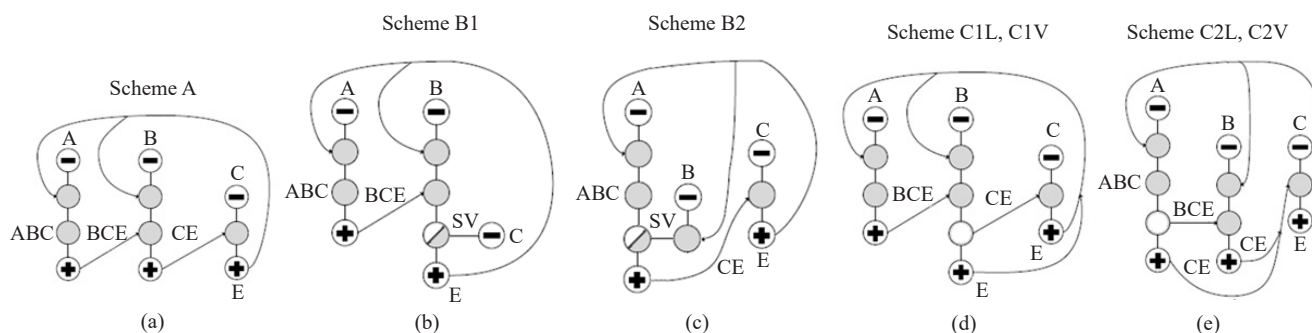


Fig. 2. Transformation of the base scheme graph: (a) graph of Scheme A, (b) graph of Scheme B1, (c) graph of Scheme B2, (d) graphs of Schemes C1L and C1V, (e) graphs of Schemes C2L and C2V (letter L means side draw in the liquid phase, and letter V—in the vapor phase)

The initial scheme (Fig. 1) is transformed into a graph (Fig. 2a). In this graph, edges denote vapor and liquid flows within and between columns. The vertices are the cross sections bounding the column sections. By combining two vertices adjacent along the oriented edges CE and BCE, the graph can be simplified to the graphs shown in Figs. 2b and 2c, which depict schemes having partially coupled heat and material flows. Performing the simplification operation on the graphs (Figs. 2b and 2c) along the undirected edges of the side vapor (SV) extraction phase results in graphs (Figs. 2d and 2e) that display schemes involving complex columns with side extraction in both vapor (C1V and C2V) and liquid (C1L and C2L) phases. The side draws are located downstream of the extractive section in the respective columns. Thus, four different variants of schemes including complex columns were synthesized from the basic Scheme A (Fig. 3):

- Scheme B1, in which columns EC2 and RC are combined in a complex with PTCDC;
- Scheme B2, in which columns EC1 and EC2 are combined in a complex with PTCDC;

- Schemes C1L and C1V are obtained on the basis of Scheme B1, in them side flow draw in vapor phase (C1V) or in liquid phase (C1L) is organized from EC2 to RC;
- Schemes C2L and C2V are obtained on the basis of Scheme B2, in them from column EC1 to column EC2 the side flow draw in steam phase (C2V) or in liquid phase (C2L) is organized.

At the next stage, the optimal operating parameters of the synthesized variants of schemes were determined. Initial data and product flow quality was set the same as for Scheme A. Total heat duty in the column reboilers was used as an optimization criterion as follows.

Optimization of schemes including complexes with PTCDC

At transition to complexes with PTCDC, the pressure in the integrated apparatuses should be equalized. In Scheme B1, the pressure in column EC1 and the basic Scheme A is 50 kPa; in the main column of the PTCDC complex and side section, the pressure was set equal

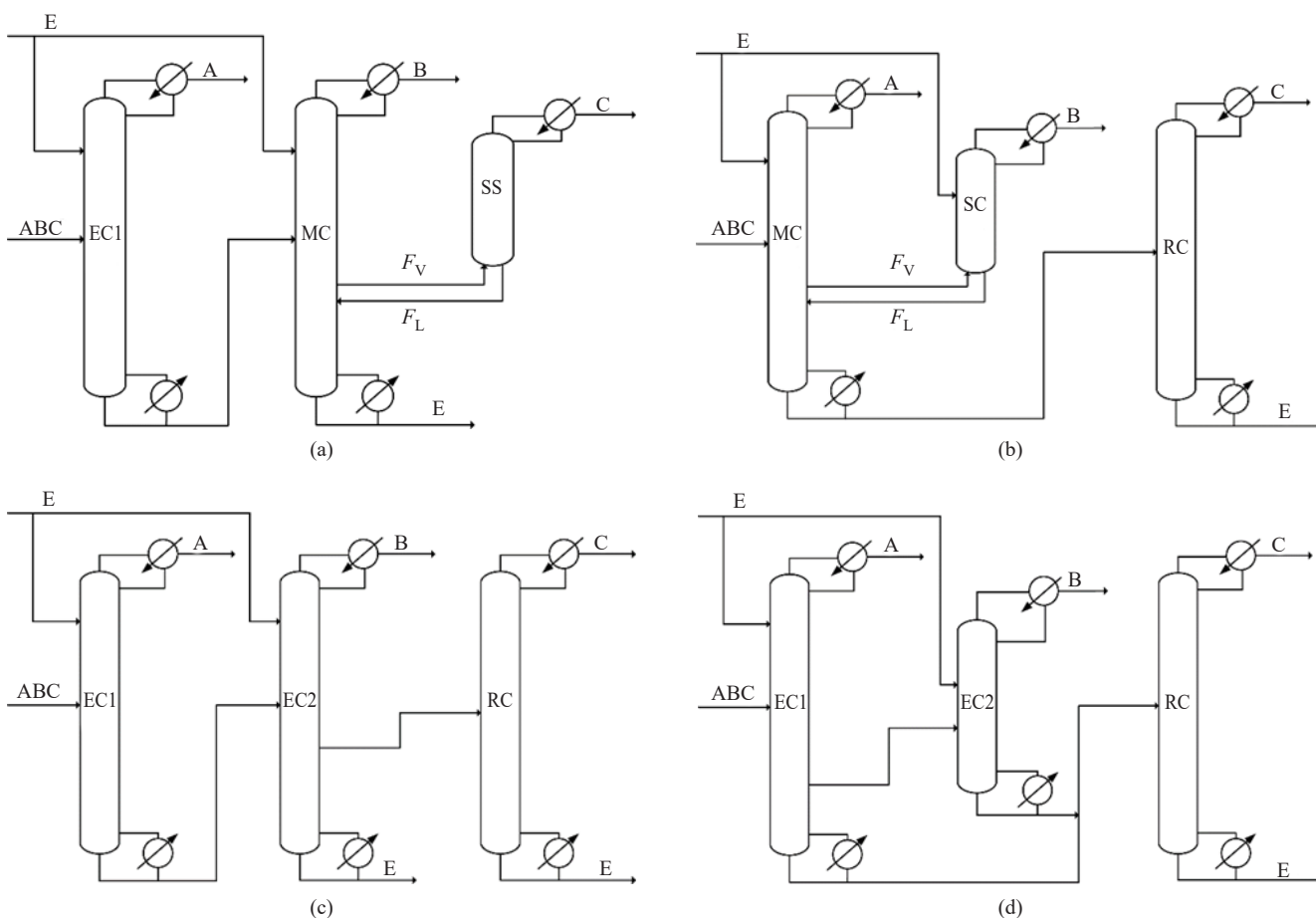


Fig. 3. Schemes involving columns with side sections and side draws: (a) Scheme B1, (b) Scheme B2, (c) Scheme C1L/C1V, (d) Scheme C2L/C2V. EC1 and EC2 are extractive columns; RC is the entrainer regeneration column; MC is the main column of the complex with partially thermally coupled distillation columns; SS is a side section; SC is a side column

to 25 kPa. In Scheme B2, the pressure in the main column and side section was set equal to 50 kPa; in the RC, as well as in the RC of the basic Scheme A, the corresponding pressure was 25 kPa. The optimized parameters were the amount of steam flow extraction into the side section (F_V) and the side draw plate location (N_{SD}). Other parameters such as temperature (T_E), entrainer flow rate (F_E), position of feed plates (N_F) in the columns, and entrainer inlet plates (N_E) were fixed according to their optimum values determined for Scheme A.

Since there were no changes in the mode of operation of columns EC1 (for Scheme B1) and CR (for Scheme B2), these parameters were not reoptimized.

Optimization of complexes with PTCDC was carried out according to the following algorithm:

- 1) setting the N_{SD} ;
- 2) setting the F_V ;
- 3) calculating the value of heat duty in the reboilers of the main column Q_{reb}^{MC} ;
- 4) returning to step 2, setting a new F_V value, controlling the distillate quality of the side section (or side column) by changing the distillate flow rate F_D^{SS} (F_D^{SC}), until Q_{reb}^{MC} reaches the minimum value;
- 5) returning to step 1, setting a new N_{SD} value. Repeating steps 1–4 until the minimum value of Q_{reb}^{MC} is reached.

The optimization results of Schemes B1 and B2 are shown in Table 2.

Optimization of schemes including columns with side draw

Scheme C1 group. Since Schemes C1L and C1V are obtained by transforming the graph of Scheme B1 and

differ only in the aggregate state of the side extraction flow, the procedure of their optimization is identical. Because the composition of the feed flow of this column in Schemes C1L and C1V differs from the composition in the basic Scheme A, the number of plates in the RC was selected at the first stage. The selection was based on an analysis of the dependence Q_{reb}^{RC} on the number of plates.

Additional optimized variables comprised the amount of side liquid extraction flow FL (Scheme C1L) or steam extraction F_V (Scheme C1V) from EC2 to the RC, as well as the location of the side extraction plate (N_{SD}) and the feed plate in the RC (N_F).

Other parameters, such as the number of plates in EC1 and EC2, entrainer temperature and flow rate, position of feed and extracting agent feed plates in EC1 and EC2, were set the same as in Scheme B1. The optimization criterion (target function) was the minimum of the total duty on the reboilers of columns EC2 (Q_{reb}^{EC2}) and CR (Q_{reb}^{RC}). The optimization procedure was as follows:

- 1) setting the N_{SD} ;
- 2) setting the amount of side flow F_L (or F_V);
- 3) determining the optimum feed plate in RC N_F^{RC} ;
- 4) repeating steps 2–3 until the minimum value of $\sum Q_{reb} = Q_{reb}^{EC2} + Q_{reb}^{RC}$ is reached;
- 5) returning to step 1;
- 6) repeating steps 1–5 before reaching the minimum value of $\sum Q_{reb}$.

The optimization results of Schemes C1L and C1V are shown in Table 3.

Scheme C2 group. Since Schemes C2L and C2V are obtained by transforming the graph of Scheme B2 and differ only in the aggregate state of the side flow draw,

Table 2. Optimal operating parameters of Schemes B1 and B2

| Column | N_{total} | N_E | N_F | N_{SD} | F_E , kg/h | F_V , kg/h | R | Q_{reb} , kW | $\sum Q_{reb}$, kW |
|--------------|-------------|-------|-------|----------|--------------|--------------|------|----------------|---------------------|
| Scheme B1 | | | | | | | | | |
| EC1 | 46 | 10 | 16 | – | 6614 | – | 6.40 | 2417 | 3604 |
| Main column | 27 | 5 | 14 | 19 | 988 | 972 | 0.25 | 1187 | |
| Side section | 5 | – | – | – | – | – | 0.25 | – | |
| Scheme B2 | | | | | | | | | |
| Main column | 51 | 10 | 16 | 48 | 6614 | 3423 | 6.16 | 3021 | 3779 |
| Side column | 14 | 5 | – | – | 988 | – | 0.36 | – | |
| RC | 13 | – | 5 | – | – | – | 0.75 | 758 | |

Table 3. Optimal operating parameters of Schemes C1L and C1V

| Column | N_{total} | N_E | N_F | N_{SD} | F_E , kg/h | $F_L (F_V)$, kg/h | R | Q_{reb} , kW | $\sum Q_{reb}$, kW |
|------------|-------------|-------|-------|----------|--------------|--------------------|------|----------------|---------------------|
| Scheme C1L | | | | | | | | | |
| EC1 | 46 | 10 | 16 | – | 6614 | – | 6.40 | 2417 | 3663 |
| EC2 | 27 | 5 | 14 | 19 | 988 | 4650 | 0.25 | 564 | |
| RC | 11 | – | 4 | – | – | – | 0.40 | 682 | |
| Scheme C1V | | | | | | | | | |
| EC1 | 46 | 10 | 16 | – | 6614 | – | 6.40 | 2417 | 3604 |
| EC2 | 27 | 5 | 14 | 19 | 988 | 899 | 0.25 | 1139 | |
| RC | 13 | – | 6 | – | – | – | 0.26 | 48 | |

the procedure of their optimization is identical. Because the composition of its feed differs from the composition in Scheme A, the number of plates in EC2 was selected at the first stage. The selection of the number of plates was performed at fixed entrainer flow rates in EC1 and EC2, as well as the position of the side extraction plate and its number. Further optimized variables were the amount of side liquid extraction flow F_L (Scheme C2L) or steam extraction F_V (Scheme C2V) from EC1 to EC2, the position of the side extraction plate (N_{SD}). As calculations have shown, the composition of the RC feed flow in Schemes C2L and C2V in comparison with Scheme A practically did not change; for this reason, optimization of parameters of this column was not carried out.

The further optimization procedure was as follows:

- 1) setting the N_{SD} in EC1;
- 2) setting the amount of side flow F_L (or F_V);
- 3) varying N_{SD} and N_F in EC2 until reaching the minimum value of Q_{reb}^{EC2} ;
- 4) specifying the position of N_F in the RC;
- 5) calculating $\sum Q_{reb}$ for the entire scheme;
- 6) returning to step 2;
- 7) repeating steps 2–6 until reaching the minimum value of $\sum Q_{reb}$;
- 8) returning to step 1;
- 9) repeating steps 1–8 until reaching the minimum value of $\sum Q_{reb}$.

The optimization results of Schemes C2L and C2V are shown in Table 4.

Table 4. Optimal operating parameters of Schemes C2L and C2V

| Column | N_{total} | N_E | N_F | N_{SD} | F_E , kg/h | $F_L (F_V)$, kg/h | R | Q_{reb} , kW | $\sum Q_{reb}$, kW |
|------------|-------------|-------|-------|----------|--------------|--------------------|------|----------------|---------------------|
| Scheme C2L | | | | | | | | | |
| EC1 | 51 | 10 | 16 | 48 | 6614 | 4250 | 6.20 | 2549 | 3800 |
| EC2 | 15 | 4 | 12 | – | 988 | – | 0.36 | 491 | |
| RC | 13 | – | 5 | – | – | – | 0.77 | 760 | |
| Scheme C2V | | | | | | | | | |
| EC1 | 51 | 10 | 16 | 47 | 6614 | 3008 | 7.62 | 3357 | 4192 |
| EC2 | 16 | 4 | 10 | – | 988 | – | 0.29 | 73 | |
| RC | 13 | – | 5 | – | – | – | 0.78 | 762 | |

RESULTS AND DISCUSSION

Six different variants of the schemes of ED of THF–EAc–water mixture, including columns with side sections and side draws, were considered in the course of the conducted studies. Comparison of the proposed scheme variants with the prototype scheme (Scheme A) by the criterion of total energy consumption is presented in Table 5. Reduction of energy consumption ΔQ_{reb} was calculated by the formula:

$$\Delta Q_{\text{reb}} = \left(\sum Q_{\text{reb}}^A - \sum Q_{\text{reb}}^i \right) / \sum Q_{\text{reb}}^A \times 100\%, \quad (1)$$

where $\sum Q_{\text{reb}}^A$ is the total energy consumption in the column reboilers of Scheme A, $\sum Q_{\text{reb}}^i$ is the total energy consumption in the reboilers of columns of the scheme including a complex with PTCDC or a column with side extraction.

Among the schemes including complexes with PTCDC, it can be seen that the maximum reduction of energy consumption by 5.9% relative to the prototype Scheme A is provided by Scheme B1, in which the complex with PTCDC is obtained by thermal bonding of columns EC2 and RC of Scheme A. Thermal bonding of columns EC1 and EC2 in Scheme B2 gives significantly lower energy savings (1.36%). The different energy efficiency of Schemes B1 and B2 is explained by different reflux ratios in columns RC and EC2 of Scheme A, which are prototypes of the side section (side column) in Schemes B1 and B2, respectively: $R^{\text{RC}} = 0.75$ and $R^{\text{EC2}} = 0.3$. Thus, the obtained results are consistent with the criterion for evaluating the energy efficiency of the application of complexes with PTCDC in the ED.¹ It should also be noted that the reflux ratio in the side section of Scheme B1 is three times lower than the reflux ratio in the RC of Scheme A. This can be explained by the fact that the concentration of water in the steam flow entering the side section is 9 times higher than in the feed flow of the RC of Scheme A. The reflux ratio in the side column of Scheme B2 has a slightly higher value as compared to the reflux ratio in EC2 of Scheme A. This is explained by the fact that about three times more THF

falls in the side section than in the bottom flow of EC1; thus, to obtain EAc of a given quality in the distillate of the side column, a slightly higher reflux ratio is required.

Scheme C1V is characterized by the same energy efficiency as Scheme B1.

In Scheme C1V, the reduction of total energy consumption occurs mainly due to a significant reduction in the duty on the reboilers of the RC (by 94%, compared to the RC of Scheme A). This is due to several reasons. First, the amount of RC feed flow in Scheme C1V is less than in Scheme A due to most of the DMSO in Scheme C1V being released in the column bottom with side extraction. Secondly, the water concentration in the RC feed flow in Scheme C1V is about 70 wt %, while in Scheme A it is 8 wt %. Thirdly, the Scheme C1V RC feed is supplied in the vapor phase, while the Scheme A RC feed is supplied in the liquid phase.

The energy efficiency of Scheme C1L is less than that of Scheme C1V. This is due to the amount of liquid side draw being 5.2 times greater than that of vapor side draw, while the concentration of DMSO in the liquid-phase side flow is already 86 wt % (instead of 30 wt % for the Scheme C1V). Thus, the RC feed flow in Scheme C1L is substantially greater than in Scheme C1V. In addition, the feed to the RC of Scheme C1L is supplied in the liquid phase, so there is no additional source of steam in this column.

The insignificant total reduction of energy consumption (0.81%) in Scheme C2L can be explained by the small reduction in energy consumption in the EC2 reboilers due to the heat contributed by the entrance into it of the withdrawal flow from EC1, which also leads to an increase in the concentration of DMSO in the column. However, energy costs increase by about the same amount in the reboilers of EC1 due to the side extraction flow carrying a certain amount of heat with it, which reduces the concentration of DMSO. Thus, the total positive energy effect is absent in this case due to a redistribution of duty on the reboilers of columns EC1 and EC2.

In Scheme C2P, total energy consumption increases by 9.4% as compared to the basic Scheme A. This significant

Table 5. Comparison of total energy consumption of the considered schemes

| Parameter | Scheme A | Scheme B1 | Scheme B2 | Scheme C1L | Scheme C1V | Scheme C2L | Scheme C2V |
|-----------------------------|----------|-----------|-----------|------------|------------|------------|------------|
| $\sum Q_{\text{reb}}$, kW | 3831 | 3604 | 3779 | 3663 | 3604 | 3800 | 4192 |
| ΔQ_{reb} , % | – | 5.9 | 1.36 | 4.4 | 5.9 | 0.8 | –9.4 |

¹ Anokhina E.A. Extractive distillation in complexes with partially coupled heat and material flows. Dr. Sci. Thesis (Eng.). Moscow; 2020. 549 p. (in Russ.).]

increase in energy consumption is explained by the flow of side extraction in the vapor phase reflux ratio $R = 6.40$ (as in EC1 of Schemes A and C1V) containing such a quantity of THF that prevents the extraction of EAc of a given quality in EC2. Thus, in order to maintain the required concentration of EAc in EC2, it is necessary to increase the reflux ratio (up to 7.62) in EC1, which leads to a significant increase in the duty on its reboilers. In addition, the steam flow of the side extraction carries a significant amount of heat, which requires replenishing.

CONCLUSIONS

Thus, it can be concluded that the organization of side draw from one EC to another in two-stage ED THF–EAc–water mixture schemes does not lead to a reduction of total energy consumption. Conversely, the organization of side draw from EC to CR can reduce the total energy consumption in the column reboilers by 4.4% at side draw in the liquid phase and by 5.9% at draw in the vapor phase. It should be noted that Scheme B1, which includes a complex with PTCDC obtained by thermal bonding of EC and RC, as well as

Scheme C1V, in which draw in the vapor phase from EC to RC is carried out, are characterized by the same energy efficiency (5.9%). The final choice of the variant for practical implementation can be made after modeling the dynamic behavior of these schemes.

Acknowledgments

This study was financially supported by the State Assignment of the Russian Federation, grant No. FSFZ-2023-0003.

Authors' contribution

D.G. Rudakov—planning and conducting research, analyzing research materials, writing the manuscript.

S.M. Kharlamov—conducting research, analyzing research materials.

P.S. Klausner—analyzing research materials, writing the manuscript.

E.A. Anokhina—management and scientific consulting, analyzing research materials.

A.V. Timoshenko—formulation of the scientific concept, general management.

The authors declare no conflicts of interest.

REFERENCES

1. Wittmann G., Karg E., Mühl A., Bodamer O.A., Túri S. Comparison of tetrahydrofuran and ethyl acetate as extraction solvents for urinary organic acid analysis. *J. Inherit. Metab. Dis.* 2008;31(1):73–80. <https://doi.org/10.1007/s10545-007-0767-8>
2. Yang A., Su Y., Shi T., *et al.* Energy-efficient recovery of tetrahydrofuran and ethyl acetate by triple-column extractive distillation: entrainer design and process optimization. *Front. Chem. Sci. Eng.* 2022;16(5):303–315. <https://doi.org/10.1007/s11705-021-2044-z>
3. Timoshenko A.V., Anokhina E.A., Morgunov A.V., Rudakov D.G. Application of the partially thermally coupled distillation flowsheets for the extractive distillation of ternary azeotropic mixtures. *Chem. Eng. Res. Des.* 2015;104(3):139–155. <https://doi.org/10.1016/j.cherd.2015.07.007>
4. Gerbaud V., Rodriguez-Donis I., Hegely L., Lang P., Denes F., You X.-Q. Review of extractive distillation. Process design, operation, optimization and control. *Chem. Eng. Res. Des.* 2019;141:229–271. <https://doi.org/10.1016/j.cherd.2018.09.020>
5. Valdez J.A., Patino-Herrera R., Martinez A.A., Perez E. Separation of the cyclohexane-benzene mixture by the extractive distillation process using ethylene glycol as a solvent. *Chem. Eng. Process.* 2024;196:109686. <https://doi.org/10.1016/j.cep.2024.109686>
6. Rudakov D.G., Klausner P.S., Ramochnikov D.A., Anokhina E.A., Timoshenko A.V. Efficiency of heat pumps in extractive rectification of the allyl alcohol–allyl acetate mixture with different compositions of the feed: Part 1. Application of heat pumps in schemes with two-selection columns. *Theor. Found. Chem. Eng.* 2023;57(4):770–778. <https://doi.org/10.1134/S0040579523040231>

СПИСОК ЛИТЕРАТУРЫ

1. Wittmann G., Karg E., Mühl A., Bodamer O.A., Túri S. Comparison of tetrahydrofuran and ethyl acetate as extraction solvents for urinary organic acid analysis. *J. Inherit. Metab. Dis.* 2008;31(1):73–80. <https://doi.org/10.1007/s10545-007-0767-8>
2. Yang A., Su Y., Shi T., *et al.* Energy-efficient recovery of tetrahydrofuran and ethyl acetate by triple-column extractive distillation: entrainer design and process optimization. *Front. Chem. Sci. Eng.* 2022;16(5):303–315. <https://doi.org/10.1007/s11705-021-2044-z>
3. Timoshenko A.V., Anokhina E.A., Morgunov A.V., Rudakov D.G. Application of the partially thermally coupled distillation flowsheets for the extractive distillation of ternary azeotropic mixtures. *Chem. Eng. Res. Des.* 2015;104(3):139–155. <https://doi.org/10.1016/j.cherd.2015.07.007>
4. Gerbaud V., Rodriguez-Donis I., Hegely L., Lang P., Denes F., You X.-Q. Review of extractive distillation. Process design, operation, optimization and control. *Chem. Eng. Res. Des.* 2019;141:229–271. <https://doi.org/10.1016/j.cherd.2018.09.020>
5. Valdez J.A., Patino-Herrera R., Martinez A.A., Perez E. Separation of the cyclohexane-benzene mixture by the extractive distillation process using ethylene glycol as a solvent. *Chem. Eng. Process.* 2024;196:109686. <https://doi.org/10.1016/j.cep.2024.109686>
6. Rudakov D.G., Klausner P.S., Ramochnikov D.A., Anokhina E.A., Timoshenko A.V. Efficiency of heat pumps in extractive rectification of the allyl alcohol–allyl acetate mixture with different compositions of the feed: Part 1. Application of heat pumps in schemes with two-selection columns. *Theor. Found. Chem. Eng.* 2023;57(4):770–778. <https://doi.org/10.1134/S0040579523040231>

7. Ma J., Wang X., Zhou Y., Du Y., Wang B. Energy-saving process development for the purification of propylene glycol based on MVR heat pump distillation combined with thermally coupled technology. *Sep. Purif. Technol.* 2024;329:125064. <https://doi.org/10.1016/j.seppur.2023.125064>
8. Wu T., Wang C., Liu J., Zhuang Y., Du J. Design and 4E analysis of heat pump-assisted extractive distillation processes with preconcentration for recovering ethyl-acetate and ethanol from wastewater. *Chem. Eng. Res. Des.* 2024;201:510–522. <https://doi.org/10.1016/j.cherd.2022.12.011>
9. Klauzner P.S., Rudakov D.G., Anokhina E.A., Timoshenko A.V. Energy efficiency of diabatic distillation schemes for an acetone–toluene–*n*-butanol mixture with an entrainer in the first column. *Tonk. Khem. Tekhnol. = Fine Chem. Technol.* 2023;18(1):7–20. <https://doi.org/10.32362/2410-6593-2023-18-1-7-20>
10. Voinov N.A., Zemtsov D.A., Deryagina N.V., Bogatkova A.V., Zhukova O.P. A study of diabatic distillation in a column with a low pressure drop. *Chem. Eng. Res. Des.* 2022;185:1–13. <https://doi.org/10.1016/j.cherd.2022.06.033>
11. Fang J., Li Z., Huang G., Li H., Li C. Externally heat-integrated multiple diabatic distillation columns (EHIm_{DC}): Basic concept and general characteristics. *Ind. Eng. Chem. Res.* 2020;59(4):1668–1681. <https://doi.org/10.1021/acs.iecr.9b05841>
12. Gutiérrez-Guerra R., Segovia-Hernández J.G. Novel approach to design and optimize heat-integrated distillation columns using Aspen Plus and an optimization algorithm. *Chem. Eng. Res. Des.* 2023;196:13–27. <https://doi.org/10.1016/j.cherd.2023.06.015>
13. Pan C., Qiu X., Guo J., Liu Y., Feng B., Li G., Gai H., Song H., Xiao M., Huang T., Zhu Q. Efficient purification of *n*-butanol by thermally coupled extractive distillation with mixed entrainer. *Sep. Purif. Technol.* 2024;336:126365. <https://doi.org/10.1016/j.seppur.2024.126365>
14. Anokhina E.A., Yakutin R.I., Timoshenko A.V. Purifying benzene from thiophene by extractive distillation using columns with side withdrawal in the vapor phase. *Theor. Found. Chem. Eng.* 2021;55(5):880–887. <https://doi.org/10.1134/S0040579521040205> [Original Russian Text: Anokhina E.A., Yakutin R.I., Timoshenko A.V. Purifying benzene from thiophene by extractive distillation using columns with side withdrawal in the vapor phase. *Teoreticheskie osnovy khimicheskoi tekhnologii.* 2021;55(5):578–586 (in Russ.). <https://doi.org/10.31857/S0040357121040011>]
15. Sun S., Fu L., Yang A., Shen W. An intensified energy-saving architecture for side-stream extractive distillation of four-azeotrope mixtures considering economic, environmental and safety criteria simultaneously. *Sep. Purif. Technol.* 2023;310:123132. <https://doi.org/10.1016/j.seppur.2023.123132>
16. Yang A., Kong Z.Y., Sunarso J., Su Y., Wang G., Zhu S. Insights on sustainable separation of ternary azeotropic mixture tetrahydrofuran/ethyl acetate/water using hybrid vapor recompression assisted side-stream extractive distillation. *Sep. Purif. Technol.* 2022;290:120884. <https://doi.org/10.1016/j.seppur.2022.120884>
17. Head D.L., McCart C.G. The thermal decomposition of DMSO. *Tetrahedron Lett.* 1973;14(16):1405–1408. [https://doi.org/10.1016/S0040-4039\(01\)95955-6](https://doi.org/10.1016/S0040-4039(01)95955-6)
18. Yang J., Pan X., Yu M., Cui P., Ma Y., Wang Y., Gao J. Vapor-liquid equilibrium for binary and ternary systems of tetrahydrofuran, ethyl acetate and *N*-methyl pyrrolidone at pressure 101.3 kPa. *J. Mol. Liq.* 2018;268:19–25. <https://doi.org/10.1016/j.molliq.2018.07.038>
19. Xie Q., Wan H., Guan G.F. Isobaric vapor-liquid equilibrium for tetrahydrofuran-water-*n*-hexane system. *Chem. Eng.* 2010;38(4):61–72.
7. Ma J., Wang X., Zhou Y., Du Y., Wang B. Energy-saving process development for the purification of propylene glycol based on MVR heat pump distillation combined with thermally coupled technology. *Sep. Purif. Technol.* 2024;329:125064. <https://doi.org/10.1016/j.seppur.2023.125064>
8. Wu T., Wang C., Liu J., Zhuang Y., Du J. Design and 4E analysis of heat pump-assisted extractive distillation processes with preconcentration for recovering ethyl-acetate and ethanol from wastewater. *Chem. Eng. Res. Des.* 2024;201:510–522. <https://doi.org/10.1016/j.cherd.2022.12.011>
9. Клаузнер П.С., Рудаков Д.Г., Анохина Е.А., Тимошенко А.В. Оценка энергетической эффективности схем неадиабатической ректификации смеси ацетон–толуол–*n*-бутанол с использованием экстрактивного агента в первой колонне. *Тонкие химические технологии.* 2023;18(1):7–20. <https://doi.org/10.32362/2410-6593-2023-18-1-7-20>
10. Voinov N.A., Zemtsov D.A., Deryagina N.V., Bogatkova A.V., Zhukova O.P. A study of diabatic distillation in a column with a low pressure drop. *Chem. Eng. Res. Des.* 2022;185:1–13. <https://doi.org/10.1016/j.cherd.2022.06.033>
11. Fang J., Li Z., Huang G., Li H., Li C. Externally heat-integrated multiple diabatic distillation columns (EHIm_{DC}): Basic concept and general characteristics. *Ind. Eng. Chem. Res.* 2020;59(4):1668–1681. <https://doi.org/10.1021/acs.iecr.9b05841>
12. Gutiérrez-Guerra R., Segovia-Hernández J.G. Novel approach to design and optimize heat-integrated distillation columns using Aspen Plus and an optimization algorithm. *Chem. Eng. Res. Des.* 2023;196:13–27. <https://doi.org/10.1016/j.cherd.2023.06.015>
13. Pan C., Qiu X., Guo J., Liu Y., Feng B., Li G., Gai H., Song H., Xiao M., Huang T., Zhu Q. Efficient purification of *n*-butanol by thermally coupled extractive distillation with mixed entrainer. *Sep. Purif. Technol.* 2024;336:126365. <https://doi.org/10.1016/j.seppur.2024.126365>
14. Анохина Е.А., Якутин Р.И., Тимошенко А.В. Очистка бензола от тиофена экстрактивной ректификацией с применением колонн с боковым отбором в паровой фазе. *Теоретические основы химической технологии.* 2021;55(5):578–586. <https://doi.org/10.31857/S0040357121040011>
15. Sun S., Fu L., Yang A., Shen W. An intensified energy-saving architecture for side-stream extractive distillation of four-azeotrope mixtures considering economic, environmental and safety criteria simultaneously. *Sep. Purif. Technol.* 2023;310:123132. <https://doi.org/10.1016/j.seppur.2023.123132>
16. Yang A., Kong Z.Y., Sunarso J., Su Y., Wang G., Zhu S. Insights on sustainable separation of ternary azeotropic mixture tetrahydrofuran/ethyl acetate/water using hybrid vapor recompression assisted side-stream extractive distillation. *Sep. Purif. Technol.* 2022;290:120884. <https://doi.org/10.1016/j.seppur.2022.120884>
17. Head D.L., McCart C.G. The thermal decomposition of DMSO. *Tetrahedron Lett.* 1973;14(16):1405–1408. [https://doi.org/10.1016/S0040-4039\(01\)95955-6](https://doi.org/10.1016/S0040-4039(01)95955-6)
18. Yang J., Pan X., Yu M., Cui P., Ma Y., Wang Y., Gao J. Vapor-liquid equilibrium for binary and ternary systems of tetrahydrofuran, ethyl acetate and *N*-methyl pyrrolidone at pressure 101.3 kPa. *J. Mol. Liq.* 2018;268:19–25. <https://doi.org/10.1016/j.molliq.2018.07.038>
19. Xie Q., Wan H., Guan G.F. Isobaric vapor-liquid equilibrium for tetrahydrofuran-water-*n*-hexane system. *Chem. Eng.* 2010;38(4):61–72.

20. Rajedran M., Renganarayanan S., Srinivasan D. Salt effect in phase equilibria and heat of mixing: effect of dissolved inorganic salts on the liquid-liquid equilibria of ethyl acetate-2-propanol-water system and the vapor-liquid equilibria and heat of mixing of its constituent binaries. *Fluid Ph. Equilib.* 1991;70(1): 65–106. [https://doi.org/10.1016/0378-3812\(91\)85005-F](https://doi.org/10.1016/0378-3812(91)85005-F)
21. Sassa Y., Konishi R., Katayama T. Isothermal vapor-liquid equilibrium data of DMSO [dimethyl sulfoxide] solutions by total pressure method. DMSO-acetone, DMSO-tetrahydrofuran, and DMSO-ethyl acetate systems. *J. Chem. Eng. Data.* 1974;19(1):44–48. <https://doi.org/10.1021/je60060a004>
22. Zhang Z., Lv M., Huang D., Jia P., Sun D., Li W. Isobaric Vapor Liquid Equilibrium for the Extractive Distillation of Acetonitrile + Water Mixtures Using Dimethyl Sulfoxide at 101.3 kPa. *J. Chem. Eng. Data.* 2013;58(12):3364–3369. <https://doi.org/10.1021/je400531a>
20. Rajedran M., Renganarayanan S., Srinivasan D. Salt effect in phase equilibria and heat of mixing: effect of dissolved inorganic salts on the liquid-liquid equilibria of ethyl acetate-2-propanol-water system and the vapor-liquid equilibria and heat of mixing of its constituent binaries. *Fluid Ph. Equilib.* 1991;70(1): 65–106. [https://doi.org/10.1016/0378-3812\(91\)85005-F](https://doi.org/10.1016/0378-3812(91)85005-F)
21. Sassa Y., Konishi R., Katayama T. Isothermal vapor-liquid equilibrium data of DMSO [dimethyl sulfoxide] solutions by total pressure method. DMSO-acetone, DMSO-tetrahydrofuran, and DMSO-ethyl acetate systems. *J. Chem. Eng. Data.* 1974;19(1):44–48. <https://doi.org/10.1021/je60060a004>
22. Zhang Z., Lv M., Huang D., Jia P., Sun D., Li W. Isobaric Vapor Liquid Equilibrium for the Extractive Distillation of Acetonitrile + Water Mixtures Using Dimethyl Sulfoxide at 101.3 kPa. *J. Chem. Eng. Data.* 2013;58(12):3364–3369. <https://doi.org/10.1021/je400531a>

About the Authors

Danila G. Rudakov, Cand. Sci. (Eng.), Associate Professor, Department of Chemistry and Technology of Basic Organic Synthesis, M.V. Lomonosov Institute of Fine Chemical Technologies, MIREA – Russian Technological University (78, Vernadskogo pr., Moscow, 119454, Russia). E-mail: rudakov@mirea.ru. Scopus Author ID 37018548000, ResearcherID M-5241-2014, RSCI SPIN-code 2366-9449, <https://orcid.org/0000-0002-9892-7909>

Sergey M. Kharlamov, Student, M.V. Lomonosov Institute of Fine Chemical Technologies, MIREA – Russian Technological University (78, Vernadskogo pr., Moscow, 119454, Russia). E-mail: sergeykharlamov.79@gmail.com. <https://orcid.org/0000-0003-4470-6323>

Pavel S. Klauzner, Cand. Sci. (Eng.), Assistant, Department of Chemistry and Technology of Basic Organic Synthesis, M.V. Lomonosov Institute of Fine Chemical Technologies, MIREA – Russian Technological University (78, Vernadskogo pr., Moscow, 119454, Russia). E-mail: klauzner@mirea.ru. ResearcherID AAJ-7842-2021, RSCI SPIN-code 6922-6509, <https://orcid.org/0000-0001-5844-549X>

Elena A. Anokhina, Dr. Sci. (Eng.), Professor, Department of Chemistry and Technology of Basic Organic Synthesis, M.V. Lomonosov Institute of Fine Chemical Technologies, MIREA – Russian Technological University (78, Vernadskogo pr., Moscow, 119454, Russia). E-mail: anokhina.ea@mail.ru. Scopus Author ID 6701718055, ResearcherID E-5022-2016, RSCI SPIN-code 8161-7762

Andrey V. Timoshenko, Dr. Sci. (Eng.), Professor, Department of Chemistry and Technology of Basic Organic Synthesis, M.V. Lomonosov Institute of Fine Chemical Technologies, MIREA – Russian Technological University (78, Vernadskogo pr., Moscow, 119454, Russia). E-mail: timoshenko@mirea.ru. Scopus Author ID 56576076700, ResearcherID Y-8709-2018, RSCI SPIN-code 5687-7930, <https://orcid.org/0000-0002-6511-7440>

Об авторах

Рудаков Данила Григорьевич, к.т.н., доцент кафедры химии и технологии основного органического синтеза, Институт тонких химических технологий им. М.В. Ломоносова, ФГБОУ ВО «МИРЭА – Российский технологический университет» (119454, Россия, Москва, пр-т Вернадского, д. 78). E-mail: rudakov@mirea.ru. Scopus Author ID 37018548000, ResearcherID M-5241-2014, SPIN-код РИНЦ 2366-9449, <https://orcid.org/0000-0002-9892-7909>

Харламов Сергей Максимович, студент, Институт тонких химических технологий им. М.В. Ломоносова, ФГБОУ ВО «МИРЭА – Российский технологический университет» (119454, Россия, Москва, пр-т Вернадского, д. 78). E-mail: sergeykhharlamov.79@gmail.com. <https://orcid.org/0000-0003-4470-6323>

Клаузнер Павел Сергеевич, к.т.н., ассистент, кафедра химии и технологии основного органического синтеза, Институт тонких химических технологий им. М.В. Ломоносова, ФГБОУ ВО «МИРЭА – Российский технологический университет» (119454, Россия, Москва, пр-т Вернадского, д. 78). E-mail: klauzner@mirea.ru. ResearcherID AAJ-7842-2021, SPIN-код РИНЦ 6922-6509, <https://orcid.org/0000-0001-5844-549X>

Анохина Елена Анатольевна, д.т.н., профессор кафедры химии и технологии основного органического синтеза, Институт тонких химических технологий им. М.В. Ломоносова, ФГБОУ ВО «МИРЭА – Российский технологический университет» (119454, Россия, Москва, пр-т Вернадского, д. 78). E-mail: anokhina.ea@mail.ru. Scopus Author ID 6701718055, ResearcherID E-5022-2016, SPIN-код РИНЦ 8161-7762

Тимошенко Андрей Всеволодович, д.т.н., профессор кафедры химии и технологии основного органического синтеза, Институт тонких химических технологий им. М.В. Ломоносова, ФГБОУ ВО «МИРЭА – Российский технологический университет» (119454, Россия, Москва, пр-т Вернадского, д. 78). E-mail: timoshenko@mirea.ru. Scopus Author ID 56576076700, ResearcherID Y-8709-2018, SPIN-код РИНЦ 5687-7930, <https://orcid.org/0000-0002-6511-7440>

Translated from Russian into English by H. Moshkov

Edited for English language and spelling by Thomas A. Beavitt

UDC 57.088.2

<https://doi.org/10.32362/2410-6593-2025-20-2-107-118>

EDN QVQVOC



RESEARCH ARTICLE

Production of the recombinant hemagglutinin protein of the swine influenza virus A/H1N1 and analysis of its physicochemical and antigenic properties

Elena D. Avdonina^{1,✉}, Kristina A. Pervoykina¹, Ludmila V. Verkhovskaya¹, Dmitriy N. Shcherbinin¹, Natalia Yu. Viskova¹, Irina S. Kruzhkova^{1,2}, Maria A. Ilina², Larisa V. Kudriavtseva², Lyudmila V. Kolobukhina^{1,2}, Maksim M. Shmarov¹, Natalya A. Antipyat², Alexander L. Gintsburg¹, Igor N. Tyurin²

¹ The Gamaleya National Center of Epidemiology and Microbiology, Ministry of Health of the Russian Federation, Moscow, 123098 Russia

² Infectious Disease Clinical Hospital No. 1, Moscow City Health Department, Moscow, 125367 Russia

✉ Corresponding author, e-mail: avdonina.yelena@mail.ru

Abstract

Objectives. To analyze the physicochemical and antigenic properties of recombinant hemagglutinin protein of swine influenza virus strain A/H1N1 (swH1-His) obtained by transduction of suspension line HEK293 with recombinant human adenovirus serotype 5.

Methods. The *de novo* assembly of the target hemagglutinin gene was performed via the polymerase chain reaction. Recombinant adenovirus recAd5-swH1-His was obtained using the AdEasy™ Adenoviral Vector System kit. Accumulation of preparative amounts of recombinant protein was performed by transduction of recAd5-swH1-His suspension culture of HEK293 cells in a wave-type bioreactor. Recombinant hemagglutinin was isolated from the culture medium by metal-chelate affinity purification on a sorbent. The actual molecular mass and its correspondence to the expected value, as well as the presence of histidine residues were shown by electrophoresis and Western blot. The antigenic specificity of swH1-His was determined by indirect enzyme-linked immunosorbent assay with specific sera.

Results. Recombinant hemagglutinin swH1-His was obtained in the amount of 1.2 mg from 50 mL of culture fluid. The compliance of its mass with the declared molecular mass (≈ 70 kDa) was confirmed along with the presence of cross-linking with histidine residues. The antigenic specificity of swH1-His in reaction with sera was demonstrated.

Conclusions. The physicochemical and antigenic characteristics of recombinant protein hemagglutinin of swine influenza A/H1N1 (swH1-His) obtained by transduction of HEK293 cells with recombinant human adenovirus of serotype 5 were determined. The obtained recombinant hemagglutinin can be used as an antigen for animal and human influenza diagnostic purposes.

Keywords

recombinant protein, recombinant human serotype 5 virus, purification of recombinant protein, antigenic specificity, enzyme-linked immunosorbent assay

Submitted: 15.08.2024

Revised: 18.12.2024

Accepted: 18.02.2025

For citation

Avdonina E.D., Pervoykina K.A., Verkhovskaya L.V., Shcherbinin D.N., Viskova N.Yu., Kruzhkova I.S., Ilina M.A., Kudriavtseva L.V., Kolobukhina L.V., Shmarov M.M., Antipyat N.A., Gintsburg A.L., Tyurin I.N. Production of the recombinant hemagglutinin protein of the swine influenza virus A/H1N1 and analysis of its physicochemical and antigenic properties. *Tonk. Khim. Tekhnol. = Fine Chem. Technol.* 2025;20(2):107–118. <https://doi.org/10.32362/2410-6593-2025-20-2-107-118>

НАУЧНАЯ СТАТЬЯ

Получение и анализ физико-химических и антигенных свойств рекомбинантного белка гемагглютини́на вируса свиного гриппа А/Н1N1

Е.Д. Авдонина¹✉, К.А. Первойкина¹, Л.В. Верховская¹, Д.Н. Щербинин¹, Н.Ю. Вискова¹, И.С. Кружкова^{1,2}, М.А. Ильина², Л.В. Кудрявцева², Л.В. Колобухина^{1,2}, М.М. Шмаров¹, Н.А. Антипят², А.Л. Гинцбург¹, И.Н. Тюрин²

¹ Национальный исследовательский центр эпидемиологии и микробиологии имени почетного академика Н.Ф. Гамалеи Министерства Здравоохранения Российской Федерации, Москва, 123098 Россия

² Инфекционная клиническая больница № 1, Департамент здравоохранения города Москвы, Москва, 123098 Россия

✉ Автор для переписки, e-mail: avdonina.yelena@mail.ru

Аннотация

Цели. Анализ физико-химических и антигенных свойств рекомбинантного белка гемагглютини́на вируса свиного гриппа штамма А/Н1N1 — swH1-His — полученного путем трансдукции суспензионной линии НЕК293 рекомбинантным аденовирусом человека 5-го серотипа.

Методы. Сборку целевого гена гемагглютини́на *de novo* проводили методом полимеразной цепной реакции. Рекомбинантный аденовирус recAd5-swH1-His получали с помощью набора AdEasy™ Adenoviral Vector System, накопление препаративных количеств рекомбинантного белка проводили методом трансдукции recAd5-swH1-His суспензионной культуры клеток НЕК293 в биореакторе волнового типа. Методом металл-хелатной аффинной очистки на сорбенте выделили рекомбинантный гемагглютинин из культуральной среды. Методами электрофореза и вестерн-блота определили его молекулярную массу, показали ее соответствие ожидаемой, а также наличие гистидиновых остатков. Методом непрямого иммуноферментного анализа со специфическими сыворотками установили антигенную специфичность swH1-His.

Результаты. В ходе работы получили рекомбинантный гемагглютинин swH1-His в количестве 1.2 мг из 50 мл культуральной жидкости, доказали соответствие его массы заявленной молекулярной массе (≈ 70 кДа) и наличие сшивки с гистидиновыми остатками, а также показали антигенную специфичность swH1-His в реакции с сыворотками.

Выводы. Определены физико-химическая и антигенная характеристики рекомбинантного белка гемагглютини́на свиного гриппа А/Н1N1 (swH1-His), полученного трансдукцией клеток НЕК293 рекомбинантным аденовирусом человека 5-го серотипа. В дальнейшем полученный рекомбинантный гемагглютинин может быть использован как антиген для диагностики гриппа животных и человека.

Ключевые слова

рекомбинантный белок, рекомбинантный вирус человека 5-го серотипа, выделение рекомбинантного белка, антигенная специфичность, иммуноферментный анализ

Поступила: 15.08.2024
Доработана: 18.12.2024
Принята в печать: 18.02.2025

Для цитирования

Авдонина Е.Д., Первойкина К.А., Верховская Л.В., Щербинин Д.Н., Вискова Н.Ю., Кружкова И.С., Ильина М.А., Кудрявцева Л.В., Колобухина Л.В., Шмаров М.М., Антипят Н.А., Гинцбург А.Л., Тюрин И.Н. Получение и анализ физико-химических и антигенных свойств рекомбинантного белка гемагглютини́на вируса свиного гриппа А/Н1N1. *Тонкие химические технологии*. 2025;20(2): 107–118. <https://doi.org/10.32362/2410-6593-2025-20-2-107-118>

INTRODUCTION

Influenza is an acute respiratory infectious disease that circulates among the worldwide population, involving seasonal rises in morbidity. The high contagiousness and significant propensity to mutations of the influenza virus allow it to adapt quickly to the immunity formed by classical seasonal vaccines [1]. Therefore, the development of broad-spectrum influenza vaccines aimed at generating an immune response to conserved (low-covariable) sequences of influenza virus proteins remains relevant [2–5]. Such vaccines currently under active development in Russia [6, 7].

When assessing the effectiveness of vaccination, it is important to develop test systems for determining antibody titers in immunized people. Enzyme-linked immunosorbent assay (ELISA)-based test systems are well suited for this objective. Their integral parameter is the presence of an antigen that meets such criteria as availability of production and purification, as well as compliance of antigenic properties with the native protein.

Several different expression systems are currently available for the production of recombinant proteins. Although the choice of systems for recombinant protein production depends on the specific objectives, the most common goal is to obtain a sufficient amount of protein that is as similar in structure as possible to its natural form. Since protein glycosylation has a significant influence on physical (stacking, solubility, molecular weight, etc.) and biological (bioavailability, immunogenicity) properties of the obtained protein [8], the matching of the glycosylation profile of the synthesized recombinant protein to the native one often becomes a key factor.

The optimal expression system for obtaining complex eukaryotic recombinant proteins is mammalian cells. When expression conditions are close to natural, proteins can be obtained having a certain degree of glycosylation strongly approximating the native form [9]. This approach is particularly well suited for research tasks where convenient availability must be combined with the most natural form of recombinant proteins.

Among mammalian cells, there are two widely used cell lines as producers: the cell line derived from human embryonic kidney 293 (HEK293) cells and Chinese hamster ovary (CHO) cells. Although the latter option gives a high yield of recombinant protein (3–8 g/L) with complex glycosylation, it also associated with long and laborious work to breed a stable producer line. In an experimental laboratory, it is generally preferable to obtain protein by transient transfection, where CHO culture is inferior to HEK cells in terms of the complexity of transfection staging and the level of recombinant protein production [8]. HEK293 cells are also notable for the absence of oncogenic potential and low immunogenicity of the recombinant proteins produced due to the absence of structural modifications that are not characteristic of humans [10]. The variant of this line in the form of suspension has an undoubted advantage. When adapted to a serum-free medium, the suspension is optimal for scaling up the process and obtaining recombinant product without the excessive protein load (e.g., albumin) added by serum used in the cultivation of adherent HEK293 cells.

HEK293 is ubiquitously used to produce viral vectors. Due to the presence of adenoviral E1A/B genes responsible for auxiliary functions, adenoviral and adeno-associated viral vectors—in particular, human adenovirus serotype 5 (Ad5)—are produced in HEK293 cell culture [10].

While the production of recombinant proteins in vitro through transduction of cell culture with the human adenoviral vector Ad5 is not currently common, such an approach has considerable potential. Together with the advantages of the HEK293 suspension line, such a tandem can provide efficient production of recombinant protein requiring minimal economic costs and purification efforts.

In this study, we first produced a recombinant adenovirus (recAd5) expressing the hemagglutinin gene of swine influenza type A strain H1N1 (swH1-His) in the HEK293 cell line. After being affinity-purified on sorbent, the physicochemical and antigenic properties of the recombinant protein expressed in the culture medium were characterized.

MATERIALS AND METHODS

De novo assembly of the swine influenza hemagglutinin gene swH1-His

The *de novo* gene assembly was performed using the block method as described by Lei Young and Qihan Dong [11]. Oligonucleotides comprising sequential forward and reverse primers of 65 nucleotides each were selected for gene assembly (see Table 1). The primers were synthesized at Eurogen (Russia). The GeneRuller SM0311 DNA molecular weight marker (*Thermo Fisher Scientific*, USA) was used in this study.

At the first stage, four primers were taken into polymerase chain reaction (PCR) and combined into blocks of 200 base pairs (bp). For each reaction, the quantity of external primers contributed was 10 pmol and internal primers—0.01 pmol. Pfu DNA polymerase (*ELK Biotechnology*, China) was used. Primers were annealed at 55°C. After detecting amplicons by horizontal electrophoresis in 1.5% agarose gel (*Thermo Fisher Scientific*, USA), fragments were excised from the gel and purified on a single Cleanup mini column (*Evrogen*, Russia). Next, overlap extension polymerase chain reaction (OE-PCR) was performed using 100 ng of purified amplicons and Pfu polymerase. At the third stage, standard PCR was performed with primers *swH1-His_out-F* (5'-CGAGCCTAAGCTTCTAGATAAGATGCCGCCACCATGCTTGGACCTGTATGCTGC-3') and *swH1-His_out-R* (5'-TATCTAGATCCGGTGGATCGGATTCATTAGTGATGATGGTGATGGTGATGG-3').

The obtained swH1-His gene (full sequence is given in Table 2) was cloned by simple linear iterative clustering (SLIC) into the shuttle plasmid pShuttle-CMV hydrolyzed by Eco32I site from the AdEasy™ Adenoviral Vector System kit (*Stratagene*, USA) to obtain the plasmid pShuttle-swH1-His.

Production of recAd5 expressing the hemagglutinin gene of swine influenza type A strain H1N1 (swH1-His)

Lipofectamine® 2000 Reagent (*Thermo Fisher Scientific*, USA) was used for transfection according to the protocol. After transfection, cells were harvested, and three freeze-thaw cycles were performed to obtain viral efflux. The titer of the recombinant recAd5-swH1-His virus obtained was determined in the plaque formation reaction on HEK293 adherent cell culture at a confluence of 70%. The cytopathic effect (CPE) induced by recAd5-swH1-His was observed for 4 days.

To analyze the presence of sequences within the recAd5-swH1-His genome, DNA was isolated, and PCR carried out with product detection by agarose gel electrophoresis. The primer sequences for each sequence are presented in Table 3.

Accumulation of preparative amounts of swH1-His protein in culture fluid

To accumulate a preparative amount of recombinant hemagglutinin, the suspension cell line HEK293 was transduced with recAd5-swH1-His virus.

Adherent and suspension cell cultures of human embryonic kidney HEK293 were obtained from the Cell Culture Collection of the Tissue Culture Laboratory of the Tissue Culture Division of the D.I. Ivanovskiy Institute of Virology of the N.F. Gamaleya National Research Center of Epidemiology and Microbiology of the Ministry of Health of the Russian Federation. Cells were cultured in a wave-type bioreactor in Biostat® CultiBag RM 5L cell culture bags (*Sartorius AG*, Germany) in CDM4-HEK293 HyClone™ culture medium (*Cytiva*, USA) supplemented with 2 g/L sodium bicarbonate (*PanEco*, Russia), 1 g/L Poloxamer 188 (*Corning*, USA) and 4 mM L-glutamine (*PanEco*, Russia) at 37°C and 5% CO₂. After reaching a concentration of $1 \cdot 10^6$ cells/mL, the culture was aseptically supplemented with 10 mL of viral suspension

containing recAd5-swH1-His adenovirus at a titer of 10^8 PFU/mL (plaque-forming units per mL) per 100 mL of medium.

Transduced cells were incubated for 3 days until 50–60% CPE was achieved. The percentage of live cells pre-stained with methylene blue was determined by visual counting in a Goryaev chamber (hemocytometer). After centrifuging the obtained cell suspension at 7700g for 20 min at room temperature (20°C), the supernatant was collected and stored at –70°C.

Metal-chelate affinity purification on sorbent

To a 50 mL volume of culture fluid containing the target protein, 1M potassium phosphate buffer (*Merck*, Germany) and sodium chloride (*Merck*, Germany) were added to a final concentration of 50 and 300 mM, respectively, and pH 8.0.

After washing 0.3 mL of the sorbent, Ni activated agarose (*Thermo Fisher Scientific*, USA) with 1 mL buffer A (50 mM potassium phosphate buffer with pH 8.0 and 300 mM sodium chloride), the sorbent precipitate was separated by centrifugation for 1 min at 3000 rpm. The procedure was repeated twice.

Following the transferal of the prepared sorbent was transferred to a tube with 50 mL of culture fluid containing 50 mM potassium phosphate buffer and 300 mM sodium chloride, the mixture was incubated on a shaker at 100 rpm for 16 h (overnight) at +22°C. Next, the supernatant was removed by centrifuging at 3000 rpm. The sorbent precipitate was then washed three times in 1 mL of buffer A.

Elution of protein from the sorbent was performed by rocking on a shaker at 180 rpm for 5 min using 1 mL of buffer B, consisting of 50 mM potassium phosphate buffer (pH 8.0) containing 300 mM sodium chloride and 250 mM methylimidazole (pH 12). After precipitating the sorbent by low-speed centrifugation (1 min at

3000 rpm), the supernatant was collected and dialyzed against 50 mM potassium phosphate buffer (pH 8.0).

The concentration of the affinity-purified protein antigen preparation was measured at 280 nm wavelength on a NanoDrop 2000 spectrophotometer (*Thermo Fisher Scientific*, USA). The preparation was stored at -20°C .

Electrophoretic analysis of swH1-His protein

Proteins were fractionated by electrophoresis in a 12% polyacrylate gel containing sodium dodecyl sulfate (SDS-PAGE) in Laemmli buffer system using a Mini-Protean 3 Cell vertical gel apparatus (*BIO-RAD*, USA). Protein molecular weight was determined using the PageRuler™ Plus Prestained Protein Ladder marker (*Thermo Fisher Scientific*, USA).

Samples for electrophoresis were applied at a loading rate of 1–4 μg of protein per track. Prior to being applied to the gel, samples were placed in denaturing (+) conditions using 2 \times Laemmli Sample Buffer (*Merck*, Germany), bringing the volume with distilled water to 40 μL (if necessary). Samples were heated at 95°C for 5–7 min and samples were added to the wells of the gel. A PageRuler™ Plus Prestained Protein Ladder molecular weight marker was used.

Electrophoresis was performed at a constant current of 20 mA/gel in SDS-PAGE Running Buffer, the components of which were 25 mM Tris-HCl, 0.25 M glycine and 0.1% sodium dodecyl sulfate (SDS), pH 8.3.

At the end of electrophoretic separation, the gel was scanned on a Gel Doc™ EZ device (*BIO-RAD*, USA), in the appropriate program to obtain a digital image and assess the electrophoretic purity of the preparation and the molecular weight of the target protein.

Western blot analysis of swH1-His protein

Following electrophoresis of the analyzed samples in SDS-PAGE, the proteins were transferred from the gel to the membrane by semi-dry transfer on a Trans-Blot® SD Semi-Dry Transfer Cell (*BIO-RAD*, USA) at a constant current of 250 mA over a 7×8 cm gel area.

At the end of transfer, 0.2 μm thick Nitrocellulose Membranes (*BIO-RAD*, USA) were washed three times in distilled water for 10 min each, then free sites on the membrane were blocked with working buffer: 20 mM

phosphate buffered saline solution (PBS), pH 7.2–7.4, containing 0.1% polysorbate 20 (Tween 20) and 1% casein, for 30 min at 37°C on a shaker. The membrane was then incubated in the same buffer solution containing peroxidase-labeled mAb-a-His-HRP¹ monoclonal antibodies to histidine sequence (*Sigma-Aldrich*, Germany) at a working dilution of 1/5000 on a shaker at 22°C for 16 h (overnight). Following incubation, the membrane was first washed with distilled water, then washed three times for 10 min each with 20 mM PBS (pH 7.2) + 0.1% Tween 20 buffer on a shaker. Chemiluminescent detection of the target protein-conjugate complex was performed using Amersham ECL Prime Western Blotting Detection Reagents (*GE HealthCare*, USA) followed by immunoreplica scanning on an Amersham Imager 600 (*GE HealthCare*, USA).

Study of antigenic specificity of the target protein swH1-His in reaction with specific sera by indirect ELISA method

Indirect ELISA was performed according to the standard procedure. The obtained recombinant swH1-His protein and commercial recombinant hemagglutinin protein of influenza A virus strain H1N1/Salifornia/2009 (*Abcam*, UK) were used as antigen.

The sorption dose of the protein was 1 $\mu\text{g}/\text{mL}$ in 50 mM K-carbonate buffer, pH 9.6. Blocking of unbound sites was performed with an inert protein solution—1% Blosker™ Casein (*Thermo Fisher Scientific*, USA). Antiviral monoclonal antibodies to human IgG—Goat anti-Human Fc-specific IgG HRP (*Sigma-Aldrich*, Germany)—were added at a working dilution of 1/5000. One-component TMB-substrate² (*Sigma-Aldrich*, Germany) was used for immune complex manifestation. Optical density was measured at wavelength $\lambda = 450$ nm using iEMS Reader MF Thermo Labsystems tablet spectrophotometer (*Thermo Fisher Scientific*, USA). The antibody titer was taken as the inverse of the highest serum dilution in which the optical absorbance was 2 times higher than background.

Statistical processing of the results

Statistical processing of the results was performed in GraphPad Prism program (*Dotmatics*, Canada). The geometric mean titer method was used for statistical processing with 95% confidence interval (CI).

¹ HRP is horseradish peroxidase.

² TMB is stabilized solution of 3,3',5,5'-tetramethylbenzidine hydrochloride.

RESULTS AND DISCUSSION

De novo assembly of the swine influenza hemagglutinin gene swH1-His

The hemagglutinin gene of Influenza A virus A/swine/Illinois/A01672343/2017(H1N1) strain (NCBI³ Protein ID—AQU12415, NCBI GenBank—KY593239.1) was chosen to create the modified gene. The transmembrane domain and cytoplasmic domain were removed *in silico* and replaced with a spacer (GSSAS) and 10 codons encoding histidine. After optimizing the nucleotide sequence of the structural part of the swH1-His gene for the frequency of codon composition of *Homo sapiens* genes, donor and acceptor splice sites, direct and inverted repeats, some restriction sites were removed.

Gene assembly was performed by PCR using the block method as described by Lei Young and Qihan Dong [11] with certain modifications: in the first step, a 200 bp amplicon was obtained from four primers (Fig. 1); at the second stage, the obtained short amplicons were assembled to a full-size gene, as a result of which all fragments complete each other, and at the third stage, a full-size DNA fragment of 1708 bp was amplified with external primers (Fig. 2) and cloned into a plasmid vector to obtain the pShuttle-swH1-His plasmid.

Production of recAd5 expressing the hemagglutinin gene of swine influenza type A strain H1N1 (swH1-His)

In the plaque formation reaction, the titer of recombinant adenovirus recAd5-swH1-His in the cell lysate was $2 \cdot 10^8$ PFU/mL.

PCR with product detection by agarose gel electrophoresis (Fig. 3) confirmed the presence of the swH1-His gene sequence in the DNA of recombinant human adenovirus serotype 5 (hexon), as well as the absence of the sequence of the E1 region of human adenovirus serotype 5.

Accumulation of preparative amounts of the target protein swH1-His in culture fluid

As shown in previous studies [12], the best parameters for accumulation of the target recombinant protein in the culture medium when using the adenovector system are an infection dose of 200 PFU/cell and 3 days of incubation with achievement of 50–60% CPE.

From the clarified culture fluid, 1 mL of a solution of recombinant swH1-His protein with a concentration of 1.2 mg/mL was obtained by metal-chelate affinity extraction in volume.

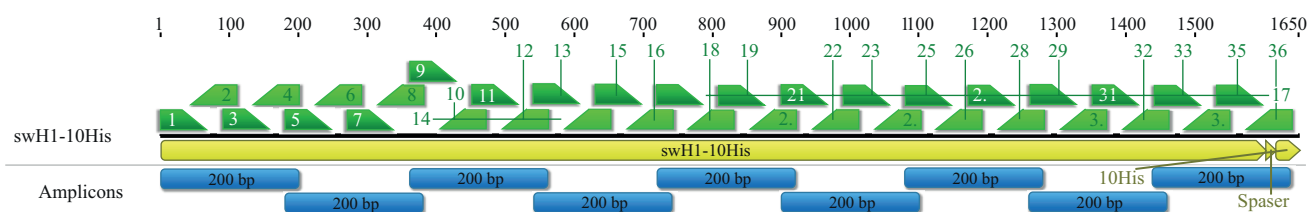


Fig. 1. Scheme for obtaining blocks of 200 base pairs (bp) using four primer amplification

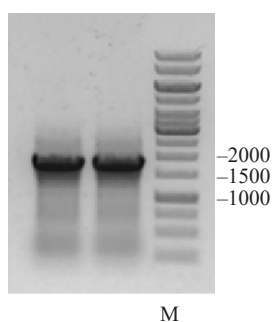


Fig. 2. Electropherogram of the results of amplification of the full-length swH1-His gene with terminal primers swH1-His_out-F and swH1-His_out-R. The amplicon size is 1708 bp, two repeats. M is the molecular weight marker

³ NCBI — National Center for Biotechnology Information. <https://www.ncbi.nlm.nih.gov/>. Accessed June 10, 2023.

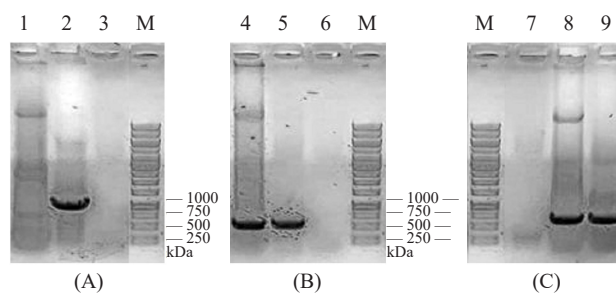


Fig. 3. Electropherogram of PCR analysis of DNA isolated from transduced cells with the recombinant adenovirus recAd5-swH1-His.

(A) PCR with primers for the E1 region of the adenovirus:

- (1) recAd5-swH1-His,
- (2) positive reaction control—1060 bp,
- (3) negative reaction control.

(B) PCR with primers for adenovirus hexon:

- (4) recAd5-swH1-His,
- (5) positive reaction control—580 bp,
- (6) negative reaction control.

(C) PCR with primers for the swH1-His gene:

- (7) negative reaction control,
- (8) recAd5-swH1-His,
- (9) positive reaction control—670 bp.

M is the molecular weight marker

Physicochemical properties of recombinant swH1-His hemagglutinin

The obtained recombinant swH1-His protein was analyzed by protein electrophoresis in 12% SDS-PAGE under denaturing conditions. The molecular mass of the recombinant swH1-His protein and its conformity to the reported molecular mass were determined. The results of electrophoresis in SDS-PAGE are shown in Fig. 4.

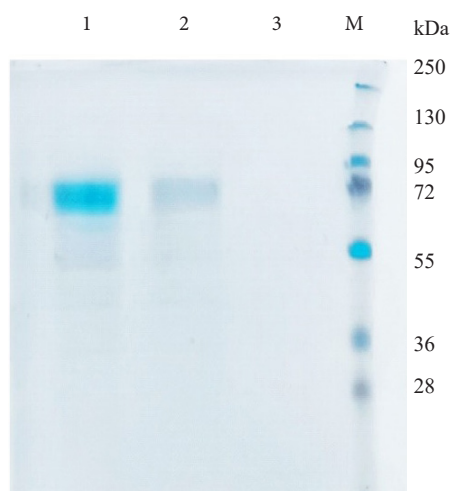


Fig. 4. Electropherogram of purified swH1-His protein:

- (1) swH1-His protein (1st elution)—4 µg/track, (2) swH1-His protein (2nd elution)—1 µg/track, (3) "tailings" (sample after adsorption on Ni-agarose). M is the marker molecular weight

According to electrophoresis data, the molecular mass of the recombinant swH1-His protein is ≈ 70 kDa, which corresponds to the full-size hemagglutinin molecule of influenza A virus. The presence of 10 histidine residues in

the purified recombinant swH1-His protein was confirmed by immunoblotting with monoclonal antibodies specific to the sequence of histidine residues (Fig. 5).

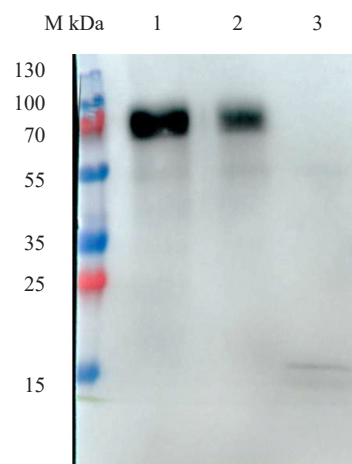


Fig. 5. Immunoreplica of purified swH1-His protein:

- (1) swH1-His protein (1st elution)—4 µg/track, (2) swH1-His protein (2nd elution)—1 µg/track, (3) "tailings" (sample after adsorption on Ni-agarose). M is the marker molecular weight

Antigenic properties of recombinant swH1-His hemagglutinin

The antigenic activity of purified recombinant hemagglutinin swH1-His was characterized by indirect ELISA. For this purpose, specific sera of people who had had influenza were used. The diagnosis of influenza was made on the basis of clinical signs and positive PCR for influenza A/H1N1 RNA in a nasopharyngeal swab.

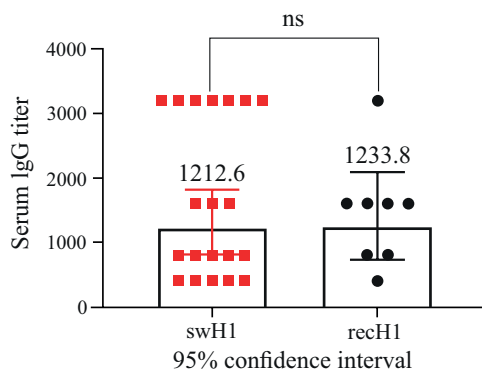


Fig. 6. Geometric mean titers of specific IgG in the blood sera of people who have had influenza to the swH1-His recombinant protein and to the recH1 commercial recombinant protein

During the period of recollection (on day 10–12 of the disease and later), serum was isolated from blood was obtained from patients using a standard method. All patients signed an informed consent form. The study complied with generally accepted medical and ethical standards, the principles of the Declaration of Helsinki of the World Medical Association (2013), and national laws and standards of the Russian Federation and the Rules of Good Clinical Practice (ICH GCP⁴), adopted in the Russian Federation (GOST R 52379-2005⁵).

In order to compare antigenic activity, serum samples were tested by indirect ELISA against the obtained swH1-His protein and commercial recombinant hemagglutinin protein of influenza A virus strain H1N1/California/2009 (recH1). The results of the indirect ELISA are shown in Fig. 6.

According to ELISA data, antigenic activity occurred in the swH1-His protein in reaction with sera of transfected people. However, the titers of specific antibodies to the obtained recombinant swH1-His antigen and to the branded commercial antigen recH1 did not show reliable differences. This indicates the potential possibility of using swH1-His as an antigen in an ELISA test system for the detection of specific antibodies.

CONCLUSIONS

In the course of this study, recombinant human adenovirus of the fifth serotype expressing the hemagglutinin gene of swine influenza type A strain H1N1 (swH1-His) containing 10 histidine residues was obtained by transduction of human embryonic kidney cell line HEK293.

The recombinant protein comprising hemagglutinin of swine influenza type A strain H1N1 (swH1-His) was affinity purified from the culture medium. The yield of highly purified swH1-His protein was 24 mg/L. The molecular mass of the purified protein was as reported (≈ 70 kDa); the authenticity of the cross-linking of the recombinant protein to the histidine sequence was confirmed by immunoblotting data.

Indirect ELISA confirmed the antigenic specificity of the swH1-His protein in reaction with specific blood sera of influenza-infected subjects. In future work, the obtained swH1-His protein will be used as an antigen in ELISA test system to assess the immunogenicity of vector vaccines for influenza prophylaxis.

Acknowledgments

The funding was provided by the Autonomous Nonprofit Organization “Moscow Center for Healthcare Innovations” within the Agreement No. 1603-46/23, dated May 16, 2023, for the grant to implement the scientific and practical project in medicine.

Authors' contributions

E.D. Avdonina—protein purification by batch method, interpretation of the results of the study, writing and revising the text.

K.A. Pervoykina—gene synthesis and obtaining recombinant adenovirus.

L.V. Verkhovskaya—dot-blot, proteins electrophoresis in PAAG, Western blot.

D.N. Shcherbinin—gene design, synthesis, and production of recombinant adenovirus.

N.Yu. Viskova—obtaining preparative quantities of recombinant antibodies in culture fluid.

I.S. Kruzhkova—preparation of a bank of specific blood sera from patients who have had influenza A virus.

⁴ ICH GCP—International Conference on Harmonization of Technical Requirements for Registration of Pharmaceuticals for Human Use; ICH).

⁵ GOST R 52379-2005. National Standard of the Russian Federation. Good Clinical Practice. Moscow: Standartinform; 2006 (in Russ.).

M.A. Ilyina—preparation of a bank of specific blood sera from patients who have had influenza A virus.

L.V. Kudriavtseva—developing conditions for enzyme-linked immunosorbent assay with specific sera from patients who have had influenza A virus.

L.V. Kolobukhina—preparing the medical documentation for work with specific blood sera of patients who have had influenza A virus.

M.M. Shmarov—concept and design of the study, approval of the final version of the of the article for publication.

N.A. Antipyat—research idea, developing conditions for enzyme-linked immunosorbent assay with specific sera of blood of patients who have had influenza A virus.

A.L. Gintsburg—research idea and concept, approval of the final version of the article for publication.

I.N. Tyurin—concept and design of the study, coordination of medical documentation, approval of the final version of the article for publication.

The authors declare no conflicts of interest.

REFERENCES

1. Becker T., Elbahesh H., Reperant L.A., Rimmelzwaan G.F., Osterhaus A.D.M.E. Influenza Vaccines: Successes and Continuing Challenges. *J. Infect. Dis.* 2021;224(12 Suppl. 2): S405–S419. <https://doi.org/10.1093/infdis/jiab269>
2. Lim M.L., Komarasamy T.V., Adnan N.A.A.B., Radhakrishnan A.K., Balasubramaniam V.R.M.T. Recent Advances, Approaches and Challenges in the Development of Universal Influenza Vaccines. *Influenza Other Respir. Viruses.* 2024;18(3):e13276. <https://doi.org/10.1111/irv.13276>
3. Jang Y.H., Seong B.L. The Quest for a Truly Universal Influenza Vaccine. *Front. Cell. Infect. Microbiol.* 2019;9:344. <https://doi.org/10.3389/fcimb.2019.00344>
4. Sautto G.A., Kirchenbaum G.A., Ross T.M. Towards a universal influenza vaccine: different approaches for one goal. *Virol. J.* 2018;15(1):17. <https://doi.org/10.1186/s12985-017-0918-y>
5. Wang W.-C., Sayedahmed E.E., Sambhara S., Mittal S.K. Progress towards the Development of a Universal Influenza Vaccine. *Viruses.* 2022;14(8):1684. <https://doi.org/10.3390/v14081684>
6. Tsybalova L.M., Stepanova L.A., Kotlyarov R.Yu., Blokhina E.A., Shuklina M.A., Mardanova E.S., Korotkov A.V., Potapchuk M.V., Ravin N.V. Strengthening the effectiveness of the candidate influenza vaccine by combining conserved sequences of hemagglutinin and M2 protein. *Epidemiologiya i Vaktsinoprofilaktika = Epidemiology and Vaccine Prophylaxis.* 2017;16(3):65–70 (in Russ.). <https://doi.org/10.31631/2073-3046-2017-16-3-65-70>
7. Sychev I.A., Kopeikin P.M., Tsvetkova E.V., Cheredova K.V., Mil'man B.L., Shamova O.V., Isakova-Sivak I.N., Desheva Yu.A. Induction of cross-reactive antibodies in mice immunized with conserved influenza A virus neuraminidase-derived linear B-cell epitopes. *Infektsiya i immunitet = Russ. J. Infection and Immunity.* 2021;11(3):463–472 (in Russ.). <https://doi.org/10.15789/10.15789/2220-7619-IOC-1343>
8. Croset A., Delafosse L., Gaudry J.-P., Arod C., Glez L., Losberger C., Begue D., Krstanovic A., Robert F., Vilbois F., Chevalet L., Antonsson B. Differences in the glycosylation of recombinant proteins expressed in HEK and CHO cells. *J. Biotechnol.* 2012;161(3):336–348. <https://doi.org/10.1016/j.jbiotec.2012.06.038>
9. Schütz A., Bernhard F., Berrow N., Buyel J.F., Ferreira-da-Silva F., Hastraete J., van den Heuvel J., Hoffmann J.-E., de Marco A., Peleg Y., Suppmann S., Unger T., Vanhoucke M., Witt S., Remans K. A concise guide to choosing suitable gene expression systems for recombinant protein production. *STAR Protoc.* 2023;4(4):102572. <https://doi.org/10.1016/j.xpro.2023.102572>

СПИСОК ЛИТЕРАТУРЫ

1. Becker T., Elbahesh H., Reperant L.A., Rimmelzwaan G.F., Osterhaus A.D.M.E. Influenza Vaccines: Successes and Continuing Challenges. *J. Infect. Dis.* 2021;224(12 Suppl. 2): S405–S419. <https://doi.org/10.1093/infdis/jiab269>
2. Lim M.L., Komarasamy T.V., Adnan N.A.A.B., Radhakrishnan A.K., Balasubramaniam V.R.M.T. Recent Advances, Approaches and Challenges in the Development of Universal Influenza Vaccines. *Influenza Other Respir. Viruses.* 2024;18(3):e13276. <https://doi.org/10.1111/irv.13276>
3. Jang Y.H., Seong B.L. The Quest for a Truly Universal Influenza Vaccine. *Front. Cell. Infect. Microbiol.* 2019;9:344. <https://doi.org/10.3389/fcimb.2019.00344>
4. Sautto G.A., Kirchenbaum G.A., Ross T.M. Towards a universal influenza vaccine: different approaches for one goal. *Virol. J.* 2018;15(1):17. <https://doi.org/10.1186/s12985-017-0918-y>
5. Wang W.-C., Sayedahmed E.E., Sambhara S., Mittal S.K. Progress towards the Development of a Universal Influenza Vaccine. *Viruses.* 2022;14(8):1684. <https://doi.org/10.3390/v14081684>
6. Цыбалова Л.М., Степанова Л.А., Котляров Р.Ю., Блохина Е.А., Шуклина М.А., Марданова Е.С., Коротков А.В., Потапчук М.В., Равин Н.В. Усиление эффективности кандидатной вакцины против гриппа сочетанием консервативных последовательностей гемагглютинаина и М2 белка. *Эпидемиология и Вакцинопрофилактика.* 2017;16(3):65–70. <https://doi.org/10.31631/2073-3046-2017-16-3-65-70>
7. Сычев И.А., Копейкин П.М., Цветкова Е.В., Чередова К.В., Мильман Б.Л., Шамова О.В., Исакова-Сивак И.Н., Дешева Ю.А. Индукция перекрестно-реактивных антител у мышей, иммунизированных консервативными линейными В-клеточными эпитопами нейраминидазы вируса гриппа А. *Инфекция и иммунитет.* 2021;11(3):463–472. <https://doi.org/10.15789/10.15789/2220-7619-IOC-1343>
8. Croset A., Delafosse L., Gaudry J.-P., Arod C., Glez L., Losberger C., Begue D., Krstanovic A., Robert F., Vilbois F., Chevalet L., Antonsson B. Differences in the glycosylation of recombinant proteins expressed in HEK and CHO cells. *J. Biotechnol.* 2012;161(3):336–348. <https://doi.org/10.1016/j.jbiotec.2012.06.038>
9. Schütz A., Bernhard F., Berrow N., Buyel J.F., Ferreira-da-Silva F., Hastraete J., van den Heuvel J., Hoffmann J.-E., de Marco A., Peleg Y., Suppmann S., Unger T., Vanhoucke M., Witt S., Remans K. A concise guide to choosing suitable gene expression systems for recombinant protein production. *STAR Protoc.* 2023;4(4):102572. <https://doi.org/10.1016/j.xpro.2023.102572>

10. Tan E., Chin C.S.H., Lim Z.F.S., Ng S.K. HEK293 Cell Line as a Platform to Produce Recombinant Proteins and Viral Vectors. *Front. Bioeng. Biotechnol.* 2021;9:796991. <https://doi.org/10.3389/fbioe.2021.796991>
11. Young L., Dong Q. Two-step total gene synthesis method. *Nucleic Acids Res.* 2004;32(7):e59. <https://doi.org/10.1093/nar/gnh058>
12. Sedova E.S., Shcherbinin D.N., Bandelyuk A.S., Verkhovskaya L.V., Viskova N.Yu., Avdonina E.D., Prokofiev V.V., Ryabova E.I., Esmagambetov I.B., Pervoykina K.A., Bogacheva E.A., Lysenko A.A., Shmarov M.M. Method for obtaining recombinant antibodies produced by a cell line transduced with recombinant adenoviruses. *Tonk. Khim. Tekhnol. = Fine Chem. Technol.* 2023;18(1):48–64. <https://doi.org/10.32362/2410-6593-2023-18-1-48-64>
10. Tan E., Chin C.S.H., Lim Z.F.S., Ng S.K. HEK293 Cell Line as a Platform to Produce Recombinant Proteins and Viral Vectors. *Front. Bioeng. Biotechnol.* 2021;9:796991. <https://doi.org/10.3389/fbioe.2021.796991>
11. Young L., Dong Q. Two-step total gene synthesis method. *Nucleic Acids Res.* 2004;32(7):e59. <https://doi.org/10.1093/nar/gnh058>
12. Седова Е.С., Щербинин Д.Н., Банделюк А.С., Верховская Л.В., Вискова Н.Ю., Авдонина Е.Д., Прокофьев В.В., Рябова Е.И., Есмагамбетов И.Б., Первойкина К.А., Богачева Е.А., Лысенко А.А., Шмаров М.М. Способ получения рекомбинантных антител, продуцируемых клеточной линией, трансдуцированной рекомбинантными аденовирусами. *Тонкие химические технологии.* 2023;18(1):48–64. <https://doi.org/10.32362/2410-6593-2023-18-1-48-64>

About the Authors

Elena D. Avdonina, Junior Researcher, Laboratory of Molecular Biotechnology, N.F. Gamaleya National Research Center for Epidemiology and Microbiology (The Gamaleya National Center), Ministry of Health of the Russian Federation (18, Gamaleya ul., Moscow, 123098, Russia). E-mail: avdonina.yelena@mail.ru. <https://orcid.org/0000-0001-8059-9743>

Kristina A. Pervoykina, Junior Researcher, Laboratory of Molecular Biotechnology, N.F. Gamaleya National Research Center for Epidemiology and Microbiology (The Gamaleya National Center), Ministry of Health of the Russian Federation (18, Gamaleya ul., Moscow, 123098, Russia). E-mail: uk-ru123@yandex.ru. Scopus Author ID 57698990900, <https://orcid.org/0000-0003-0780-5998>

Ludmila V. Verkhovskaya, Cand. Sci. (Biol.), Leading Researcher, Laboratory of Molecular Biotechnology, N.F. Gamaleya National Research Center for Epidemiology and Microbiology (The Gamaleya National Center), Ministry of Health of the Russian Federation (18, Gamaleya ul., Moscow, 123098, Russia). E-mail: verkhov@mail.ru. RSCI SPIN-code 5529-5909, <https://orcid.org/0000-0002-4731-1629>

Dmitriy N. Shcherbinin, Cand. Sci. (Biol.), Researcher, Laboratory of Molecular Biotechnology, N.F. Gamaleya National Research Center for Epidemiology and Microbiology (The Gamaleya National Center), Ministry of Health of the Russian Federation (18, Gamaleya ul., Moscow, 123098, Russia). E-mail: dim284@inbox.ru. Scopus Author ID 36599350900, ResearcherID E-7682-2014, RSCI SPIN-code 7743-6517, <https://orcid.org/0000-0002-8518-1669>

Natalia Yu. Viskova, Researcher, Laboratory of Molecular Biotechnology, N.F. Gamaleya National Research Center for Epidemiology and Microbiology (The Gamaleya National Center), Ministry of Health of the Russian Federation (18, Gamaleya ul., Moscow, 123098, Russia). E-mail: apr2004@mail.ru. <https://orcid.org/0000-0002-6476-3520>

Irina S. Kruzhkova, Infectious Disease Specialist, Infectious Diseases Clinical Hospital No. 1, Moscow City Health Department (63, Volokolamskoye sh., Moscow, 125367, Russia); Researcher, N.F. Gamaleya National Research Center for Epidemiology and Microbiology (The Gamaleya National Center), Ministry of Health of the Russian Federation (18, Gamaleya ul., Moscow, 123098, Russia), E-mail: irina-kru@yandex.ru. <http://orcid.org/0000-0002-1983-481X>

Maria A. Ilina, Head of the Moscow Center for Chronic Infectious Diseases, Tick-Borne Infections, Travel Medicine and Vaccine Prevention, Infectious Diseases Clinical Hospital No. 1, Moscow City Health Department (63, Volokolamskoye sh., Moscow, 125367, Russia). E-mail: ilina_mar@list.ru. <http://orcid.org/0000-0003-4227-5363>

Larisa V. Kudriavtseva, Head of Laboratory and Diagnostic Department, Infectious Diseases Clinical Hospital No. 1, Moscow City Health Department (63, Volokolamskoye sh., Moscow, 125367, Russia). E-mail: drkudriavtsevalv@yandex.ru. <http://orcid.org/0000-0001-7516-9490>

Lyudmila V. Kolobukhina, Dr. Sci. (Med.), Professor, Head of the Laboratory of Respiratory Viral Infections with Drug Testing, N.F. Gamaleya National Research Center for Epidemiology and Microbiology (The Gamaleya National Center), Ministry of Health of the Russian Federation (18, Gamaleya ul., Moscow, 123098, Russia); Infectious Disease Specialist, Infectious Diseases Clinical Hospital No. 1, Moscow City Health Department (63, Volokolamskoye sh., Moscow, 125367, Russia). E-mail: lkolobuchina@yandex.ru. Scopus Author ID 6601956811, <http://orcid.org/0000-0001-5775-3343>

Maksim M. Shmarov, Dr. Sci. (Biol.), Head of the Laboratory of Molecular Biotechnology, N.F. Gamaleya National Research Center for Epidemiology and Microbiology (The Gamaleya National Center), Ministry of Health of the Russian Federation (18, Gamaleya ul., Moscow, 123098, Russia). E-mail: ribozym@mail.ru. Scopus Author ID 6507322279, ResearcherID D-8662-2014, RSCI SPIN-code 4874-2578, <https://orcid.org/0000-0002-5268-1296>

Natalya A. Antipyat, Deputy Chief Physician for Medical Affairs, Infectious Diseases Clinical Hospital No. 1, Moscow City Health Department (63, Volokolamskoye sh., Moscow, 125367, Russia). E-mail: natadoc70@bk.ru. Scopus Author ID 57207693166, <http://orcid.org/0000-0001-8578-2838>

Alexander L. Gintsburg, Full Member of the Russian Academy of Sciences, Dr. Sci. (Biol.), Professor, Director of the N.F. Gamaleya National Research Center for Epidemiology and Microbiology (The Gamaleya National Center), Ministry of Health of the Russian Federation (18, Gamaleya ul., Moscow, 123098, Russia); Head of the Department of Infectology and Virology, I.M. Sechenov First Moscow State Medical University (Sechenov University) (8-2, Trubetskaya ul., Moscow, 119991, Russia). E-mail: gintsburg@gamaleya.org. Scopus Author ID 7005111491 RSCI SPIN-code 7626-0373, <https://orcid.org/0000-0003-1769-5059>

Igor N. Tyurin, Chief Physician, Infectious Diseases Clinical Hospital No 1, Moscow City Health Department (63, Volokolamskoye sh., Moscow, 125367, Russia). E-mail: tyurin.dti@yandex.ru. Scopus Author ID 56895933300, <http://orcid.org/0000-0002-5696-1586>

Об авторах

Авдонина Елена Дмитриевна, младший научный сотрудник, лаборатория молекулярной биотехнологии, ФГБУ «Национальный исследовательский центр эпидемиологии и микробиологии имени почетного академика Н.Ф. Гамалеи», Министерство здравоохранения Российской Федерации (123098, Россия, Москва, ул. Гамалеи, д. 18). E-mail: avdonina.yelena@mail.ru. <https://orcid.org/0000-0001-8059-9743>

Первойкина Кристина Алексеевна, младший научный сотрудник, лаборатория молекулярной биотехнологии, ФГБУ «Национальный исследовательский центр эпидемиологии и микробиологии имени почетного академика Н.Ф. Гамалеи», Министерство здравоохранения Российской Федерации (123098, Россия, Москва, ул. Гамалеи, д. 18). E-mail: uk-ru123@yandex.ru. Scopus Author ID 57698990900, <https://orcid.org/0000-0003-0780-5998>

Верховская Людмила Викторовна, к.б.н., ведущий научный сотрудник, лаборатория молекулярной биотехнологии, ФГБУ «Национальный исследовательский центр эпидемиологии и микробиологии имени почетного академика Н.Ф. Гамалеи», Министерство здравоохранения Российской Федерации (123098, Россия, Москва, ул. Гамалеи, д. 18). E-mail: verkhov@mail.ru. SPIN-код РИНЦ 5529-5909, <https://orcid.org/0000-0002-4731-1629>

Щербинин Дмитрий Николаевич, к.б.н., научный сотрудник, лаборатория молекулярной биотехнологии, ФГБУ «Национальный исследовательский центр эпидемиологии и микробиологии имени почетного академика Н.Ф. Гамалеи», Министерство здравоохранения Российской Федерации (123098, Россия, Москва, ул. Гамалеи, д. 18). E-mail: dim284@inbox.ru. Scopus Author ID 36599350900, ResearcherID E-7682-2014, SPIN-код РИНЦ 7743-6517, <https://orcid.org/0000-0002-8518-1669>

Вискова Наталья Юрьевна, научный сотрудник, лаборатория клеточной микробиологии, ФГБУ «Национальный исследовательский центр эпидемиологии и микробиологии имени почетного академика Н.Ф. Гамалеи», Министерство здравоохранения Российской Федерации (123098, Россия, Москва, ул. Гамалеи, д. 18). E-mail: apr2004@mail.ru. <https://orcid.org/0000-0002-6476-3520>

Кружкова Ирина Сергеевна, врач-инфекционист, ГБУЗ «Инфекционная клиническая больница № 1 Департамента здравоохранения г. Москвы» (125367, Россия, Москва, Волоколамское шоссе, д. 63); научный сотрудник, ФГБУ «Национальный исследовательский центр эпидемиологии и микробиологии имени почетного академика Н.Ф. Гамалеи», Министерство здравоохранения Российской Федерации (123098, Россия, Москва, ул. Гамалеи, д. 18). E-mail: irina-kru@yandex.ru. <http://orcid.org/0000-0002-1983-481X>

Ильина Мария Аркадьевна, заведующая Московским центром хронических инфекционных заболеваний, клещевых инфекций, медицины путешествий и вакцинопрофилактики, ГБУЗ «Инфекционная клиническая больница № 1 Департамента здравоохранения г. Москвы» (125367, Россия, Москва, Волоколамское шоссе, д. 63). E-mail: ilina_mar@list.ru. <http://orcid.org/0000-0003-4227-5363>

Кудрявцева Лариса Васильевна, заведующая лабораторно-диагностическим отделением, ГБУЗ «Инфекционная клиническая больница № 1 Департамента здравоохранения г. Москвы» (125367, Россия, Москва, Волоколамское шоссе, д. 63). E-mail: drkudriavtsevalv@yandex.ru. <http://orcid.org/0000-0001-7516-9490>

Колобухина Людмила Васильевна, д.м.н., профессор, руководитель лаборатории респираторных вирусных инфекций с апробацией лекарственных средств, ФГБУ «Национальный исследовательский центр эпидемиологии и микробиологии имени почетного академика Н.Ф. Гамалеи», Министерство здравоохранения Российской Федерации (123098, Россия, Москва, ул. Гамалеи, д. 18); врач-инфекционист, ГБУЗ «Инфекционная клиническая больница № 1 Департамента здравоохранения г. Москвы» (125367, Россия, Москва, Волоколамское шоссе, д. 63). E-mail: lkolobuchina@yandex.ru. Scopus Author ID 6601956811, <http://orcid.org/0000-0001-5775-3343>

Шмаров Максим Михайлович, д.б.н., заведующий лабораторией молекулярной биотехнологии, ФГБУ «Национальный исследовательский центр эпидемиологии и микробиологии имени почетного академика Н.Ф. Гамалеи», Министерство здравоохранения Российской Федерации (123098, Россия, Москва, ул. Гамалеи, д. 18). E-mail: ribozym@mail.ru. Scopus Author ID 6507322279, ResearcherID D-8662-2014, SPIN-код РИНЦ 4874-2578, <https://orcid.org/0000-0002-5268-1296>

Антипят Наталья Александровна, заместитель главного врача по медицинской части, ГБУЗ «Инфекционная клиническая больница № 1 Департамента здравоохранения г. Москвы» (125367, Россия, Москва, Волоколамское шоссе, д. 63). E-mail: natadoc70@bk.ru. Scopus Author ID 57207693166, <http://orcid.org/0000-0001-8578-2838>

Гинцбург Александр Леонидович, академик Российской академии наук, д.б.н., профессор, директор ФГБУ «Национальный исследовательский центр эпидемиологии и микробиологии имени почетного академика Н.Ф. Гамалеи», Министерство здравоохранения Российской Федерации (123098, Россия, Москва, ул. Гамалеи, д. 18); заведующий кафедрой инфектологии и вирусологии, ФГАОУ ВО Первый МГМУ им. И.М. Сеченова (Сеченовский университет), Министерство здравоохранения Российской Федерации (119048, Россия, Москва, ул. Трубецкая, д. 8, стр. 2). E-mail: gintzburg@gamaleya.org. Scopus Author ID 7005111491, SPIN-код РИНЦ 7626-0373, <https://orcid.org/0000-0003-1769-5059>

Тюрин Игорь Николаевич, главный врач, ГБУЗ «Инфекционная клиническая больница № 1 Департамента здравоохранения г. Москвы» (125367, Россия, Москва, Волоколамское шоссе, д. 63). E-mail: tyurin.dti@yandex.ru. Scopus Author ID 56895933300, <http://orcid.org/0000-0002-5696-1586>

Translated from Russian into English by H. Moshkov

Edited for English language and spelling by Thomas A. Beavitt

UDC 577.152.321; 620.3

<https://doi.org/10.32362/2410-6593-2025-20-2-119-136>

EDN LWMGXO



REVIEW ARTICLE

New nanostructured carriers for cellulase immobilization

Alexandrina M. Sulman✉, Vladimir P. Molchanov✉, Daria V. Balakshina, Olga V. Grebennikova,
Valentina G. Matveeva

Tver State Technical University, Tver, 170026 Russia

✉ Corresponding author, e-mail: A.M. Sulman, alexsulman@mail.ru; V.P. Molchanov, molchanov@science.tver.ru

Abstract

Objectives. Cellulase is a multienzyme complex that breaks down cellulose contained in plant cell walls. Cellulase consists of three types of enzymes: endoglucanase, exoglucanase, and β -glucosidase, each of which is involved in the destruction of certain chemical bonds in cellulose. Nanobiocatalysts based on cellulase immobilized on nanostructured carriers are used for catalytic hydrolysis of biomass waste, as well as in the food industry and for environmental protection. This article reviews scientific developments in the immobilization of cellulase on nanostructured carriers.

Methods. The article analyzes scientific papers published over the past five years that concerned the main aspects of immobilization of cellulase, an enzyme for processing cellulose biomass waste, on nanostructured carriers. The article examines methods of cellulase immobilization, the morphology of nanostructured carriers, and the factors affecting the enzyme activity and allowing one to achieve maximum conversion of cellulose-containing waste of plant origin.

Results. Nanostructured carriers have a large surface area, providing high immobilization efficiency, and also create a favorable environment for activating cellulase and increasing its stability. This allows one to create nanobiocatalysts for efficient conversion of cellulose substrate. The conducted analysis of the latest trends shows that positive changes have occurred in immobilization methods and carrier compositions over the past five years. The article describes such nanostructured carriers as graphene layers, polymer nanoparticles, nanohydrogels, nanofibers, silica nanoparticles, hierarchical porous materials, and magnetic nanoparticles.

Conclusions. Magnetically separable carriers increase the reliability of the biocatalyst and facilitate biocatalytic processes. The use of magnetic nanoparticles is especially advantageous due to their easy separation and the possibility of extracting the nanobiocatalyst for reuse.

Keywords

cellulase, immobilization methods, nanostructured carriers, processing of lignocellulosic biomass

Submitted: 24.10.2024

Revised: 17.12.2024

Accepted: 18.02.2025

For citation

Sulman A.M., Molchanov V.P., Balakshina D.V., Grebennikova O.V., Matveeva V.G. New nanostructured carriers for cellulase immobilization. *Tonk. Khim. Tekhnol. = Fine Chem. Technol.* 2025;20(2):119–136. <https://doi.org/10.32362/2410-6593-2025-20-2-119-136>

ОБЗОРНАЯ СТАТЬЯ

Новые наноструктурированные носители для иммобилизации целлюлаз

А.М. Сульман✉, В.П. Молчанов✉, Д.В. Балакшина, О.В. Гребенникова, В.Г. Матвеева

Тверской государственной технической университет, Тверь, 170026 Россия

✉ Автор для переписки, e-mail: А.М. Сульман, alexsulman@mail.ru; В.П. Молчанов, molchanov@science.tver.ru

Аннотация

Цели. Целлюлаза — мультиферментный комплекс, расщепляющий целлюлозу, содержащуюся в клеточных стенках растений. В состав целлюлазы входят ферменты трех видов: эндоглюканазы, экзоглюканазы и β -глюкозидазы, каждый из которых участвует в процессах разрушения определенных химических связей в целлюлозе. Нанобиокатализаторы на основе целлюлазы, иммобилизованной на наноструктурированных носителях, используются для каталитического гидролиза отходов биомассы, а также в пищевой промышленности и для защиты окружающей среды. Цель настоящего исследования — представить обзор научных разработок по иммобилизации целлюлазы на наноструктурированных носителях.

Методы. Проанализированы опубликованные за последние пять лет научные работы, касающиеся основных аспектов иммобилизации целлюлазы — фермента для переработки отходов целлюлозной биомассы — на наноструктурированных носителях. Рассмотрены методы иммобилизации целлюлазы, морфология наноструктурированных носителей, а также факторы, влияющие на активность ферментов и позволяющие достичь максимальной конверсии целлюлозосодержащих отходов растительного происхождения.

Результаты. Наноструктурированные носители обладают большой площадью поверхности, обеспечивая высокую эффективность иммобилизации, а также создают благоприятную среду для активизации целлюлазы и увеличения ее стабильности. Это позволяет создавать нанобиокатализаторы для эффективного превращения целлюлозного субстрата. Проведенный анализ последних тенденций показывает, что за последние пять лет в методах иммобилизации и составах носителей произошли положительные изменения. Описаны такие наноструктурированные носители, как слои графена, полимерные наночастицы, наногидрогели, нановолокна, кремнеземные наночастицы, иерархические пористые материалы и магнитные наночастицы.

Выводы. Магниторазделяемые носители повышают надежность биокатализатора и облегчают биокаталитические процессы. Использование магнитных наночастиц особенно выгодно ввиду их легкого отделения и возможности извлечения нанобиокатализатора для повторного использования.

Ключевые слова

целлюлаза, методы иммобилизации, наноструктурированные носители, переработка лигноцеллюлозной биомассы

Поступила: 24.10.2024

Доработана: 17.12.2024

Принята в печать: 18.02.2025

Для цитирования

Сульман А.М., Молчанов В.П., Балакшина Д.В., Гребенникова О.В., Матвеева В.Г. Новые наноструктурированные носители для иммобилизации целлюлаз. *Тонкие химические технологии*. 2025;20(2):119–136. <https://doi.org/10.32362/2410-6593-2025-20-2-119-136>

1. INTRODUCTION

The scarcity of conventional fuels and trend toward their gradual abandonment due to environmental concerns necessitate the development of processes for processing plant waste into biofuels. Current technologies for processing lignocellulosic biomass into biofuels include many stages, of which the decomposition of cellulose to fermentable sugars (providing a substrate for bioethanol production) is the most important [1]. To ensure environmental safety in the processing of lignocellulosic biomass, biocatalytic processes involving enzymes that decompose cellulose to glucose are widely used [2–5]. However, the industrial use of such enzymes is limited by

their low thermal stability, the presence of a wide range of impurities in enzymatic preparations, and the difficulty of separating enzymes from processing products, as well as the impossibility of their reuse. These disadvantages can be minimized or completely eliminated by immobilizing enzymes on various carriers. Such carriers preserve the secondary and tertiary structure of the enzyme to create favorable conditions for its interaction with the substrate. The optimal carrier can be selected based on the enzyme type and the features of the technological process [6, 7].

The attention of researchers is particularly drawn to the processes of enzyme immobilization on nanostructured carriers to form nanobiocatalysts [8–13]. Nanostructured carriers are materials containing nanometer-sized

elements (usually from 1 to 100 nm), including nanoparticles (NPs) of various shapes, nanorods, and nanofibers. Unlike conventional granular carriers, nanostructured materials minimize diffusion limitations of substrate mass transfer. In addition, their developed surface area favors the effective immobilization of enzymes to improve their location on the surface, which increases enzymatic activity [14, 15].

The present study reviews scientific developments in the immobilization of cellulase on nanostructured carriers. Cellulase is a multienzyme complex that breaks down cellulose contained in plant cell walls. Cellulase consists of three types of enzymes: endoglucanases, exoglucanases, and β -glucosidases, each of which is involved in the destruction of certain chemical bonds in cellulose [10, 16].

Lignocellulosic biomass contains polysaccharides (cellulose and hemicellulose), as well as the aromatic polymer lignin, the presence of which suppresses cellulose hydrolysis. Immobilization of cellulase on nanostructured carriers not only stabilizes the biocatalyst and makes it possible to reuse it, but also changes the surface charge of the enzyme, reducing its nonspecific binding to lignin and increasing its affinity for cellulose [17, 18]. In order to use cellulase to effectively hydrolyze cellulose [19], lignocellulosic biomass wastes generally require delignification using laccase from *Trichoderma asperellum* (another enzymatic catalyst) or by co-immobilizing several enzymes on a single carrier [20–22].

This review discusses publications of the last five years that study cellulase immobilized on nanostructured carriers. Particular attention is paid to cellulase immobilization methods, as well as to the types of nanostructured carriers, including magnetically separable ones. The advantages of using immobilized cellulase are described based on the analysis of biocatalytic processes for processing cellulose-containing biomass to obtain sugars.

2. CELLULASE IMMOBILIZATION METHODS

Known methods of immobilization of cellulase on nanostructured carriers include adsorption, encapsulation, entrapment in a polymer matrix, covalent attachment, and cross-linking [23]. The most common method is covalent binding by the formation of chemical bonds between functional groups in the cellulase molecule and reactive groups on the carrier surface. Due to its strong covalent bonds, the immobilized

cellulase is highly stable and reusable while maintaining a sufficiently high activity. This immobilization method is necessary in industries where the stability of cellulase and the possibility of its reuse are especially important. At the same time, in industries where simplicity and cost-effectiveness are of primary importance—e.g., in small-scale agriculture or the food industry—preference is often given to physical adsorption, cross-linking, or entrapment methods [24]. Ultimately, the choice of cellulase immobilization method should be guided by specific application requirements and a reasonable balance between performance, stability, and cost.

2.1. Adsorption

The physical adsorption method has been used to immobilize cellulase on metal–organic frameworks (MOFs) [25, 26], composites based on iron oxide and acid-activated montmorillonites [27], as well as multiwalled carbon nanotubes (MWCNTs) [28]. Important adsorption factors are high surface area, a suitable carrier pore size, and opposite net charges of the enzyme and the carrier [29].

Costantini *et al.* [30] showed that, while pretreatment of lignocellulosic biomass with ionic liquids can be used to facilitate its hydrolysis, such ionic liquids may lead to the enzyme's destruction. Zhou *et al.* [25] studied the resistance of nanobiocatalysts based on several MOFs (with different metals) and physically adsorbed cellulase to ionic liquids. Zhou *et al.* [26] also found that the most effective way to protect immobilized cellulase from the negative effect of ionic liquids on enzymatic activity or to reduce desorption is to modify the carrier surface before adsorption. Enzyme desorption can be reduced by surface treatment with zeolitic imidazolate frameworks (ZIF-8, i.e., MOFs that consist of Zn^{2+} and 2-methylimidazole ligands), charge-changing compounds (e.g., chitosan), or hydrophobicity-changing macromolecules (such as polyethylene glycol) (Fig. 1).

Modification of Zr-containing MOF UiO-66¹ with amino groups increases the enzyme content on the carrier (from 220 to 350 mg/g) due to the formation of additional “anchors” (NH_2 groups) on the carrier surface [31].

Some studies demonstrated the possibility of modifying the biocatalyst following enzyme adsorption. Adsorption of cellulase on carbon nanotubes followed by treatment with sodium alginate provides increased stability of the biocatalyst [28]. In this case, the gradual decrease in activity with each reaction cycle (following seven cycles of repeated hydrolysis of carboxymethyl cellulose, the activity of immobilized cellulase remains

¹ UiO is University of Oslo (Norwegian—Universitetet i Oslo).

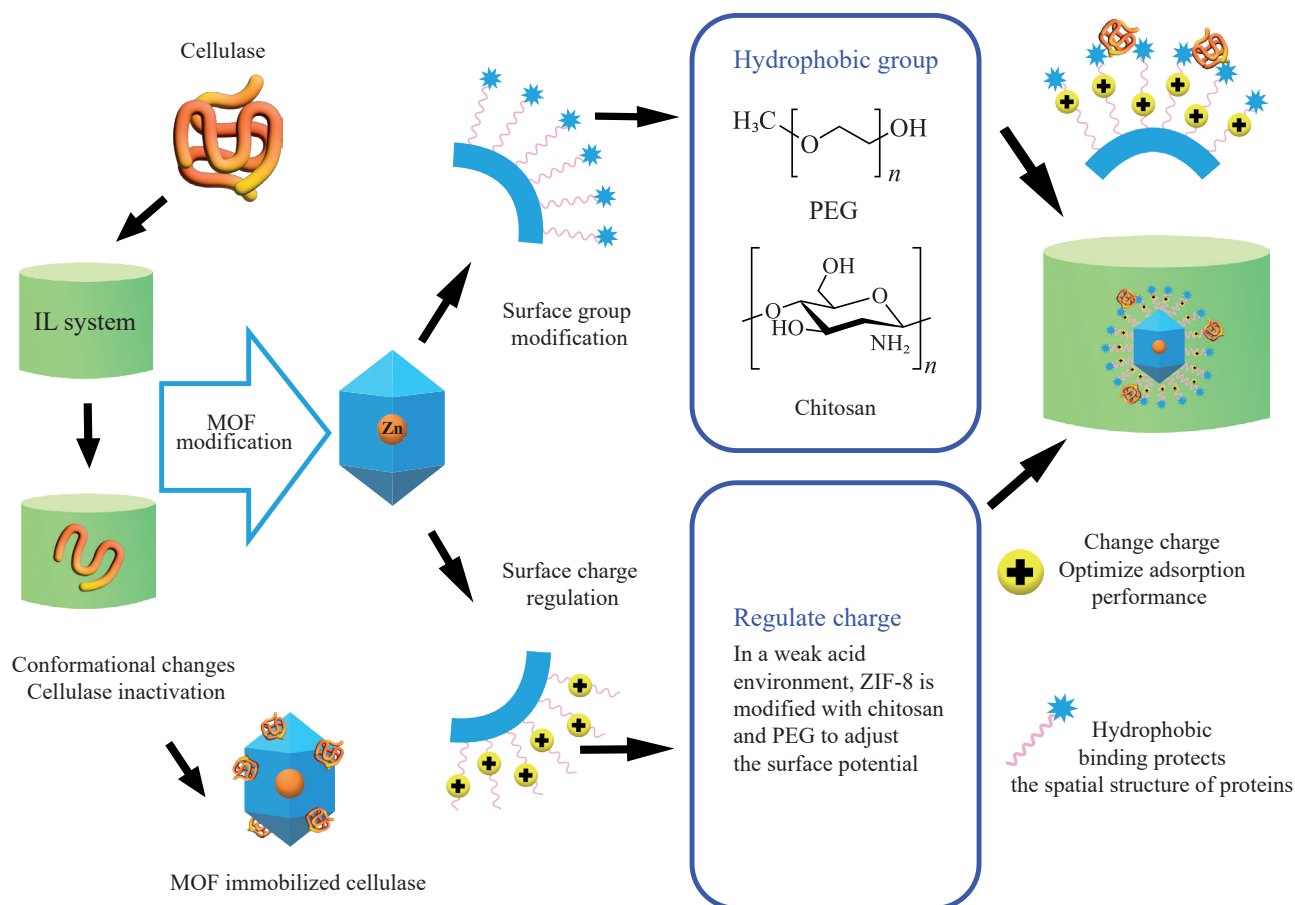


Fig. 1. Functional modification of ZIF-8 (modification of surface groups/regulation of surface charge) and its effect on immobilized cellulase (protection of the spatial structure of the enzyme) [26]. PEG is polyethylene glycol; IL system is ionic liquid system; MOF are metal-organic frameworks

at the level of 71.5%) is caused by weak noncovalent interactions between cellulase and the carrier (MWCNTs). After 30-day storage of immobilized and soluble cellulase, the enzyme activity remains at the level of 71.2 and 56.8% of the initial activity, respectively. Thus, the slightly increased stability of cellulase during storage following immobilization is considered an important condition for its industrial application. An original method of cellulase immobilization was proposed by Zhu and colleagues. After adsorbing the enzyme on $\text{Fe}_3\text{O}_4+\text{C}$ NPs by means of electrostatic interactions, they coated these NPs with a thin layer of precipitated silica, which enhanced the adsorption of cellulase (the enzyme content on the carrier reached 200 mg/g) at the same time as preserving its enzymatic functions [32].

In order to obtain effective biocatalysts by adsorption of cellulase, carriers may be modified or functionalized. In the case of modification after adsorption, the applied outer layer should be sufficiently porous or swollen to ensure contact of cellulase with the cellulose substrate. Potential disadvantages of the adsorption method are

a relatively low immobilization efficiency and the possibility of enzyme desorption during the reaction, leading to contamination of the final product.

2.2. Entrapment/encapsulation

Entrapment represents an irreversible immobilization method in which cellulase is retained in a porous matrix or polymer network without forming direct bonds with the carrier material. According to this approach, only the molecules of substrates and products are allowed to move in the pores, while the enzyme is prevented from leaching out of the biocatalyst. Therefore, a suitable pore size is critical for the selection of the carrier. Entrapment can enhance enzyme stability, reduce enzyme leaching, and protect the enzyme from adverse effects of the reaction environment, thus preventing cellulase deactivation. In contrast to entrapment, encapsulation separates the enzyme from the reaction environment by means of a permeable and porous organic/inorganic polymer. The creation of a microenvironment by encapsulation protects the enzyme molecules from adverse conditions that are

commonly observed in lignocellulosic hydrolysates due to inhibitory agents [23, 24, 33].

Wu *et al.* [34] immobilized several enzymes including cellulase using Zr-containing MOFs UiO-66 with different mesopores (6.46, 7.55, and 10.80 nm). By using UiO-66 with a pore size of 6.46 nm, the maximum enzyme adsorption for cellulase of 203.9 mg/g was achieved without damaging the enzyme structure. According to the authors, significantly increased stability of the immobilized enzyme cellulase+UiO-66 was achieved due to the optimal ratio of the pore size of the carrier material and the size of the enzyme molecule. Since the cellulase molecule has a prolate ellipsoidal shape with a diameter (minor axis) of 4–6.5 nm and a length (major axis) of 18–21.5 nm,² pores of the corresponding sizes provide more effective immobilization. Wu *et al.* [35] also showed cellulase could be firmly retained on the carrier by the addition of 4.6-nm mesopores to microporous UiO-66 to increase the stability of the immobilized cellulase. In particular, the results showed that the UiO-66 carrier provided high cellulase immobilization efficiency (265 mg/g) at a residual enzymatic activity of about 83% after six cycles. Analysis of the Michaelis–Menten equation showed that the Michaelis constant (13.355 mg/mL) and maximum reaction rate (1.311 mg/(mL·min)) of the immobilized cellulase were higher than those of the soluble enzyme (14.525 mg/mL and 0.732 mg/(mL·min), respectively).

Mesoporous Zn-based MOFs were also used for encapsulation of cellulase by coprecipitation of the enzyme and MOF precursors [36]. This increased the immobilized enzyme content to 350 mg/g to improve mass transfer due to the formation of structural defects during the formation of large pores in the MOF. The encapsulated cellulase retained 77% of the initial activity after four cycles.

Self-assembly of chitosan around cellulase by salting out from a mixed solution [30] led to the formation of a nanohybrid, which was deposited on alginate beads. The resulting nanobiocatalyst demonstrated increased stability and efficiency in the hydrolysis of sugarcane bagasse. The Michaelis constant increased by 3% for the immobilized nanohybrid compared to native cellulase (11.9 and 11.5 mg/mL, respectively). This could be due to the alginate matrix forming a barrier to limit the enzyme affinity for the substrate. The maximum rate for the immobilized nanohybrid was reduced compared to soluble cellulase (1.1 and 1.2 mM/min, respectively) due to the concentration gradient created by the nanohybrid within the alginate beads, which decreased the hydrolysis rate. The slight decrease in the maximum rate for the

immobilized nanohybrid indicated the possibility for carboxymethyl cellulose to diffuse into the alginate beads due to its water solubility.

Thus, the most important advantage of enzyme immobilization by entrapment/encapsulation is its high robustness, although drawbacks such as co-adsorption and loss of structural integrity may limit its attractiveness. Furthermore, as in physical adsorption, the cellulase entrapment/encapsulation method is effective only if the enzyme is easily accessible within the nanomaterial.

2.3. Covalent attachment

Although covalent attachment is often preferred due to its provision of increased enzyme stability, it requires functionalization of carriers that do not initially contain functional groups [37, 38]. In addition, a suitable coupling agent is needed to maintain the enzyme conformation. The most commonly used bifunctional coupling agent is glutaraldehyde, which does not require the presence of any catalyst due to its interaction with the amino groups of the side amino acid residues and the NH₂ groups of the carrier [39]. Despite the short length of the glutaraldehyde molecule (0.75 nm) [40], this is sufficient to prevent nonspecific adsorption of the enzyme. Although longer-molecular-length coupling agents such as tetradecanedioic and docosandioic dicarboxylic acids with approximate chain lengths of 1.4 and 2.2 nm, respectively, have also been investigated, the interaction of the terminal carboxyl groups with the amino-functionalized carriers (to form a peptide bond) requires elevated temperatures and/or the presence of a catalyst [41, 42]. In the case of carriers such as graphene oxide with carboxyl groups on the surface, the coupling agents (dicarboxylic acids) are first activated by carbodiimide followed by reaction with *N*-hydroxysuccinimide to create a functional group for enzyme attachment [43].

Cellulase covalently immobilized using glutaraldehyde on amino-functionalized magnetic Fe₃O₄ nanoparticles (MNPs) coated with silica (Fe₃O₄+SiO₂) showed an activity of 3341 EA/g in the hydrolysis of carboxymethyl cellulose, which was 83.5% of the activity of the native enzyme [44]. The Michaelis constants and the maximum reaction rates for the immobilized and soluble cellulase were 0.0125 and 0.015 mg/mL, and 5.0 and 0.833 mmol/min, respectively, indicating a slight decrease in the affinity for the substrate and catalytic efficiency of the immobilized cellulase. A study of the stability of the immobilized enzyme in five repeated cycles demonstrated the retention of 44% of the

² Worldwide Protein Data Bank, <https://www.rcsb.org/#Category-analyze>. Accessed February 17, 2025.

initial activity. When using immobilized cellulase for the enzymatic saccharification of pretreated poplar wood [44], the maximum conversion of enzymatic saccharification (at 50°C and pH 4.5) was 38.4% over 72 h.

Targeted functionalization of the carrier may be critical for efficient covalent attachment of the enzyme. Gao *et al.* [45] prepared graphene oxide as a carrier for immobilization of cellulase by covalent binding. Graphene oxide was activated by esterification with 2-[(4-aminophenyl)sulfonyl]ethyl hydrogen sulfate (SESA) as a hydrophobic spacer. After modifying the resulting complex by diazotizing the acid, it was possible to covalently immobilize cellulase on it. Compared with soluble cellulase, the thermal and operational stability of the immobilized cellulase was significantly improved. At 50°C, the half-life of immobilized cellulase (533 min) was six times higher than that of soluble cellulase (89 min). In addition, the affinity between immobilized cellulase and the substrate (2.19 g/L) was more favorable than that of soluble cellulase (3.84 g/L). This suggests that immobilized cellulase has a higher catalytic efficiency. Here, it should be noted that the reliability of covalent attachment of cellulase is hampered by the complex

functionalization procedure, which significantly reduces the attractiveness of this method.

Covalently immobilized and catalytically active enzymes on microgel particles can be obtained using reactive groups of amino acid residues (e.g., amino groups from lysine residues, thiol groups from cysteine residues, and carboxylic groups from aspartic or glutamic acids) and reactive groups in microgels (e.g., epoxides, and *N*-hydroxysuccinimide and maleimide esters). The main problem of immobilization is the presence of identical reactive groups in the target enzyme (e.g., several solvent-accessible lysine residues on the surface of cellulase). In this case, multipoint immobilization may occur to reduce the flexibility of the enzyme structure and potentially reduce its catalytic activity. Zou *et al.* [46] proposed a strategy for oriented single-point site-specific covalent immobilization of the enzyme in a microgel. They considered doping with sortase (transpeptidase) as a highly selective tool for conjugation of peptides or proteins [47]. *Staphylococcus aureus* sortase A recognizes the amino acid sequence LPETG in the protein to form a reactive thioether intermediate sortase A–protein (Fig. 2a), which

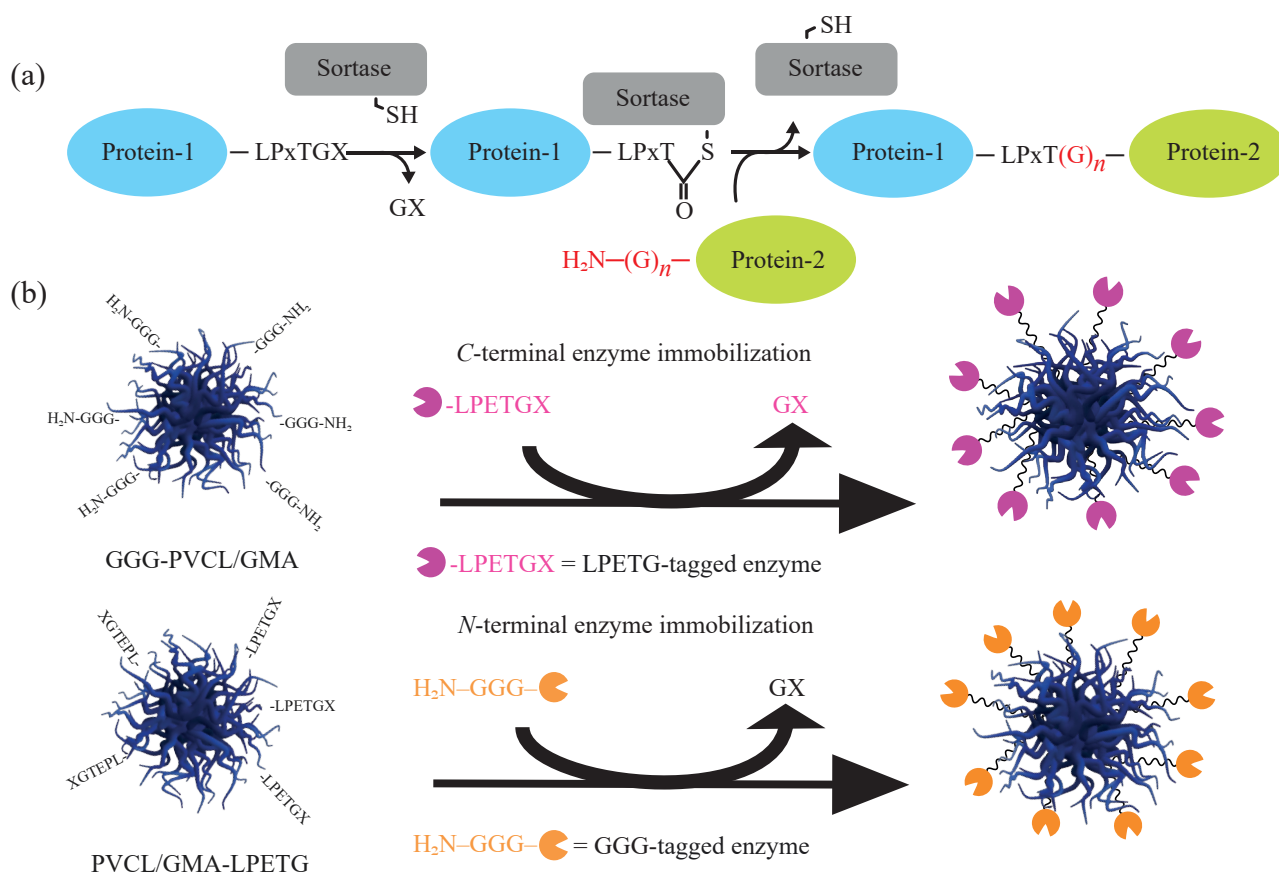


Fig. 2. (a) Sortase-catalyzed protein–protein conjugation using LPETG-labeled and GGG-labeled proteins as substrates. (b) Both conjugation variants (*N*- and *C*-terminal) are shown to confirm the effectiveness of a microgel-based carrier for enzyme immobilization: *C*-terminal immobilization (top); *N*-terminal immobilization (bottom) [46]

is subsequently cleaved by a nucleophile (e.g., the amino group of the *N*-terminal oligoglycine tag in another protein). As a result, a stable amide bond is formed and sortase A is released [46]. In that work, Zou *et al.* improved the principle of peptide synthesis in catalytic microgels to create a universal platform for enzyme immobilization on poly(*N*-vinylcaprolactam)/glycidyl methacrylate (PVCL/GMA) microgels.

To ensure the possibility of enzyme conjugation using both options (*N*- or *C*-terminal immobilization), two immobilization approaches are used. *C*-terminal enzymes labeled with LPETG are immobilized by coupling to H₂N–GGG–PVCL/GMA, whereas *N*-terminal enzymes labeled with GGG are doped with PVCL/GMA–LPETG–COOH microgels (Fig. 2b). For testing covalent immobilization, biotechnologically significant enzymes were selected, including cellulase A2M2 (*N*-terminal enzyme).

According to the presented examples, a possible disadvantage of covalent attachment of cellulase may be the complexity of chemical modification of the carrier and/or enzyme.

2.4. Cross-linking

Cross-linking of enzymes into aggregates (CLEA) permits their immobilization without the use of carriers. Such cross-linking can be achieved by interaction with

glutaraldehyde [48]. However, the activity of cross-linked enzyme aggregates was found to depend on the type of cross-linking agent, which can affect the density of CLEA [49].

If precipitated cross-linked aggregates of cellulases are combined with MNPs, an additional advantage consists in the increased ease of manipulation of the magnetic nanobiocatalyst [50].

An original method for obtaining multienzyme hybrid nanoflowers (ECG-NFs) was implemented by Khan *et al.* [51] by cross-linking three enzymes of the cellulase complex: cellobiohydrolase (CBH), endoglucanase (EG), and β -glucosidase (BG). Cross-linking was performed using the recombinant enzymes EG–Linker–ELP (elastin-like polypeptide)–His₆ (EGLEH), CBH–Linker–ELP–His₆ (CBHLEH), and Glu–Linker–ELP–His₆ (GLEH). Figure 3 presents the processes of cross-linking of the enzymes and their catalyzed reaction of cellulose hydrolysis to glucose. The formation of hybrid nanoflowers is assumed to generally occur in two main stages [52]. In the first stage (“nucleation”), GLEH, CBHLEH, and EGLEH bind to Cu²⁺ to form a complex compound involving the appearance of copper phosphate crystals. In the second stage (“growth”), the amino groups of GLEH, CBHLEH, and EGLEH combine with Cu²⁺ by the coordination reaction of protein ions and Cu²⁺ to form nanocrystals, which can provide binding sites for GLEH, CBHLEH,

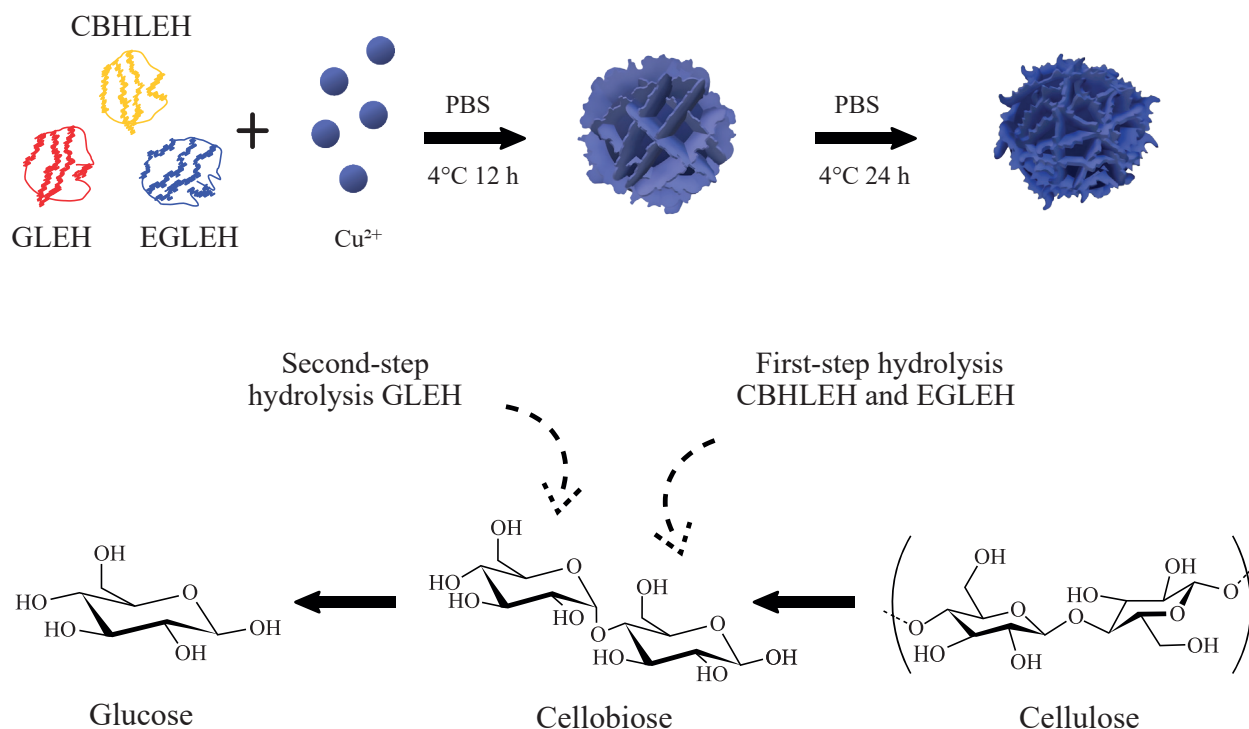


Fig. 3. Diagram of the ECG-NF formation and the functional cellulase action mechanisms. PBS is polybutylene succinate [51]

and EGLN during the growth process. The continuous growth of NPs leads to the formation of mature nanoaggregates. In this case, the spatial structure of enzyme aggregates is the key to successful catalysis. The constructed system of multienzyme hybrid nanoflowers was used for a one-pot cascade conversion of cellulose to glucose. Compared with the native multienzyme system, the ECG-NFs nanoflowers demonstrated better physical stability, thermal stability, and storage stability. Moreover, the enzymatic activity of ECG-NFs was retained at 61.59% after eight repeated reaction cycles. The kinetic constants of the immobilized and native enzymes (Michaelis constants 9.33 and 9.54 g/L, respectively; maximum reaction rate, 0.0056 and 0.0048 g/(L·min), respectively) also indicate increased cellulase affinity and activity following co-immobilization. The total enzymatic activity of ECG-NFs increased by a factor of 1.12 compared to the native enzyme in the process of converting microcrystalline cellulose into glucose. Thus, it is expected that the effect of co-immobilization of several enzymes will be successfully used in industrial production conditions.

A potential drawback of this immobilization method is a decrease in activity due to limited access to the active site if the cross-linked aggregates are too dense.

3. TYPES OF NANOSTRUCTURED CARRIERS

The main nanostructured carriers used for cellulase immobilization are nanoporous materials (MOF, biochars, porous silica), nanohydrogels, and polymeric NPs and MNPs [10]. Most of these carriers have been used for enzyme immobilization for many years, but over the past five years, significant technological changes have occurred in the production or modification of these nanomaterials to increase the efficiency of immobilization processes and improve the characteristics of nanobiocatalysts created on their basis.

3.1. Nanosized porous materials

Pota *et al.* [53] proposed the co-immobilization of β -glucosidase and cellulase by adsorption on folded mesoporous silica NPs with a hierarchical structure of open pores having a smaller (wrinkled silica NPs, WSN) and larger (WSN synthesized by using pentanol, WSN-p) distance between the folds. The results showed that the best biocatalyst is the one obtained by co-immobilization of β -glucosidase and cellulase at the WSN-p distance. In this case, the fraction of adsorbed enzymes reaches 20%, which corresponds to their content at the level of 100 mg/g of the carrier. During testing in the reaction of hydrolysis of cellulose extracted from the leaves of

loquat *Eriobotrya japonica*, the biocatalyst demonstrated a conversion of 82% and an activity of 72 $\mu\text{mol}/(\text{min}\cdot\text{g})$. The biocatalyst retained 83% of its initial activity after nine cycles of repeated use. In addition, it had better stability over a wide temperature range than the mixture of soluble enzymes, retaining 72% of the maximum conversion value at temperatures up to 90°C.

Chen *et al.* [54] compared mesoporous silicas (MS) with average pore sizes of 17.6 and 3.8 nm (MS-17.6 and MS-3.8, respectively) and determined that larger pores, the sizes of which are similar to the major axis of the cellulase molecule, provide higher immobilization efficiency: the adsorption value was 410 mg/g for MS-17.6 and 315 mg/g for MS-3.8. On the other hand, the pores of the carrier with a diameter of 3.8 nm, close to the size of the minor axis of the cellulase molecule, provide higher activity (up to 67% of the activity of the native enzyme at 60°C) compared to cellulase on MS-17.6, which after immobilization retained only 26.6% of the activity of the native enzyme under the same conditions. Chen *et al.* [54] assumed that, in the case when the average pore size of the carrier is similar to the minor axes of the enzyme molecules, the immobilized cellulase retains active sites and demonstrates the highest activity. And in the case of the MS-17.6 carrier, the enzyme molecules penetrate into the pores, creating a dense and ordered structure, which probably hinders the conformational flexibility of cellulase necessary for the interaction between cellulase and the substrate.

3.2. Nanogels

Zarei *et al.* [55] proposed a simple two-stage approach to the fabrication of a conductive nanohydrogel composed of poly- ϵ -caprolactone and the cationic macromolecule of phosphine oxide. For this purpose, a cationic nanohydrogel was synthesized by electrospinning in the form of fibers with a diameter of about 469 nm, followed by *in situ* polymerization of polyaniline nanorods. The resulting nanohydrogel was used to immobilize cellulase, the activity of which was studied in the reaction of carboxymethyl cellulose hydrolysis. High immobilization efficiency (96%) was observed after optimization of such parameters as pH, temperature, processing time, and enzyme concentration in the mixture. The immobilized enzyme retained almost 90% of its initial activity after four weeks of storage and 73% of the initial activity after nine cycles of repeated use. The kinetic parameters (Michaelis constant and maximum reaction rate) showed values of 2.9 g/L and 7.6 g/(L·min) for immobilized cellulase and 1.5 g/L and 6.8 g/(L·min) for the native enzyme, respectively. The increase in the Michaelis constant after immobilization indicates that the reaction reaches its maximum catalytic efficiency

at slightly higher substrate concentrations. This may be due to limited substrate access to the active site of the enzyme and/or changes in the enzyme conformation and a decrease in the possibility of enzyme–substrate complex formation. The increase in the maximum reaction rate for immobilized cellulase compared to the native enzyme may be due to increased enzyme stability after immobilization.

Ariaeenejad *et al.* [56] created efficient nanohydrogel–enzyme systems with excellent stability and activity for practical use of cellulase in the hydrolysis of lignocellulosic biomass, and presented a strategy for the synthesis of new three-dimensional hydrogels from carboxymethyl cellulose copolymers of 2-acrylamido-2-methylpropane sulfonate and acrylamide. Graphene oxide nanosheets were used as a filling and cross-linking agent creating hydrogen bonds between polymer chains to obtain three-dimensional networks. The effect of graphene oxide content on the efficiency of the synthesized structures during conjugation with a model enzyme, cellulase, was studied. Immobilization of cellulase in graphene oxide–reinforced hydrogels resulted in a noticeable retention (at the level of 60%) of its maximum activity at a temperature of 90°C, as well as a significant increase in its specific activity and stability during storage. Compared with soluble cellulase, the immobilized enzyme containing graphene oxide hydrogels showed a noticeable (154.8%) increase in the conversion of alkali-treated sugar beet pulp, while the original cellulase hydrogel showed only a 66.7% increase under the same conditions.

Hedaiatnia *et al.* [22] obtained an efficient immobilized bifunctional enzymatic complex cellulase/xylanase on a hydrogel carrier with increased stability and activity, which was subsequently used for the hydrolysis of lignocellulosic biomass. The initial hydrogel (SA–CH) was synthesized by radical polymerization of chitosan (CH) and sodium alginate (SA) solutions in the presence of a cross-linking agent and acrylic monomers. The hydrogel nanocarrier (SA–CH/NCs) was synthesized by adding nanocellulose (NCs) to SA–CH. The activity and stability of native cellulase and xylanase and immobilized bienzyme complexes (PersiCelXyn1+SA–CH and PersiCelXyn1+SA–CH/NCs) were investigated in the hydrolysis of sugar beet pulp to produce a hydrolysate containing fermentable sugar and serving as a substrate for lactic acid production. The Michaelis constant values for native enzymes and the PersiCelXyn1+SA–CH and PersiCelXyn1+SA–CH/NCs complexes were found to be 2.84, 0.89, and 0.58 mg/mL, respectively. Different values demonstrated different affinities of the enzymes for the substrate. During the immobilization process, the enzyme conformation may change, and various

diffusion effects and steric hindrances may alter the enzyme microenvironment, which affects its affinity for the substrate after immobilization. The decrease in the Michaelis constant for the immobilized enzymes compared to their soluble form indicates an increase in the affinity for the substrate after immobilization. This decrease was more pronounced in the case of the PersiCelXyn1+SA–CH/NCs hydrogel compared to PersiCelXyn1+SA–CH. It is possible that the presence of nanocellulose in the matrix of this hydrogel caused a more intense interaction of the substrate with the enzyme, which in turn led to an increase in the affinity of the enzyme for its substrate. The maximum reaction rates for PersiCelXyn1+SA–CH and PersiCelXyn1+SA–CH/NCs were 74.19 and 103.79 $\mu\text{mol}/(\text{mg}\cdot\text{min})$, respectively, while for the native form this value was 58.70 $\mu\text{mol}/(\text{mg}\cdot\text{min})$. Since the maximum reaction rate parameter represents the rate of enzymatic reaction at saturating substrate concentrations, its higher values for immobilized enzymes indicate that, when saturated with the substrate, they ensure a higher reaction rate than the soluble enzyme. Thus, the addition of NCs to the hydrogel network allowed one to obtain a modified hybrid nanocarrier for immobilizing bienzyme complexes with an increased specific activity compared to the original hydrogel and, ultimately, to increase the catalytic activity of the immobilized enzyme.

3.3. Polymeric particles

Polymeric NPs can be useful for surface covalent attachment of enzymes if the polymer structure contains the necessary functional groups. Wang *et al.* [57] obtained polymeric NPs from a cross-linked copolymer of styrene and maleic anhydride by precipitation polymerization without a stabilizer, followed by covalent attachment of cellulase through anhydride groups.

Self-assembling micelles of the poly(styrene)-*b*-poly(styrene-*alt*-maleic anhydride) polymer modified with nitrilotriacetic acid (NTA), the further modification of which with Ni^{2+} ions made it possible to attach bacterial His₆-cellulase, were successfully used by Lu *et al.* [58] to obtain core–shell NPs with cellulase molecules in the outer layer (Fig. 4).

Lu *et al.* [58] showed that cellulase immobilized on polymer NPs after incubation for 24 h produced approximately twice as much reducing sugar (50 mg/L) as the soluble enzyme (30 mg/L). The stability of the immobilized cellulase was also tested, and it was found that, after two-week storage at 48°C or storage for 48 h at room temperature, the activity of the immobilized cellulase did not undergo significant changes. Lu *et al.* explained the activity and stability of the immobilized enzyme by the specific orientation of proteins on the surface of the

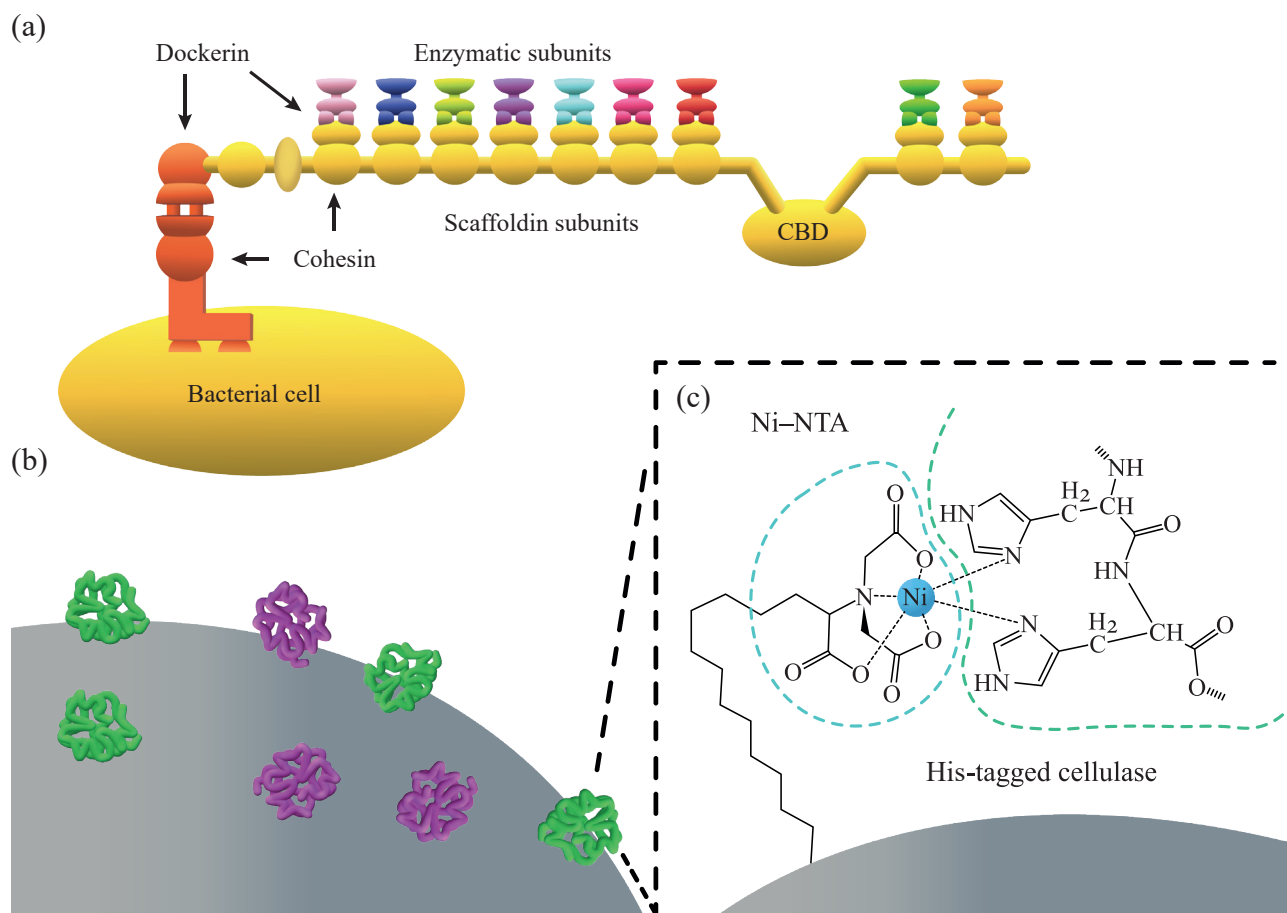


Fig. 4. (a) Structural organization of the cellulosome in *Clostridium thermocellum* cells, (b) functionalized Ni-NTA micelles for cellulase immobilization, and (c) the interaction of Ni-NTA with cellulase molecules tagged with His₆ [58]

NPs and in the active sites, as well as by the more effective action of the immobilized enzyme on the substrate.

3.4. Magnetic nanostructured carriers

Magnetically responsive nanostructured carriers are usually based on MNPs. The use of MNPs for the development of nanobiocatalysts has rapidly increased in recent years due to the simplicity of magnetic separation, which allows for the repeated use of nanobiocatalysts and makes the processes involving them more reliable, as well as economically and environmentally beneficial. MNPs (most often, iron oxide NPs) are usually prefunctionalized to ensure the possibility of enzyme attachment. For this purpose, MNPs are coated either with silicon dioxide followed by the addition of functional amino groups [44, 59–68] or with polymers containing reactive groups (e.g., chitosan or other functional polymers) [69–75]. The addition of metal ions (e.g., copper) to amino-functionalized MNPs improves the immobilization of cellulase due to its affinity for the metal [76]. Under optimal

operating conditions (Cu/MNP ratio = 1, cellulase/MNP ratio = 0.11, pH 6), the relative activity and content of immobilized enzyme on MNPs were 91% and 164 mg/g, respectively. Abbaszadeh and Hejazi showed [76] that immobilized cellulase tested in the hydrolysis reaction of carboxymethyl cellulose taken at a concentration of 1% exhibits greater stability than the soluble enzyme. In addition, the immobilized enzyme retained 73% of its initial activity after five cycles of use.

For better protection of iron oxide MNPs, Poorakbar *et al.* [77] first formed a gold shell around the MNPs and then a silica shell, followed by functionalization with polyethylene glycol and L-aspartic acid for covalent attachment of cellulase (Fig. 5). Covalent binding of the enzyme was confirmed by Fourier transform infrared spectroscopy. The binding efficiency was 84% as determined by the Bradford method. During filter paper hydrolysis, the immobilized cellulase showed 88% of the activity of the native enzyme and retained 73% of its initial catalytic activity after 9 h (with an activity of 0.78 mmol/mL) [77].

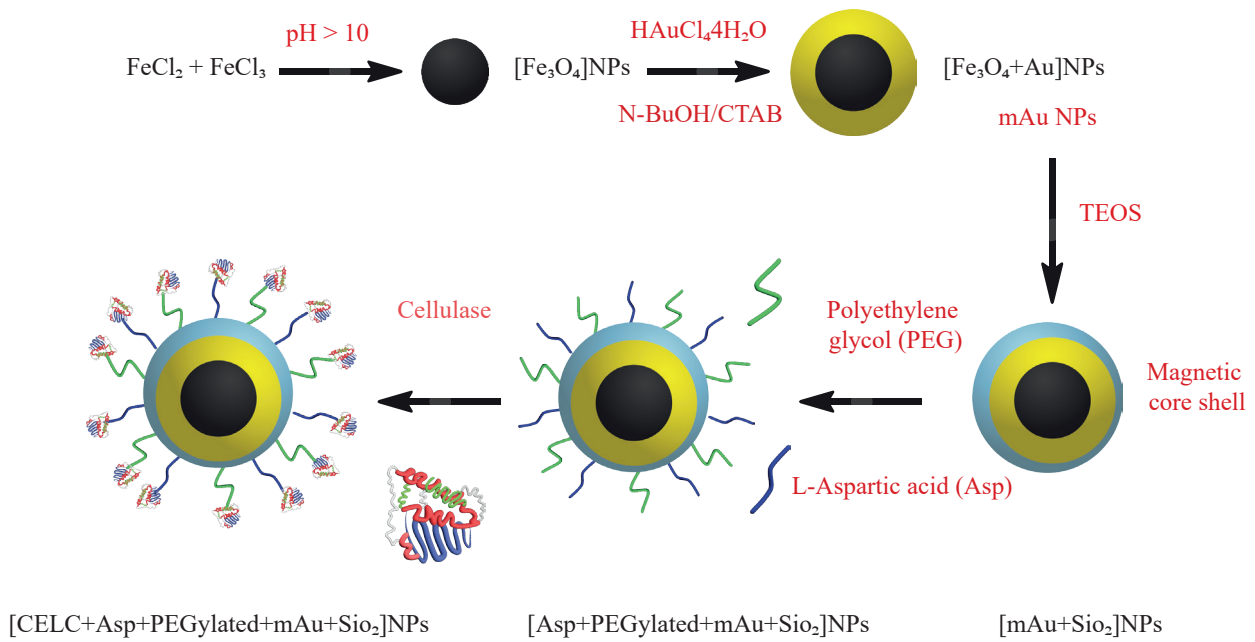


Fig. 5. Synthesis of core-shell gold MNP as a new nanocarrier and the immobilization of cellulase on it to obtain biocatalysts [77]

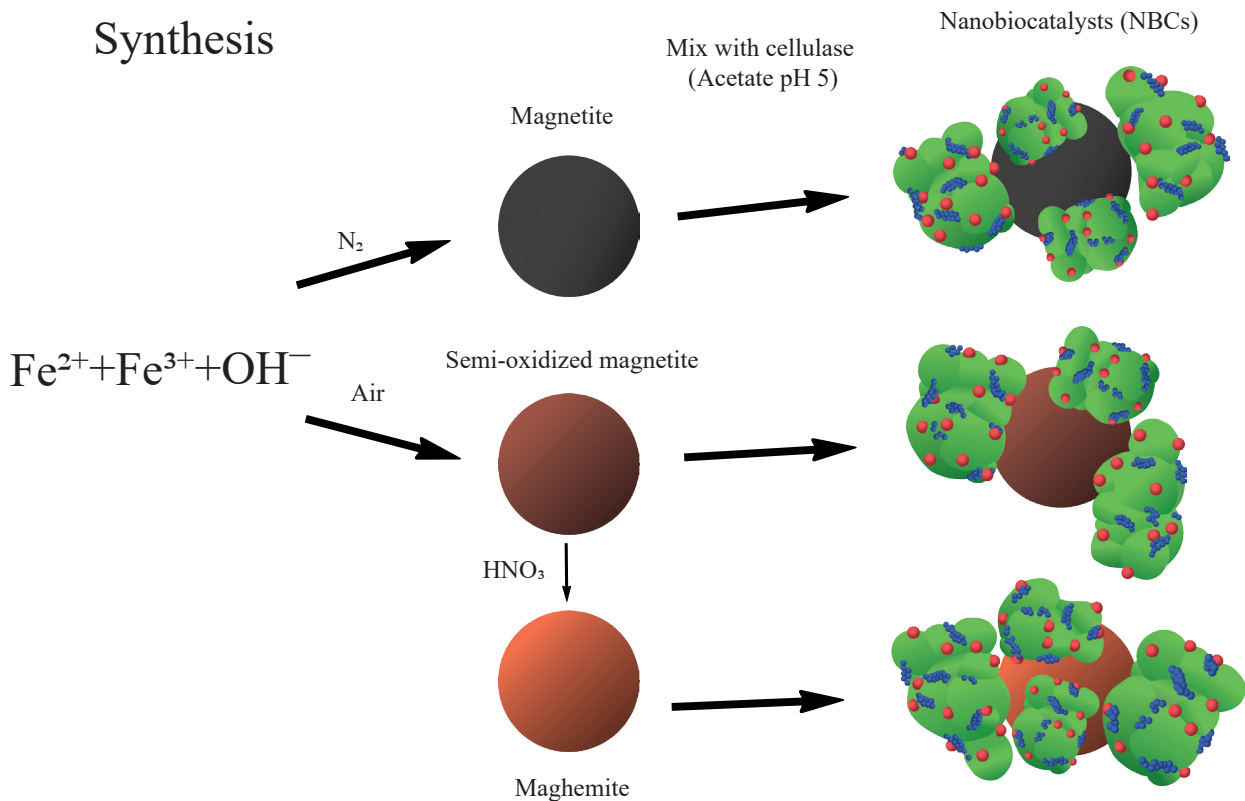


Fig. 6. MNP synthesis for cellulase immobilization [80]

Another method for synthesizing a magnetic nanobiocatalyst [78, 79] involves introducing MNPs into porous or polymeric materials. For example, the porous material used by Zhang *et al.* [79] was

mesoporous silicon dioxide SBA-15 with pores 7–9 nm in diameter, inside which Fe_3O_4 ·MNPs were formed. Cellulase immobilization was carried out by adsorption at pH 4.8 and a temperature of 4°C for 24 h. In the

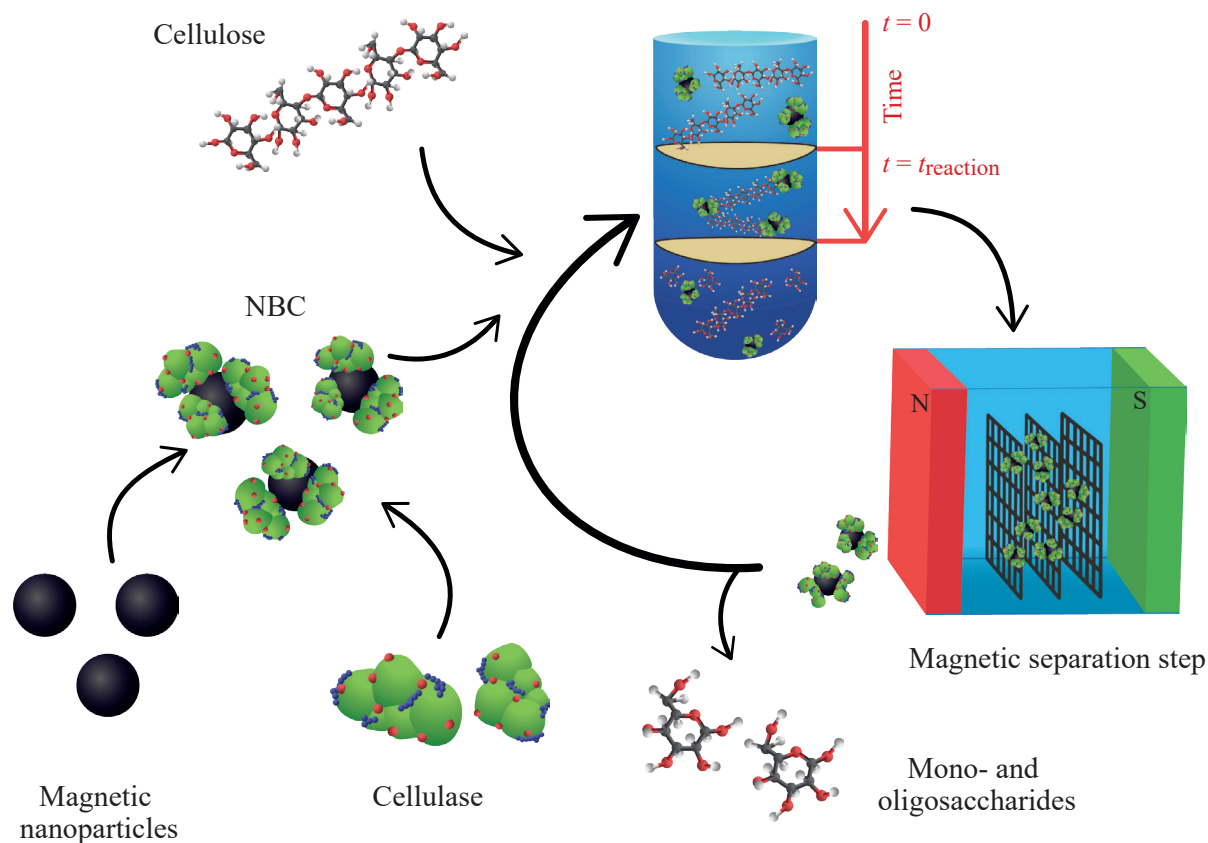


Fig. 7. Cellulose conversion and magnetic separation of nanobiocatalysts (NBC) [80]

hydrolysis of cellulose in the presence of immobilized cellulase, a glucose yield of 86.2% was achieved.

Magnetite NPs without a carrier are also used for cellulase adsorption, as shown in Fig. 6 [80]. For cellulase immobilization, three types of iron oxide NPs were synthesized: nitrogen-synthesized magnetite (MNP-N₂), air-synthesized semi-oxidized magnetite (MNP-Air), and nitric acid-oxidized magnetite NPs (MNP-Ox).

The catalytic activity of immobilized cellulase was investigated in the hydrolysis of carboxymethyl cellulose and filter paper. In all cases, the obtained nanobiocatalyst with magnetite as a carrier demonstrated better absolute activity (4.28 and 0.82 units/(g·h) for the catalyst on magnetite and maghemite, respectively) and relative enzymatic activity at lower pH values, as well as at higher and lower temperatures. This indicates an improvement in the thermal and mechanical stability of magnetite-based nanobiocatalysts, which is a desirable effect in enzyme immobilization.

Another important effect of cellulase immobilization is an increase in long-term catalytic stability. The presented nanobiocatalysts demonstrate long-term stability for 42 days without loss of catalytic activity,

while the activity of the native enzyme during this time drops to 40%. However, the most important positive effect is the possibility of reusing nanobiocatalysts by magnetic separation. Schnell *et al.* [80] achieved 95% recovery of magnetic nanobiocatalysts after use in six consecutive reaction cycles (Fig. 7).

Similar magnetite NPs were also synthesized by Ingle *et al.* [81] using glutaraldehyde to immobilize cellulase by covalent binding. During hydrolysis of the cellulose substrate (sugar cane cake powder), cellulose conversion for 24 h was achieved at a level of 93% for the native enzyme and 89% for cellulase immobilized on MNPs.

4. CONCLUSIONS

Nanobiocatalysts based on cellulase immobilized on nanostructured carriers are used for the catalytic hydrolysis of biomass waste, as well as in the food industry and for environmental protection purposes. The analysis of recent trends presented in this review shows that positive changes have occurred in the immobilization methods and carrier compositions over the past five years.

One of the most striking examples involves oriented single-point site-specific immobilization of the enzyme in

a microgel by sortase-catalyzed protein conjugation, which increases the immobilization targeting and improves the subsequent interaction of the enzyme with cellulose.

Another example demonstrates the possibility of using an unusual carrier structure (folded mesoporous silica NPs) for the production of effective and stable nanobiocatalysts by simple adsorption of cellulase due to the unique nature and morphology of the carrier. Cellulase adsorbed in this way turned out to be very stable and active due to preliminary modification of the carrier with macromolecules that change the charge or hydrophobicity–hydrophilicity balance.

Carrier-free multienzyme hybrid nanoflowers could be used to achieve a similar goal by forming combined enzymatic structures with high affinity for cellulose biomass.

The use of magnetically separable carriers increases the reliability of the biocatalyst and facilitates biocatalytic

processes, thus providing the possibility of extracting the magnetic nanobiocatalyst.

Acknowledgments

This work was supported by the Russian Science Foundation (project No. 24-79-10042, <https://rscf.ru/project/24-79-10042/>).

Authors' contributions

A.M. Sulman and **V.P. Molchanov**—writing (original draft preparation).

D.V. Balakshina and **O.V. Grebennikova**—literature analysis and preparation of graphic material.

V.G. Matveeva—conceptualization, review, and editing.

All authors have read and agreed to the published version of the manuscript.

The authors declare no conflicts of interest.

REFERENCES

1. Houfani A.A., Anders N., Spiess A.C., Baldrian P., Benallaoua S. Insights from enzymatic degradation of cellulose and hemicellulose to fermentable sugars – a review. *Biomass Bioenergy*. 2020;134(20):105481. <https://doi.org/10.1016/j.biombioe.2020.105481>
2. Arumugam A., Malolan V.V., Ponnusami V. Contemporary Pretreatment Strategies for Bioethanol Production from Corncobs. *Waste Biomass Valor*. 2021;12(4):577–612. <https://doi.org/10.1016/j.wbi.2020.10.090>
3. Behera S.S., Ray R.C. Solid state fermentation for production of microbial cellulases: Recent advances and improvement strategies. *Int. J. Biol. Macromol.* 2016;86:656–669. <https://doi.org/10.1016/j.ijbiomac.2015.10.090>
4. Cirujano F.G., Dhakshinamoorthy A. Challenges and opportunities for the encapsulation of enzymes over porous solids for Biodiesel production and Cellulose valorization into Glucose. *ChemCatChem*. 2021;13(22):4679–4693. <http://doi.org/10.1002/cctc.202100943>
5. Tabah B., Pulidindi I.N., Chitturi V.R., Varvak A., Foran E., Gedanken A. Solar-energy-driven conversion of biomass to bioethanol: A sustainable approach. *J. Mater. Chem. A*. 2017;5(30):15486–15506. <http://doi.org/10.1039/C7TA03083E>
6. Zanuso E., Gomes D.G., Ruiz H.A., Teixeira J.A., Domingues L. Enzyme immobilization as a strategy towards efficient and sustainable lignocellulosic biomass conversion into chemicals and biofuels: current status and perspectives. *Sustainable Energy Fuels*. 2021;5(17):4233–4247. <http://doi.org/10.1039/D1SE00747E>
7. Sulman E.M., Matveeva V.G., Bronstein L.M. Design of biocatalysts for efficient catalytic processes. *Current Opinion in Chemical Engineering*. 2019;26:1–8. <http://doi.org/10.1016/j.coche.2019.06.005>
8. Ramirez N., Serey M., Illanes A., Piumetti M., Ottone C. Immobilization strategies of photolyases: Challenges and perspectives for DNA repairing application. *J. Photochem. Photobiol. B*. 2021;215:112113. <https://doi.org/10.1016/j.jphotobiol.2020.112113>
9. Zhang S., Bilal M., Zdarta J., Cui J., Kumar A., Franco M., Ferreira L.F.R., Iqbal H.M.N. Biopolymers and nanostructured materials to develop pectinases-based immobilized nano-biocatalytic systems for biotechnological applications. *Food Res. Int.* 2021;140:109979. <https://doi.org/10.1016/j.foodres.2020.109979>

10. Gan J., Iqbal H.M.N., Show P.L., *et al.* Upgrading recalcitrant lignocellulosic biomass hydrolysis by immobilized cellulolytic enzyme-based nanobiocatalytic systems: a review. *Biomass Conv. Bioref.* 2024;14(1):4485–4509. <http://doi.org/10.1007/s13399-022-02642-7>
11. Holyavka M.G., Goncharova S.S., Redko Y.A., *et al.* Novel biocatalysts based on enzymes in complexes with nano- and micromaterials. *Biophys. Rev.* 2023;15(1):1127–1158. <http://doi.org/10.1007/s12551-023-01146-6>
12. Ahmed Z., Arshad A., Bilal M., *et al.* Nano-biocatalytic Systems for Cellulose de-polymerization: A Drive from Design to Applications. *Top. Catal.* 2023;66:592–605. <http://doi.org/10.1007/s11244-023-01785-9>
13. Zdarta J., Kołodziejczak-Radzimska A., Bachosz K., Rybarczyk A., Bilal M., Iqbal H.M.N., Buszewski B., Jesionowski T. Nanostructured supports for multienzyme co-immobilization for biotechnological applications: Achievements, challenges and prospects. *Adv. Colloid Interface Sci.* 2023;315:102889. <https://doi.org/10.1016/j.cis.2023.102889>
14. Cipolatti E.P., Valerio A., Henriques R.O., Moritz D.E., Ninow J.L., Freire D.M.G., Manoel E.A., Fernandez-Lafuente R., de Oliveira D. Nanomaterials for biocatalyst immobilization – State of the art and future trends. *RSC Adv.* 2016;6:104675–104692. <https://doi.org/10.1039/C6RA22047A>
15. Cavalcante F.T.T., de A. Falcão I.R., da S. Souza J.E., Rocha T.G., de Sousa I.G., Cavalcante A.L.G., de Oliveira A.L.B., de Sousa M.C.M., dos Santos J.C.S. Designing of Nanomaterials-Based Enzymatic Biosensors: Synthesis, Properties, and Applications. *Electrochem.* 2021;2(1): 149–184. <http://doi.org/10.3390/electrochem2010012>
16. Sudhir Singh A.P., Singhania R.R., Larroche C., Li Z. (Eds.). *Biomass, Biofuels, Biochemicals; Advances in Enzyme Catalysis and Technologies*. 1st ed. Amsterdam, The Netherlands: Elsevier; 2020. 472 p. ISBN 978-044-464114-4
17. Paul M., Mohapatra S., Kumar Das Mohapatra P., Thatoi H. Microbial cellulases – An update towards its surface chemistry, genetic engineering and recovery for its biotechnological potential. *Bioresour. Technol.* 2021;340:125710. <https://doi.org/10.1016/j.biortech.2021.125710>
18. Zhou Z., Ju X., Chen J., Wang R., Zhong Y., Li L. Charge-oriented strategies of tunable substrate affinity based on cellulase and biomass for improving in situ saccharification: a review. *Bioresour. Technol.* 2020;319:124159. <https://doi.org/10.1016/j.biortech.2020.124159>
19. Shanmugam S., Krishnaswamy S., Chandrababu R., Veerabagu U., Pugazhendhi A., Mathimani T. Optimal immobilization of *Trichoderma asperellum* laccase on polymer coated Fe₃O₄@SiO₂ nanoparticles for enhanced biohydrogen production from delignified lignocellulosic biomass. *Fuel.* 2020;273:117777. <https://doi.org/10.1016/j.fuel.2020.117777>
20. Giannakopoulou A., Patila M., Spyrou K., Chalmpes N., Zarafeta D., Skretas G., Gournis D., Stamatis H. Development of a four-enzyme magnetic nanobiocatalyst for multi-step cascade reactions. *Catalysts.* 2019;9(12):995. <https://doi.org/10.3390/catal9120995>
21. Marino M.A., Fulaz S., Tasic L. Magnetic Nanomaterials as Biocatalyst Carriers for Biomass Processing: Immobilization Strategies, Reusability, and Applications. *Magnetochemistry.* 2021;7(10):133. <https://doi.org/10.3390/magnetochemistry7100133>
22. Hedayatnia S., Ariaeenejad S., Kumleh H.H., Mirzaei H.H., Shakeri F., Motamedi E. Lactic acid production enhancement using metagenome-derived bifunctional enzyme immobilized on chitosan-alginate/nanocellulose hydrogel. *Bioresour. Technol. Rep.* 2024;25:101749. <https://doi.org/10.1016/j.biteb.2023.101749>
23. Maghraby Y.R., El-Shabasy R.M., Ibrahim A.H., Azzazy H.M.E. Enzyme Immobilization Technologies and Industrial Applications. *ACS Omega.* 2023;8(6):5184–5196. <https://doi.org/10.1021/acsomega.2c07560>
24. Xu C., Tong S., Sun L., Gu X. Cellulase immobilization to enhance enzymatic hydrolysis of lignocellulosic biomass: An all-inclusive review. *Carbohydr. Polym.* 2023;321:121319. <https://doi.org/10.1016/j.carbpol.2023.121319>
25. Zhou M., Ju X., Zhou Z., Yan L., Chen J., Yao X., Xu X., Li L.-Z. Development of an immobilized cellulase system based on metal-organic frameworks for improving ionic liquid tolerance and in situ saccharification of bagasse. *ACS Sustainable Chem. Eng.* 2019;7(23):19185–19193. <https://doi.org/10.1021/acssuschemeng.9b05175>
26. Zhou M., Yan L., Chen H., Ju X., Zhou Z., Li L. Development of functionalized metal-organic frameworks immobilized cellulase with enhanced tolerance of aqueous-ionic liquid media for *in situ* saccharification of bagasse. *Fuel.* 2021;304:121484. <https://doi.org/10.1016/j.fuel.2021.121484>
27. Wu L.M., Zeng Q.H., Ding R., Tu P.P., Xia M.Z. Fe₃O₄/Acid activated montmorillonite/cellulase composites: Preparation, structure, and enzyme activity. *Appl. Clay Sci.* 2019;179(13):105129. <http://doi.org/10.1016/j.clay.2019.105129>
28. Li L.-J., Xia W.-J., Ma G.-P., Chen Y.-L., Ma Y.-Y. A study on the enzymatic properties and reuse of cellulase immobilized with carbon nanotubes and sodium alginate. *AMB Express.* 2019;9:112. <https://doi.org/10.1186/s13568-019-0835-0>
29. Costantini A., Venezia V., Pota G., Bifulco A., Califano V., Sannino F. Adsorption of cellulase on wrinkled silica nanoparticles with enhanced inter-wrinkle distance. *Nanomaterials.* 2020;10(9):1799. <https://doi.org/10.3390/nano10091799>
30. Saha K., Verma P., Sikder J., Chakraborty S., Curcio S. Synthesis of chitosan-cellulase nanohybrid and immobilization on alginate beads for hydrolysis of ionic liquid pretreated sugarcane bagasse. *Renew. Energy.* 2019;133:66–76. <http://doi.org/10.1016/j.renene.2018.10.014>
31. Ahmed I.N., Yang X.-L., Dubale A.A., Li R.-F., Ma Y.-M., Wang L.-M., Hou G.-H., Guan R.-F., Xie M.-H. Hydrolysis of cellulose using cellulase physically immobilized on highly stable zirconium based metal-organic frameworks. *Bioresour. Technol.* 2018;270:377–382. <https://doi.org/10.1016/j.biortech.2018.09.077>
32. Zhu Y., Han J., Wu J., Li Y., Wang L., Mao Y., Wang Y. A two-step method for the synthesis of magnetic immobilized cellulase with outstanding thermal stability and reusability. *New J. Chem.* 2021;45(13):6144–6150. <https://doi.org/10.1039/D0NJ06037B>

33. Singh N., Dhanya B.S., Verma M.L. Nano-immobilized biocatalysts and their potential biotechnological applications in bioenergy production. *Mater. Sci. Energy Technol.* 2020;3:808–824. <https://doi.org/10.1016/j.mset.2020.09.006>
34. Wu J., Han J., Mao Y., Wang L., Wang Y., Li Y., Wang Y. Bionic mineralization growth of UIO-66 with bovine serum for facile synthesis of Zr-MOF with adjustable mesopores and its application in enzyme immobilization. *Sep. Purif. Technol.* 2022;297(16):121505. <http://doi.org/10.1016/j.seppur.2022.121505>
35. Wu J., Wang Y., Han J., Wang L., Li C., Mao Y., Wang Y. A method of preparing mesoporous Zr-based MOF and application in enhancing immobilization of cellulase on carrier surface. *Biochem. Eng. J.* 2022;180:108342. <http://doi.org/10.1016/j.bej.2022.108342>
36. Zhang X., Zheng S., Tao J., Wang X. *In Situ* Encapsulation of Cellulase in a Novel Mesoporous Metal-Organic Framework. *Catal. Lett.* 2022;152(70):699–706. <https://doi.org/10.1007/s10562-021-03672-y>
37. Amaro-Reyes A., Diaz-Hernandez A., Gracida J., Garcia-Almendarez B.E., Escamilla-Garcia M., Arredondo-Ochoa T., Regalado C. Enhanced performance of immobilized xylanase/filter paper-ase on a magnetic chitosan support. *Catalysts.* 2019;9(11):966. <http://doi.org/10.3390/catal9110966>
38. Zheng T., Yang L., Ding M., Huang C., Yao J. Metal-organic framework promoting high-solids enzymatic hydrolysis of untreated corncob residues. *Bioresour. Technol.* 2022;344(Pt. A):126163. <https://doi.org/10.1016/j.biortech.2021.126163>
39. Mo H., Qiu J., Yang C., Zang L., Sakai E., Chen J. Porous biochar/chitosan composites for high performance cellulase immobilization by glutaraldehyde. *Enzym. Microb. Technol.* 2020;138:109561. <https://doi.org/10.1016/j.enzmictec.2020.109561>
40. Salem M., Mauguen Y., Prange T. Revisiting glutaraldehyde cross-linking: The case of the Arg-Lys intermolecular doublet. *Acta Crystallogr. Sect. F: Struct. Biol. Cryst. Commun.* 2010;66(Pt. 3):225–228. <https://doi.org/10.1107/s1744309109054037>
41. Yamato K., Yoshida Y., Kumamoto Y., Isogai A. Surface modification of TEMPO-oxidized cellulose nanofibers, and properties of their acrylate and epoxy resin composite films. *Cellulose.* 2022;29(5):2839–2853. <https://doi.org/10.1007/s10570-021-04131-y>
42. Handoko, Panigrahi N.R., Arora P.S. Two-component redox organocatalyst for peptide bond formation. *J. Am. Chem. Soc.* 2022;144(8):3637–3643. <https://doi.org/10.1021/jacs.1c12798>
43. Paz-Cedeno F.R., Carceller J.M., Iborra S., Donato R.K., Godoy A.P., Veloso de Paula A., Monti R., Corma A., Masarin F. Magnetic graphene oxide as a platform for the immobilization of cellulases and xylanases: Ultrastructural characterization and assessment of lignocellulosic biomass hydrolysis. *Renew. Energy.* 2021;164:491–501. <https://doi.org/10.1016/j.renene.2020.09.059>
44. Huang YY., Zhan P., Wang F., *et al.* Cellulase immobilized onto amino-functionalized magnetic Fe₃O₄@SiO₂ nanoparticle for poplar deconstruction. *Chem. Pap.* 2022;76:5807–5817. <https://doi.org/10.1007/s11696-022-02292-z>
45. Gao J., Lu C.-L., Wang Y., Wang S.-S., Shen J.-J., Zhang J.-X., Zhang Y.-W. Rapid immobilization of cellulase onto graphene oxide with a hydrophobic spacer. *Catalysts.* 2018;8(5):180. <https://doi.org/10.3390/catal8050180>
46. Zou Z., Gau E., El-Awaad I., Jakob F., Pich A., Schwaneberg U. Selective Functionalization of Microgels with Enzymes by Sortagging. *Bioconjug. Chem.* 2019;30(11):2859–2869. <https://doi.org/10.1021/acs.bioconjchem.9b00568>
47. Cambria E., Renggli K., Ahrens C.C., Cook C.D., Kroll C., Krueger A.T., Imperiali B., Griffith L.G. Covalent Modification of Synthetic Hydrogels with Bioactive Proteins via Sortase-Mediated Ligation. *Biomacromolecules.* 2015;16(8):2316–2326. <https://doi.org/10.1021/acs.biomac.5b00549>
48. Hojnik Podrepsek G., Knez Z., Leitgeb M. Activation of cellulase cross-linked enzyme aggregates (CLEAs) in scCO₂. *J. Supercrit. Fluids.* 2019;154:104629. <http://doi.org/10.1016/j.supflu.2019.104629>
49. Blanco-Llamero C., Garcia-Garcia P., Senorans F.J. Cross-Linked Enzyme Aggregates and Their Application in Enzymatic Pretreatment of Microalgae: Comparison Between CLEAs and Combi-CLEAs. *Front. Bioeng. Biotechnol.* 2021;9:794672. <https://doi.org/10.3389/fbioe.2021.794672>
50. Ifko D., Vasic K., Knez Z., Leitgeb M. (Magnetic) cross-linked enzyme aggregates of cellulase from *T. reesei*: A stable and efficient biocatalyst. *Molecules.* 2023;28(3):1305. <https://doi.org/10.3390/molecules28031305>
51. Han J., Feng H., Wu J., Li Y., Zhou Y., Wang L., Luo P., Wang Y. Construction of multienzyme co-immobilized hybrid nanoflowers for an efficient conversion of cellulose into glucose in a cascade reaction. *J. Agric. Food Chem.* 2021;69(28):7910–7921. <https://doi.org/10.1021/acs.jafc.1c02056>
52. Ge J., Lei J., Zare R.N. Protein–inorganic hybrid nanoflowers. *Nat. Nanotechnol.* 2012;7(7):428–432. <https://doi.org/10.1038/nnano.2012.80>
53. Pota G., Sapienza Salerno A., Costantini A., Silvestri B., Passaro J., Califano V. Co-immobilization of Cellulase and β-Glucosidase into Mesoporous Silica Nanoparticles for the Hydrolysis of Cellulose Extracted from *Eriobotrya japonica* Leaves. *Langmuir.* 2022;38(18):5481–5493. <https://doi.org/10.1021/acs.langmuir.2c00053>
54. Chen B., Qiu J., Mo H., Yu Y., Ito K., Sakai E., Feng H. Synthesis of mesoporous silica with different pore sizes for cellulase immobilization: Pure physical adsorption. *New J. Chem.* 2017;41(17):9338–9345. <https://doi.org/10.1039/C7NJ00441A>
55. Zarei A., Alihosseini F., Parida D., Nazir R., Gaan S. Fabrication of Cellulase Catalysts Immobilized on a Nanoscale Hybrid Polyaniline/Cationic Hydrogel Support for the Highly Efficient Catalytic Conversion of Cellulose. *ACS Appl. Mater. Interfaces.* 2021;13(42):49816–49827. <https://doi.org/10.1021/acsami.1c12263>
56. Ariaeenejad S., Motamedi E., Hosseini Salekdeh G. Stable cellulase immobilized on graphene oxide@CMC-g-poly(AMPS-co-AAm) hydrogel for enhanced enzymatic hydrolysis of lignocellulosic biomass. *Carbohydr. Polym.* 2020;230:115661. <https://doi.org/10.1016/j.carbpol.2019.115661>

57. Wang Y., Chen D., Wang G., Zhao C., Ma Y., Yang W. Immobilization of cellulase on styrene/maleic anhydride copolymer nanoparticles with improved stability against pH changes. *Chem. Eng. J.* 2018;336:152–159. <https://doi.org/10.1016/j.cej.2017.11.030>
58. Lu L., Zhang L., Yuan L., Zhu T., Chen W., Wang G., Wang Q. Artificial Cellulosome Complex from the Self-Assembly of Ni-NTA-Functionalized Polymeric Micelles and Cellulases. *ChemBioChem.* 2019;20(11):1394–1399. <https://doi.org/10.1002/cbic.201900061>
59. Kaur P., Taggar M.S., Kalia A. Characterization of magnetic nanoparticle-immobilized cellulases for enzymatic saccharification of rice straw. *Biomass Convers. Biorefin.* 2021;11(3):955–969. <https://doi.org/10.1007/s13399-020-00628-x>
60. Kumar S., Morya V., Gadhavi J., Vishnoi A., Singh J., Datta B. Investigation of nanoparticle immobilized cellulase: Nanoparticle identity, linker length and polyphenol hydrolysis. *Heliyon.* 2019;5(5):e01702. <https://doi.org/10.1016/j.heliyon.2019.e01702>
61. Yu D., Ma X., Huang Y., Jiang L., Wang L., Han C., Yang F. Immobilization of cellulase on magnetic nanoparticles for rice bran oil extraction in a magnetic fluidized bed. *Int. J. Food Eng.* 2022;18(1):15–26. <https://doi.org/10.1515/ijfe-2021-0111>
62. Marino M.A., Moretti P., Tasic L. Immobilized commercial cellulases onto amino-functionalized magnetic beads for biomass hydrolysis: Enhanced stability by non-polar silanization. *Biomass Convers. Biorefin.* 2022;13(10):1007. <https://doi.org/10.1007/s13399-021-01798-y>
63. Rong G.-X., Lv Z.-X., Pan Z.-J., Zhang S.-L., Deng P. Covalent immobilization of cellulase onto amino and graphene oxide functionalized magnetic Fe₂O₃/Fe₃O₄@SiO₂ nanocomposites. *J. Nanosci. Nanotechnol.* 2021;21(9):4749–4757. <https://doi.org/10.1166/jnn.2021.19127>
64. Yi J., Qiu M., Zhu Z., Dong X., Andrew Decker E., McClements D.J. Robust and recyclable magnetic nanobiocatalysts for extraction of anthocyanin from black rice. *Food Chem.* 2021;364:130447. <https://doi.org/10.1016/j.foodchem.2021.130447>
65. Huang W., Pan S., Li Y., Yu L., Liu R. Immobilization and characterization of cellulase on hydroxy and aldehyde functionalized magnetic Fe₂O₃/Fe₃O₄ nanocomposites prepared via a novel rapid combustion process. *Int. J. Biol. Macromol.* 2020;162:845–852. <https://doi.org/10.1016/j.ijbiomac.2020.06.209>
66. Kumar A., Singh S., Nain L. Magnetic nanoparticle immobilized cellulase enzyme for saccharification of paddy straw. *Int. J. Curr. Microbiol. Appl. Sci.* 2018;7(05):881–893. <http://dx.doi.org/10.20546/ijemas.2018.704.095>
67. Dal Magro L., Silveira V.C.C., Weber de Menezes E., Benvenuti E.V., Nicolodi S., Hertz P.F., Klein M.P., Rodrigues R.C. Magnetic biocatalysts of pectinase and cellulase: Synthesis and characterization of two preparations for application in grape juice clarification. *Int. J. Biol. Macromol.* 2018;115:35–44. <https://doi.org/10.1016/j.ijbiomac.2018.04.028>
68. Rashid S.S., Mustafa A.H., Rahim M.H.A., Gunes B. Magnetic nickel nanostructure as cellulase immobilization surface for the hydrolysis of lignocellulosic biomass. *Int. J. Biol. Macromol.* 2022;209:1048–1053. <https://doi.org/10.1016/j.ijbiomac.2022.04.072>
69. Javid A., Amiri H., Kafrani A.T., Rismani-Yazdi H. Post-hydrolysis of cellulose oligomers by cellulase immobilized on chitosan-grafted magnetic nanoparticles: A key stage of butanol production from waste textile. *Int. J. Biol. Macromol.* 2022;207:324–332. <https://doi.org/10.1016/j.ijbiomac.2022.03.013>
70. Zanuso E., Ruiz H.A., Domingues L., Teixeira J.A. Magnetic Nanoparticles as Support for Cellulase Immobilization Strategy for Enzymatic Hydrolysis Using Hydrothermally Pretreated Corn Cob Biomass. *BioEnergy Res.* 2022;15(4):1946–1957. <http://doi.org/10.1007/s12155-021-10384-z>
71. Asar M.F., Ahmad N., Husain Q. Chitosan modified Fe₃O₄/graphene oxide nanocomposite as a support for high yield and stable immobilization of cellulase: Its application in the saccharification of microcrystalline cellulose. *Prep. Biochem. Biotechnol.* 2020;50(5):460–467. <https://doi.org/10.1080/10826068.2019.1706562>
72. Diaz-Hernandez A., Gracida J., Garcia-Almendarez B.E., Regalado C., Nunez R., Amaro-Reyes A. Characterization of magnetic nanoparticles coated with chitosan: A potential approach for enzyme immobilization. *J. Nanomater.* 2018;2018:9468574. <https://doi.org/10.1155/2018/9468574>
73. Cui J., Li L., Kou L., Rong H., Li B., Zhang X. Comparing Immobilized Cellulase Activity in a Magnetic Three-Phase Fluidized Bed Reactor under Three Types of Magnetic Field. *Ind. Eng. Chem. Res.* 2018;57(32):10841–10850. <https://doi.org/10.1021/acs.iecr.8b02195>
74. Hosseini S.H., Hosseini S.A., Zohreh N., Yaghoubi M., Pourjavadi A. Covalent immobilization of cellulase using magnetic poly(ionic liquid) support: Improvement of the enzyme activity and stability. *J. Agric. Food Chem.* 2018;66(4):789–798. <https://doi.org/10.1021/acs.jafc.7b03922>
75. Sanchez-Ramirez J., Martinez-Hernandez J.L., Lopez-Campos R.G., Segura-Ceniceros E.P., Saade H., Ramos-Gonzalez R., Neira-Velazquez M.G., Medina-Morales M.A., Aguilar C.N., Ilyina A. Laccase Validation as Pretreatment of Agave Waste Prior to Saccharification: Free and Immobilized in Superparamagnetic Nanoparticles Enzyme Preparations. *Waste Biomass Valorization.* 2018;9(2):223–234. <https://doi.org/10.1007/s12649-016-9774-z>
76. Abbaszadeh M., Hejazi P. Metal affinity immobilization of cellulase on Fe₃O₄ nanoparticles with copper as ligand for biocatalytic applications. *Food Chem.* 2019;290:47–55. <https://doi.org/10.1016/j.foodchem.2019.03.117>
77. Poorakbar E., Saboury A.A., Laame Rad B., Khoshnevisan K. Immobilization of Cellulase onto Core-Shell Magnetic Gold Nanoparticles Functionalized by Aspartic Acid and Determination of its Activity. *Protein J.* 2020;39(4):328–336. <https://doi.org/10.1007/s10930-020-09906-z>
78. Jannah Sulaiman N., Mansor A.F., Rahman R.A., Illias R.M., Shaarani S.M. Adsorption Kinetics of Cellulase and Xylanase Immobilized on Magnetic Mesoporous Silica. *Chem. Eng. Technol.* 2019;42(9):1825–1833. <https://doi.org/10.1002/ceat.201800657>
79. Zhang Y., Jin P., Liu M., Pan J., Yan Y., Chen Y., Xiong Q. A novel route for green conversion of cellulose to HMF by cascading enzymatic and chemical reactions. *AIChE J.* 2017;63(11):4920–4932. <http://doi.org/10.1002/aic.15841>

80. Schnell F., Kube M., Berensmeier S., Schwaminger S.P. Magnetic Recovery of Cellulase from Cellulose Substrates with Bare Iron Oxide Nanoparticles. *ChemNanoMat*. 2019;5(4):422–426. <http://doi.org/10.1002/cnma.201800658>
81. Ingle A.P., Rathod J., Pandit R., da Silva S.S., Rai M. Comparative evaluation of free and immobilized cellulase for enzymatic hydrolysis of lignocellulosic biomass for sustainable bioethanol production. *Cellulose*. 2017;24(12):5529–5540. <http://doi.org/10.1007/s10570-017-1517-1>

About the Authors

Alexandrina M. Sulman, Cand. Sci. (Chem.), Associate Professor, Department of Biotechnology, Chemistry and Standardization, Tver State Technical University (22, Afanasiya Nikitina nab., Tver, 170026, Russia). E-mail: alexsulman@mail.ru. Scopus Author ID 57147926100, ResearcherID ABC-4215-2020, RSCI SPIN-code 6520-1380, <https://orcid.org/0000-0002-6845-3431>

Vladimir P. Molchanov, Dr. Sci. (Eng.), Professor, Department of Biotechnology, Chemistry and Standardization, Tver State Technical University (22, Afanasiya Nikitina nab., Tver, 170026, Russia). E-mail: molchanov@science.tver.ru. Scopus Author ID 57146992100, ResearcherID U-3736-2019, RSCI SPIN-code 7265-3331, <https://orcid.org/0000-0003-3038-0406>

Daria V. Balakshina, Master Student, Tver State Technical University (22, Afanasiya Nikitina nab., Tver, 170026, Russia). E-mail: dasha.balakshina.01@bk.ru. <https://orcid.org/0009-0002-0551-8469>

Olga V. Grebennikova, Cand. Sci. (Chem.), Associate Professor, Department of Biotechnology, Chemistry and Standardization, Tver State Technical University (22, Afanasiya Nikitina nab., Tver, 170026, Russia). E-mail: olechkamatveeva@mail.ru. Scopus Author ID 57219406141, ResearcherID A-9397-2014, RSCI SPIN-code 2995-9094, <https://orcid.org/0000-0002-8888-1783>

Valentina G. Matveeva, Dr. Sci. (Chem.), Professor, Department of Biotechnology, Chemistry and Standardization, Tver State Technical University (22, Afanasiya Nikitina nab., Tver, 170026, Russia). E-mail: matveeva@science.tver.ru. Scopus Author ID 7004479390, ResearcherID B-1120-2014, RSCI SPIN-code 8005-3995, <https://orcid.org/0000-0002-3291-4865>

Об авторах

Сульман Александрина Михайловна, к.х.н., доцент кафедры биотехнологии, химии и стандартизации, ФГБОУ ВО «Тверской государственный технический университет» (170026, Россия, Тверь, набережная Афанасия Никитина, д. 22). E-mail: alexsulman@mail.ru. Scopus Author ID 57147926100, ResearcherID ABC-4215-2020, SPIN-код РИНЦ 6520-1380, <https://orcid.org/0000-0002-6845-3431>

Молчанов Владимир Петрович, д.т.н., профессор кафедры биотехнологии, химии и стандартизации, ФГБОУ ВО «Тверской государственный технический университет» (170026, Россия, Тверь, набережная Афанасия Никитина, д. 22). E-mail: molchanov@science.tver.ru. Scopus Author ID 57146992100, ResearcherID U-3736-2019, SPIN-код РИНЦ 7265-3331, <https://orcid.org/0000-0003-3038-0406>

Балакшина Дарья Вадимовна, студент магистратуры, ФГБОУ ВО «Тверской государственный технический университет» (170026, Россия, Тверь, набережная Афанасия Никитина, д. 22). E-mail: dasha.balakshina.01@bk.ru. <https://orcid.org/0009-0002-0551-8469>

Гребенникова Ольга Валентиновна, к.х.н., доцент кафедры биотехнологии, химии и стандартизации, ФГБОУ ВО «Тверской государственный технический университет» (170026, Россия, Тверь, набережная Афанасия Никитина, д. 22). E-mail: olechkamatveeva@mail.ru. Scopus Author ID 57219406141, ResearcherID A-9397-2014, SPIN-код РИНЦ 2995-9094, <https://orcid.org/0000-0002-8888-1783>

Матвеева Валентина Геннадьевна, д.х.н., профессор кафедры биотехнологии, химии и стандартизации, ФГБОУ ВО «Тверской государственный технический университет» (170026, Россия, Тверь, набережная Афанасия Никитина, д. 22). E-mail: matveeva@science.tver.ru. Scopus Author ID 7004479390, ResearcherID B-1120-2014, SPIN-код РИНЦ 8005-3995, <https://orcid.org/0000-0002-3291-4865>

Translated from Russian into English by V. Glyanchenko

Edited for English language and spelling by Thomas A. Beavitt

Synthesis and processing of polymers and polymeric composites
Синтез и переработка полимеров и композитов на их основе

UDC 66.085.3+547.599.6

<https://doi.org/10.32362/2410-6593-2025-20-2-137-145>

EDN JYMQMK



RESEARCH ARTICLE

***N*-[(1*RS*)-camphane-2-ylidene]aniline: A novel efficient liquid UV absorber for 3D printing**

Nina V. Sidorenko¹, Marat A. Vaniev¹, Iurii M. Mkrтчyan¹, Nikita A. Salykin², Andrey A. Vernigora¹, Ivan A. Novakov¹

¹ Volgograd State Technical University, Volgograd, 400005 Russia

² SIBUR-Innovations, SIBUR Holding, Tomsk, 634058 Russia

✉ Corresponding author, e-mail: nvsidorenko@vstu.ru

Abstract

Objectives. To investigate the effectiveness of *N*-[(1*RS*)-camphanyl-2-ylidene]aniline as an ultraviolet (UV) absorber in 3D printing using digital light processing.

Methods. Polymerization process parameters were determined using a Netzsch DSC 204 F1 Phoenix differential scanning calorimeter equipped with an OmniCure S2000 UV irradiation attachment (400–500 nm filter). Samples were printed on a Minicube ULTRA 3D printer using a 405-nm LED light source. Dimensional accuracy during printing was evaluated according to ISO 52902:2019. Mechanical properties were determined using a Zwick/Roell Zwicki Z5.0 universal testing machine, while heat deflection temperature was measured on a Gotech HDT-HV-2000-3 device.

Results. The conversion degree of double bonds determined from differential scanning calorimetry results for a photopolymerizable composition containing camphor anil are almost identical to that for the composition without a UV absorber. The high gel fraction content in the samples indicates the formation of cross-linked polymers. The level of physical and mechanical properties, as determined in tensile and flexural parameters, is largely unaffected by the use of the type of UV absorbers considered. Tensile strength values are comparable to those of oligocarbonate methacrylate OCM-2-based materials produced under radiation polymerization conditions. Dimensional deviation for materials containing camphor anils is smaller than for compositions without a UV absorber or for compositions using a triazole derivative as an absorber.

Conclusions. The effectiveness of camphor anils as UV absorbers in the photopolymerizable composition is confirmed. With high dimensional accuracy in printing, it is possible to produce densely cross-linked polymers offering desirable physicomechanical properties and heat deflection temperatures.

Keywords

UV absorber, camphor anils, 3D printing, differential scanning calorimetry, oligocarbonate methacrylate

Submitted: 21.10.2024

Revised: 10.12.2024

Accepted: 20.02.2025

For citation

Sidorenko N.V., Vaniev M.A., Mkrтчyan Iu.M., Salykin N.A., Vernigora A.A., Novakov I.A. *N*-[(1*RS*)-camphane-2-ylidene]aniline: A novel efficient liquid UV absorber for 3D printing. *Tonk. Khim. Tekhnol. = Fine Chem. Technol.* 2025;20(2):137–145. <https://doi.org/10.32362/2410-6593-2025-20-2-137-145>

НАУЧНАЯ СТАТЬЯ

N-[(1RS)-камфан-2-илиден]анилин — новый эффективный жидкий УФ-абсорбер для 3D-печати в условиях фотохимического инициирования

Н.В. Сидоренко¹✉, М.А. Ваниев¹, Ю.М. Мкртчян¹, Н.А. Салыкин², А.А. Вернигора¹, И.А. Новаков¹

¹ Волгоградский государственный технический университет, Волгоград, 400005 Россия

² ООО «СИБУР-Инновации», ПАО «СИБУР Холдинг», Томск, 634058 Россия

✉ Автор для переписки, e-mail: nvsidorenko@vstu.ru

Аннотация

Цели. Оценка эффективности применения N-[(1RS)-камфан-2-илиден]анилина в качестве ультрафиолетового (УФ) абсорбера при 3D-печати методом цифровой обработки света (digital light processing, DLP).

Методы. Параметры процесса полимеризации определялись на дифференциальном сканирующем калориметре Netzsch DSC 204 F1 Phoenix с приставкой УФ-облучения OmniCure S2000 (светофильтр 400–500 нм). Образцы печатали на 3D-принтере Minicube ULTRA со светодиодным источником излучения 405 нм. Линейную точность при печати оценивали по ГОСТ Р 59586-2021 (ISO 52902:2019). Прочностные характеристики определяли с использованием универсальной испытательной машины Zwick/Roell Zwicki Z5.0, деформационную теплостойкость — на приборе Gotech HDT-HV-2000-3.

Результаты. Значения степени превращения двойных связей, определенные по результатам дифференциальной сканирующей калориметрии для фотополимеризующейся композиции (ФПК), содержащей анилы камфоры, практически совпадают с таковыми для композиции без УФ-абсорбера. Высокое содержание гель-фракции в образцах свидетельствует о получении густосетчатых полимеров. Уровень достигаемых физико-механических свойств, определяемых показателями при растяжении и изгибе, практически не зависит от типа рассматриваемых УФ-абсорберов. Значения прочности при растяжении близки к характеристикам материалов на основе олигокарбонатметакрилата ОКМ-2, получаемым в условиях радиационной полимеризации. Отклонение от линейных размеров для материалов, содержащих анилы камфоры, меньше, чем при отсутствии в составе ФПК УФ-абсорбера или при использовании в качестве такового производного триазола.

Выводы. Подтверждена эффективность применения анилов камфоры в составе ФПК в качестве УФ-абсорбера. При высокой линейной точности печати реализуемо получение густосетчатых полимеров с высоким уровнем физико-механических характеристик и деформационной теплостойкости.

Ключевые слова

УФ-абсорбер, анилы камфоры, 3D-печать, дифференциальная сканирующая калориметрия, олигокарбонатметакрилат

Поступила: 21.10.2024

Доработана: 10.12.2024

Принята в печать: 20.02.2025

Для цитирования

Сидоренко Н.В., Ваниев М.А., Мкртчян Ю.М., Салыкин Н.А., Вернигора А.А., Новаков И.А. N-[(1RS)-камфан-2-илиден]анилин — новый эффективный жидкий УФ-абсорбер для 3D-печати в условиях фотохимического инициирования. *Тонкие химические технологии*. 2025;20(2):137–145. <https://doi.org/10.32362/2410-6593-2025-20-2-137-145>

INTRODUCTION

Already widespread modern 3D printing technologies based on the use of oligomeric compositions that are reactive under photo-initiated polymerization conditions (VAT photopolymerization) [1–4] generally involve the use of a component or combination of components that act as a limiter of the polymer layer thickness during layer-by-layer build-up of the product under UV irradiation. Dyes and pigments used as such components [5–8] include those originally intended for the production of printed circuit boards [9, 10].

In addition, it is worth noting the presence of ultraviolet (UV) absorbers traditionally used in paints and varnishes, as well as in thermoplastics [1, 11, 12]. Since currently used components are not without drawbacks, the search for new effective UV absorbers for use in digital light processing (DLP) printing technology becomes a pressing issue. In particular, dyes can migrate into polymer optically transparent elements of printers that come into contact with photopolymerizable compositions (PPC), while pigments are prone to sedimentation settling during long-term printing. Industrial UV absorbers, which

generally consist of powders of varying dispersion, have limited solubility in multicomponent oligomeric compositions.

The chemical structures of camphane- and aniline-based compounds synthesized in previous works provided grounds to consider their potential applicability as UV absorbers for 3D printing [13]. Since there is no information of this kind in the scientific and technical literature, the present work set out to provide a comprehensive assessment of the efficiency of using one of the representatives of liquid camphor anils (*N*-[(1RS)-camphane-2-ylidene]aniline) as a UV absorber in PPC formulations.

MATERIALS AND METHODS

The model PPC consisted of oligocarbonate methacrylate OCM-2 (bis-(methacryloxyethylene carbonate)-diethyleneglycol, *Polyketone*, Russia), a bis-acylphosphine oxide (BAPO) (phenylbis(2,4,6-trimethylbenzoyl)-phosphine oxide photoinitiator, Omnirad 819, *IGM Resins*, Netherlands), (2-(2-hydroxy-5-methylphenyl)benzotriazole (*Tokyo Chemical Industry Co.*, Japan), a triazole derivative (hereinafter triazole), was used as a comparative sample of the UV absorber. To determine the theoretical thermal effect, thermal polymerization was initiated with benzoyl peroxide purified by recrystallization (*Vekton*, Russia). Cyclohexane of chemically pure grade (*Vekton*, Russia) served as a solvent for UV spectroscopy. The experimentally determined concentrations of BAPO and UV absorbers that allow 3D printing with the same printer settings were 1.0 and 0.5% of the oligomer mass, respectively.

The PPC was obtained by mixing the ingredients. The mixtures were kept at 50°C for 1–3 h until the formation of homogeneous solutions. The characteristic parameters of the obtained PPC polymerization were determined in accordance with GOST R 56755-2015¹ (ISO 11357-5) on a DSC 204 F1 Phoenix differential scanning calorimeter (*Netzsch*, Germany) equipped with a compressor cooling system and an OmniCure S2000 UV irradiation attachment using a light filter transmitting in the 400–500 nm region at an irradiation power of 1 W/cm²

in standard aluminum crucibles. The total flow of inert gas (argon) was 90 mL/min.

The theoretical thermal effect of polymerization, whose value was used to calculate the degree of conversion, was determined using differential scanning calorimetry (DSC) in dynamic mode (temperature scanning mode) by heating a sample of the OCM-2 oligomer containing dissolved benzoyl peroxide (0.5%) to 170°C at a rate of 5°C/min. The average of 5 measurements was 271.7 J/g, which is in fairly good agreement with the calculated data (271.0 J/g) based on the thermal effects known for methacrylates [14]. The thermal effects of photopolymerization were determined by performing two measurements equivalent in terms of sample exposure conditions and then subtracting the second measurement from the first. A similar calculation method was used in [15].

All samples were printed on a MiniCube ULTRA 3D printer (*Minicube*, Russia) equipped with a 405 nm LED light source. The preparation and slicing of print jobs was performed in specialized MiniCube Studio software. The specified layer thickness was 0.03 mm, while the number of layers, taking into account the supports, was 2375. After printing, washing with isopropanol, and mechanical removal of supports, the samples were dried at room temperature for 30 min. Post-polymerization was carried out at 60°C for 60 min on each side on a FormCure installation (*Formlabs*, USA) equipped with LEDs having an emission wavelength of 405 nm. UV spectra were recorded on a UV-2600 device (*Shimadzu*, Japan) in standard quartz cuvettes with an optical path length of 10 mm.

The intensity of the 3D printer LED source at the bottom of a standard container was measured using a UVpad E UV radiometer (*Opsytec Dr. Gröbel*, Germany).

Linear accuracy during printing was assessed according to GOST R 59586-2021² (ISO 52902:2019).

To determine the amount of gel fraction, extraction with boiling toluene was carried out for 24 h using a Soxhlet apparatus.

The strength characteristics of the samples were determined using a Zwick Z5.0 universal testing machine (*Zwick/Roell*, Germany) in accordance with GOST 34370-2017³ (ISO 527-1:2012): a sample of

¹ GOST R 56755-2015. National Standard of the Russian Federation. Plastics. Differential scanning calorimetry (DSC). Part 5. Determination of characteristic reaction-curve temperatures and times, enthalpy of reaction and degree of conversion. Moscow: Standartinform; 2016 (in Russ.).

² GOST R 59586-2021. National Standard of the Russian Federation. Additive technologies. Test artifacts. Geometric capability assessment of additive manufacturing systems. Moscow: Russian Institute of Standardization; 2016 (in Russ.).

³ GOST 34370-2017. Interstate Standard. Plastics. Determination of tensile properties. Part 1: General principles. Moscow: Standartinform; 2018 (in Russ.).

type 4 (GOST 11262-2017⁴ (ISO 527-2:2012)) was characterized at a speed of 100 mm/min, while a sample of 80 × 10 × 4 mm bar type (GOST 4648-2014⁵ (ISO 178:2010)) was tested at a speed of 2 mm/min.

Heat deflection temperature (HDT) was determined in accordance with GOST 12021-2017⁶ (ISO 75-2:2013) using a Gotech HDT-HV-2000-3 (Gotech Inc., China) device. The samples were comprised of 80 × 10 × 4 mm bar. The heating rate was 2°C/min, while bending stresses were 0.45 and 1.8 MPa, respectively. Shore D hardness was measured in accordance with GOST 24621-2015⁷ (ISO 868:2003) using a TH210 portable hardness tester (Time Group Inc., China).

RESULTS AND DISCUSSION

Previously [16], we used a detailed visual comparison to demonstrate the possibility of using camphor anils as UV absorbers for 3D printing. As such, it was deemed necessary to numerically evaluate not only the detailing during printing, but also the complex of properties of the resulting materials. The motivation for choosing OCM-2 as the base oligomer consisted in the possibility of 3D printing samples without any additional components, such as adhesion modifiers or wetting modifiers. Detailed information, including information on the synthesis, properties of OCM-2 and the physical and mechanical characteristics of polymers based thereupon, is given in [17, 18].

The DSC method was used to obtain sets of values of the total enthalpies of reactions, whose averaged values were then used to calculate the degree of conversion. The results are presented in Table 1.

Table 1. Enthalpy of reaction and conversion degree of the photopolymerizable composition at 20°C

| UV absorber | Total enthalpy of reaction, J/g | Degree of conversion, % |
|------------------|---------------------------------|-------------------------|
| Without absorber | 220.9 | 81.0 |
| Triazole | 206.3 | 75.9 |
| Camphor anil | 219.5 | 80.8 |

It can be seen from the obtained data that the degree of conversion at 20°C does not reach 90% in all cases. However, the values for the PPC-containing camphor anils practically coincide with those for the composition without a UV absorber. Increasing the temperature to values created in the printing zone (30–40°C depending on the device) should promote a deeper polymerization, which is demonstrated by the values obtained when processing the results of experiments conducted at different temperatures (Table 2).

Table 2. Conversion degree of the photopolymerizable composition at different temperatures

| Temperature, °C | Conversion degree, % | |
|-----------------|----------------------|--------------|
| | Without UV absorbers | Camphor anil |
| 20 | 81.0 | 80.8 |
| 30 | 91.1 | 93.1 |
| 40 | 95.9 | 93.5 |

Considering that the post-processing of the samples includes not only the rapid removal of unpolymerized PPC residues from the samples with isopropanol and drying, but also the stage of post-polymerization at an elevated temperature, it was assumed that the final degree of conversion of the oligomer into a polymer would be higher than that calculated from the DSC results. The degree of curing achieved under real conditions (3D printing with subsequent post-processing) was determined using gel-sol analysis. The content of the gel fraction in the samples, which was 98.2–98.3%, indicates the production of densely networked polymers and the practical absence of a significant effect of UV absorbers in the studied concentration on the formation of three-dimensionally cross-linked products.

An assessment of the physical and mechanical characteristics obtained under 3D printing conditions of materials (Tables 3 and 4) showed that the level of achieved properties determined by the indicators under tension and bending is practically independent of the UV absorber used; moreover, the difference in values is within the limits of measurement error.

⁴ GOST 11262-2017. Interstate Standard. Plastics. Tensile test method. Moscow: Standartinform; 2018 (in Russ.).

⁵ GOST 4648-2014. Interstate Standard. Plastics. Method of static bending test. Moscow: Standartinform; 2016 (in Russ.).

⁶ GOST 12021-2017. Interstate Standard. Plastics and ebonite. Method for determination of temperature of deflection under load. Moscow: Standartinform; 2018 (in Russ.).

⁷ GOST 24621-2015. Interstate Standard. Plastics and ebonite. Determination of indentation hardness by means of a durometer (Shore hardness). Moscow: Standartinform; 2018 (in Russ.).

Table 3. Properties of materials under bending stress conditions

| UV absorber | Modulus of elasticity, GPa | Maximum force, MPa | Relative elongation at maximum force, % | Force at failure, MPa | Relative elongation at failure, % |
|------------------|----------------------------|--------------------|---|-----------------------|-----------------------------------|
| Without absorber | 3.06 | 116.2 | 5.9 | 112.4 | 7.0 |
| Triazole | 3.09 | 117.6 | 6.1 | 114.2 | 7.0 |
| Camphor anil | 3.10 | 117.4 | 5.7 | 115.6 | 6.0 |

Table 4. Properties of materials under tensile stress conditions and Shore D hardness

| UV absorber | Tensile strength, MPa | Relative elongation, % | Shore D hardness, conventional units |
|------------------|-----------------------|------------------------|--------------------------------------|
| Without absorber | 79.0 | 4.8 | 89 |
| Triazole | 80.4 | 5.5 | 89 |
| Camphor anil | 78.4 | 4.4 | 89 |

It should be noted that the obtained tensile strength values are 20% higher than similar values for samples formed under conditions of material initiation, as well as being close in values to materials obtained under conditions of radiation polymerization [17]. Apparently, this is due to the absence of a temperature gradient during polymerization realized under the conditions of the 3D printing method used at the selected layer thickness and the consequent minimization of internal stress.

The differences in the values of heat deflection for different component compositions of PPC (Table 5) are within the limits of experimental error.

Table 5. Heat deflection temperature

| UV absorber | Bending stress, MPa | T , °C |
|------------------|---------------------|----------|
| Without absorber | 0.45 | 91 |
| | 1.8 | 72 |
| Triazole | 0.45 | 88 |
| | 1.8 | 69 |
| Camphor anil | 0.45 | 90 |
| | 1.8 | 69 |

Linear accuracy during printing, which is of decisive importance in additive technologies, was assessed using a standard sample (Fig. 1).

The numerical values given in Table 5 confirm the possibility of using camphor anil to obtain samples having a smaller deviation from the linear dimensions than in

the absence of a UV absorber in the PPC composition or when using triazole as such. In general, the deviation of the linear accuracy does not exceed 1% (Table 6).

It should be noted that the absorption of anil camphor in the UV range (Fig. 2) in the region of maximum emission (406–409 nm) changes insignificantly (from 0.042 to 0.036), whereas in case of triazole it decreases more than twofold (from 0.056 to 0.024). Apparently, this is the reason for the greater linear accuracy when printing using anil camphor as a UV absorber.

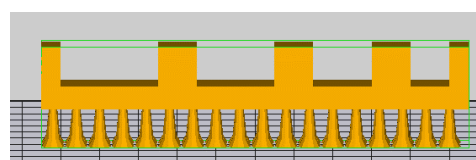


Fig. 1. Sample model for determining linear accuracy

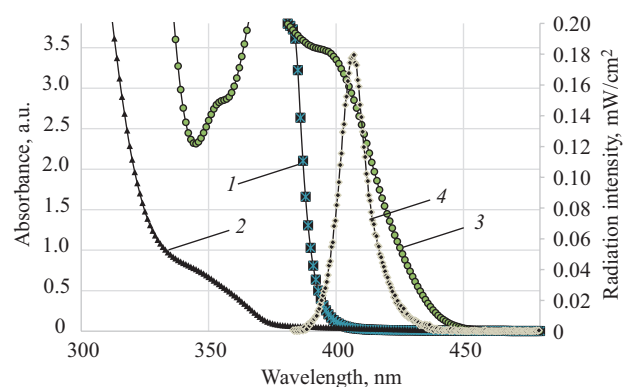


Fig. 2. UV spectra of triazole (1), camphor anil (2), and photoinitiator BAPO (3); emission spectrum of the 3D printer radiation source (4)

Table 6. Results of linear accuracy determination during printing

| Specified size, mm | Deviation from specified size, % | | |
|-----------------------|----------------------------------|----------|--------------|
| | Without absorber | Triazole | Camphor anil |
| Block dimensions | | | |
| 55 | 1.22 | 1.29 | 1.00 |
| 5 | 0.93 | 1.00 | 0.09 |
| 8 | 1.11 | 1.42 | 0.64 |
| Distance between tabs | | | |
| 5 | -0.07 | -0.11 | -0.16 |
| 7.5 | -0.05 | -0.09 | -0.05 |
| 10 | -0.04 | -0.05 | -0.04 |
| 12.5 | -0.09 | -0.20 | -0.04 |
| End tabs | | | |
| 2.5 | 0.05 | 0.24 | 0.18 |
| 5 | 0.15 | 0.22 | 0.18 |
| 5 | 0.24 | 0.22 | 0.15 |
| 5 | 0.47 | 0.24 | 0.07 |
| 2.5 | 0.16 | 0.20 | 0.09 |

CONCLUSIONS

Thus, the analysis of the totality of the obtained results confirms the efficiency of using camphor anil in the PPC composition as a UV absorber. With high linear printing accuracy, it is possible to obtain densely meshed polymers characterized by desirable physicochemical characteristics and heat deflection temperature.

Acknowledgments

The study was funded by the Russian Science Foundation grant No. 22-13-20062, <https://rscf.ru/project/22-13-20062/>, and the Volgograd Oblast Administration grant under Agreement No. 2 dated May 31, 2024 using the park of analytical instruments of the Center for Collective Use “Physicochemical

Research Methods” of the Volgograd State Technical University.

Authors' contributions

N.V. Sidorenko—research concept, DSC measurements, initial manuscript drafting.

M.A. Vaniev—adjustment of the experimental plan, final manuscript preparation.

Iu.M. Mkrtchyan—3D printing, post-processing, property determination, and linear accuracy determination.

N.A. Salykin—synthesis of camphor anil, preparation of photocurable composition, gel-sol analysis, DSC data processing.

A.A. Vernigora—extraction and purification of camphor anil.

I.A. Novakov—adjustment of the experimental plan, final manuscript preparation.

The authors declare no conflicts of interest.

REFERENCES

1. Al Rashid A., Ahmed W., Khalid M.Y., Koç M. Vat photopolymerization of polymers and polymer composites: Processes and applications. *Addit. Manuf.* 2021;47:102279. <https://doi.org/10.1016/j.addma.2021.102279>
2. Lalatovic A., Vaniev M.A., Sidorenko N.V., Gres I.M., Dyachenko D. Y., Makedonova Y.A. A review on Vat Photopolymerization 3D-printing processes for dental application. *Dent. Mater.* 2022;38(11):e284–e296. <https://doi.org/10.1016/j.dental.2022.09.005>
3. Caussin E., Moussally C., Le Goff S., Fasham T., Troizier-Cheyne M., Tapie L., François P. Vat photopolymerization 3D printing in dentistry: A comprehensive review of actual popular technologies. *Materials.* 2024.;17(4):950. <https://doi.org/10.3390/ma17040950>
4. Dileep C., Jacob L., Umer R., Butt H. Review of Vat photopolymerization 3D Printing of Photonic Devices. *Addit. Manuf.* 2024. P. 104189. <https://doi.org/10.1016/j.addma.2024.104189>
5. Seo J.W., Kim G.M., Choi Y., Cha J.M., Bae H. Improving printability of digital-light-processing 3D bioprinting via photoabsorber pigment adjustment. *Int. J. Mol. Sci.* 2022;23(10):5428. <https://doi.org/10.3390/ijms23105428>
6. Gastaldi M., Cardano F., Zanetti M., Viscardi G., Barolo C., Bordiga S., Magdassi S., Fin A., Roppolo I. Functional dyes in polymeric 3D printing: applications and perspectives. *ACS Mater. Lett.* 2021;3(1):1–17. <https://doi.org/10.1021/acsmaterialslett.0c00455>
7. Kowsari K., Zhang B., Panjwani S., Chen Z., Hingorani H., Akbari S., Fang N.X., Ge Q. Photopolymer formulation to minimize feature size, surface roughness, and stair-stepping in digital light processing-based three-dimensional printing. *Addit. Manuf.* 2018;24:627–638. <https://doi.org/10.1016/j.addma.2018.10.037>
8. Gong H., Bickham B.P., Woolley A.T., Nordin G.P. Custom 3D printer and resin for 18 μm \times 20 μm microfluidic flow channels. *Lab Chip.* 2017;17(17):2899–2909. <https://doi.org/10.1039/c7lc00644f>
9. Endo A., Yamasaki S., Uno S. *Lithographic Printing Plate Precursor and Method of Producing Printing Plate*: USA Pat. US 7939240. Publ. 10.05.2011.
10. Kunita K., Yamasaki S. *Planographic Printing Plate Precursor Using a Polymerizable Composition*: Pat. EP 3182204. Publ. 21.06.2017.
11. Bail R., Hong J.Y., Chin B.D. Effect of a red-shifted benzotriazole UV absorber on curing depth and kinetics in visible light initiated photopolymer resins for 3D printing. *J. Ind. Eng. Chem.* 2016;38:141–145. <https://doi.org/10.1016/j.jiec.2016.04.017>
12. Kolb C., Lindemann N., Wolter H., Sextl G. 3D-printing of highly translucent ORMOCER[®]-based resin using light absorber for high dimensional accuracy. *J. Appl. Polym. Sci.* 2021;138(3):49691. <https://doi.org/10.1002/app.49691>
13. Novakov I.A., Brunilin R.V., Vernigora A.A., Davidenko A.V., Deshevov P.P., Navrotskii M.B. *Method for Producing D-Camphor Anils*: RF Pat. 2750161. Publ. 22.06.2021 (in Russ.).
14. Chesnokov S.A., Zakharina M.Y., Shaplov A., Lozinskaya E.I., Malyshkina I.A., Abakumov G.A., Vidal F., Vygodskii Y.S. Photopolymerization of Poly(ethylene glycol) dimethacrylates: The influence of ionic liquids on the formulation and the properties of the resultant polymer materials. *J. Polym. Sci. Part A: Polym. Chem.* 2010;48(11):2388–2409. <https://doi.org/10.1002/pola.24008>

СПИСОК ЛИТЕРАТУРЫ

1. Al Rashid A., Ahmed W., Khalid M.Y., Koç M. Vat photopolymerization of polymers and polymer composites: Processes and applications. *Addit. Manuf.* 2021;47:102279. <https://doi.org/10.1016/j.addma.2021.102279>
2. Lalatovic A., Vaniev M.A., Sidorenko N.V., Gres I.M., Dyachenko D.Y., Makedonova Y.A. A review on Vat Photopolymerization 3D-printing processes for dental application. *Dent. Mater.* 2022;38(11):e284–e296. <https://doi.org/10.1016/j.dental.2022.09.005>
3. Caussin E., Moussally C., Le Goff S., Fasham T., Troizier-Cheyne M., Tapie L., François P. Vat photopolymerization 3D printing in dentistry: A comprehensive review of actual popular technologies. *Materials.* 2024.;17(4):950. <https://doi.org/10.3390/ma17040950>
4. Dileep C., Jacob L., Umer R., Butt H. Review of Vat photopolymerization 3D Printing of Photonic Devices. *Addit. Manuf.* 2024. P. 104189. <https://doi.org/10.1016/j.addma.2024.104189>
5. Seo J.W., Kim G.M., Choi Y., Cha J.M., Bae H. Improving printability of digital-light-processing 3D bioprinting via photoabsorber pigment adjustment. *Int. J. Mol. Sci.* 2022;23(10):5428. <https://doi.org/10.3390/ijms23105428>
6. Gastaldi M., Cardano F., Zanetti M., Viscardi G., Barolo C., Bordiga S., Magdassi S., Fin A., Roppolo I. Functional dyes in polymeric 3D printing: applications and perspectives. *ACS Mater. Lett.* 2021;3(1):1–17. <https://doi.org/10.1021/acsmaterialslett.0c00455>
7. Kowsari K., Zhang B., Panjwani S., Chen Z., Hingorani H., Akbari S., Fang N.X., Ge Q. Photopolymer formulation to minimize feature size, surface roughness, and stair-stepping in digital light processing-based three-dimensional printing. *Addit. Manuf.* 2018;24:627–638. <https://doi.org/10.1016/j.addma.2018.10.037>
8. Gong H., Bickham B.P., Woolley A.T., Nordin G.P. Custom 3D printer and resin for 18 μm \times 20 μm microfluidic flow channels. *Lab Chip.* 2017;17(17):2899–2909. <https://doi.org/10.1039/c7lc00644f>
9. Endo A., Yamasaki S., Uno S. *Lithographic Printing Plate Precursor and Method of Producing Printing Plate*: USA Pat. US 7939240. Publ. 10.05.2011.
10. Kunita K., Yamasaki S. *Planographic Printing Plate Precursor Using a Polymerizable Composition*: Pat. EP 3182204. Publ. 21.06.2017.
11. Bail R., Hong J.Y., Chin B.D. Effect of a red-shifted benzotriazole UV absorber on curing depth and kinetics in visible light initiated photopolymer resins for 3D printing. *J. Ind. Eng. Chem.* 2016;38:141–145. <https://doi.org/10.1016/j.jiec.2016.04.017>
12. Kolb C., Lindemann N., Wolter H., Sextl G. 3D-printing of highly translucent ORMOCER[®]-based resin using light absorber for high dimensional accuracy. *J. Appl. Polym. Sci.* 2021;138(3):49691. <https://doi.org/10.1002/app.49691>
13. Новиков И.А., Брунилин Р.В., Вернигора А.А., Давиденко А.В., Дешевов П.П., Навроцкий М.Б. *Способ получения анилов D-камфоры*: пат. 2750161 РФ. Заявка № 2020140906; заявл. 11.12.2020; опубл. 22.06.2021.
14. Chesnokov S.A., Zakharina M.Y., Shaplov A., Lozinskaya E.I., Malyshkina I.A., Abakumov G.A., Vidal F., Vygodskii Y.S. Photopolymerization of Poly(ethylene glycol) dimethacrylates: The influence of ionic liquids on the formulation and the properties of the resultant polymer materials. *J. Polym. Sci. Part A: Polym. Chem.* 2010;48(11):2388–2409. <https://doi.org/10.1002/pola.24008>

15. Buravov B.A., Al-Khamzawi A., Bochkarev E.S., Grichishkina N.Kh., Borisov S.V., Sidorenko N.V., Tuzhikov O.I., Tuzhikov O.O. Synthesis of new photo-cured phosphorus-containing oligoestermethacrylates with a spacer in the structure. *Fine Chem. Technol.* 2022;17(5):410–426. <https://doi.org/10.32362/2410-6593-2022-17-5-410-426>
16. Sidorenko N.V., Mkrtychyan Yu.M., Vaniev M.A., Popov N.I., Vernigora A.A., Davidenko A.V., Salykin N.A., Novakov I.A. *Use of D-Camphor Anils as UV Absorbers of Photopolymerizable Compositions for 3D Printing*: RF Pat. 2794337. Publ. 17.04.2023 (in Russ.).
17. Sivergin Yu.M., Pernikis R.Ya., Kireeva S.M. *Поликарбонат(мет)акрилаты (Polycarbonate(met)acrylates)*. Riga: Zinatne; 1988. 213 p. (in Russ.). ISBN 5-7966-0036-2
18. Matveeva I.A., Shashkova V.T., Lyubimov A.V., Lyubimova G.V., Koltsova L.S., Shienok A.I., Zaichenko N.L., Levin P.P. Luminescent Properties of Polycarbonate Methacrylates Containing Organic Fluorescent Dyad. *Coatings*. 2023;13(6):1071. <https://doi.org/10.3390/coatings13061071>
15. Буравов Б.А., Аль-Хамзави А., Бочкарев Е.С., Гричишкина Н.Х., Борисов С.В., Сидоренко Н.В., Тужиков О.И., Тужиков О.О. Синтез новых фотоотверждаемых фосфорсодержащих олигоэфирметакрилатов со спейсером в структуре. *Тонкие химические технологии*. 2022;17(5): 410–426. <https://doi.org/10.32362/2410-6593-2022-17-5-410-426>
16. Сидоренко Н.В., Мкртчян Ю.М., Ваниев М.А., Попов Н.И., Вернигора А.А., Давиденко А.В., Салыкин Н.А., Новаков И.А. *Использование анилов D-камфоры в качестве УФ-абсорберов фотополимеризующихся композиций для 3D-печати*: пат. 2794337 РФ. Заявка № 2022132607А; заявл. 13.12.2022; Оpubл. 17.04.2023.
17. Сивергин Ю.М., Перникис Р.Я., Киреева С.М. *Поликарбонат(мет)акрилаты*. Рига: Зинатне; 1988. 213 с. ISBN 5-7966-0036-2
18. Matveeva I.A., Shashkova V.T., Lyubimov A.V., Lyubimova G.V., Koltsova L.S., Shienok A.I., Zaichenko N.L., Levin P.P. Luminescent Properties of Polycarbonate Methacrylates Containing Organic Fluorescent Dyad. *Coatings*. 2023;13(6):1071. <https://doi.org/10.3390/coatings13061071>

About the Authors

Nina V. Sidorenko, Cand. Sci. (Eng.), Associate Professor, Department of Chemistry and Processing Technology of Elastomers, Volgograd State Technical University (28, pr. im. V.I. Lenina, Volgograd, 400005, Russia). E-mail: nvsidorenko@vstu.ru. ResearcherID A-9544-2014, Scopus Author ID 16308435400, RSCI SPIN-code 5155-3692, <https://orcid.org/0000-0002-6113-290X>

Marat A. Vaniev, Dr. Sci. (Eng.), Head of the Department of Chemistry and Processing Technology of Elastomers, Volgograd State Technical University (28, pr. im. V.I. Lenina, Volgograd, 400005, Russia). E-mail: vaniev@vstu.ru. Scopus Author ID 14063995400, RSCI SPIN-code 9260-2745, <https://orcid.org/0000-0001-6511-5835>

Yurii M. Mkrtychyan, Assistant, Department of Chemistry and Processing Technology of Elastomers, Volgograd State Technical University (28, pr. im. V.I. Lenina, Volgograd, 400005, Russia). E-mail: m.sc.yuri@vstu.ru. RSCI SPIN-code 1363-6544, <https://orcid.org/0009-0008-6119-8125>

Nikita A. Salykin, Specialist (Spectroscopy and Thermal Analysis), Analytical R&D Support Center of SIBUR-INNOVATIONS LLC, SIBUR Holding (2, bld. 270, Kuzovlevsky tract, Tomsk, 634067, Russia). E-mail: behefun@gmail.com. Scopus Author ID 57415508300, RSCI SPIN-code 7262-9636, <https://orcid.org/0000-0003-3380-0568>

Andrey A. Vernigora, Senior Lecturer, Organic Chemistry Department, Volgograd State Technical University (28, pr. im. V.I. Lenina, Volgograd, 400005, Russia). E-mail: vernigora.andrey@vstu.ru. Scopus Author ID 57191338560, RSCI SPIN-code 8776-4755, <https://orcid.org/0000-0001-6456-0910>

Ivan A. Novakov, Academician at the Russian Academy of Sciences, Dr. Sci. (Chem.), Head of the Department of Analytical, Physical Chemistry and Physical Chemistry of Polymers, President of the Volgograd State Technical University (28, pr. im. V.I. Lenina, Volgograd, 400005, Russia). E-mail: president@vstu.ru. Scopus Author ID 7003436556, ResearcherID I-4668-2015, RSCI SPIN-code 2075-5298, <https://orcid.org/0000-0002-0980-6591>

Об авторах

Сидоренко Нина Владимировна, к.т.н., доцент кафедры «Химия и технология переработки эластомеров», ФГБОУ ВО «Волгоградский государственный технический университет» (400005, Россия, Волгоград, пр-т им. В.И. Ленина, д. 28). E-mail: nvsidorenko@vstu.ru. ResearcherID A-9544-2014, Scopus Author ID 16308435400, SPIN-код РИНЦ 5155-3692, <https://orcid.org/0000-0002-6113-290X>

Ваниев Марат Абдурахманович, д.т.н., доцент, заведующий кафедрой «Химия и технология переработки эластомеров», ФГБОУ ВО «Волгоградский государственный технический университет» (400005, Россия, Волгоград, пр-т им. В.И. Ленина, д. 28). E-mail: vaniev@vstu.ru. Scopus Author ID 14063995400, SPIN-код РИНЦ 9260-2745, <https://orcid.org/0000-0001-6511-5835>

Мкртчян Юрий Мушегович, ассистент, кафедра «Химия и технология переработки эластомеров», ФГБОУ ВО «Волгоградский государственный технический университет» (400005, Россия, Волгоград, пр-т им. В.И. Ленина, д. 28). E-mail: m.sc.yuri@vstu.ru. SPIN-код РИНЦ 1363-6544, <https://orcid.org/0009-0008-6119-8125>

Салькин Никита Андреевич, специалист (спектроскопия и термический анализ), Центр аналитической поддержки НИОКР, ООО «СИБУР-ИННОВАЦИИ», ПАО «СИБУР Холдинг» (634067, Россия, г. Томск, Кузовлевский тракт, д. 2, стр. 270). E-mail: behefun@gmail.com. Scopus Author ID 57415508300, SPIN-код РИНЦ 7262-9636, <https://orcid.org/0000-0003-3380-0568>

Вернигора Андрей Александрович, старший преподаватель, кафедра «Органическая химия», ФГБОУ ВО «Волгоградский государственный технический университет» (400005, Россия, Волгоград, пр-т им. В.И. Ленина, д. 28). E-mail: vernigora.andreyu@gmail.com. Scopus Author ID 57191338560, SPIN-код РИНЦ 8776-4755, <https://orcid.org/0000-0001-6456-0910>

Новаков Иван Александрович, академик Российской академии наук, д.х.н., профессор, президент, заведующий кафедрой «Аналитическая, физическая химия и физико-химия полимеров», ФГБОУ ВО «Волгоградский государственный технический университет» (400005, Россия, Волгоград, пр-т им. В.И. Ленина, д. 28). E-mail: president@vstu.ru. Scopus Author ID 7003436556, ResearcherID I-4668-2015, SPIN-код РИНЦ 2075-5298, <https://orcid.org/0000-0002-0980-6591>

Translated from Russian into English by M. Povorin

Edited for English language and spelling by Thomas A. Beavitt

Synthesis and processing of polymers and polymeric composites
Синтез и переработка полимеров и композитов на их основе

UDC 541.68

<https://doi.org/10.32362/2410-6593-2025-20-2-146-155>

EDN DTICXX



RESEARCH ARTICLE

Gas permeability of films based on low-density polyethylene–ethylene-vinyl acetate blends with cellulosic fillers

Pavel G. Shelenkov^{1,2,✉}, Petr V. Pantyukhov^{1,2}, Anatoly A. Olkhov^{1,2}, Anatoly A. Popov^{1,2}

¹ Emanuel Institute of Biochemical Physics, Russian Academy of Sciences, Moscow, 119334 Russia

² Plekhanov Russian University of Economics, Moscow, 117997 Russia

✉ Corresponding author, e-mail: shell1183@mail.ru

Abstract

Objectives. The work set out to characterize the gas permeability properties of biocomposite materials based on synthetic polymers and natural fillers.

Methods. The studied materials were blends of low-density polyethylene (LDPE) and ethylene–vinyl acetate (EVA) copolymer, with different LDPE/EVA ratios, as well as biocomposites based on these polymers with natural cellulosic fillers (wood flour (WF) and microcrystalline cellulose (MCC)). The coefficients of gas permeability, diffusion, and oxygen solubility were determined in the obtained composites using the manometric method. The dependence of the diffusion properties of LDPE/EVA blends and biocomposites made of LDPE/EVA/natural filler on the EVA content in the composite was considered.

Results. We demonstrated that, as the EVA content in the polymer matrix increases, so also do its solubility and coefficients of gas permeability and oxygen diffusion. The variation in the diffusion characteristics of biocomposite materials obtained using solid filler particles that differ significantly in shape is characterized. The presented interpretation of the obtained results explains the decrease in diffusion in terms of increased rigidity of biocomposites.

Conclusions. An increase in the EVA content in blends with LDPE leads to a linear increase in the gas permeability for oxygen, as well as enhanced diffusion and solubility of oxygen in the film. Upon adding a cellulosic filler, the gas permeability of the composites drops almost twofold. The decrease in gas permeability is associated with the morphology of the filler particles increasing the path of gas molecules. Oxygen solubility for composites with MCC and WF is not the same due to the shape of the filler particles. Rough and more elongated WF particles form a more rigid, less permeable structure of the biocomposite than smooth spherical MCC particles.

Keywords

gas permeability, diffusion, microcrystalline cellulose, wood flour, ethylene-vinyl acetate copolymer blends, biocomposites

Submitted: 03.10.2024

Revised: 29.11.2024

Accepted: 21.02.2025

For citation

Shelenkov P.G., Pantyukhov P.V., Olkhov A.A., Popov A.A. Gas permeability of films based on low-density polyethylene–ethylene-vinyl acetate blends with cellulosic fillers. *Tonk. Khim. Tekhnol. = Fine Chem. Technol.* 2025;20(2):146–155. <https://doi.org/10.32362/2410-6593-2025-20-2-146-155>

НАУЧНАЯ СТАТЬЯ

Газопроницаемость пленок на основе смесей полиэтиленов низкой плотности – сэвиленов с целлюлозосодержащими наполнителями

П.Г. Шеленков^{1,2,✉}, П.В. Пантюхов^{1,2}, А.А. Ольхов^{1,2}, А.А. Попов^{1,2}

¹ Институт биохимической физики им. Н.М. Эмануэля Российской академии наук, Москва, 119334 Россия

² Российский экономический университет им. Г.В. Плеханова, Москва, 115054 Россия

✉ Автор для переписки, e-mail: shell1183@mail.ru

Аннотация

Цели. Изучение свойств газопроницаемости биокomпозитных материалов на основе синтетических полимеров и природных наполнителей.

Методы. Объектами исследования являлись смеси полиэтилена низкой плотности (ПЭНП) и сополимера этилена с винилацетатом (СЭВА), при различном соотношении ПЭНП/СЭВА, а также биокomпозиты на основе данных полимеров с природными целлюлозосодержащими наполнителями (древесная мука (ДМ) и микрокристаллическая целлюлоза (МКЦ)). У полученных композитов манометрическим методом определяли коэффициенты газопроницаемости, диффузии и растворимости по кислороду. Рассматривалась зависимость диффузионных свойств полимерных смесей состава ПЭНП/СЭВА и биокomпозитов состава ПЭНП/СЭВА/природный наполнитель от содержания СЭВА в композитах.

Результаты. Показано, что с увеличением содержания СЭВА в полимерной матрице увеличивается коэффициент газопроницаемости, коэффициент диффузии кислорода и его растворимость. Показана разница диффузионных характеристик биокomпозиционных материалов, полученных с использованием твердых частиц наполнителей, существенно различающихся по своей форме. Дана интерпретация полученных результатов, объясняющая снижение диффузии повышением жесткости биокomпозитов.

Выводы. С повышением содержания СЭВА в смеси с ПЭНП линейно увеличивается газопроницаемость по кислороду. Также при этом увеличиваются диффузия и растворимость кислорода в пленке. При введении целлюлозосодержащего наполнителя, газопроницаемость композитов падает практически в два раза. Очевидно, что снижение газопроницаемости связано с морфологией частиц наполнителя, увеличивающего путь молекулам газа. Растворимость кислорода для композитов с МКЦ и ДМ не одинакова, что связано с формой частиц наполнителей. Шероховатые и более вытянутые частицы ДМ формируют более жесткую, менее проницаемую структуру биокomпозита, чем гладкие сферические частицы МКЦ.

Ключевые слова

газопроницаемость, диффузия, микрокристаллическая целлюлоза, древесная мука, смеси сополимера этилена с винилацетатом, биокomпозиты

Поступила: 03.10.2024

Доработана: 29.11.2024

Принята в печать: 21.02.2025

Для цитирования

Шеленков П.Г., Пантюхов П.В., Ольхов А.А., Попов А.А. Газопроницаемость пленок на основе смесей полиэтиленов низкой плотности – сэвиленов с целлюлозосодержащими наполнителями. *Тонкие химические технологии*. 2025;20(2):146–155. <https://doi.org/10.32362/2410-6593-2025-20-2-146-155>

INTRODUCTION

The most inert of the polyolefins, polyethylene undergoes slow degradation in the environment [1]. At the same time, it holds the first place in terms of production volumes among the whole class of polyolefins. The valuable properties combined in this material have led to the widespread use of polyethylene in industry and for domestic purposes [2]. Polyethylene does not react with alkalis, is resistant to acids and salts, and is inert to the action of microbiota from the environment [3–4]. At the same time, polyethylene offers gas and vapor

permeability. Gas permeation through the films can be considered as a two-stage diffusion of liquid. In the first stage, the diffusant is equilibrated by the film surface, while in the second stage, it diffuses towards a lower chemical potential. The gas permeability of the films determines whether the material can be used for packaging purposes. For certain packaged products, the gas permeability of the film should be high, while for others, conversely, it should be minimal [5]. Thus, this characteristic determines the scope of application of the material [6]. The gas permeation rate of a film depends largely on temperature [7]. Thus, R. Ahvenainen [8]

proposed to conduct a study of automatic packaging at 10, 15, 20, and 25°C to determine O₂ and CO₂ gas permeation rates of selected films and film laminates at these temperatures. Then, as noted by the authors [9], an attempt was made to apply the Arrhenius equation to develop models to predict the gas permeation rates of selected polymer films and film laminates at different temperatures. It is found that film thickness and test temperature have a significant effect on gas permeability. However, the gas permeation rate of films is more affected by their thickness than temperature.

A recent study has shown that in some partially crystallizing polymers (gutta-percha, polyethylene, polyamide) after reaching the limiting orientation of macromolecules, gas permeability decreases due to an additional increase in the degree of crystallinity or an increase in the packing density of amorphous polymer regions [10].

The change in gas permeability values (P) is due to the change in the diffusion coefficient (D), while the gas solubility coefficient does not change significantly when the film sorbs organic solvents. The gas permeability values of polyethylene for O₂, N₂, CO₂ are not affected by the relative humidity of the gases. Meanwhile, the gas permeability of a mixture of gases often depends on the high solubility of one of the gases included in the mixture. Thus, P.V. Kozlov and G.I. Braginskii in their study of polyethylene in relation to a mixture of ethane and butane-4 showed that the permeability of the mixture increases with increasing butane concentration as compared to the calculated value, which is based on the initial P coefficients [11]. The anomaly of the values of gas permeability and CO₂ diffusion coefficients is associated with high values of carbon dioxide sorption by polyethylene. This phenomenon was also noted in other works.

Many researchers have obtained bulk nanocomposite structures by introducing nanoparticles—i.e., fillers having at least one size smaller than 100 nm—into polymer matrices. This has proven to be one of the most promising directions in the development of packaging materials with improved mass transfer properties. The expected role of these inclusions is to achieve a significant reduction in mass transfer properties compared to the original matrix. The filler particles act as physical barriers to diffusion and penetration of diffusing molecules, which must follow a more tortuous path. This phenomenon is called the tortuosity effect or increase in the length of the diffusion path. However, N.N. Barashkov [12] concluded that tortuosity, the main mechanism proposed to explain the decrease in permeability of nanocomposites, often fails to explain the effect of nanoparticles on the barrier properties of nanocomposites.

Note that the analysis of current experience published on various profile forums, websites of organizations, as well as in scientific journals allows us to conclude that the use of biodegradable composites and polymers derived from various renewable sources is currently preferred [13]. The use of eco-friendly materials helps to protect the environment as these materials degrade rapidly in it. Thus, the number of products made from renewable resources has been increasing rapidly in recent years. Applications of green products include food packaging, drug delivery, tissue engineering, medical implants, composite technologies and eco-friendly sorbents [14].

In recent years, interest in the use of biodegradable materials has been increasing due to their eco-friendly, renewable and environmentally friendly properties. In addition, certain specific properties such as low toxicity and density, biocompatibility and biodegradability favor their replacement of synthetic materials. Certain authors have pointed out the importance of cellulose, chitin and starch for the development of environmentally friendly composites [15, 16]. These fillers have played a significant role in the success of developing high strength composites [17].

In [18], lignosulfonates (a byproduct of wood processing) were introduced into polypropylene, which led to an increase in thermal stability. The introduction of more than 50 wt % wood flour (WF) into ethylene-vinyl acetate (EVA) copolymer [19] significantly increased the thermal oxidation resistance of the material due to the diffusion of polyphenolic components (natural antioxidants) from wood into the synthetic polymer during compounding. Thus, biocomposites with wood components are well protected from oxidative degradation during processing and can withstand several recycling cycles.

There are many works devoted to the study of polyethylene composites with natural polymeric fillers such as starch, cellulose, cellulose-containing particles, chitosan, etc. [20–23]. These composites are created to impart biodegradable properties to traditional polyolefins. To improve adhesion between polar natural filler and nonpolar polyethylene matrix, combining additives (compatibilizers) are introduced. One such additive is EVA. In our previous studies, EVA-based superconcentrates filled with WF and microcrystalline cellulose (MCC) were obtained and investigated [24–26]. In these works, biocomposites made from previously obtained superconcentrates were investigated by dilution with low density polyethylene (LDPE). Biocomposites with WF content of 30, 40, 50, 50, 60, 70 wt % were investigated in [27]. When the filler content was higher than 30 wt %, a significant decrease in the complex of mechanical properties was observed. In this study, the filler content for all biocomposites was selected at

Table 1. Characteristics of fillers

| Filler | Cellulose, % | Lignin, % | Pentosans, % | Others, % |
|----------------------------------|--------------|-----------|--------------|-----------|
| Wood flour (WF) | 46 | 20 | 29 | 5 |
| Microcrystalline cellulose (MCC) | 100 | – | – | – |

Table 2. Characteristics of synthetic polymers

| No. | Polymer | Vinyl acetate group content | | Melt flow index (MFI), g/10 min | Tensile strength, MPa | Elongation at break, % | Density, g/cm ³ |
|-----|----------------|-----------------------------|--------|---------------------------------|-----------------------|------------------------|----------------------------|
| | | wt % | mol. % | | | | |
| 1 | EVA 28025 | 28 | 11 | 24.8–25.2 | >12.0 | >850 | 0.950–0.952 |
| 2 | LDPE 10803-020 | – | – | 1.8–2.2 | >12.2 | >550 | 0.917–0.920 |

30 wt % as comprising the limiting filler content in the polymer matrix while maintaining acceptable operational and technological characteristics. The aim of the work was to study their gas permeability in order to determine possible applications.

MATERIALS AND METHODS

For the composites manufacturing, LDPE grade 10803-020 produced by *Ufaorgsintez* (Russia), EVA grade EA 28025 produced by *LG Chem* (South Korea) were used. The fillers used were MCC grade 101 produced by *PO Progress* (Kemerovo, Russia) and WF, comprising a blend of coniferous and deciduous trees supplied by *Novotop* (Moscow, Russia). The fillers were pre-dried at 105°C to constant weight (~5 h), then sieved through a sieve with a mesh diameter of 100 µm. Table 1 shows the composite of the fillers, Table 2 shows the characteristics of the initial synthetic polymers (LDPE and EVA).

Binary (LDPE/EVA) and ternary (LDPE/EVA/filler) composites were created having different ratios of LDPE/EVA in the blend (Table 3).

The composites were made on UBL6175BL laboratory heated rollers (*Dongguan BaoPin International Precision Instruments Co.*, China) at roll temperatures of 130 and 150°C and a mixing speed of 8 rpm. After milling the obtained composites using a PM 120 knife mill (*Vibrotechnik*, Russia), they were thermally pressed using a GT-7014-H press (*Gotech Testing Machines Inc.*, Taiwan) at 140°C and a plate clamping force of 15 tons for 2 min; cooling was performed in air. The resultant films having a thickness of 250–270 µm were then used to determine the density and oxygen gas permeability.

Table 3. Component ratios in binary (LDPE/ EVA) and ternary (LDPE/ EVA/filler) composites

| Binary composites | | | |
|--------------------|----------------------|---------------------------------------|-----------|
| No. | LDPE content, wt % | EVA content, wt % | |
| 1 | 100 | 0 | |
| 2 | 80 | 20 | |
| 3 | 70 | 30 | |
| 4 | 60 | 40 | |
| 5 | 50 | 50 | |
| 6 | 40 | 60 | |
| 7 | 20 | 80 | |
| 8 | 0 | 100 | |
| Ternary composites | | | |
| No. | Natural filler, wt % | LDPE/ EVA ratio in the polymer matrix | |
| | | LDPE, wt % | EVA, wt % |
| 1 | 30 | 70 | 0 |
| 2 | | 57 | 13 |
| 3 | | 50 | 20 |
| 4 | | 40 | 30 |
| 5 | | 35 | 35 |
| 6 | | 0 | 70 |

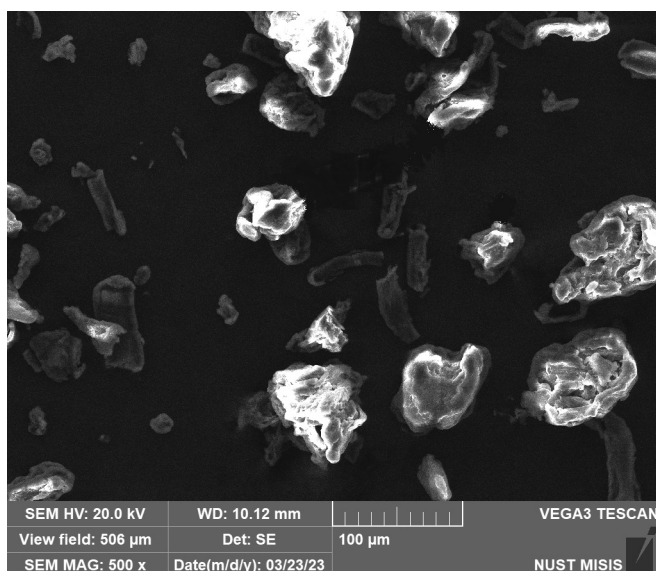
Gas permeability was measured on a VAC-VI instrument (*Labthink*, China) according to ISO 15105-2:2003¹. The gas permeability was measured in oxygen (O₂) at a chamber temperature of 30°C with a measurement range of 0 to 100000 cm³/m² · 24 h · 0.1 MPa. In addition to the gas permeability coefficient, the diffusion coefficient and solubility coefficient were also determined. ISO 15105-2:2003 provides a formula for calculating gas permeability:

$$\text{GTR} = \frac{V_C}{R \cdot T \cdot P_h \cdot A} \cdot \frac{dp}{dt},$$

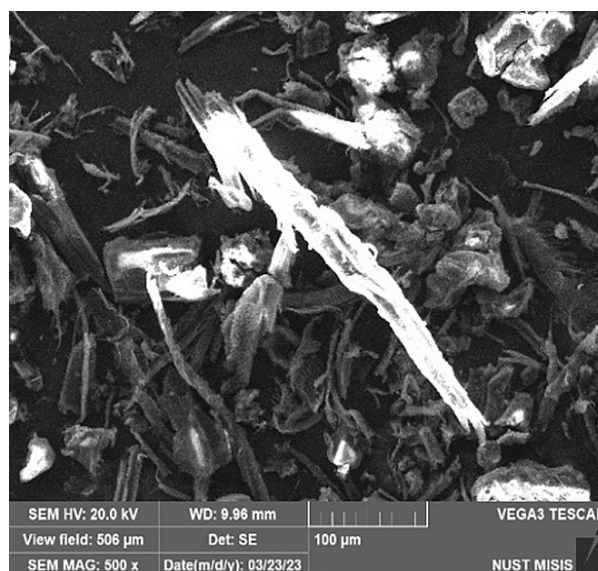
where GTR is gas transmission rate; V_C is the volume of the lower pressure chamber, liters, T is temperature, K; P_h is the gas pressure in the high pressure chamber, Pa; A is the area of the sample through which the diffusion gas passes, m²; R is the universal gas constant, J·K⁻¹·mol⁻¹; $\frac{dp}{dt}$ is the pressure change over

time in the low-pressure chamber, Pa/s. Multiplying GTR by the average thickness of the sample, we obtain the gas permeability coefficient P .

Microphotographs of filler particles were obtained by scanning electron microscopy (SEM). A Vega 3SB scanning electron microscope (*TESCAN GROUP*, Czech Republic) was used, having an accelerating voltage of 20 kV, a working distance from 9 to 15 mm, and a platinum coating.



(a)



(b)

Fig. 2. Microphotographs of filler particles: (a) MCC, (b) WF. Scanning electron microscopy (SEM)

RESULTS AND DISCUSSION

The oxygen gas permeability of films with double (PE/EVA) and ternary composites (PE/EVA/filler) was studied. Figure 1 shows the dependencies of the gas permeability coefficient on the EVA content in the polymer matrix for double and ternary composites. The gas permeability coefficient values increase with increasing EVA content in double blends with LDPE, this dependence has a linear form.

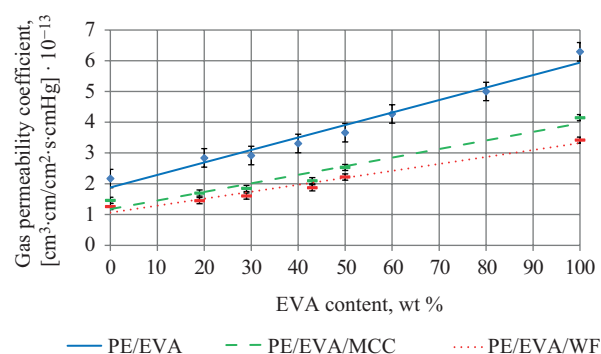


Fig. 1. Dependence of oxygen gas permeability coefficient on EVA content in the polymer matrix

At introduction of 30 wt % of natural filler, the gas permeability decreases almost two-fold. The gas

¹ ISO 15105-2:2003. Interstate Standard. Plastics. Film and sheeting. Determination of gas-transmission rate. Part 2: Equal-pressure method. Moscow: Standartinform; 2010. 12 p. (in Russ.).]

permeability of composites with WF is less than that of composites with MCC. At the same time the type of dependence does not change, while the curve is unaffected by the introduction of filler. The difference in the values of gas permeability coefficients for composites with MCC and WF can be explained in terms of the different morphology of filler particles. The shape and size of filler particles were investigated using SEM. Microphotographs of the particles are presented in Fig. 2.

As can be seen from Fig. 2, WF particles are more elongated and branched, while MCC particles are more spherical in shape and have a smooth surface. Accordingly, the greater the filler particle length, the longer the diffusion path of the gas passing through the film. When films are fabricated by pressing, the WF particles are arranged uniformly in its plane, i.e., perpendicular to the direction of oxygen flow through the film. It was shown in [28] that the diffusion rate was 1 or 2 orders of magnitude higher in the axial direction of the wood fibers than in the radial direction. The diffusion of oxygen through wood was studied in [29] to evaluate the oxidation of wine stored for extended periods of time in oak barrels. The study shows that the very low rate of oxygen diffusion through wood depends on the type of wood. An approximate scheme of the gas path through films with spherical and cylindrical filler particles is shown in Fig. 3. The oxygen diffusion path length can additionally be influenced by the contact area of the filler particles with the polymer matrix. Here, the free volume of the polymer is smaller when the contact area with the filler is larger. The interface surface of biocomposites made of polyethylene with WF was studied in [30] along with the structure of biocomposites based on polyethylene filled with WF or oilseed flax stems. When the free volume of the polymer decreases, the gas permeability should decrease. These factors explain the lower gas permeability of biocomposites with WF compared to MCC. It was shown in [30] that biocomposites with WF absorbed oxygen significantly. Oxygen sorption with oxidation of low molecular weight substances can explain the lower gas permeability of biocomposites with WF.

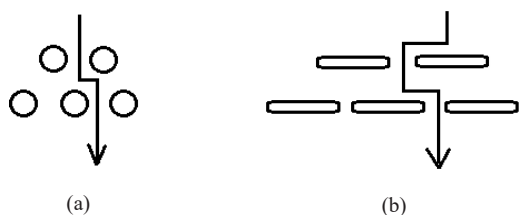


Fig. 3. Model of diffusion of a gas molecule in a polymer filled with particles of spherical (a) and cylindrical (b) shapes

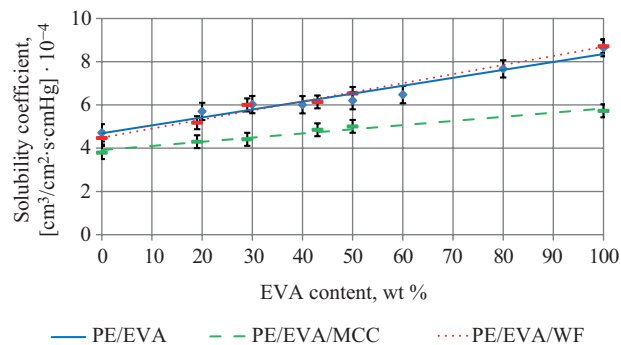


Fig. 4. Dependence of oxygen solubility coefficient on EVA content in the polymer matrix

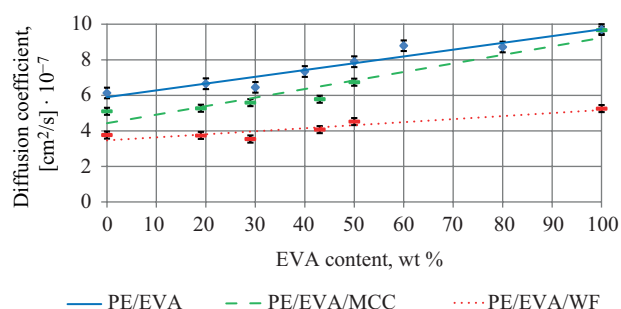


Fig. 5. Dependence of oxygen diffusion coefficient on EVA content in the polymer matrix

Figures 4 and 5 show the dependencies of the diffusion coefficient and oxygen solubility coefficient in the films of ternary and double composites on the EVA content in the polymer matrix. With increasing EVA content in the blend, a linear increase in the values of these two parameters is observed. Oxygen solubility in biocomposites containing WF is the same as in composites without filler, while the presence of MCC particles markedly reduces oxygen solubility in the composite. Fragments of EVA macromolecules, which have a certain mobility, can shift upon introduction of gas molecules. This occurs for the pure polymer and for biocomposites with MCC. However, the stiffer polymer chains have less mobility. Biocomposites with WF particles are less elastic (stiffer), as can be seen when comparing their mechanical properties. Thus, it was shown in [24] that the elongation at break of biocomposites with WF is about 5 times lower than that with MCC. At the same time, the elastic modulus of biocomposites with WF is significantly higher than that of composites with MCC (Table 4). Prior to the creation of ternary biocomposites, we investigated the change in elastic modulus of highly filled binary EVA biocomposites with natural fillers (WF and MCC). Table 4 shows the values of elastic modulus of highly filled biocomposites with filler

content (WF or MCC) of 50 wt %. The presented values allow us to conclude that biocomposites with WF are much stiffer than biocomposites with MCC. It can be seen that the composites with WF have a higher modulus. Due to the increased stiffness of biocomposites with WF and the increased path length of diffusing gas molecules, a significant difference with the original polymer matrix in terms of diffusion coefficient is observed (Fig. 5).

Table 4. Modulus of elasticity of EVA 28025 based composites

| Tensile modulus of elasticity, MPa | | |
|------------------------------------|-------------|------------|
| Without filler | MCC 50 wt % | WF 50 wt % |
| 23 ± 2 | 108 ± 5 | 176 ± 5 |

The obtained results are not only important for the physical chemistry of polymers, but also have applied significance. When using biocomposites as raw materials for the production of packaging films, the oxygen gas permeability index for such products is of crucial importance since determining the shelf life of food products. By obtaining an understanding the dependence of gas permeability on the shape of filler particles and the ability to vary their shape and content in the polymer matrix of the composite, it is possible to create biocomposite materials with specified gas-permeability parameters.

REFERENCES

- Chamas A., Moon H., Zheng J., Qiu Y., Tabassum T., Jang J.H., Abu-Omar M., Scott S.L., Suh S. Degradation Rates of Plastics in the Environment. *ACS Sustainable Chem. Eng.* 2020;8(9): 3494–3511. <https://doi.org/10.1021/acssuschemeng.9b06635>
- Wang Y., Feng G., Lin N., Lan H., Li Q., Yao D., Tang J. A review of degradation and life prediction of polyethylene. *Appl. Sci.* 2023;13(5):3045. <https://doi.org/10.3390/app13053045>
- Ali S.S., Elsamahy T., Al-Tohamy R., Zhu D., Mahmoud Y.A.G., Koutra E., Metwally M.A., Kornaros M., Sun J. Plastic wastes biodegradation: Mechanisms, challenges and future prospect. *Sci. Total Environ.* 2021;780:146590. <https://doi.org/10.1016/j.scitotenv.2021.146590>
- Tiago G.A.O., Mariquito A., Martins-Dias S., Marques A.C. The problem of polyethylene waste – recent attempts for its mitigation. *Sci. Total Environ.* 2023;892:164629. <https://doi.org/10.1016/j.scitotenv.2023.164629>
- Kantelberg R., Achenbach T., Kirch A., Reineke S. In-plane oxygen diffusion measurements in polymer films using time-resolved imaging of programmable luminescent tags. *Sci. Rep.* 2024;14(1):5826. <https://doi.org/10.1038/s41598-024-56237-5>
- Zaikov G.E. (Ed.). *Polimernye plenki (Polymer Films)*: transl. from Engl. St. Petersburg: Professiya; 2005. 352 p. (in Russ.).

CONCLUSIONS

The diffusion properties of biocomposite materials based on LDPE and EVA and having MCC or WF as fillers were studied. An increase in the EVA content in blends with LDPE was shown to lead to a linear increase in the oxygen gas permeability along with enhanced diffusion and oxygen solubility coefficients in the film. Upon adding cellulose-containing filler, the gas permeability of the composites is reduced approximately two-fold. The decrease in gas permeability is probably due to the morphology of the filler particles. While the oxygen solubility for composites with MCC and WF is not the same, it may also be related to the morphology of filler particles. The rough and elongated WF particles form a stiffer and less permeable structure than the smooth spherical MCC particles. The established regularities can be used to evaluate and predict the barrier properties of film materials made of biocomposites with fillers having different morphologies.

Acknowledgments

A.A. Olkhov thanks Plekhanov Russian University of Economics for financial support.

Authors' contributions

P.G. Shelenkov—conducting the study.

P.V. Pantyukhov—approval of the final version of the article.

A.A. Olkhov—preparing and editing the text of the article.

A.A. Popov—development of the research concept.

The authors declare no conflicts of interest.

СПИСОК ЛИТЕРАТУРЫ

- Chamas A., Moon H., Zheng J., Qiu Y., Tabassum T., Jang J.H., Abu-Omar M., Scott S.L., Suh S. Degradation Rates of Plastics in the Environment. *ACS Sustainable Chem. Eng.* 2020;8(9):3494–3511. <https://doi.org/10.1021/acssuschemeng.9b06635>
- Wang Y., Feng G., Lin N., Lan H., Li Q., Yao D., Tang J. A review of degradation and life prediction of polyethylene. *Appl. Sci.* 2023;13(5):3045. <https://doi.org/10.3390/app13053045>
- Ali S.S., Elsamahy T., Al-Tohamy R., Zhu D., Mahmoud Y.A.G., Koutra E., Metwally M.A., Kornaros M., Sun J. Plastic wastes biodegradation: Mechanisms, challenges and future prospect. *Sci. Total Environ.* 2021;780:146590. <https://doi.org/10.1016/j.scitotenv.2021.146590>
- Tiago G.A.O., Mariquito A., Martins-Dias S., Marques A.C. The problem of polyethylene waste – recent attempts for its mitigation. *Sci. Total Environ.* 2023;892:164629. <https://doi.org/10.1016/j.scitotenv.2023.164629>
- Kantelberg R., Achenbach T., Kirch A., Reineke S. In-plane oxygen diffusion measurements in polymer films using time-resolved imaging of programmable luminescent tags. *Sci. Rep.* 2024;14(1):5826. <https://doi.org/10.1038/s41598-024-56237-5>
- Полимерные пленки*; пер. с англ.; под ред. Г.Е. Заикова. СПб.: Профессия; 2010. 352 с.

7. Exama A., Arul J., Lencki R.W., Lee L.Z., Toupin C. Suitability of plastic films for modified atmosphere packaging of fruits and vegetables. *J. Food Sci.* 1993;58(6):1365–1370. <https://doi.org/10.1111/j.1365-2621.1993.tb06184.x>
8. Ahvenainen R. Active and inteligente packaging: An introduction. In: Ahvenainen R. (Ed.). *Novel Food Packaging Technology*. Cambridge: Published in CRC Press, Boca, Raton, Boston, New York, Washinton, DC and Published by Woodhead Publishing, Ltd.; 2003. P. 5–21. <http://doi.org/10.1533/9781855737020.1.5>
9. Yasuda H., Clark H.G., Stannett V. Permeability. In: *Encyclopedia Polymer Science and Technology*. 1969;9:794–807.
10. Khaliq M.H., Gomes R., Fernandes C., Nóbrega J., Carneiro O.S., Ferrás L.L. On the use of high viscosity polymers in the fused filament fabrication process. *Rapid Prototyping J.* 2017;23(4):727. <https://doi.org/10.1108/rpj-02-2016-0027>
11. Kozlov P.V., Bragin'skii G.I. *Khimiya i tekhnologiya polimernykh plenok (Chemistry and Technology of Polymer Films)*. Moscow: Iskusstvo; 1965. 624 p. (in Russ.).
12. Barashkov N.N. *Polimernye kompozity: poluchenie, svoystva, primeneniye (Polymer Composites: Preparation, Properties, Application)*. Moscow: Nauka; 1984. 129 p. (in Russ.).
13. Blanchard R., Ogunsona E.O., Hojabr S., Berry R., Mekonnen T.H. Synergistic cross-linking and reinforcing enhancement of rubber latex with cellulose nanocrystals for glove applications. *ACS Appl. Polym. Mater.* 2020;2(2):887–898. <https://doi.org/10.1021/acsapm.9b01117>
14. Varghese S.A., Pulikkalparambil H., Rangappa S.M., Siengchin S., Parameswaranpillai J. Novel biodegradable polymer films based on poly(3-hydroxybutyrate-co-3-hydroxyvalerate) and *Ceiba pentandra* natural fibers for packaging applications. *Food Packaging and Shelf Life.* 2020;25(5):100538. <https://doi.org/10.1016/j.fpsl.2020.100538>
15. Bordyugova S. S., Belyanskaya E. V., Zaitseva A. A., Pashchenko O. A., Konovalova O. V. Indicator of gas permeability of biodegradable films based on gelatin. *Nauchnyi vestnik Luganskogo gosudarstvennogo agrarnogo universiteta = Scientific Bulletin of Lugansk State Agrarian University.* 2021;4(13):84–90 (in Russ.).
16. Kuzmin A., Ashori A., Pantyukhov P., Zhou Y., Guan L., Hu C. Mechanical, thermal, and water absorption properties of HDPE/barley straw composites incorporating waste rubber. *Sci. Rep.* 2024;14:25232. <https://doi.org/10.1038/s41598-024-76337-6>
17. Kristine V.A. Polysaccharides for biodegradable packaging materials: past, present, and future (Brief Review). *Polymers.* 2023;15(2):451. <https://doi.org/10.3390/polym15020451>
18. Schneider M., Finimundi N., Podzorova M., Pantyukhov P., Poletto M. Assessment of morphological, physical, thermal, and thermal conductivity properties of polypropylene/lignosulfonate blends. *Materials.* 2021;14(3):543. <https://doi.org/10.3390/ma14030543>
19. Shelenkov P.G., Pantyukhov P.V., Aleshinskaya S.V., Maltsev A.A., Abushakhmanova Z.R., Popov A.A., Saavedra-Arias J.J., Poletto M. Thermal stability of highly filled cellulosic biocomposites based on ethylene-vinyl acetate copolymer. *Polymers.* 2024;16(15):2103. <https://doi.org/10.3390/polym16152103>
20. Pantyukhov P.V., Khvatov A.V., Monakhova T.V., Popov A.A., Kolesnikova N.N. The Degradation of Materials Based on Low-Density Polyethylene and Natural Fillers. *Int. Polym. Sci. Technol.* 2018;40(5):55–58. <https://doi.org/10.1177/0307174X1304000511> [Original Russian Text: Pantyukhov P.V., Khvatov A.V., Monakhova T.V., Popov A.A., Kolesnikova N.N. Destruction of the materials made of PELD and natural fillers. *Plasticheskie Massy.* 2012;2:40–42 (in Russ.).
7. Exama A., Arul J., Lencki R.W., Lee L.Z., Toupin C. Suitability of plastic films for modified atmosphere packaging of fruits and vegetables. *J. Food Sci.* 1993;58(6):1365–1370. <https://doi.org/10.1111/j.1365-2621.1993.tb06184.x>
8. Ahvenainen R. Active and inteligente packaging: An introduction. In: Ahvenainen R. (Ed.). *Novel Food Packaging Technology*. Cambridge: Published in CRC Press, Boca, Raton, Boston, New York, Washinton, DC and Published by Woodhead Publishing, Ltd.; 2003. P. 5–21. <http://doi.org/10.1533/9781855737020.1.5>
9. Yasuda H., Clark H.G., Stannett V. Permeability. In: *Encyclopedia Polymer Science and Technology*. 1969;9:794–807.
10. Khaliq M.H., Gomes R., Fernandes C., Nóbrega J., Carneiro O.S., Ferrás L.L. On the use of high viscosity polymers in the fused filament fabrication process. *Rapid Prototyping J.* 2017;23(4):727. <https://doi.org/10.1108/rpj-02-2016-0027>
11. Козлов П.В., Брагинский Г.И. *Химия и технология полимерных пленок*. М.: Искусство; 1965. 624 с.
12. Барашков Н.Н. *Полимерные композиты: получение, свойства, применение*. М.: Наука; 1984. 129 с.
13. Blanchard R., Ogunsona E.O., Hojabr S., Berry R., Mekonnen T.H. Synergistic cross-linking and reinforcing enhancement of rubber latex with cellulose nanocrystals for glove applications. *ACS Appl. Polym. Mater.* 2020;2(2):887–898. <https://doi.org/10.1021/acsapm.9b01117>
14. Varghese S.A., Pulikkalparambil H., Rangappa S.M., Siengchin S., Parameswaranpillai J. Novel biodegradable polymer films based on poly(3-hydroxybutyrate-co-3-hydroxyvalerate) and *Ceiba pentandra* natural fibers for packaging applications. *Food Packaging and Shelf Life.* 2020;25(5):100538. <https://doi.org/10.1016/j.fpsl.2020.100538>
15. Бордюгова С.С., Белянская Е.В., Зайцева А.А., Пащенко О.А., Коновалова О.В. Показатели газопроницаемости биодegradируемых пленок на основе желатина. *Научный вестник Луганского государственного аграрного университета.* 2021;4(13):84–90.
16. Kuzmin A., Ashori A., Pantyukhov P., Zhou Y., Guan L., Hu C. Mechanical, thermal, and water absorption properties of HDPE/barley straw composites incorporating waste rubber. *Sci. Rep.* 2024;14:25232. <https://doi.org/10.1038/s41598-024-76337-6>
17. Kristine V.A. Polysaccharides for biodegradable packaging materials: past, present, and future (Brief Review). *Polymers.* 2023;15(2):451. <https://doi.org/10.3390/polym15020451>
18. Schneider M., Finimundi N., Podzorova M., Pantyukhov P., Poletto M. Assessment of morphological, physical, thermal, and thermal conductivity properties of polypropylene/lignosulfonate blends. *Materials.* 2021;14(3):543. <https://doi.org/10.3390/ma14030543>
19. Shelenkov P.G., Pantyukhov P.V., Aleshinskaya S.V., Maltsev A.A., Abushakhmanova Z.R., Popov A.A., Saavedra-Arias J.J., Poletto M. Thermal stability of highly filled cellulosic biocomposites based on ethylene-vinyl acetate copolymer. *Polymers.* 2024;16(15):2103. <https://doi.org/10.3390/polym16152103>
20. Пантюхов П.В., Хватов А.В., Монахова Т.В., Попов А.А., Колесникова Н.Н. Деструкция материалов на основе ПЭВД и природных наполнителей. *Пластические массы.* 2012;2:40–42. <https://www.elibrary.ru/item.asp?id=17743233>
21. Шабарин А.А., Шабарин А.А., Водяков В.Н., Кузьмин А.М. Биоразлагаемые композиционные материалы на основе полиолефинов и пивной дробины. *Вестник Технологического университета.* 2016;19(17):67–70.

21. Shabarin A.A., Shabarin A.A., Vodiakov V.N., Kuzmin A.M. Biodegradable composite materials based on polyolefins and beer pellets. *Vestnik Tekhnologicheskogo universiteta = Herald of Technological University*. 2016;19(17):67–70 (in Russ.).
22. Lukanina Yu.K., Pantyukhov P.V., Khvatov A.V., Koroleva A.V., Kolesnikova N.N., Likhachev A.N., Popov A.A. Bio-damage of materials based on polyethylene and wood flour. *Vse materialy. Entsiklopedicheskiy spravochnik = All Materials. Encyclopedic Reference Manual*. 2014;1:2–7 (in Russ.).
23. Rogovina S.Z., Lomakin S.M., Aleksanyan K.V., et al. The structure, properties, and thermal destruction of biodegradable blends of cellulose and ethylcellulose with synthetic polymers. *Russ. J. Phys. Chem. B*. 2012;6:416–424. <https://doi.org/10.1134/S1990793112060048>
[Original Russian Text: Rogovina S.Z., Lomakin S.M., Aleksanyan K.V., Prut E.V. The structure, properties, and thermal destruction of biodegradable blends of cellulose and ethylcellulose with synthetic polymers. *Khimicheskaya Fizika*. 2012;31(6):54–62 (in Russ.).]
24. Shelenkov P.G., Pantyukhov P.V., Poletto M., Popov A.A. Influence of vinyl acetate content and melt flow index of ethylene-vinyl acetate copolymer on physico-mechanical and physico-chemical properties of highly filled biocomposites. *Polymers*. 2023;15(12):2639. <https://doi.org/10.3390/polym15122639>
25. Shelenkov P.G., Pantyukhov P.V., Popov A.A. Mechanical properties of superconcentrates based on ethylene-vinyl acetate copolymer and microcrystalline cellulose. *Mater. Sci. Forum*. 2020;992:306–310. <https://doi.org/10.4028/www.scientific.net/MSF.992.306>
26. Shelenkov P.G., Pantyukhov P.V., Popov A.A. Highly filled biocomposites based on ethylene-vinyl acetate copolymer and wood flour. *IOP Conf. Ser.: Mater. Sci. Eng.* 2018;369(1):012043. <https://doi.org/10.1088/1757-899X/369/1/012043>
27. Pantyukhov P., Zykova A., Popov A. Ethylene-octene copolymer-wood flour/oil flax straw biocomposites: Effect of filler type and content on mechanical properties. *Polym. Eng. Sci.* 2017;57(7):756–763. <https://doi.org/10.1002/pen.24626>
28. Sorz J., Hietz P. Gas diffusion through wood: implications for oxygen supply. *Trees*. 2006;20:34–41. <https://doi.org/10.1007/s00468-005-0010-x>
29. Alamo-Sanza del M., Cárcel L.M., Nevares I. Characterization of the oxygen transmission rate of oak wood species used in cooperage. *J. Agric. Food Chem.* 2017;65(3):648–655. <https://doi.org/10.1021/acs.jafc.6b05188>
30. Zykova A.K., Pantyukhov P.V., Kolesnikova N.N., Monakhova T.V., Popov A.A. Influence of filler particle size on physical properties and biodegradation of biocomposites based on low-density polyethylene and lignocellulosic fillers. *J. Polym. Environ.* 2018;26:1343–1354. <https://doi.org/10.1007/s10924-017-1039-9>
22. Луканина Ю.К., Пантюхов П.В., Хватов А.В., Королева А.В., Колесникова Н.Н., Лихачев А.Н., Попов А.А. Биоповреждение материалов на основе полиэтилена и древесной муки. *Все материалы. Энциклопедический справочник*. 2014;1:2–7.
23. Роговина С.З., Ломакин С.М., Алексанян К.В., Прут Э.В. Структура, свойства и термическая деструкция биоразлагаемых смесей на основе целлюлозы и этилцеллюлозы с синтетическими полимерами. *Химическая физика*. 2012;31(6):54–62.
24. Shelenkov P.G., Pantyukhov P.V., Poletto M., Popov A.A. Influence of vinyl acetate content and melt flow index of ethylene-vinyl acetate copolymer on physico-mechanical and physico-chemical properties of highly filled biocomposites. *Polymers*. 2023;15(12):2639. <https://doi.org/10.3390/polym15122639>
25. Shelenkov P.G., Pantyukhov P.V., Popov A.A. Mechanical properties of superconcentrates based on ethylene-vinyl acetate copolymer and microcrystalline cellulose. *Mater. Sci. Forum*. 2020;992:306–310. <https://doi.org/10.4028/www.scientific.net/MSF.992.306>
26. Shelenkov P.G., Pantyukhov P.V., Popov A.A. Highly filled biocomposites based on ethylene-vinyl acetate copolymer and wood flour. *IOP Conf. Ser.: Mater. Sci. Eng.* 2018;369(1):012043. <https://doi.org/10.1088/1757-899X/369/1/012043>
27. Pantyukhov P., Zykova A., Popov A. Ethylene-octene copolymer-wood flour/oil flax straw biocomposites: Effect of filler type and content on mechanical properties. *Polym. Eng. Sci.* 2017;57(7):756–763. <https://doi.org/10.1002/pen.24626>
28. Sorz J., Hietz P. Gas diffusion through wood: implications for oxygen supply. *Trees*. 2006;20:34–41. <https://doi.org/10.1007/s00468-005-0010-x>
29. Alamo-Sanza del M., Cárcel L.M., Nevares I. Characterization of the oxygen transmission rate of oak wood species used in cooperage. *J. Agric. Food Chem.* 2017;65(3):648–655. <https://doi.org/10.1021/acs.jafc.6b05188>
30. Zykova A.K., Pantyukhov P.V., Kolesnikova N.N., Monakhova T.V., Popov A.A. Influence of filler particle size on physical properties and biodegradation of biocomposites based on low-density polyethylene and lignocellulosic fillers. *J. Polym. Environ.* 2018;26:1343–1354. <https://doi.org/10.1007/s10924-017-1039-9>

About the Authors

Pavel G. Shelenkov, Postgraduate Student, N.M. Emanuel Institute of Biochemical Physics, Russian Academy of Sciences (4, Kosygina ul., Moscow, 119334, Russia); Higher Engineering School “New Materials and Technologies,” Plekhanov Russian University of Economics (36, Stremyanniy per., Moscow, 115054, Russia). E-mail: shell1183@mail.ru. Scopus Author ID 57202800500, <https://orcid.org/0009-0007-5282-6321>

Petr V. Pantyukhov, Cand. Sci. (Chem.), Senior Researcher, N.M. Emanuel Institute of Biochemical Physics, Russian Academy of Sciences (4, Kosygina ul., Moscow, 119334, Russia); Higher Engineering School “New Materials and Technologies,” Plekhanov Russian University of Economics (36, Stremyanniy per., Moscow, 115054, Russia). E-mail: pantyukhov@mail.ru. Scopus Author ID 55368433100, ResearcherID I-9817-2014, RSCI SPIN-code 8841-5962, <https://orcid.org/0000-0001-8967-2089>

Anatoly A. Olkhov, Dr. Sci. (Chem.), Senior Researcher, N.M. Emanuel Institute of Biochemical Physics, Russian Academy of Sciences (4, Kosygina ul., Moscow, 119334, Russia); Leading Researcher, Scientific Laboratory “Advanced Composite Materials and Technologies,” Plekhanov Russian University of Economics (36, Stremyanniy per., Moscow, 115054, Russia). E-mail: aolkhov72@yandex.ru. Scopus Author ID 6602363287, ResearcherID F-9265-2017, RSCI SPIN-code 4674-8406

Anatoly A. Popov, Dr. Sci. (Chem.), Professor, Deputy Director, N.M. Emanuel Institute of Biochemical Physics, Russian Academy of Sciences (4, Kosygina ul., Moscow, 119334, Russia); Head of the Basic Department of Chemistry of Innovative Materials and Technologies, Plekhanov Russian University of Economics (36, Stremyanniy per., Moscow, 115054, Russia). E-mail: anatoly.popov@mail.ru. Scopus Author ID 7402986626, ResearcherID I-9835-2014, RSCI SPIN-code 5556-7816, <https://orcid.org/0000-0002-8006-6215>

Об авторах

Шеленков Павел Геннадьевич, аспирант, ФГБУН Институт биохимической физики им. Н.М. Эмануэля Российской академии наук (199334, Россия, Москва, ул. Косыгина, д. 4); Высшая инженерная школа «Новые материалы и технологии», ФГБОУ ВО «Российский экономический университет им. Г.В. Плеханова» (115054, Россия, Москва, Стремянный пер., д. 36). E-mail: shell1183@mail.ru. Scopus Author ID 57202800500, <https://orcid.org/0009-0007-5282-6321>

Пантюхов Петр Васильевич, к.х.н., старший научный сотрудник, ФГБУН Институт биохимической физики им. Н.М. Эмануэля Российской академии наук (199334, Россия, Москва, ул. Косыгина, д. 4); ведущий научный сотрудник, Научная школа «Химия и технология полимерных материалов», ФГБОУ ВО «Российский экономический университет им. Г.В. Плеханова» (115054, Россия, Москва, Стремянный пер., д. 36). E-mail: pantyukhov@mail.ru. Scopus Author ID 55368433100, ResearcherID I-9817-2014, SPIN-код РИНЦ 8841-5962, <https://orcid.org/0000-0001-8967-2089>

Ольхов Анатолий Александрович, д.х.н., старший научный сотрудник, ФГБУН Институт биохимической физики им. Н.М. Эмануэля Российской академии наук (199334, Россия, Москва, ул. Косыгина, д. 4); ведущий научный сотрудник, Научная лаборатория «Перспективные композиционные материалы и технологии», ФГБОУ ВО «Российский экономический университет им. Г.В. Плеханова» (115054, Россия, Москва, Стремянный пер., д. 36). E-mail: aolkhov72@yandex.ru. Scopus Author ID 6602363287, ResearcherID F-9265-2017, SPIN-код РИНЦ 4674-8406

Попов Анатолий Анатольевич, д.х.н., профессор, заместитель директора, ФГБУН Институт биохимической физики им. Н.М. Эмануэля Российской академии наук (199334, Россия, Москва, ул. Косыгина, д. 4); заведующий базовой кафедрой химии инновационных материалов и технологий, ФГБОУ ВО «Российский экономический университет им. Г.В. Плеханова» (115054, Россия, Москва, Стремянный пер., д. 36). E-mail: anatoly.popov@mail.ru. Scopus Author ID 7402986626, ResearcherID I-9835-2014, SPIN-код РИНЦ 5556-7816, <https://orcid.org/0000-0002-8006-6215>

Translated from Russian into English by H. Moshkov

Edited for English language and spelling by Thomas A. Beavitt

UDC 544.032

<https://doi.org/10.32362/2410-6593-2025-20-2-156-166>

EDN DKIJFP



RESEARCH ARTICLE

The influence of lanthanum content in the $\text{Fe}_2\text{O}_3\text{--Li}_2\text{O--La(OH)}_3$ system on phase formation and properties of composite material

Yuliya S. Elkina✉, Vitaly A. Vlasov, Elena N. Lysenko, Anatoly P. Surzhikov

National Research Tomsk Polytechnic University, Tomsk, 634050 Russia

✉ Corresponding author, e-mail: ysm7@tpu.ru

Abstract

Objectives. To study the effect of varying lanthanum content in the $\text{Fe}_2\text{O}_3\text{--Li}_2\text{O--La(OH)}_3$ system on phase formation and corresponding structural and electromagnetic properties of a lithium-ferrite composite material obtained using high-temperature ceramic technology.

Methods. Following the addition of lanthanum occurred at the initial stage of mixing the $\text{Fe}_2\text{O}_3/\text{Li}_2\text{CO}_3/\text{La(OH)}_3$ components in a certain weight ratio, the obtained samples were sent for preliminary synthesis at a temperature of 900°C for 240 min in an air atmosphere and sintering in a dilatometer at a temperature of 1100°C for 120 min. The microstructure and properties of the sintered composite samples were studied using X-ray phase analysis (XRD), thermogravimetry (TG), differential scanning calorimetry (DSC), and scanning electron microscopy.

Results. XRD analysis confirmed the formation of a two-phase structure following solid-phase synthesis, consisting of the magnetic phase of lithium ferrite $\text{Li}_{0.5}\text{Fe}_{2.5}\text{O}_4$ and the perovskite-like phase LaFeO_3 . XRD carried out after sintering showed that the high-temperature heating process did not affect the changes in the phase composition of the sample phases. Dilatometric shrinkage curves obtained after sintering showed that the addition of La reduces the rate of compaction of the samples at the stage of their heating. The sintered samples were characterized by a density of 4.34, 3.84, 3.93 g/cm³ and a porosity of 0.7, 16, and 18%, respectively, having an increased mass content of La(OH)_3 at the synthesis stage. A decrease in the grain sizes was also observed. An increase in the amount of lanthanum hydroxide La(OH)_3 additive from 0 to 4.4 and 13.9 wt % led to an increase in the concentration of the synthesized LaFeO_3 phase in the samples to 4.2 and 16.6 wt %, resulting in decreased specific saturation magnetization values from 59.4 to 58.2 and 49.7 G·cm³/g and the initial magnetic permeability from 41.6 to 22.8 and 19.5, respectively. TG and DSC showed that high-temperature sintering of lithium ferrite without additives leads to the predominant formation of the disordered β -phase $\text{Li}_{0.5}\text{Fe}_{2.5}\text{O}_4$, which has a reduced Curie temperature of 626°C. This process is associated with a violation of the stoichiometric composition of the samples for lithium and oxygen due to the release of these elements from the samples during high-temperature sintering.

Conclusions. The high values of the Curie temperature of 631°C confirm that the addition of lanthanum during the production of lithium ferrite prevents the violation of the stoichiometric composition of the ferrite during sintering due to the construction of an additional LaFeO_3 lattice. The addition of lanthanum was also found to lead to a significant increase in specific electrical resistance from $5 \cdot 10^2$ to $6 \cdot 10^9$ and $1 \cdot 10^{12}$ Ohm·cm, which may be associated with both a change in the microstructure of the samples and a change in their phase composition.

Keywords

lithium ferrite, lanthanum, magnetic properties, electrical properties, structure, rare earth element

Submitted: 11.09.2024

Revised: 08.11.2024

Accepted: 19.02.2025

For citation

Elkina Yu.S., Vlasov V.A., Lysenko E.N., Surzhikov A.P. The influence of lanthanum content in the $\text{Fe}_2\text{O}_3\text{-Li}_2\text{O-La(OH)}_3$ system on phase formation and properties of composite material. *Tonk. Khim. Tekhnol. = Fine Chem. Technol.* 2025;20(2):156–166. <https://doi.org/10.32362/2410-6593-2025-20-2-156-166>

НАУЧНАЯ СТАТЬЯ

Влияние содержания лантана в системе $\text{Fe}_2\text{O}_3\text{-Li}_2\text{O-La(OH)}_3$ на фазообразование и свойства композиционного материала

Ю.С. Елькина✉, В.А. Власов, Е.Н. Лысенко, А.П. Суржигов

Национальный исследовательский Томский политехнический университет, Томск, 634050 Россия

✉ Автор для переписки, e-mail: ysm7@tpu.ru

Аннотация

Цели. Исследование влияния содержания лантана в системе $\text{Fe}_2\text{O}_3\text{-Li}_2\text{O-La(OH)}_3$ на фазообразование, а также структурные и электромагнитные свойства композиционного материала на основе литиевого феррита, полученного с помощью высокотемпературной керамической технологии.

Методы. Введение лантана происходило на начальном этапе смешивания компонентов $\text{Fe}_2\text{O}_3/\text{Li}_2\text{CO}_3/\text{La(OH)}_3$ в определенном весовом соотношении, затем полученные образцы были направлены на предварительный синтез при температуре 900°C в течение 240 мин в атмосфере воздуха и дальнейшее спекание в dilatометре при температуре 1100°C в течение 120 мин. Методами рентгенофазового анализа (РФА), термогравиметрии (ТГ), дифференциально-сканирующей калориметрии (ДСК), а также сканирующей электронной микроскопии проведено исследование микроструктуры и свойств исследуемых композиционных образцов.

Результаты. Методом РФА установлено, что после твердофазного синтеза происходит образование двухфазной структуры, состоящей из магнитной фазы литиевого феррита $\text{Li}_{0.5}\text{Fe}_{2.5}\text{O}_4$ и перовскитоподобной фазы LaFeO_3 . Проведение РФА после спекания показало, что процесс высокотемпературного нагрева не оказал влияния на изменения фазового состава образцов. Dilатометрические кривые усадки, полученные во время спекания, показали, что введение La уменьшает скорость уплотнения образцов на стадии их нагрева. Спеченные образцы характеризовались плотностью 4.34, 3.84, 3.93 г/см³ и пористостью 0.7, 16 и 18% с увеличением на этапе синтеза массового содержания La(OH)_3 . Также наблюдалось уменьшение размеров зерна. Увеличение количества добавки La(OH)_3 с 0 до 4.4 и 13.9 мас. % привело к увеличению в образцах концентрации фазы LaFeO_3 до 4.2 и 16.6 мас. %, что явилось причиной снижения значений удельной намагниченности насыщения соответственно с 59.4 до 58.2 и 49.7 Гс·см³/г и начальной магнитной проницаемости с 41.6 до 22.8 и 19.5. С помощью ТГ и ДСК показано, что высокотемпературное спекание литиевого феррита без добавок приводит к преимущественному формированию разупорядоченной β -фазы $\text{Li}_{0.5}\text{Fe}_{2.5}\text{O}_4$, имеющей заниженное значение температуры Кюри 626°C . Данный процесс связан с нарушением стехиометрического состава образцов по литию и кислороду вследствие выхода данных элементов из образцов во время высокотемпературного спекания.

Выводы. Введение лантана при получении литиевого феррита препятствует во время спекания нарушению стехиометрического состава феррита за счет построения дополнительной решетки LaFeO_3 , что подтверждено высокими значениями температуры Кюри 631°C . Также установлено, что введение лантана приводит к значительному увеличению удельного электрического сопротивления с $5 \cdot 10^2$ до $6 \cdot 10^9$ и $1 \cdot 10^{12}$ Ом·см, что может быть связано как с изменением микроструктуры образцов, так и с изменением их фазового состава.

Ключевые слова

литиевый феррит, лантан, магнитные свойства, электрические свойства, структура, редкоземельный элемент

Поступила: 11.09.2024

Доработана: 08.11.2024

Принята в печать: 19.02.2025

Для цитирования

Елькина Ю.С., Власов В.А., Лысенко Е.Н., Суржигов А.П. Влияние содержания лантана в системе $\text{Fe}_2\text{O}_3\text{-Li}_2\text{O-La(OH)}_3$ на фазообразование и свойства композиционного материала. *Тонкие химические технологии.* 2025;20(2):156–166. <https://doi.org/10.32362/2410-6593-2025-20-2-156-166>

INTRODUCTION

The number of studies focused on ferrites, including lithium-containing ferrites having various technological applications, continues to grow steadily each year. Due to its high Curie temperature and saturation magnetization, lithium ferrite $\text{Li}_{0.5}\text{Fe}_{2.5}\text{O}_4$ is used in microwave devices, as well as cathode materials in lithium-ion batteries and gas sensors [1–4]. All these applications, in one way or another, rely on a certain combination of magnetic and electrical properties of this ferrite. To achieve such various combinations, metal ions such as Ti, Zn, Ni, Mg, Mn, Co, etc. are added into the lithium ferrite. Studies [5–8] have shown that certain characteristics can be improved by varying different substitution combinations; however, in many cases this leads to a deterioration of other desired characteristics. Therefore, it becomes necessary to develop methods for improving the electrophysical and magnetic properties of lithium ferrites.

Recently, researchers have been actively investigating the properties of various ferrites with rare earth elements [9–13]. Unpaired 4f electrons located in the outer orbital level of rare earth elements play a major role in the occurrence of magnetic anisotropy due to their orbital shape [10]. This means that the addition of such ions as samarium, lanthanum, gadolinium, etc. to spinel ferrites can change their electrical and magnetic properties. At the same time, there are very few studies devoted to the research of the influence of various rare-earth elements on the properties of lithium ferrites.

It is known that in addition to varying the composition of ferrites due to the inclusion of certain components, the method of obtaining ferrites also affects their properties [3, 10, 12, 14–16]. In the case of traditional and widespread ceramic technology, oxides and carbonates are used as starting reagents to produce ferrites. Based on data from [17], it was shown that during solid-phase interaction of $\text{Sm}_2\text{O}_3/\text{Fe}_2\text{O}_3/\text{Li}_2\text{CO}_3$ reagents in different weight ratios no substituted lithium ferrite phase is formed, but two phases including unsubstituted lithium ferrite $\text{Li}_{0.5}\text{Fe}_{2.5}\text{O}_4$ and SmFeO_3 are formed and affect the final properties of the ferrite.

In this study, the structure and properties of lithium ferrite modified with lanthanum were investigated by X-ray diffraction phase analysis (XRD), thermogravimetry (TG), differential scanning calorimetry (DSC) and scanning electron microscopy (SEM) methods.

MATERIALS AND METHODS

The initial reagents for preparation of lanthanum-modified lithium ferrite were iron oxide Fe_2O_3 (pure for analysis, *Vekton*, Russia), lithium carbonate Li_2CO_3 (extra pure 20-2, *Vekton*, Russia) and lanthanum hydroxide La(OH)_3 (99.99%, *MOS International Co.*, China). The weight ratios of these components $\text{Fe}_2\text{O}_3/\text{Li}_2\text{CO}_3/\text{La(OH)}_3$ were 91.5/8.5/0 wt % (sample N0), 87.3/8.3/4.4 wt % (sample N1), and 78.2/7.9/13.9 wt % (sample N2).

Prior to mixing, the powders were dried in an oven for 120 min at 200°C to remove excess moisture. Mixing of these components was carried out in an E-max ball mill (*Retsch*, Germany) using steel balls with a diameter of 5 mm at 300 rpm for 15 min. Next, the samples were compacted by cold pressing in the form of tablets on a PGr-10 manual hydraulic press (*LabTuls*, Russia). Preliminary synthesis of the obtained samples was carried out in a laboratory furnace at 900°C for 240 min in air atmosphere. Then the samples were ground in an agate mortar and 12 wt % polyvinyl alcohol (95.3%, *MCD Chemicals*, China) was added to the obtained powders. Finally, the powders were compacted into tablets and sintered in a DIL 402C dilatometer (*Netzsch*, Germany) at 1100°C for 2 h.

The phase composition of the obtained samples was studied by XRD on an ARL X'TRA diffractometer (*Thermo Fisher Scientific*, Switzerland) using Cu-K_α radiation. The measurement range was $2\theta = 10^\circ\text{--}90^\circ$. Powder Cell 2.5 software with the International Center for Diffraction Data (ICDD¹) PDF-4+ database was used for phase identification and quantification.

With the help of TG and DSC analyses, the Curie temperature (T_C) and thermal effects during heating of the samples in a thermal analyzer in STA 449C Jupiter (*Netzsch*, Germany) were investigated. The Curie temperature T_C was obtained by differentiating the TG curve of lithium ferrite into a derivative thermogravimetric curve (DTG), whose peak corresponds to the Curie temperature value according to the methodology presented in [18]. The thermal analysis was performed with the application of an external magnetic field during the entire heating process up to 900°C.

The microstructural features of the lithium samples were studied by SEM on a TM-3000 device (*Hitachi*, Japan).

The saturation magnetization (σ_s) was measured at room temperature using an H-04 pulse magnetometer (*TSU*, Russia). The initial magnetic permeability was

¹ URL: <http://www.icdd.com>. Accessed February 13, 2023.

measured using the inductive method on a Keysight E4980AL precision LCR meter (Agilent, USA). The temperature dependence of the electrical resistivity of the samples was measured using the two-probe method according to the method described in [19].

RESULTS AND DISCUSSION

At the first stage of obtaining the composite material, a solid-phase interaction reaction was carried out between the initial components in a certain weight ratio specified in the experimental procedure.

The qualitative and quantitative phase composition of the samples following synthesis was determined from the XRD results (Table 1 and Fig. 1), which confirmed the formation of two distinct phases: spinel phase $\text{Li}_{0.5}\text{Fe}_{2.5}\text{O}_4$ (PDF No. 01-070-5669¹) and perovskite-like phase with orthorhombic structure LaFeO_3 (PDF No. 01-077-99802¹). The presence of reflexes at $2\theta \approx 15^\circ$, 23° , and 26° , as well as the lattice parameter $\sim 8.33 \text{ \AA}$, which are in agreement with literature data [20], indicate the formation of ordered cubic phase $\alpha\text{-Li}_{0.5}\text{Fe}_{2.5}\text{O}_4$ [21].

The formation of the secondary phase proceeds according to the following mechanism (1):



The concentration of the secondary phase depends on the content of the added initial reagent La(OH)_3 such that, with an increase of the added lanthanum ions, the content of LaFeO_3 increases. Thus, on the basis of XRD analysis it can be seen that the reaction of solid-phase interaction between the initial reagents proceeds without the addition of La into the crystal structure of lithium ferrite, that is, the formation of a two-phase composite. Presumably, the reaction in the synthesis process between the initial

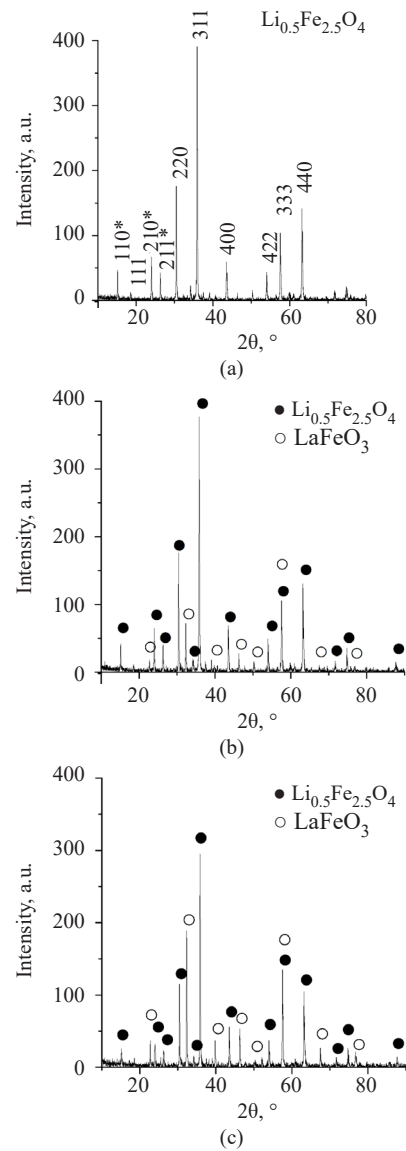
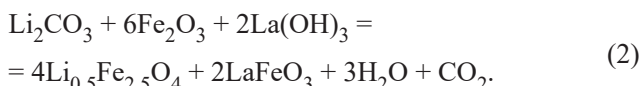


Fig. 1. X-ray diffraction patterns of samples after synthesis, where is (a) N0; (b) N1; (c) N2

Table 1. Phase composition of synthesized samples

| Sample | Phase composition | Lattice parameters, \AA | Concentration, wt % |
|--------|--|--|---------------------|
| N0 | $\text{Li}_{0.5}\text{Fe}_{2.5}\text{O}_4$ | $a = b = c = 8.3328 (\pm 0.002)$ | 100 |
| | LaFeO_3 | – | – |
| N1 | $\text{Li}_{0.5}\text{Fe}_{2.5}\text{O}_4$ | $a = b = c = 8.3279 (\pm 0.002)$ | 95.7 |
| | LaFeO_3 | $a = 5.5549 (\pm 0.002)$ $b = 7.8495 (\pm 0.003)$ $c = 5.5477 (\pm 0.003)$ | 4.3 |
| N2 | $\text{Li}_{0.5}\text{Fe}_{2.5}\text{O}_4$ | $a = b = c = 8.3310 (\pm 0.002)$ | 81.9 |
| | LaFeO_3 | $a = 5.5501 (\pm 0.002)$ $b = 7.8613 (\pm 0.003)$ $c = 5.5572 (\pm 0.003)$ | 18.1 |

reactants Fe₂O₃/Li₂CO₃/La(OH)₃ proceeds according to scheme (2):



Next, the sintering process was carried out and the dilatometric curves shown in Fig. 2 were obtained.

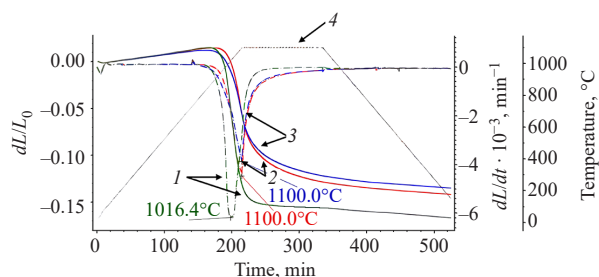


Fig. 2. Dilatometric curves obtained by sintering samples at 1100°C (shrinkage curve—solid lines, shrinkage rate—dotted lines): 1 (green lines) sample N0; 2 (red lines) sample N1; 3 (blue lines) sample N2; 4 temperature program

Up to the temperature of non-isothermal heating 800°C, material expansion occurs in all samples, which is associated with an increase in the volume of gas pores. Then there is a sharp change in the length of samples at a temperature of about 900°C, which is associated with

their densification. At the same time, the shrinkage rate of sample N0 is higher than that of N1 and N2. By the end of isothermal curing, sample N0 shows the highest shrinkage. From the shrinkage curves, it can be seen that the addition of lanthanum reduces the shrinkage rate of the samples at the stage of heating and that the shrinkage rate of samples N1 and N2 is almost the same.

The data obtained by measuring the hydrostatic density and porosity indicated in Table 2 confirmed the dilatometry data. With the addition of lanthanum, there is a decrease in density (ρ_{hydr}) and an increase in porosity of samples (Q).

X-ray diffraction patterns of the samples after the sintering process are shown in Fig. 3.

XRD after sintering showed that the qualitative content of phases did not change after this process and that sintered samples contain phases Li_{0.5}Fe_{2.5}O₄ and LaFeO₃. During sintering (Table 3), the quantitative content of phases in sample N1 practically does not change, while for sample N2 there is a slight decrease in the concentration of Li_{0.5}Fe_{2.5}O₄ phase and an increase in the amount of secondary phase LaFeO₃ in comparison with the synthesis data.

SEM images of the surface of the samples are shown in Fig. 4. The images of samples N1 and N2, which confirm the conclusions about the formation of a two-phase product after sintering, clearly show two contrasts [17] that correspond to the ferrite phase (gray shade) and

Table 2. Density and porosity of composite samples

| Sample | Density ρ_{hydr} , g/cm ³ | Porosity Q, % | Grain size D, μm |
|--------|--|---------------|-----------------------------|
| N0 | 4.34 | 0.7 | 4.78 |
| N1 | 3.84 | 16.0 | 1.63 |
| N2 | 3.93 | 18.0 | 1.57 |

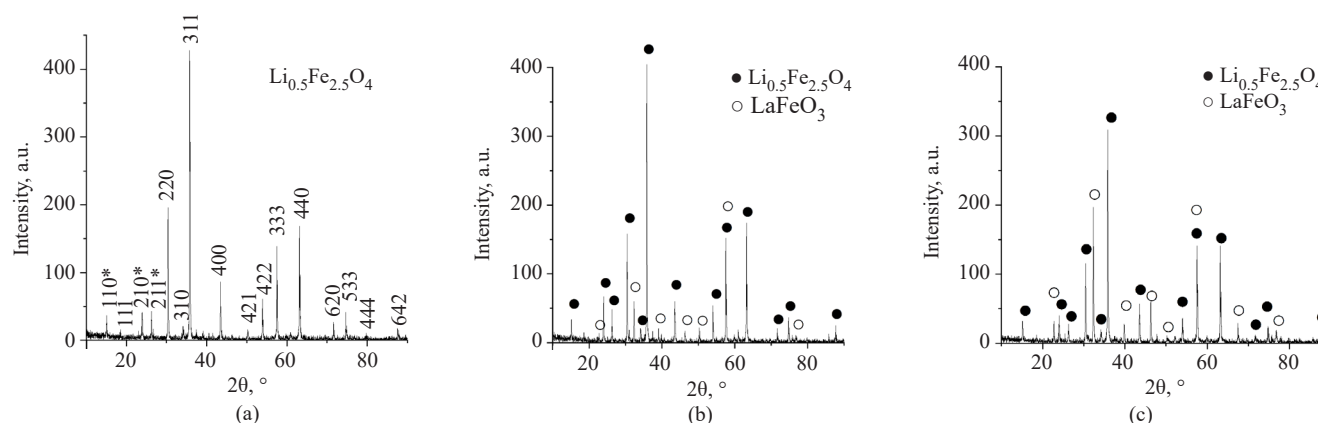


Fig. 3. X-ray diffraction patterns of samples after sintering: (a) N0; (b) N1; (c) N2

Table 3. Phase composition of sintered samples

| Sample | Phase composition | Lattice parameters, Å | Concentration, wt % |
|--------|--|--|---------------------|
| N0 | $\text{Li}_{0.5}\text{Fe}_{2.5}\text{O}_4$ | $a = b = c = 8.3327 (\pm 0.002)$ | 100 |
| | LaFeO_3 | – | – |
| N1 | $\text{Li}_{0.5}\text{Fe}_{2.5}\text{O}_4$ | $a = b = c = 8.3275 (\pm 0.002)$ | 95.8 |
| | LaFeO_3 | $a = 5.5506 (\pm 0.002)$ $b = 7.8418 (\pm 0.003)$ $c = 5.5838 (\pm 0.003)$ | 4.2 |
| N2 | $\text{Li}_{0.5}\text{Fe}_{2.5}\text{O}_4$ | $a = b = c = 8.3304 (\pm 0.002)$ | 83.4 |
| | LaFeO_3 | $a = 5.5539 (\pm 0.002)$ $b = 7.8593 (\pm 0.003)$ $c = 5.5535 (\pm 0.003)$ | 16.6 |

the LaFeO_3 phase (white shade). The addition of La also affects the microstructure of the final ceramic samples. The values of average grain size are given in Table 2. While the addition of La leads to a decrease in the grain size of the ferrite phase [22], the concentration of the rare earth element does not significantly affect the further change of this parameter.

In this work, the electrical resistivity (ρ) was also investigated. The sharp increase in electrical resistivity with increasing additive content shown in Table 4 may be due to an increase in the amount of secondary phase LaFeO_3 , as well as the high porosity and low density

of the samples. Studies of the saturation specific magnetization (σ_s) showed that a slight decrease in this parameter occurs with the addition of La in small amounts. More significant changes occur in the initial magnetic permeability (μ_0) of ferrite [17, 23–27]. This is probably due to the quantitative increase of the LaFeO_3 phase, which is antiferromagnetic in nature and behaves as a paramagnetic under certain circumstances.

Furthermore, thermal analysis of the sintered specimens was carried out, the graphs of which are shown in Fig. 5. As shown in [17–19, 21], the thermal endothermic effect on the DSC curve in the temperature

Table 4. Electrical and magnetic properties of samples

| Sample | ρ , Ohm·cm | σ_s , G·cm ³ /g | μ_0 | T_C , °C |
|--------|-------------------|-----------------------------------|---------|------------|
| N0 | $5 \cdot 10^2$ | 59.4 | 41.6 | 626 |
| N1 | $6 \cdot 10^9$ | 58.2 | 22.8 | 631 |
| N2 | $1 \cdot 10^{12}$ | 49.7 | 19.5 | 630 |

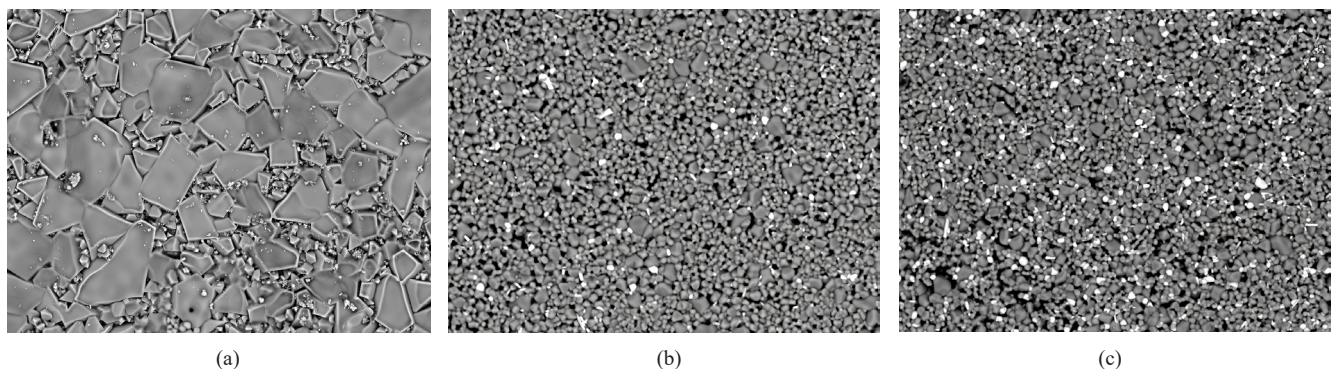


Fig. 4. SEM images of lithium ferrite modified with lanthanum: (a) N0; (b) N1; (c) N2

region $\sim 700\text{--}760^\circ\text{C}$ is associated with the phase transition from the ordered α -phase to the disordered β -phase of the unsubstituted lithium ferrite $\text{Li}_{0.5}\text{Fe}_{2.5}\text{O}_4$.

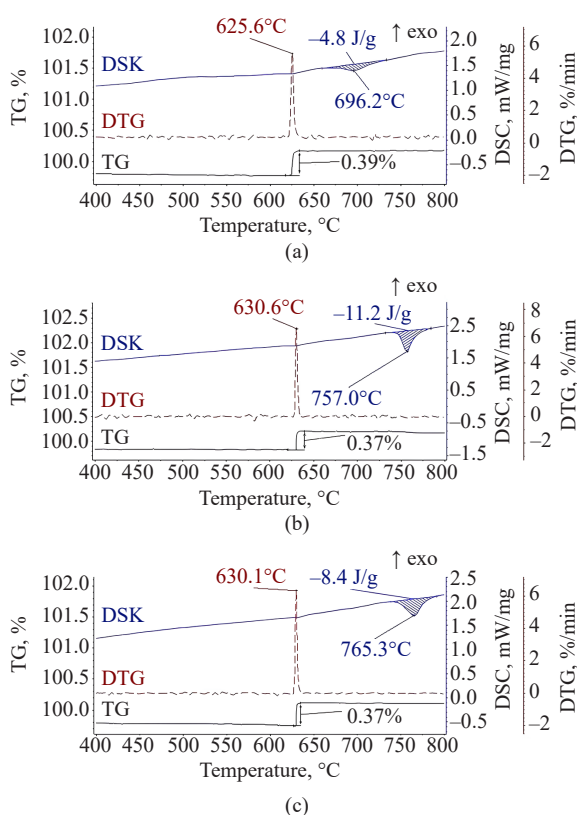


Fig. 5. Thermogravimetric and differential calorimetric curves obtained after sintering at 1100°C

As was shown in [17, 18, 21, 28], the enthalpy of the $\alpha \rightarrow \beta$ $\text{Li}_{0.5}\text{Fe}_{2.5}\text{O}_4$ transition is 12–13 J/g according to the peak area of DSC analysis of ferrite. In our study, the value of enthalpy parameter for sample N0 decreased by more than 60%. For samples N1 and N2, the value of enthalpy reduction was about 10 and 30%, respectively. It is also worth noting that with increasing lanthanum content, the temperature range of the thermal effect shifts to higher temperatures from $660\text{--}730^\circ\text{C}$ (sample N0) to $732\text{--}783^\circ\text{C}$ and $740\text{--}790^\circ\text{C}$ for N1 and N2, respectively. Table 3 shows the T_C values for different samples. The T_C value for lithium ferrite N0 is slightly underestimated compared to samples N1 and N2, whose temperature is close to that reported in the studies [17, 18, 21].

It is suggested that the underestimated values of Curie temperature and DSC peak areas in lithium ferrite $\text{Li}_{0.5}\text{Fe}_{2.5}\text{O}_4$ without the addition of lanthanum indicate a disordered ferrite structure during high-temperature sintering due to the loss of oxygen and lithium by the

sample [20]. As shown in [18, 21], partial formation of disordered phase $\beta\text{-Li}_{0.5}\text{Fe}_{2.5}\text{O}_4$ occurs during sintering. The addition of La prevents the disordered stoichiometric composition of sintered lithium ferrite due to the rearrangement of the internal crystal structure.

CONCLUSIONS

In the present study, the influence of lanthanum content in the $\text{Fe}_2\text{O}_3\text{-Li}_2\text{O-L}(\text{OH})_3$ system on phase formation is investigated along with the structural and electromagnetic properties of composite material based on lithium ferrite $\text{Li}_{0.5}\text{Fe}_{2.5}\text{O}_4$. The confirmed formation of two-phase composite during the sample synthesis process consists of spinel phase $\alpha\text{-Li}_{0.5}\text{Fe}_{2.5}\text{O}_4$ and perovskite-like phase LaFeO_3 , whose concentrations depend on the ratios of initial components and do not change significantly during high-temperature sintering.

The study of structural characteristics showed that the increase in lanthanum concentration at the synthesis stage leads to a decrease in density and increase in porosity of sintered samples. The addition of lanthanum also influences the ordering of the ferrite structure during high-temperature sintering to prevent violation of its stoichiometric composition. There is a slight deterioration in magnetic properties and a significant improvement in electrical properties.

The data confirm the utility of small additions of lanthanum as a means of modifying the properties of lithium ferrite with rare-earth elements for potential use in microwave technology.

Further research in this area will be aimed at varying the small amounts of added lanthanum, as well as changing the temperature and time modes of sintering in order to obtain denser and less porous ferrite ceramics offering a good combination of electromagnetic properties.

Acknowledgments

The research was supported by the Ministry of Science and Higher Education of the Russian Federation in part of the science program (project FSWW-2023-0011).

Authors' contributions

Yu.S. Elkina—investigation, methodology, formal analysis, writing the original draft.

V.A. Vlasov—formal analysis, investigation, supervision.

E.N. Lysenko—validation, data curation.

A.P. Surzhikov—conceptualization, funding acquisition.

The authors declare no conflicts of interest.

REFERENCES

1. Ahmad M., Shahid M., Alanazi Y.M., Rehman A. ur., Asif M., Dunnill C.W. Lithium ferrite ($\text{Li}_{0.5}\text{Fe}_{2.5}\text{O}_4$): synthesis, structural, morphological and magnetic evaluation for storage devices. *J. Mater. Res. Technol.* 2022;18:3386–3395. <https://doi.org/10.1016/j.jmrt.2022.03.113>
2. Khot S.S., Shinde N.S., Basavaiah N., Watawe S.C., Vaidya M.M. Magnetic properties of LiZnCu ferrite synthesized by the microwave sintering method. *J. Magn. Magn. Mater.* 2015;374:182–186. <https://doi.org/10.1016/j.jmmm.2014.08.039>
3. Aravind G., Raghasudha M., Ravinder D., Manivel Raja M., Meena S.S., Bhatt P., Hashim M. Study of structural and magnetic properties of Li–Ni nanoferrites synthesized by citrate-gel auto combustion. *Ceram. Int.* 2016;42(2): 2941–2950. <https://doi.org/10.1016/j.ceramint.2015.10.077>
4. Nikishina E.E. Heterophase synthesis of cobalt ferrite. *Fine Chem. Technol.* 2021;16(6):502–511. <https://doi.org/10.32362/2410-6593-2021-16-6-502-511>
5. Isaev I.M., Kostishin V.G., Korovushkin V.V., et al. Magnetic and Radio-Absorbing Properties of Polycrystalline $\text{Li}_{0.33}\text{Fe}_{2.29}\text{Zn}_{0.21}\text{Mn}_{0.17}\text{O}_4$ Spinel Ferrite. *Tech. Phys.* 2021;66(11):1216–1220. <https://doi.org/10.1134/S1063784221090085>
[Original Russian Text: Isaev I.M., Kostishin V.G., Korovushkin V.V., Salogub D.V., Shakirzyanov R.I., Timofeev A.V., Mironovich A.Yu. Magnetic and Radio-Absorbing Properties of Polycrystalline $\text{Li}_{0.33}\text{Fe}_{2.29}\text{Zn}_{0.21}\text{Mn}_{0.17}\text{O}_4$ Spinel Ferrite. *Zhurnal tekhnicheskoi fiziki.* 2021;91(9):1376–1380 (in Russ.). <https://doi.org/10.21883/JTF.2021.09.51217.74-21>]
6. Isaev I.M., Kostishin V.G., Korovushkin V.V., et al. Crystal chemistry and magnetic properties of polycrystalline spinel ferrites $\text{Li}_{0.33}\text{Fe}_{2.29}\text{Zn}_{0.21}\text{Mn}_{0.17}\text{O}_4$. *Russ. J. Inorg. Chem.* 2021;66(12): 1917–1924. <https://doi.org/10.1134/S0036023621120056>
[Original Russian Text: Isaev I.M., Kostishin V.G., Korovushkin V.V., Shipko M.N., Timofeev A.V., Mironovich A.Yu., Salogub D.V., Shakirzyanov R.I. Crystal chemistry and magnetic properties of polycrystalline spinel ferrites $\text{Li}_{0.33}\text{Fe}_{2.29}\text{Zn}_{0.21}\text{Mn}_{0.17}\text{O}_4$. *Zhurnal neorganicheskoi khimii.* 2021;66(12):1792–1800 (in Russ.). <https://doi.org/10.31857/S0044457X21120059>]
7. Kareva K.V., Suraev A.S., Chervinskaya A.S., Dotsenko O.A., Kushnarev B.O., Minin R.V., Zhuravlev V.A., Wagner D.V. Structural characteristics and magnetic properties of $\text{Ni}_{1-x}\text{Zn}_x\text{Fe}_2\text{O}_4$ ferrimagnets synthesized by the ceramic method. *Izvestiya vuzov. Fizika.* 2023;66(12):5–11 (in Russ.).
8. Punda A.Yu., Gafarova K.P., Zhivulin V.E., Chernukha A.S., Zykova A.R., Gudkova S.A., Pesin L.A., Vyatkin G.P., Vinnik D.A. Synthesis and structure of barium hexaferrite $\text{BaFe}_{12-x}\text{In}_x\text{O}_{19}$ ($x = 0-1$). *Zhurnal obshchei khimii.* 2024;94(2):285–291 (in Russ.). <https://doi.org/10.3157/s0044460x24020149>
9. Maksoud M.I.A.A., El-Ghandour A., Ashour A.H., Atta M.M., Abdelhaleem S., El-Hanbaly A.H., Fahim R.A., Kassem S.M., Shalaby M.S., Awed A.S. La^{3+} doped $\text{LiCo}_{0.25}\text{Zn}_{0.25}\text{Fe}_2\text{O}_4$ spinel ferrite nanocrystals: Insights on structural, optical and magnetic properties. *J. Rare Earths.* 2021;39(1):75–82. <https://doi.org/10.1016/j.jre.2019.12.017>
10. Khan M.A., Sabir M., Mahmood A., Asghar M., Mahmood K., Khan M.A., Ahmad I., Sher M., Warsi M.F. High frequency dielectric response and magnetic studies of $\text{Zn}_{1-x}\text{Tb}_x\text{Fe}_2\text{O}_4$ nanocrystalline ferrites synthesized via micro-emulsion technique. *Magn. Magn. Mater.* 2014;360:188–192. <https://doi.org/10.1016/j.jmmm.2014.02.059>
11. Ahmad I., Abbas T., Ziya A.B., Maqsood A. Structural and magnetic properties of erbium doped nanocrystalline Li–Ni ferrites. *Ceram. Int.* 2014;40(6):7941–7945. <https://doi.org/10.1016/j.ceramint.2013.12.142>
12. Jiang J., Liangchao L., Feng X. Structural analysis and magnetic properties of Gd-doped Li–Ni ferrites prepared using rheological phase reaction method. *J. Rare Earths.* 2007;25(1):79–83. [https://doi.org/10.1016/S1002-0721\(07\)60049-0](https://doi.org/10.1016/S1002-0721(07)60049-0)
13. Mahmoudi M., Kavanlouei M., Maleki-Ghaleh H. Effect of composition on structural and magnetic properties of nanocrystalline ferrite $\text{Li}_{0.5}\text{Sm}_x\text{Fe}_{2.5-x}\text{O}_4$. *Powd. Metall. Met. Ceram.* 2015;54: 31–39. <https://doi.org/10.1007/s1106-015-9676-9>

СПИСОК ЛИТЕРАТУРЫ

1. Ahmad M., Shahid M., Alanazi Y.M., Rehman A. ur., Asif M., Dunnill C.W. Lithium ferrite ($\text{Li}_{0.5}\text{Fe}_{2.5}\text{O}_4$): synthesis, structural, morphological and magnetic evaluation for storage devices. *J. Mater. Res. Technol.* 2022;18:3386–3395. <https://doi.org/10.1016/j.jmrt.2022.03.113>
2. Khot S.S., Shinde N.S., Basavaiah N., Watawe S.C., Vaidya M.M. Magnetic properties of LiZnCu ferrite synthesized by the microwave sintering method. *J. Magn. Magn. Mater.* 2015;374:182–186. <https://doi.org/10.1016/j.jmmm.2014.08.039>
3. Aravind G., Raghasudha M., Ravinder D., Manivel Raja M., Meena S.S., Bhatt P., Hashim M. Study of structural and magnetic properties of Li–Ni nanoferrites synthesized by citrate-gel auto combustion. *Ceram. Int.* 2016;42(2): 2941–2950. <https://doi.org/10.1016/j.ceramint.2015.10.077>
4. Никишина Е.Е. Гетерофазный синтез феррита кобальта. *Тонкие химические технологии.* 2021;16(6):502–511. <https://doi.org/10.32362/2410-6593-2021-16-6-502-511>
5. Исаев И.М., Костишин В.Г., Коровушкин В.В., Салогуб Д.В., Шакирзянов Р.И., Тимофеев А.В., Миронович А.Ю. Магнитные и радиопоглощающие свойства поликристаллического феррита-шпинели $\text{Li}_{0.33}\text{Fe}_{2.29}\text{Zn}_{0.21}\text{Mn}_{0.17}\text{O}_4$. *Журн. техн. физики (ЖТФ).* 2021;91(9):1376–1380. <https://doi.org/10.21883/JTF.2021.09.51217.74-21>
6. Исаев И.М., Костишин В.Г., Коровушкин В.В., Шипко М.Н., Тимофеев А.В., Миронович А.Ю., Салогуб Д.В., Шакирзянов Р.И. Кристаллохимия и магнитные свойства поликристаллических ферритов-шпинелей $\text{Li}_{0.33}\text{Fe}_{2.29}\text{Zn}_{0.21}\text{Mn}_{0.17}\text{O}_4$. *Журн. неорган. химии.* 2021;66(12):1792–1800. <https://doi.org/10.31857/S0044457X21120059>
7. Карева К.В., Сураев А.С., Червинская А.С., Доценко О.А., Кушнарев Б.О., Минин Р.В., Журавлев В.А., Вагнер Д.В. Структурные характеристики и магнитные свойства синтезированных керамических методом ферримagnetиков $\text{Ni}_{1-x}\text{Zn}_x\text{Fe}_2\text{O}_4$. *Известия вузов. Физика.* 2023;66(12):5–11.
8. Пунда А.Ю., Гафарова К.П., Живулин В.Е., Чернуха А.С., Зыкова А.Р., Гудкова С.А., Песин Л.А., Вяткин Г.П., Винник Д.А. Синтез и структура гексаферрита бария $\text{BaFe}_{12-x}\text{In}_x\text{O}_{19}$ ($x = 0-1$). *Журн. общей химии.* 2024;94(2): 285–291. <https://doi.org/10.31857/s0044460x24020149>
9. Maksoud M.I.A.A., El-Ghandour A., Ashour A.H., Atta M.M., Abdelhaleem S., El-Hanbaly A.H., Fahim R.A., Kassem S.M., Shalaby M.S., Awed A.S. La^{3+} doped $\text{LiCo}_{0.25}\text{Zn}_{0.25}\text{Fe}_2\text{O}_4$ spinel ferrite nanocrystals: Insights on structural, optical and magnetic properties. *J. Rare Earths.* 2021;39(1):75–82. <https://doi.org/10.1016/j.jre.2019.12.017>
10. Khan M.A., Sabir M., Mahmood A., Asghar M., Mahmood K., Khan M.A., Ahmad I., Sher M., Warsi M.F. High frequency dielectric response and magnetic studies of $\text{Zn}_{1-x}\text{Tb}_x\text{Fe}_2\text{O}_4$ nanocrystalline ferrites synthesized via micro-emulsion technique. *Magn. Magn. Mater.* 2014;360:188–192. <https://doi.org/10.1016/j.jmmm.2014.02.059>
11. Ahmad I., Abbas T., Ziya A.B., Maqsood A. Structural and magnetic properties of erbium doped nanocrystalline Li–Ni ferrites. *Ceram. Int.* 2014;40(6):7941–7945. <https://doi.org/10.1016/j.ceramint.2013.12.142>
12. Jiang J., Liangchao L., Feng X. Structural analysis and magnetic properties of Gd-doped Li–Ni ferrites prepared using rheological phase reaction method. *J. Rare Earths.* 2007;25(1):79–83. [https://doi.org/10.1016/S1002-0721\(07\)60049-0](https://doi.org/10.1016/S1002-0721(07)60049-0)
13. Mahmoudi M., Kavanlouei M., Maleki-Ghaleh H. Effect of composition on structural and magnetic properties of nanocrystalline ferrite $\text{Li}_{0.5}\text{Sm}_x\text{Fe}_{2.5-x}\text{O}_4$. *Powd. Metall. Met. Ceram.* 2015;54: 31–39. <https://doi.org/10.1007/s1106-015-9676-9>

11. Ahmad I., Abbas T., Ziya A.B., Maqsood A. Structural and magnetic properties of erbium doped nanocrystalline Li-Ni ferrites. *Ceram. Int.* 2014;40(6):7941–7945. <https://doi.org/10.1016/j.ceramint.2013.12.142>
12. Jiang J., Liangchao L., Feng X. Structural analysis and magnetic properties of Gd-doped Li-Ni ferrites prepared using rheological phase reaction method. *J. Rare Earths.* 2007;25(1):79–83. [https://doi.org/10.1016/S1002-0721\(07\)60049-0](https://doi.org/10.1016/S1002-0721(07)60049-0)
13. Mahmoudi M., Kavanlouei M., Maleki-Ghaleh H. Effect of composition on structural and magnetic properties of nanocrystalline ferrite $\text{Li}_{0.5}\text{Sm}_x\text{Fe}_{2.5-x}\text{O}_4$. *Powd. Metall. Met. Ceram.* 2015;54:31–39. <https://doi.org/10.1007/s11106-015-9676-9>
14. Nikumbh A.K., Pawar R.A., Nighot D.V., Gugale G.S., Sangale M.D., Khanvilkar M.B., Nagawade A.V. Structural, electrical, magnetic and dielectric properties of rare-earth substituted cobalt ferrites nanoparticles synthesized by the co-precipitation method. *J. Magn. Magn. Mater.* 2014;355:201–209. <https://doi.org/10.1016/j.jmmm.2013.11.052>
15. Садыков С.А., Каллаев С.Н., Эмиров Р.М., Алиханов Н.М.-Р. Электрические свойства керамики BiFeO_3 , легированной Sm. *Физика твердого тела.* 2023;65(10):1727–1736. <https://doi.org/10.61011/FTT.2023.10.56320.149>
16. Хабиров Р.Р., Масс А.В., Кузьмин Р.И., Руктуев А.А., Черкасова Н.Ю., Агафонов М.Ю., Королева В.А., Миллер А.А. Особенности формирования структуры и свойств Mn-Zn-ферритов, полученных методом золь-гель синтеза. *Письма в ЖТФ.* 2024;50(9):21–26. <https://doi.org/10.61011/PJTF.2024.09.57563.19834>
17. Lysenko E.N., Vlasov V.A., Nikolaeva S.A., Nikolaev E.V. TG, DSC, XRD, and SEM studies of the substituted lithium ferrite formation from milled $\text{Sm}_2\text{O}_3/\text{Fe}_2\text{O}_3/\text{Li}_2\text{CO}_3$ precursors. *J. Therm. Anal. Calorim.* 2023;148(4):1445–1453. <https://doi.org/10.1007/s10973-022-11665-1>
18. Lysenko E.N., Surzhikov A.P., Astafyev A.L. Thermomagnetic analysis of lithium ferrites. *J. Therm. Anal. Colorim.* 2019;136(2):441–445. <https://doi.org/10.1007/s10973-018-7678-9>
19. Lysenko E.N., Nikolaeva S.A., Surzhikov A.P., Ghyngazov S.A., Plotnikova I.V., Zhuravlev A., Zhuravleva E.V. Electrical and magnetic properties of ZrO_2 -doped lithium-titanium-zinc ferrite ceramics. *Ceram. Int.* 2019;45(16):20148–20154. <https://doi.org/10.1016/j.ceramint.2019.06.282>
20. Ridley D.H., Lessoff H., Childress J.D. Effect of lithium and oxygen losses on magnetic and crystallographic properties of spinel lithium ferrite. *J. Am. Ceram. Soc.* 1970;53(6):304–311. <https://doi.org/10.1111/J.1151-2916.1970.TB12113.X>
21. Surzhikov A.P., Frangulyan T.S., Ghyngazov S.A., Lysenko E.N. Investigation of structural states and oxidation processes in $\text{Li}_{0.5}\text{Fe}_{2.5}\text{O}_{4-\delta}$ using TG analysis. *J. Therm. Anal. Calorim.* 2012;108(3):1207–1212. <https://doi.org/10.1007/s10973-011-1734-z>
22. Bulai G., Diamandescu L., Dumitru I., Gurlui S., Feder M., Caltun O.F., Effect of rare earth substitution in cobalt ferrite bulk materials. *J. Magn. Magn. Mater.* 2015;390:123–131. <https://doi.org/10.1016/j.jmmm.2015.04.089>
23. Mohanty V., Cheruku R., Vijayan L., Govindaraj G. Ce-substituted Lithium Ferrite: Preparation and Electrical Relaxation Studies. *J. Mater. Sci. Technol.* 2014;30(4):335–341. <https://doi.org/10.1016/j.jmst.2013.10.028>
24. Al-Hilli M.F., Li S., Kassim K.S. Structural analysis, magnetic and electrical properties of samarium substituted lithium-nickel mixed ferrites. *J. Magn. Magn. Mater.* 2012;324(5):873–879. <https://doi.org/10.1016/j.jmmm.2011.10.005>
25. An S.Y., Shim I.B., Kim C.S. Synthesis and magnetic properties of LiFe_5O_8 powders by a sol-gel process. *J. Magn. Magn. Mater.* 2005;290–291:1551–1554. <https://doi.org/10.1016/j.jmmm.2004.11.244>
26. Mazen S.A., Abu-Elsaad N.I. Characterization and magnetic investigations of germanium-doped lithium ferrite. *Ceram. Int.* 2014;40(7):11229–11237. <https://doi.org/10.1016/j.ceramint.2014.03.167>
27. Abdellatif M.H., El-Komy G.M., Azab A.A., Magnetic characterization of rare earth doped spinel ferrite. *J. Magn. Magn. Mater.* 2017;442:445–452. <https://doi.org/10.1016/j.jmmm.2017.07.020>

22. Bulai G., Diamandescu L., Dumitru I., Gurlui S., Feder M., Caltun O.F., Effect of rare earth substitution in cobalt ferrite bulk materials. *J. Magn. Magn. Mater.* 2015;390:123–131. <https://doi.org/10.1016/j.jmmm.2015.04.089>
23. Mohanty V., Cheruku R., Vijayan L., Govindaraj G. Ce-substituted Lithium Ferrite: Preparation and Electrical Relaxation Studies. *J. Mater. Sci. Technol.* 2014;30(4): 335–341. <https://doi.org/10.1016/j.jmst.2013.10.028>
24. Al-Hilli M.F., Li S., Kassim K.S. Structural analysis, magnetic and electrical properties of samarium substituted lithium–nickel mixed ferrites. *J. Magn. Magn. Mater.* 2012;324(5):873–879. <https://doi.org/10.1016/j.jmmm.2011.10.005>
25. An S.Y., Shim I.B., Kim C.S. Synthesis and magnetic properties of LiFe_5O_8 powders by a sol–gel process. *J. Magn. Magn. Mater.* 2005;290–291:1551–1554. <https://doi.org/10.1016/j.jmmm.2004.11.244>
26. Mazen S.A., Abu-Elsaad N.I. Characterization and magnetic investigations of germanium-doped lithium ferrite. *Ceram. Int.* 2014;40(7):11229–11237. <https://doi.org/10.1016/j.ceramint.2014.03.167>
27. Abdellatif M.H., El-Komy G.M., Azab A.A., Magnetic characterization of rare earth doped spinel ferrite. *J. Magn. Magn. Mater.* 2017;442:445–452. <https://doi.org/10.1016/j.jmmm.2017.07.020>
28. Berbenni V., Marini A., Capsoni D. Solid state reaction study of the system $\text{Li}_2\text{CO}_3/\text{Fe}_2\text{O}_3$. *Z. Naturforschung – Sect. J. Phys. Sci.* 1998;53:997–1003. <https://doi.org/10.1515/zna-1998-1212>

About the Authors

Yuliya S. Elkina, Postgraduate Student, Research Laboratory for Electronics, Semiconductors and Dielectrics, Research School of High-Energy Physics, Tomsk Polytechnic University (30, Lenina pr., Tomsk, 634034, Russia). E-mail: ysm7@tpu.ru. Scopus Author ID 58892380200, ResearcherID HHS-0003-2022, RSCI SPIN-code 6717-1540, <https://orcid.org/0000-0002-2708-9872>

Vitaly A. Vlasov, Cand. Sci. (Phys.-Math.), Senior Researcher, Research Laboratory for Electronics, Semiconductors and Dielectrics, Research School of High-Energy Physics, Tomsk Polytechnic University (30, Lenina pr., Tomsk, 634034, Russia). E-mail: vlvitan@tpu.ru. Scopus Author ID 7202194125, ResearcherID K-1257-2013, RSCI SPIN-code 2003-8431, <https://orcid.org/0000-0002-5946-2117>

Elena N. Lysenko, Dr. Sci. (Eng.), Professor, Head of the Laboratory, Research Laboratory for Electronics, Semiconductors and Dielectrics, Research School of High-Energy Physics, Tomsk Polytechnic University (30, Lenina pr., Tomsk, 634034, Russia). E-mail: lysenkoen@tpu.ru. Scopus Author ID 25027787100, ResearcherID K-1582-2013, RSCI SPIN-code 6536-9390, <https://orcid.org/0000-0002-5093-2207>

Anatoly P. Surzhikov, Dr. Sci. (Phys.-Math.), Professor, Head of the Department, Division for Testing and Diagnostics, School of Non-Destructive Testing, Tomsk Polytechnic University (30, Lenina pr., Tomsk, 634034, Russia). surzhikov@tpu.ru. Scopus Author ID 6603494148, ResearcherID K-1224-2013, RSCI SPIN-code 1875-0293, <https://orcid.org/0000-0003-2795-398X>

Об авторах

Елькина Юлия Сергеевна, аспирант, проблемная научно-исследовательская лаборатория электроники диэлектриков и полупроводников, Исследовательская школа физики высокоэнергетических процессов, ФГАОУ ВО «Национальный исследовательский Томский политехнический университет» (634050, Россия, г. Томск, пр. Ленина, д. 30). E-mail: ysm7@tpu.ru. Scopus Author ID 58892380200, ResearcherID HNS-0003-2022, SPIN-код РИНЦ 6717-1540, <https://orcid.org/0000-0002-2708-9872>

Власов Виталий Анатольевич, к.ф.-м.н., старший научный сотрудник, проблемная научно-исследовательская лаборатория электроники диэлектриков и полупроводников, Исследовательская школа физики высокоэнергетических процессов, ФГАОУ ВО «Национальный исследовательский Томский политехнический университет» (634050, Россия, г. Томск, пр. Ленина, д. 30). E-mail: vlvitan@tpu.ru. Scopus Author ID 7202194125, ResearcherID K-1257-2013, SPIN-код РИНЦ 2003-8431, <https://orcid.org/0000-0002-5946-2117>

Лысенко Елена Николаевна, д.т.н., профессор, заведующая лабораторией, проблемная научно-исследовательская лаборатория электроники диэлектриков и полупроводников, Исследовательская школа физики высокоэнергетических процессов, ФГАОУ ВО «Национальный исследовательский Томский политехнический университет» (634050, Россия, г. Томск, пр. Ленина, д. 30). E-mail: lysenkoen@tpu.ru. Scopus Author ID 25027787100, ResearcherID K-1582-2013, SPIN-код РИНЦ 6536-9390, <https://orcid.org/0000-0002-5093-2207>

Суржиков Анатолий Петрович, д.ф.-м.н., профессор, заведующий кафедрой – руководитель отделения на правах кафедры, отделение контроля и диагностики, Инженерная школа неразрушающего контроля и безопасности, ФГАОУ ВО «Национальный исследовательский Томский политехнический университет» (634050, Россия, г. Томск, пр. Ленина, д. 30). E-mail: surzhikov@tpu.ru. Scopus Author ID 6603494148, ResearcherID K-1224-2013, SPIN-код РИНЦ 1875-0293, <https://orcid.org/0000-0003-2795-398X>

Translated from Russian into English by H. Moshkov

Edited for English language and spelling by Thomas A. Beavitt

UDC 54.03; 537

<https://doi.org/10.32362/2410-6593-2025-20-2-167-184>

EDN ABZEFD



RESEARCH ARTICLE

Post-vibration activity of electrochemically activated water

Olga V. Slatinskaia, German O. Stepanov✉, Olga V. Fartushnaya, Evgenii V. Zubkov,
Anastasia D. Zatykina, Olesya M. Gizitdinova, Nikita S. Karpov, Alexey V. Smirnov,
Vladimir S. Boriskin, Natalia N. Rodionova, Anastasia O. Petrova

NPF "MATERIA MEDICA HOLDING," Moscow, 129272 Russia

✉ Corresponding author, e-mail: stepanovgo@materiamedica.ru

Abstract

Objectives. It was recently discovered that water samples with modified physicochemical properties can be obtained by successive vibration treatment of intact water together with a solution of a substance located in separate closely spaced vials. We refer to such samples as iterations. By adding the vibrational iterations into the initial substance, the physicochemical properties of the latter are changed, i.e., they demonstrate post-vibration activity. In addition, it has been shown that vibrational iterations can be obtained using water treated with a magnetic field as the initial substance. On this basis, we may hypothesize that the phenomenon of post-vibration activity is universal. To confirm this hypothesis, water treated with an electric signal having various parameters (electrochemically activated water) was used as the initial substance for the preparation of vibrational iterations.

Methods. The physicochemical properties of vibrational iterations, which were obtained from electrochemically activated water, were studied by conductometry, terahertz spectroscopy, and radiometry. The effect of the initial substance or its vibrational iterations on intact water (a neutral carrier) was evaluated by dynamic light scattering. For this purpose, the intensity of light scattering by the sample and the hydrodynamic diameter of optical heterogeneities were measured. The attenuation coefficient of an additional electric signal applied to the samples was determined.

Results. The obtained vibrational iterations differ from intact water and their mixtures with intact water in terms of specific electrical conductivity, power flux density of microwave radiation, as well as in the contribution of the main (Debye) relaxation process to the overall dielectric response. Mixtures of vibrational iterations with water also differ from intact water in terms of the size of optical heterogeneities. By analogy with the vibrational iterations for which solutions of high- and low-molecular-weight substances were used as the initial substance, vibrational iterations obtained using electrochemically activated water can be classified into different groups (fractions) according to their physicochemical characteristics. Different degrees of changes in the physicochemical characteristics are observed depending on the parameters of the electric signal used to obtain the initial substance. The efficiency of electrical signal propagation in these mixtures, as estimated by the signal strength attenuation coefficient, is additionally changed. The addition of the initial substance (electrochemically activated water) to intact water also leads to changes in the physicochemical properties of the resulting mixture compared to the control. Depending on the parameters of the electric signal used to obtain the initial substance, the magnitude of changes in the physicochemical characteristics of these mixtures similarly varies.

Conclusions. The fundamental possibility of obtaining vibrational iterations from electrochemically activated water similarly to vibrational iterations prepared in other studies, was demonstrated. This confirms the universality of the phenomenon of post-vibration activity.

Keywords

vibrational iterations, post-vibration activity, electrochemical activation, aqueous solutions, conductometry, THz spectroscopy, dynamic light scattering, optical heterogeneities

Submitted: 19.12.2024

Revised: 03.02.2024

Accepted: 21.02.2025

For citation

Slatinskaia O.V., Stepanov G.O., Fartushnaya O.V., Zubkov E.V., Zatykina A.D., Gizitdinova O.M., Karpov N.S., Smirnov A.V., Boriskin V.S., Rodionova N.N., Petrova A.O. Post-vibration activity of electrochemically activated water. *Tonk. Khim. Tekhnol. = Fine Chem. Technol.* 2025;20(2):167–184. <https://doi.org/10.32362/2410-6593-2025-20-2-167-184>

НАУЧНАЯ СТАТЬЯ

Поствибрационная активность электрохимически активированной воды

О.В. Слатинская, Г.О. Степанов✉, О.В. Фартушная, Е.В. Зубков, А.Д. Затыкина, О.М. Гизитдинова, Н.С. Карпов, А.В. Смирнов, В.С. Борискин, Н.Н. Родионова, А.О. Петрова

НПФ «Материа Медика Холдинг», Москва, 129272 Россия

✉ Автор для переписки, e-mail: stepanovgo@materiamedica.ru

Аннотация

Цели. Недавно открыто, что при последовательной вибрационной обработке интактной воды совместно с раствором вещества, находящихся в разных, вплотную расположенных пробирках, можно получить образцы воды, обладающие измененными физико-химическими свойствами. Такие образцы названы нами «вибрационными итерациями». При добавлении вибрационных итераций в исходную субстанцию, они способны изменять ее физико-химические свойства, т.е. вибрационные итерации обладают поствибрационной активностью. Кроме того, было показано, что вибрационные итерации можно получить при использовании в качестве исходной субстанции воды, обработанной магнитным полем. Это позволило предположить, что феномен поствибрационной активности имеет универсальный характер. Для подтверждения этой гипотезы в настоящем исследовании в качестве исходной субстанции для приготовления вибрационных итераций использовали воду, обработанную электрическим сигналом с различными параметрами (электрохимически активированная вода).

Методы. Изучение физико-химических свойств полученных вибрационных итераций, которые являются производными от электрохимически активированной воды, проводили методами кондуктометрии, терагерцовой спектроскопии, радиометрии. Воздействие исходной субстанции или ее вибрационных итераций на интактную воду (нейтральный носитель) оценивали методом динамического рассеяния света. Для этого измеряли интенсивность рассеяния света образцом и гидродинамический диаметр оптических гетерогенностей. Кроме этого, пропускали через образцы электрический сигнал для определения коэффициента его ослабления.

Результаты. Показано, что полученные вибрационные итерации и их смеси с водой отличаются от интактной воды по значениям удельной электропроводности, потока мощности микроволнового излучения, а также по вкладу основного (Дебаевского) релаксационного процесса в общий диэлектрический отклик. Смеси вибрационных итераций с водой также отличаются от интактной воды по размеру оптических гетерогенностей. Аналогично вибрационным итерациям, для которых в качестве исходной субстанции использовали растворы высоко- и низкомолекулярных веществ, вибрационные итерации, полученные с использованием электрохимически активированной воды, в соответствии с физико-химическими свойствами могут быть классифицированы на различные группы (фракции). Показано, что физико-химические характеристики таких групп изменяются в различной степени в зависимости от показателей электрического сигнала, использованного для получения исходной субстанции. Кроме того, в данных смесях меняется эффективность распространения электрического сигнала, оцениваемая по коэффициенту его ослабления. Внесение исходной субстанции (электрохимически активированной воды) в интактную воду также приводит к изменениям физико-химических свойств полученной смеси по сравнению с контролем. Аналогично, в зависимости от показателей электрического сигнала, использованного для получения исходной субстанции, выраженность изменений физико-химических характеристик смеси различается.

Выводы. Показана принципиальная возможность получения вибрационных итераций из электрохимически активированной воды, аналогично вибрационным итерациям растворов, использованных в других исследованиях, что является подтверждением универсальности феномена поствибрационной активности.

Ключевые слова

вибрационные итерации, поствибрационная активность, электрохимическая активация, водные растворы, кондуктометрия, ТГц-спектроскопия, динамическое рассеяние света, оптические гетерогенности

Поступила: 19.12.2024

Доработана: 03.02.2024

Принята в печать: 21.02.2025

Для цитирования

Слатинская О.В., Степанов Г.О., Фартушная О.В., Зубков Е.В., Затыкина А.Д., Гизитдинова О.М., Карпов Н.С., Смирнов А.В., Борискин В.С., Родионова Н.Н., Петрова А.О. Поствибрационная активность электрохимически активированной воды. *Тонкие химические технологии.* 2025;20(2):167–184. <https://doi.org/10.32362/2410-6593-2025-20-2-167-184>

1. INTRODUCTION

Vibrational treatment of various substances (low- and high-molecular-weight) changes their properties and imparts the ability to participate in distant interactions [1, 2–4]. It has recently been discovered that sequential vibrational treatment (crossing) of two solutions, one of which is a solution of the initial substance and the other is a neutral carrier (intact water), which are located in separate closely spaced vials, can produce water samples having different physicochemical properties from those of the neutral carrier. Such samples are called *vibrational iterations* [1]. Unlike a neutral carrier, the addition of vibrational iterations into the initial substance is capable of changing the physicochemical properties of the initial substance, i.e., vibrational iterations demonstrate post-vibration activity. Vibrational iterations differ from intact water in terms of their physicochemical properties, allowing them to be classified into groups (fractions).

It has been shown that vibrational iterations can be obtained not only from high- and low-molecular-weight substances used as the initial substance, but also from water treated with an external physical factor such as a magnetic field [5]. An earlier study of vibrational iterations prepared from magnetized water demonstrated that they differ from each other in terms of their physicochemical properties [5]. It is likely that various physical factors can be used to obtain samples demonstrating post-vibration activity. One of the types of treatment that can influence the physicochemical properties of water is electrochemical activation (ECA) [6–8]. ECA is carried out by passing through water an electric signal with defined parameters [9–17]. Thus, we assume that ECA water can be used to prepare vibration iterations.

The present study sets out to confirm the universal character of the post-vibration activity phenomenon. For this purpose, vibrational iterations were obtained from water previously subjected to electrical treatment at different signal parameters to study the possibility of their classification according to physicochemical properties into fractions demonstrating post-vibration activity. Then, the effect of different fractions of vibrational iterations on the physicochemical properties of intact water was studied by comparing the samples with the initial substance (ECA water) from which the vibrational iterations were prepared.

2. MATERIALS AND METHODS

Ultrapure water obtained using a Milli-Q Integral 5 water purification system (*Millipore*, France) was used in the study. Freshly produced purified water having specific conductivity $\sim 0.06 \mu\text{S}/\text{cm}$ was kept for at least 1 h at ambient conditions (temperature 24.5°C , humidity

45–50%, and normal atmospheric pressure). After this period, the specific conductivity of the water was $0.731 \pm 0.011 \mu\text{S}/\text{cm}$. Purified water was also present among experimental samples, where it is labeled as “intact water.”

2.1. Samples

In accordance with the purpose of the work, vibrational iterations of ECA water, their mixtures with intact water (to assess their post-vibration activity on intact water), and mixtures of ECA water with intact water (to assess its effect on intact water) were studied. To perform ECA of water, voltages less 0.8 V and more 8 V (that is more than the threshold of water electrolysis ($\sim 1.5\text{--}2.0 \text{ V}$ [18])) were selected. Electrical treatment was carried out using both a constant and a sinusoidal signal. The frequency of the sinusoidal signal was 12.6 Hz, which corresponds to the frequency of the ion cyclotron resonance of water (12.6 Hz) [6].

Thus, three groups of samples were prepared.

Group 1. Vibrational iterations of ECA water:

- vibrational iterations of water to which a constant electric signal with a voltage of 0.8 V was applied (hereinafter referred to as vibrational iterations of “ECA water 0.8 V”);
- vibrational iterations of water to which a sinusoidal electric signal with an amplitude of 0.8 V and a frequency of 12.6 Hz was applied (hereinafter referred to as vibrational iterations of “ECA water 0.8 V, 12.6 Hz”);
- vibrational iterations of water to which a constant electric signal with a voltage of 8 V was applied (hereinafter referred to as vibrational iterations of “ECA water 8 V”);
- vibrational iterations of water to which a sinusoidal electric signal with an amplitude of 8 V and a frequency of 12.6 Hz was applied (hereinafter referred to as vibrational iterations of “ECA water 8 V, 12.6 Hz”);
- vibrational iterations of water placed in a cuvette for electric treatment, but in the absence of voltage applied to the electrodes (hereinafter referred to as vibrational iterations of “ECA water 0 V”).

Group 2. Mixtures of vibrational iterations of ECA water with intact water in a volume ratio of 1 : 9 and control:

- vibrational iterations of ECA water (group 1) + intact water;
- control (mixture of “intact water + intact water”).

Group 3. Mixtures of ECA water with intact water in a volume ratio of 1 : 9 and control:

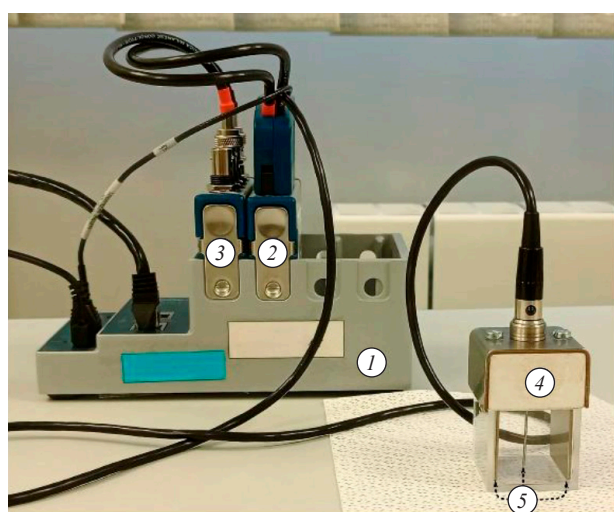
- Water to which an electrical signal with different parameters was applied (ECA water) + intact water;
- Control (mixture of “intact water + intact water”).

2.2. Obtaining electrochemically activated water: treating water with an electric signal

To obtain ECA water, we used an electric signal treatment device (*Vitek-Avtomatika*, Russia), a hardware and software complex consisting of an arbitrary waveform signal generator (NI 9263, *National Instruments*, USA) and a measuring module (NI 9215, *National Instruments*, USA) installed in a chassis (cDAQ-9185, *National Instruments*, USA). The device is operated under the control of LabView software (*National Instruments*, USA). The water incubation period was controlled using a laboratory timer (*VWR® Traceable®*, Germany). Figure 1 demonstrates the appearance and diagram of an electric signal treatment device.

An optical glass cuvette (704-001-30-10, *Hellma Analytcs*, Germany) was filled with 18 mL of ultrapure water. Two plate electrodes made of AISI 304 stainless steel were placed inside the cuvette along two opposite walls. The electrode area completely covered the corresponding wall of the cuvette. Then, for 60 min, a potential difference with the following parameters was applied to the plate electrodes:

- constant electrical signal with a voltage of 0.8 V;
- electrical sinusoidal signal with an amplitude of 0.8 V and a frequency of 12.6 Hz;
- constant electrical signal with a voltage of 8 V;
- electrical sinusoidal signal with an amplitude of 8 V and a frequency of 12.6 Hz;



(a)

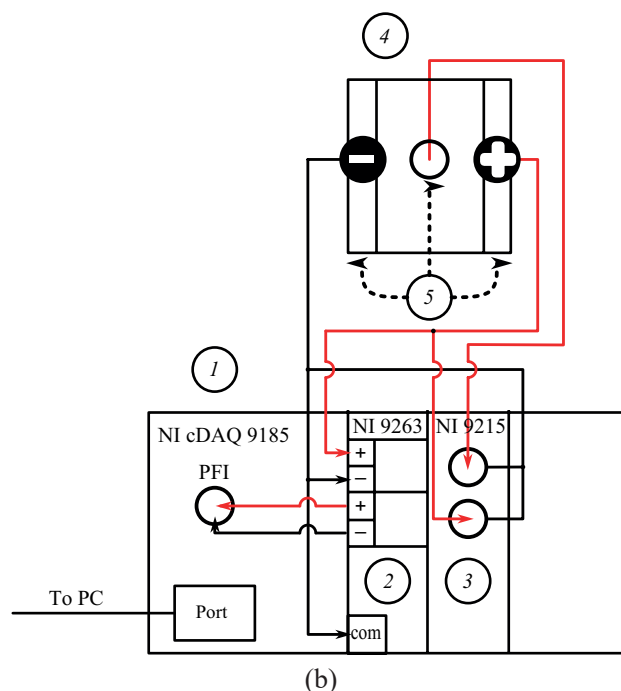
- electrical signal with a voltage of 0 V (i.e., the electrical signal generator was turned off).

In this way, 5 types of ECA water samples were obtained.

2.3. Preparation of vibrational iterations from ECA water

A row of vibrational iterations was prepared from each type of ECA water obtained in accordance with the parameters of the electrical signals applied to the electrodes (i.e., 5 different rows of vibrational iterations were obtained). Transparent borosilicate glass vials (250 mL, *Simax*, Czech Republic) were used to prepare vibrational iterations. Schematic representation of the method for preparing vibration iterations is presented in Fig. 2.

ECA water (18 mL) obtained after electric treatment was placed in a borosilicate glass vial (Fig. 2). Next, 180 mL of intact water (neutral carrier) were added to another vial. The filled vials were placed close to each other and subjected to joint vibration (MS 3 basic vortex with MS 1.21 platform, *IKA-Werke*, Germany) for 10 s at 3000 rpm, after which they were incubated for 1 min at room temperature of 24.5°C (during such process, crossing of water with the initial substance occurred). As a result, 180 mL of the zero vibrational iteration (hereinafter, I0) was obtained in the vial with intact water.



(b)

Fig. 1. (a) Photo and (b) schematic diagram of the electric signal treatment device. (1) NI cDAQ-9185 chassis; (2) NI 9263 module (arbitrary waveform generator); (3) NI 9215 module (analog-to-digital signal meter); (4) optical glass cuvette; (5) stainless steel immersed plate electrodes located along the walls of the cuvette, and a needle electrode, which is located in the center of the cuvette

To obtain vibrational iteration No. 1 (I1), a vial with 180 mL of vibrational iteration I0 was placed close to another borosilicate glass vial with intact water (neutral carrier) in a volume of 180 mL and subjected to joint (with close contact) vibration on a vortex for 10 s at 3000 rpm, after which they were incubated for 1 min at room temperature. As a result, 180 mL of vibrational iteration I1 was obtained in the vial with intact water.

The above steps were repeated to obtain vibrational iterations, up to I7 (Step 2, Fig. 2). Samples from I0 to I7 constituted a row of iterations.

Vibrational iterations of ECA water were prepared on the same day at room temperature. If the study of the properties of vibrational iterations or mixtures containing them was not conducted on the day of preparation, then on the day of analysis of vibrational iterations, they were once processed on a vortex for 10 s at 3000 rpm. Before preparing mixtures with ECA water, for 1 h it was subjected to repeated treatment with electric signal with the same parameters that were used in the primary treatment.

2.4. Preparation of mixtures with intact water

To study the ability of ECA water (substance) and vibrational iterations to change the physicochemical properties of intact water, mixtures of vibrational iterations (or ECA water, or intact water as a control) with intact water were prepared in a volume ratio of 1 : 9. The mixtures were prepared immediately before carrying out measurements. Depending on the final volume required for measurements, the mixtures were prepared in 20 or 40 mL borosilicate glass vials (*Glastechnik Grafenroda*, Germany) for radiometry or conductometry, respectively, or in 2 mL plastic test tubes (*Eppendorf*, Germany) for THz spectroscopy.

3. METHODS OF ANALYSIS

3.2. Conductometry, radiometry, and THz spectroscopy

The properties of the samples were studied by conductometry (specific electrical conductivity) and radiometry (power flux density), as described in [1] (Table 1). The study using the THz spectroscopy (determining dielectric constant ϵ_{r1} , i.e., contribution of the main (Debye) relaxation process to the overall dielectric response) was conducted in two versions:

- (1) mixing 1 part of the test sample (control or vibrational iterations of ECA water) with 99 parts of intact water as described in [1];
- (2) mixing 1 part of the test sample (control, ECA water or vibrational iterations of ECA water) with 9 parts of intact water.

The samples were subjected to the following numbers of measurements: conductometry—9; radiometry—not less than 6; THz spectroscopy—not less than 10.

In the present work, the analysis of vibrational iterations classified into fractions in accordance with [1] was carried out. Vibrational iterations can be classified into four types of fractions as compared to intact water in terms of their unique physicochemical properties, as well as according to their ability to influence the physicochemical properties of intact water and aqueous solutions (the so-called *modifying effect*). These four types of fractions were named Active, Native, Semi-Active, and Semi-Native. In the work [1], it was demonstrated that the number of Active fractions increases at the end of the iteration rows and over time during their storage, while the Active fraction exhibits stability in its physicochemical properties when mixed with other types of fractions. In the present work, only the Active and Native or Semi-Native fractions were used to study the modifying effect of vibrational iterations on intact water.

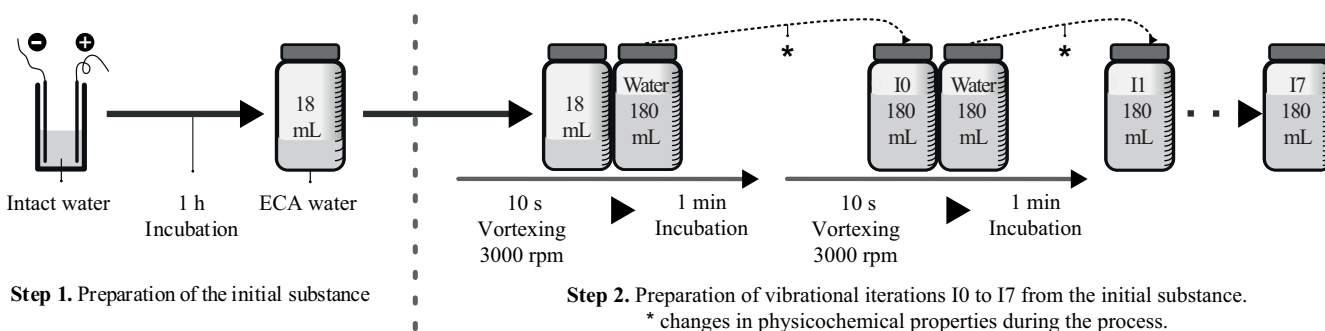


Fig. 2. Preparation of vibrational iterations of electrochemically activated water. Designations: Water is intact water (neutral carrier); ECA water is electrochemically activated water; I0 is the zero vibrational iteration of ECA water; I1 is the vibrational iteration No. 1 of ECA water, ..., I7 is the vibrational iteration No. 7 of ECA water

In addition to conductometry, radiometry, and THz spectroscopy, we used the following methods for sample analysis: dynamic light scattering and oscillography (determination of the attenuation coefficient of the signal passed through the studied sample).

3.3. Dynamic light scattering

The scattering intensity of solutions and the distribution of hydrodynamic diameters of optical heterogeneities in the range of 50–200 nm were determined on a Photocor Compact-Z analyzer (*Photocor*, Russia). The analyzer was equipped with a temperature stabilized continuous-wave semiconductor laser (80 mW of maximum output power at 638 nm wavelength) with a thermostated cell compartment ($25 \pm 0.1^\circ\text{C}$). The signal was recorded for 20 s; the number of signal accumulations was 10. The number of measurements of each sample was at least 10. To establish the particle diameter according to the Stokes–Einstein equation, the viscosity of water was taken as 0.89 mPa·s. Size distributions were calculated using the DynaLS software (version 2.8.3) supplied with the device (*Alango*, Israel).

3.4. Determination of the attenuation coefficient of the signal passed through the studied sample (oscillography)

18 mL of the mixture “ECA water + intact water” (group 3) or “vibrational iteration + intact water” (group 2) in a volume ratio of 1 : 9 were added into a clean cuvette of the electric treatment device, and electrodes were immersed in the mixture. An electric signal (of the type used to prepare ECA water) was applied for 3 min. The procedure was repeated five times. In all cases (both for supplying constant and alternating sinusoidal signals), an arbitrary waveform generator NI 9263 (*National Instruments*, USA) was connected to the plate electrodes (“–” electrode and “+” electrode) of the cuvette (Fig. 1). The signal was recorded using the NI 9215 module (*National Instruments*, USA). Two oscillograms were synchronously recorded: one between the plate electrodes, the second between one plate electrode, and

an additional needle electrode located in the center of the cuvette. Then, the attenuation coefficient was calculated.

- The attenuation coefficient for constant signals was calculated as the ratio of the average potential difference measured between the central and “–” plate electrodes to the average potential difference between the “–” and “+” plate electrodes (Fig. 1b).
- The attenuation coefficient for alternating (sinusoidal) signals was calculated as the ratio of the average amplitude of the potential difference measured between the central and plate electrodes to the average amplitude of the potential difference between the plate electrodes (Fig. 1b).

3.4. Statistical analysis

Statistical data processing was performed in RStudio 2023.09.1+494 (© 2009–2023 *R Foundation for Statistical Computing*, Vienna, Austria) using the R package version 4.2.2. The normality of distribution was assessed by the Shapiro–Wilk test, the homogeneity of variances was assessed by the Bartlett test. Groups were compared using the Student–Welch t-test and the Kruskal–Wallis test followed by Dunn’s test. Differences between groups were considered statistically significant at $p < 0.05$.

4. RESULTS AND DISCUSSION

4.1. Physicochemical properties and modifying effect of vibrational iterations of ECA water. Classification of iterations into fractions

The physicochemical properties and modifying effect of vibrational iterations I0–I7 obtained using five different types of ECA water as the initial substance were assessed. Crossing water with the initial substance (Fig. 2), five rows of vibrational iterations were obtained. For each iteration, the physicochemical properties and the effect on intact water (modifying effect) were analyzed. The results are presented in Table 2.

Based on the differences of vibrational iterations from intact water in physicochemical properties and the modifying

Table 1. Classification of vibrational iterations into fractions according to changes in physicochemical characteristics relative to intact water [1]

| Parameter (method of analysis) | Presence of differences from intact water | | | |
|---|---|-------------|-------------|--------|
| | Native | Semi-Native | Semi-Active | Active |
| Physicochemical properties (conductometry and radiometry) | – | + | – | + |
| Modifying effect (THz spectroscopy) | – | – | + | + |

Note: the test result was considered positive (“+”) if it met the acceptance criteria. Otherwise, the result was taken as negative (“–”). The acceptance criteria: the values obtained for vibrational iterations should statistically significantly ($p < 0.05$) differ from those of intact water by $\pm 5\%$ or more (by conductometry and THz spectroscopy) and by $+10\%$ or more (by radiometry). The values obtained for intact water were taken as 100%.

Table 2. Physicochemical properties and modifying effect of vibrational iterations

| Initial substance | Iteration number | | | | | | | |
|--|------------------|---------------|---------------|---------------|---------------|---------------|---------------|--------------|
| | I0 | I1 | I2 | I3 | I4 | I5 | I6 | I7 |
| Specific electrical conductivity, % | | | | | | | | |
| ECA water 0.8 V | 99.9 ± 2.2 | 107.2 ± 1.1* | 103.0 ± 3.0 | 100.9 ± 1.6 | 106.5 ± 1.2* | 119.2 ± 1.1* | 102.9 ± 0.8 | 103.4 ± 0.8 |
| ECA water 0.8 V, 12.6 Hz | 143.1 ± 15.4* | 140.3 ± 8.2* | 139.3 ± 4.5* | 143.9 ± 11.2* | 146.7 ± 5.6* | 133.7 ± 5.5* | 147.6 ± 13.5* | 142.2 ± 9.9* |
| ECA water 8 V | 121.0 ± 1.8* | 113.8 ± 1.6* | 112.6 ± 4.4* | 112.4 ± 4.7* | 112.0 ± 0.3* | 112.9 ± 1.3* | 119.5 ± 0.1* | 121.7 ± 0.6* |
| ECA water 8 V, 12.6 Hz | 108.8 ± 3.4 | 114.7 ± 6.3* | 118.8 ± 7.1* | 112.1 ± 4.4 | 112.0 ± 0.8 | 119.6 ± 5.5* | 112.2 ± 4.1 | 112.0 ± 0.8 |
| ECA water 0 V | 126.7 ± 0.2* | 111.0 ± 0.2* | 111.2 ± 0.4* | 112.2 ± 2.0* | 112.2 ± 0.9* | 112.1 ± 2.0* | 121.3 ± 4.1* | 119.2 ± 3.2* |
| Power flux density across GHz range, % | | | | | | | | |
| ECA water 0.8 V | 94.0 ± 3.1# | 103.7 ± 3.4 | 113.4 ± 4.5* | 110.8 ± 3.6# | 109.4 ± 6.5# | 87.0 ± 10.2# | 125.4 ± 10.4* | 102.9 ± 11.0 |
| ECA water 0.8 V, 12.6 Hz | 116.4 ± 5.8* | 135.8 ± 12.2* | 128.4 ± 10.2* | 141.0 ± 18.5* | 70.9 ± 1.7# | 185.6 ± 6.6* | 84.5 ± 2.8# | 182.2 ± 5.6* |
| ECA water 8 V | 167.5 ± 8.3* | 165.4 ± 14.3* | 128.1 ± 20.7* | 117.5 ± 16.6 | 96.1 ± 4.5 | 87.1 ± 5.2*# | 81.8 ± 3.3# | 107.5 ± 5.8# |
| ECA water 8 V, 12.6 Hz | 111.7 ± 14.3* | 108.2 ± 4.2* | 140.3 ± 14.5* | 119.8 ± 9.2* | 150.7 ± 24.8* | 90.4 ± 7.5# | 119.1 ± 11.3* | 88.5 ± 5.5# |
| ECA water 0 V | 100.0 ± 20.9 | 108.1 ± 16.3# | 95.6 ± 6.3 | 107.3 ± 16.0 | 117.6 ± 21.8* | 117.5 ± 12.5* | 210.1 ± 8.9 # | 107.2 ± 7.3# |
| Dielectric constant ϵ_{e1} (modifying effect) ϵ_{e1} , % | | | | | | | | |
| ECA water 0.8 V | 103.8 ± 5.3 | 99.9 ± 8.5* | 102.8 ± 9.7 | 95.2 ± 4.9 | 97.1 ± 3.1* | 102.5 ± 6.9 | 100.0 ± 6.7 | 102.9 ± 4.3 |
| ECA water 0.8 V, 12.6 Hz | 104.2 ± 5.8* | 105.4 ± 3.3* | 103.0 ± 3.7* | 101.3 ± 3.8 | 95.0 ± 5.8* | 106.0 ± 5.1* | 101.9 ± 4.2 | 107.2 ± 3.1* |
| ECA water 8 V | 99.7 ± 4.6 | 103.8 ± 7.7 | 101.3 ± 2.5 | 97.8 ± 4.4 | 99.9 ± 6.7 | 100.5 ± 4.5 | 98.5 ± 2.7 | 108.2 ± 5.2* |
| ECA water 8 V, 12.6 Hz | 98.3 ± 4.0 | 95.2 ± 6.2* | 97.5 ± 3.4 | 97.4 ± 5.1 | 99.2 ± 3.7 | 98.3 ± 4.2 | 102.6 ± 6.4 | 100.4 ± 4.1 |
| ECA water 0 V | 103.9 ± 3.7 | 105.2 ± 3.2* | 103.1 ± 7.6* | 103.2 ± 2.3 | 98.1 ± 4.3 | 101.4 ± 1.7* | 94.4 ± 7.5 | 96.8 ± 4.5 |

Table 2. Continued

| Initial substance | Iteration number | | | | | | | |
|--------------------------|------------------|-------------|-------------|-------------|-------------|-------------|-------------|-------------|
| | I0 | I1 | I2 | I3 | I4 | I5 | I6 | I7 |
| ECA water 0.8 V | Native | Active | Semi-Native | Semi-Native | Active | Semi-Native | Semi-Native | Native |
| ECA water 0.8 V, 12.6 Hz | Active | Active | Active | Semi-Native | Active | Active | Semi-Native | Active |
| ECA water 8 V | Semi-Native | Semi-Native | Semi-Native | Semi-Native | Semi-Native | Semi-Native | Semi-Native | Active |
| ECA water 8 V, 12.6 Hz | Semi-Native | Active | Semi-Native | Semi-Native | Semi-Native | Semi-Native | Semi-Native | Semi-Native |
| ECA water 0 V | Semi-Native | Active | Active | Semi-Native | Semi-Native | Active | Semi-Native | Semi-Native |

Note:

* meet the acceptance criteria (statistical significance $p < 0.05$) compared to intact water (see MATERIALS AND METHODS);

do not meet the acceptance criteria ($p < 0.05$; mean values differ less than $\pm 5\%$ according to conductometry and THz spectroscopy and less than $\pm 10\%$ according to radiometry compared to intact water);

unlabeled values: $p > 0.05$ compared to intact water.

Data are normalized to the corresponding values obtained for intact water according to the formula: $\frac{\text{Value measured for the sample}}{\text{Value measured for intact water}} \times 100\%$ and presented as Mean \pm Standard Deviation (SD).

¹ In order to obtain the parameter Dielectric constant $\epsilon_{1,99}$ parts of water were added to 1 part of each sample.

effect on intact water, all iterations were assigned to one or another fraction in accordance with [1]. Depending on the type of ECA water, which was used as initial substance to prepare vibrational iterations, the number of iterations classified into each of the fractions varied (Table 3).

Thus, among all the studied rows of vibrational iterations, the Semi-Active fraction is absent, while the Native fraction is detected only among vibrational iterations for which “ECA water 0.8 V” was used as the initial substance. In addition, vibrational iterations of “ECA water 0.8 V” show the smallest number of differences relative to the control for the studied physicochemical parameters and the greatest diversity of fractions. In the row of vibrational iterations of “ECA water 0.8 V, 12.6 Hz,” the Active fraction prevails. An increase in the intensity of the electrical signal to 8 V (for both constant and alternating signals) was shown to lead to an increase in the number of Semi-Native fractions. At the same time, for the row of vibrational iterations “ECA water 0.8 V, 12.6 Hz” and “ECA water 8 V, 12.6 Hz,” an increase in the differences in the radiation power flux density was noted.

Thus, depending on the parameters of the electrical signal for obtaining ECA water used as the initial substance in the preparation of vibrational iterations, the properties of the iterations differ. This fact indicates the fundamental similarity of vibrational iterations obtained from water treated with an external physical factor with vibrational iterations of a substance of natural origin, whose properties also specifically depend on the particular substance [1].

4.2. The influence of vibration iterations of ECA water on intact water

In order to study the influence of vibration iterations of ECA water on intact water, the following vibration iterations were selected:

- among the row of vibrational iterations of “ECA water 0 V”: I5 (Active), I3 (Semi-Native);

- among the row of vibrational iterations of “ECA water 0.8 V”: I4 (Active), I0 (Native);
- among the row of vibrational iterations of “ECA water 0.8 V, 12.6 Hz”: I1 (Active), I6 (Semi-Native);
- among the row of vibrational iterations of “ECA water 8 V”: I7 (Active), I4 (Semi-Native);
- among the row of vibrational iterations of “ECA water 8 V, 12.6 Hz”: I1 (Active), I7 (Semi-Native).

After adding the above samples to intact water in a volume ratio of 1 : 9, the resulting mixtures were analyzed using conductometry, radiometry, THz spectroscopy, dynamic light scattering, and oscillography. The measurement results were compared with the control, to which the corresponding amount of intact water had been added instead of vibrational iterations. Different vibrational iterations were shown to have different effects on intact water (Table 4).

The magnitude and direction of the changes depend on the characteristics of the electrical signal used to prepare the initial substance of vibrational iterations. Thus, each studied vibrational iteration caused changes in the radiation power of the resulting mixtures: both studied fractions of iterations obtained from “ECA water 0.8 V” decreased the radiation power, while vibrational iterations obtained from other substances increased this parameter.

It is also evident from Table 4 that the mixtures of intact water with both fractions of the rows of vibrational iterations “ECA water 0.8 V,” vibrational iterations “ECA water 0.8 V, 12.6 Hz” and vibrational iterations “ECA water 8 V” have lower light scattering intensity than the corresponding control mixture, whereas the mixture of intact water with the Semi-Native fraction of vibrational iterations “ECA water 0 V” has higher scattering intensity. The introduction of other vibrational iterations did not affect the scattering intensity of the obtained mixtures. A similar (but not entirely corresponding) situation is observed with the size of optical heterogeneities:

Table 3. Distribution by fractions in the rows of vibrational iterations prepared from each type of ECA water

| Electric signal parameters | Fraction, number | | | |
|----------------------------|------------------|-------------|--------|-------------|
| | Native | Semi-Native | Active | Semi-Active |
| 0 V | – | 6 | 2 | – |
| 0.8 V | 2 | 4 | 2 | – |
| 0.8 V, 12.6 Hz | – | 2 | 6 | – |
| 8 V | – | 7 | 1 | – |
| 8 V, 12.6 Hz | – | 7 | 1 | – |

Table 4. Changes in the physicochemical properties of intact water after addition of vibrational iterations of ECA water in 1 : 9 ratio

| Parameter | Parameters of the electric signal for processing the initial substance for vibration iterations | | | | | |
|--|---|--------------------|--------------------|--------------------|-------------------------|--------------------|
| | 0 V | | 0.8 V | | 0.8 V, 12.6 Hz | |
| | Semi-Native + ECA water | Active + ECA water | Native + ECA water | Active + ECA water | Semi-Native + ECA water | Active + ECA water |
| Specific electrical conductivity, % | 105.2 ± 3.6 | 94.9 ± 0.1 | 97.6 ± 2.9 | 91.6 ± 0.5* | 103.5 ± 0.8 | 96.7 ± 0.5 |
| Power flux density across GHz range, % | 115.4 ± 7.7* | 143.3 ± 10.9* | 86.8 ± 3.1* | 77.7 ± 1.4* | 187.8 ± 21.4* | 142.7 ± 6.1* |
| Dielectric constant ϵ_{d1} , % | 111.3 ± 3.9* | 109.3 ± 4.2* | 102.3 ± 10.8 | 97.2 ± 20.7 | 93.0 ± 8.0 | 96.1 ± 12.7 |
| Hydrodynamic diameter of optical heterogeneities, % | 87.8 ± 7.4* | 161.3 ± 20.7 | 42.9 ± 2.8* | 41.9 ± 7.1* | 38.2 ± 5.7* | 91.2 ± 5.9* |
| Scattering intensity, % | 107.1 ± 14.8* | 125.8 ± 17.6 | 61.2 ± 5.3* | 42.6 ± 1.8* | 46.6 ± 1.7* | 42.8 ± 7.0* |
| Signal intensity attenuation coefficient (sample), rel. units | Not applicable | | 0.269 ± 0.044 | 0.234 ± 0.038 | | 0.493 ± 0.005 |
| Signal intensity attenuation coefficient (control) [§] , rel. units | Not applicable | | 0.253 ± 0.008 | | 0.483 ± 0.001 | |

Table 4. Continued

| Parameter | Parameters of the electric signal for processing the initial substance for vibration iterations | | |
|--|---|--------------------|-------------------------|
| | 8 V | | 8 V, 12.6 Hz |
| | Semi-Native + ECA water | Active + ECA water | Semi-Native + ECA water |
| Specific electrical conductivity, % | 88.5 ± 4.8* | 90.2 ± 5.3* | 100.1 ± 3.2 |
| Power flux density across GHz range, % | 113.7 ± 6.0* | 139.7 ± 13.9* | 148.4 ± 6.4* |
| Dielectric constant ϵ_{r1} , % | 97.4 ± 8.1 | 97.3 ± 9.8 | 103.0 ± 13.2 |
| Hydrodynamic diameter of optical heterogeneities, % | 117.9 ± 28.5* | 134.6 ± 17.3 | 147.3 ± 12.0* |
| Scattering intensity, % | 50.7 ± 4.1* | 40.1 ± 3.2* | 97.0 ± 16.4 |
| Signal intensity attenuation coefficient (sample), rel. units | 0.482 ± 0.002 | 0.478 ± 0.012 | 0.502 ± 0.001* |
| Signal intensity attenuation coefficient (control) [§] , rel. units | 0.485 ± 0.014 | | 0.511 ± 0.002 |

Note:

* statistically significant differences from intact water, $p < 0.05$;

§ control measurements (intact water + intact water) were carried out on the day of the study of the corresponding iteration (vibrational iterations of ECA water + intact water). Data are normalized to the corresponding values obtained for intact water according to the formula: $\frac{\text{Value measured for the sample}}{\text{Value measured for intact water}} \times 100\%$. This normalization was applied to all parameters except the signal intensity

attenuation coefficient. Data are presented as Mean ± SD.

mixtures of intact water with both fractions of vibrational iterations “ECA water 0.8 V” and “ECA water 0.8 V, 12.6 Hz,” as well as the Active fractions of vibrational iterations “ECA water 8 V, 12.6 Hz” and the Semi-Native fraction of vibrational iterations “ECA water 0 V” contain optical heterogeneities of a smaller size than the control. Mixtures of intact water with the Semi-Native fraction of vibrational iterations “ECA water 8 V” and “ECA water 8 V, 12.6 Hz” contain optical heterogeneities of a larger size than the control. The resulting mixture is not affected by the addition of the remaining iterations. The specific electrical conductivity of the mixture, which decreases with the addition of both fractions from the rows of vibrational iterations “ECA water 0.8 V” and “ECA water 8 V,” does not change with the addition of the rest of the studied iterations.

The signal attenuation coefficient (according to oscillography data) decreases with the action of both fractions from the row of vibrational iterations “ECA water 8 V, 12.6 Hz” on water and increases with the action of the Active fraction of vibrational iterations “ECA water 8 V, 12.6 Hz” (Table 4). In the overwhelming majority of cases, different fractions of vibrational iterations prepared using the same electrical signal change the physicochemical properties of the resulting mixture in the same direction (compared to intact water).

In this experimental setup (a 1 : 9 mixture with intact water), it is important to note that neither the Active nor the Native/Semi-Native fractions of ECA water obtained by applying an electrical signal affect the value of the dielectric constant ϵ_1 (obtained using THz spectroscopy) of the resulting mixture as compared to the control (Table 4). However, the value of ϵ_1 of the mixture of intact water with both the Active and Semi-Native fractions of vibrational iterations of “ECA water 0 V” increases. Comparing the results obtained by THz spectroscopy (Table 2 and Table 4), it becomes clear that the degree of influence of vibrational iterations on intact water depends on the volume ratio of the mixture components. This conclusion is in agreement with the conclusion made in [19] that the reaction of the Nafion polymer depends on the method of obtaining a salt solution of a certain final concentration, including the number of cycles of mechanical action on water used. This fact indicates the regularity of the dependence of the measurement result on the method of obtaining the mixtures that we have discovered.

The established changes in the physicochemical parameters in the mixtures of vibrational iterations of ECA water relative to intact water demonstrate that intact water (neutral carrier) after the crossing procedure acquires physicochemical properties that are different from intact water, i.e., crossing leads to the formation of a new substance. However, it is also important to understand

whether the effect on intact water of the samples of the Active or Native/Semi-Native fractions is similar to that of the initial substance (i.e., the corresponding ECA water). In order to clarify this, experiments described in the next section were conducted.

4.3. Influence of ECA water on the physicochemical properties of intact water

In order to test the effect of ECA water on the physicochemical properties of intact water, one volume part of ECA water was added to nine volume parts of intact water, then the resulting mixture was analyzed using conductometry, radiometry, THz spectroscopy, dynamic light scattering, and oscillography. The results were compared with the control (for the control, the corresponding amount of intact water was added instead of ECA water). The results are presented in Table 5.

All mixtures of intact water and ECA water demonstrate differences from the control in terms of certain physical and chemical characteristics. The magnitude and direction of these differences depend on the voltage applied during the preparation of ECA water. “ECA water 0.8 V” (compared to the control—intact water) causes an increase in the specific electrical conductivity of the mixture by 22% and a decrease in the value of the signal attenuation coefficient (according to the results of oscillography), in contrast to “ECA water 8 V”, which has no effect on this indicator.

Increases in radiation power flux density (by 22% for “ECA water 0.8 V + intact water”; 63% for “ECA water 8 V + intact water”) and in diameters of optical heterogeneities (51% for “ECA water 0.8 V + intact water,” 191% for “ECA water 8 V + intact water”) are observed. At the same time, a stronger and oppositely directed effect is observed in the dynamic scattering intensity of the resulting mixture (“ECA water 0.8 V” increases this parameter in the mixture by 177%, and “ECA water 8 V” reduces by 16%).

The effect of ECA water on intact water (compared with effect of the control—intact water) differs depending on whether constant or alternating electrical treatment was used to obtain it. The addition of “ECA water 0.8 V” leading to an increase in the specific electrical conductivity, radiation power, scattering intensity and diameter of optical heterogeneities is accompanied by a decrease in the signal attenuation coefficient (according to the results of oscillography). However, the addition of “ECA water 0.8 V, 12.6 Hz” leads only to a decrease in specific electrical conductivity, which is accompanied by an increase in the signal attenuation coefficient (according to the results of oscillography). The addition of “ECA water 8 V” leading to an increase in the scattering intensity

Table 5. Effect of ECA water on the physicochemical properties of intact water (mixture in 1 : 9 ratio)

| Parameter | Parameters of the electric signal used to prepare ECA water (in ECA water + intact water mixtures) | | | | |
|--|---|----------------|----------------|----------------|----------------|
| | 0 V | 0.8 V | 0.8 V, 12.6 Hz | 8 V | 8 V, 12.6 Hz |
| Specific electrical conductivity, % | 106.2 ± 0.8* | 122.4 ± 0.3* | 93.1 ± 3.9* | 101.4 ± 3.8# | 99.5 ± 2.3 |
| Power flux density across GHz range, % | 121.2 ± 9.6* | 122.3 ± 7.9* | 121.5 ± 18.7 | 163.3 ± 8.5*# | 142.7 ± 13.8* |
| Dielectric constant ϵ_1 , % | 97.3 ± 4.5 | 106.0 ± 11.9 | 104.9 ± 12.3 | 106.1 ± 4.4# | 104.1 ± 13.5 |
| Hydrodynamic diameter of optical heterogeneities, % | 81.7 ± 21.9 | 150.8 ± 19.4* | 100.2 ± 8.2 | 291.2 ± 18.8*# | 37.6 ± 10.5* |
| Scattering intensity), % | 186.5 ± 18.7* | 277.4 ± 26.5* | 122.7 ± 23.4 | 84.2 ± 3.5* | 300.7 ± 42.6* |
| Signal intensity attenuation coefficient (sample), rel. units | Not applicable | 0.216 ± 0.016* | 0.506 ± 0.001* | 0.496 ± 0.012 | 0.507 ± 0.001* |
| Signal intensity attenuation coefficient (control), rel. units | Not applicable | 0.253 ± 0.008 | 0.483 ± 0.001 | 0.485 ± 0.014 | 0.511 ± 0.002 |

Note:

* statistically significant differences from the control, $p < 0.05$;

statistically significant differences from the ECA water 0 V and intact water mixture, $p < 0.05$. Data are normalized to the corresponding values obtained for intact water according to the formula: $\frac{\text{Value measured for the sample}}{\text{Value measured for intact water}} \times 100\%$. This normalization was applied to all

parameters except the signal intensity attenuation coefficient. Data are presented as Mean ± SD.

and a decrease in the diameter of optical heterogeneities in intact water is accompanied by an increase in the radiation power. Conversely, the addition of “ECA water 8 V, 12.6 Hz” leads to a decrease in the scattering intensity and an increase in the diameter of optical heterogeneities, which is also accompanied by an increase in the radiation power. While the signal attenuation coefficient is not changed by the addition of “ECA water 8 V” (according to the oscillography results) in water, the addition of “ECA water 8 V, 12.6 Hz” causes its decrease.

Thus, similar to the effect of vibrational iterations of ECA water on water, the effect of ECA water itself on intact water depends on the parameters of the electrical signal that was used to prepare ECA water.

4.4. Comparison of the addition of ECA water on the physicochemical properties of intact water

In order to understand whether the samples of the Active or Native/Semi-Native fractions have the same effect on the properties of intact water as that of the substance itself (corresponding ECA water), a comparison of their effects on water was carried out (Table 6). However, in

order to study the contribution of only the applied electric signal rather than the presence of contact of water with the measuring cell (and, accordingly, the immersion electrodes) in the absence of a signal, the comparison was carried out using only those indicators that did not differ between the “ECA water 0 V + intact water” sample and the control (intact water). Such characteristics were the dielectric constant ϵ_1 and the hydrodynamic diameter of optical heterogeneities (Table 6).

A higher value of dielectric constant is found in both the mixtures of water with Active and Semi-Native fractions compared to the control; moreover, in the mixture of water with the Semi-Native fraction, smaller optical heterogeneities are found as compared to the control. Nevertheless, treatment of water with an electric signal did not affect its ability or that of its vibrational iterations to change the dielectric constant of intact water. At the same time, the ability of both ECA water and its iterations to affect the size of optical heterogeneities in water is demonstrated. A pattern is observed when ECA is carried out with a constant voltage: in a mixture with intact water, the size of the optical heterogeneities increases; however, when an alternating electric signal (8 V, 12.6 Hz) is used, it decreases.

Table 6. Direction of the effect of adding ECA water and vibrational iterations prepared from it to intact water in a volume ratio of 1 : 9

| Parameter | Parameters of the electric signal for processing the initial substance for vibration iterations | | | | | | | | | | | | | | |
|---|---|-------------|--------|-----------|--------|--------|----------------|-------------|--------|-----------|-------------|--------|--------------|-------------|--------|
| | 0 V | | | 0.8 V | | | 0.8 V, 12.6 Hz | | | 8 V | | | 8 V, 12.6 Hz | | |
| | ECA water | Semi-Native | Active | ECA water | Native | Active | ECA water | Semi-Native | Active | ECA water | Semi-Native | Active | ECA water | Semi-Native | Active |
| Dielectric constant ϵ_1 , % | — | ↑ | ↑ | — | — | — | — | — | — | — | — | — | — | — | — |
| Hydrodynamic diameter of optical heterogeneities, % | — | ↓ | — | ↑ | ↓ | ↓ | — | ↓ | ↓ | ↑ | ↓ | — | ↓ | ↑ | ↓ |

Note: “↑” indicates an increase, “↓” indicates a decrease, and “—” indicates no change in the recorded characteristics compared to the control ($p < 0.05$).

Vibrational iterations (both the Active and Native/Semi-Native fractions) obtained from “ECA water 0.8 V” and “ECA water 0.8 V, 12.6 Hz” reduce the size of optical heterogeneities observed in the resulting mixture when mixed with water. The same effect is produced by the Semi-Native fractions of vibrational iteration “ECA water 8 V” and the Active fraction of vibrational iteration “ECA water 8 V, 12.6 Hz”. However, adding the Active fraction of vibrational iteration “ECA water 8 V” to water does not affect the resulting mixture, while adding the Semi-Native fraction of vibrational iteration “ECA water 8 V, 12.6 Hz” to water leads to an increase in the optical heterogeneities in the mixture.

Thus, in the overwhelming majority of the studied sample types, the effect exerted by vibrational iterations of ECA water on the size of optical heterogeneities in water differs from the effect exerted by the substance used to prepare vibrational iteration. However, the result of the effect of vibrational iterations of ECA water on the size of optical heterogeneities in water weakly depends on the parameters of the electrical signal used to prepare the substance, as well as on the fraction of vibrational iteration. Vibrational iterations predominantly cause a decrease in the size of optical heterogeneities.

5. CONCLUSIONS

1. The study of vibrational iterations of ECA water demonstrated that they follow general patterns of post-vibration activity and can be classified into fractions that differ from each other in physicochemical properties. The obtained result indicates the universality of the mechanisms of vibration treatment,

i.e., the possibility of their implementation regardless of the nature of the initial substance.

2. The use of an electric signal with a constant voltage of 0.8 V for the preparation of the initial substance allows us to obtain a greater variety of fractions of vibrational iterations. The use of an electric signal with a constant voltage of 8 V or alternating voltage of 8 V, 12.6 Hz allows us to obtain a greater number of vibrational iterations of the Semi-Native fraction. This result emphasizes that the mechanisms of formation of the post-vibration activity are sensitive to the degree and nature of external influences, which may indicate their plasticity.
3. The addition of ECA water or its vibration iterations in a volume ratio of 1 : 9 to intact water leads to a change in the physicochemical parameters of intact water. The degree of difference depends on the parameters of the electrical signal used to obtain ECA water. The degree of influence of vibration iterations on intact water depends on the volume ratio of the mixture components.
4. In the overwhelming majority of the studied types of electrical signal, the effect of vibration iterations of ECA water on the size of optical heterogeneities of water differs from the effect of the substance used to prepare the vibration iteration. However, in most cases, vibration iterations cause a decrease in the size of optical heterogeneities (regardless of the electrical signal used to obtain the sample).

Acknowledgments

The work was financially supported by NPF “Materia Medica Holding,” Moscow, Russia. The authors thank E.N. Zaytseva, A.A. Kuhninova,

I.V. Molodtsova, K.S. Peshketova, E.O. Khimich for their assistance in conducting the experiments. The authors thank A.L. Kovalchuk for assistance in preparing the manuscript, valuable comments, and suggestions.

Authors' contributions

O.V. Slatinskaia—analyzed the data and wrote the original draft of the manuscript.

G.O. Stepanov—planned the experiments, analyzed the data, and contributed to the final version of the manuscript.

O.V. Fartushnaya—planned the experiments and contributed to the final version of the manuscript.

E.V. Zubkov—planned the experiments and contributed to the final version of the manuscript.

A.D. Zatykina—carried out the experiments (THz spectroscopy).

O.M. Gizitdinova—carried out the experiments (THz spectroscopy).

N.S. Karpov—carried out the experiments (sample preparation, conductometry, oscillography).

A.V. Smirnov—carried out the experiments (radiometry, dynamic light scattering).

V.S. Boriskin—carried out the experiments (radiometry).

N.N. Rodionova—analyzed the data and contributed to the final version of the manuscript.

A.O. Petrova—planned the experiments and analyzed the data.

Conflict of interest

O.V. Slatinskaia, G.O. Stepanov, O.V. Fartushnaya, E.V. Zubkov, A.D. Zatykina, O.M. Gizitdinova, N.S. Karpov, A.V. Smirnov, V.S. Boriskin, N.N. Rodionova, and A.O. Petrova are employees of NPF "Materia Medica Holding," Moscow, Russia (full or part-time employment).

REFERENCES

1. Petrova A., Tarasov S., Gorbunov E., Stepanov G., Fartushnaya O., Zubkov E., Molodtsova I., Boriskin V., Zatykina A., Smirnov A., Zakharova S., Yaroshenko S., Ponomareva A., Petrova N., Kardash E., Ganina K., Rodionova N., Kovalchuk A. Epstein O. Phenomenon of Post-Vibration Interactions. *Symmetry*. 2024;16(8):958. <https://doi.org/10.3390/sym16080958>
2. Penkov N.V. Influence of the combined magnetic field and high dilution technology on the intrinsic emission of aqueous solutions. *Water*. 2023;15(3):599. <https://doi.org/10.3390/w15030599>
3. Penkov N. Antibodies processed using high dilution technology distantly change structural properties of IFN γ aqueous solution. *Pharmaceutics*. 2021;13(11):1864. <https://doi.org/10.3390/pharmaceutics13111864>
4. Penkov N., Penkova N. Analysis of emission infrared spectra of protein solutions in low concentrations. *Front. Phys.* 2020;8:624779. <https://doi.org/10.3389/fphy.2020.624779>
5. Novikov V.V. Effect of vibrational iterations of magnetized water on the physico-chemical properties of intact water. *Russ. Phys. J.* 2024;67(10):1718–1727. <https://doi.org/10.1007/s11182-024-03304-z>
6. Petrushanko I.I., Lobyshev V.I. Physicochemical properties of aqueous solutions obtained in a membrane electrolyzer. *Biophysics*. 2004;49(1):17–26.
7. Kerwick M.I., Reddy S.M., Chamberlai A.H.L., Holt D.M. Electrochemical disinfection, an environmentally acceptable method of drinking water disinfection? *Electrochim. Acta*. 2005;50(25–26):5270–5277. <https://doi.org/10.1016/j.electacta.2005.02.074>
8. Hanaoka K., Sun D., Lawrence R., Kamitani Y., Fernandes G. The mechanism of the enhanced antioxidant effects against superoxide anion radicals of reduced water produced by electrolysis. *Biophys. Chem.* 2004;107(1):71–82. <https://doi.org/10.1016/j.bpc.2003.08.007>
9. Novikov V.V., Yablokova E.V., Fesenko E.E. The Role of Water in the Effect of Weak Combined Magnetic Fields on Production of Reactive Oxygen Species (ROS) by Neutrophils. *Appl. Sci.* 2020;10(9):3326. <https://doi.org/10.3390/app10093326>
10. Novikov V.V., Yablokova E.V. Interaction between Highly Diluted Samples, Protein Solutions and Water in a Controlled Magnetic Field. *Appl. Sci.* 2022;12(10):5185. <https://doi.org/10.3390/app12105185>
11. Astashev M.E., Serov D.A., Sarimov R.M. Gudkov S.V. Influence of the Vibration Impact Mode on the Spontaneous Chemiluminescence of Aqueous Protein Solutions. *Phys. Wave Phen.* 2023;31:189–199. <https://doi.org/10.3103/S1541308X23030020>
12. Gudkov S.V., Penkov N.V., Baimler I.V., Lyakhov G.A., Pustovoy V.I., Simakin A.V., Sarimov R.M., Scherbakov I.A. Effect of Mechanical Shaking on the Physicochemical Properties of Aqueous Solutions. *Int. J. Mol. Sci.* 2020;21(21):8033. <https://doi.org/10.3390/ijms21218033>
13. Demangeat J-L. Water proton NMR relaxation revisited: Ultrahighly diluted aqueous solutions beyond Avogadro's limit prepared by iterative centesimal dilution under shaking cannot be considered as pure solvent. *J. Mol. Liquid.* 2022;360:119500. <https://doi.org/10.1016/j.molliq.2022.119500>
14. Sarimov R.M., Simakin A.V., Matveeva T.A., Gudkov S.V., Lyakhov G.A., Pustovoy V.I., Troitskii A.V., Shcherbakov I.A. Influence of Magnetic Fields with Induction of 7 T on Physical and Chemical Properties of Aqueous NaCl Solutions. *Appl. Sci.* 2021;11(23):11466. <https://doi.org/10.3390/app112311466>
15. Lee S.H., Jeon S.I., Kim Y.S., Lee S.K. Changes in the electrical conductivity, infrared absorption, and surface tension of partially-degassed and magnetically-treated water. *J. Mol. Liquid.* 2013;187:230–237. <https://doi.org/10.1016/j.molliq.2013.07.017>
16. Jerman I, Ogrizek L, Krapež V.P, Jan L. Molecular Signal Transfer of Highly Diluted Antibodies to Interferon-Gamma Regarding Kind, Time, and Distance of Exposition. *Int. J. Mol. Sci.* 2024;25(1):656. <https://doi.org/10.3390/ijms25010656>
17. Elia V., Marrari L.A., Napoli E. Aqueous nanostructures in water induced by electromagnetic fields emitted by EDS: A conductometric study of fullerene and carbon nanotube EDS. *J. Therm. Anal. Calorim.* 2012;107(2):843–851. <https://doi.org/10.1007/s10973-011-1484-y>
18. Rashid M.M., Al Mesfer M.K., Naseem H., Danish M. Hydrogen production by water electrolysis: a review of alkaline water electrolysis, PEM water electrolysis and high temperature water electrolysis. *Int. J. Eng. Adv. Technol.* 2015;4(3):2249–8958.
19. Ninham B.W., Bolotskova P.N., Gudkov S.V., Baranova E.N., Kozlov V.A., Shkirin A.V., Vu M.T., Bunkin N.F. Nafion swelling in salt solutions in a finite sized cell: Curious phenomena dependent on sample preparation protocol. *Polymers*. 2022;14(8):1511. <https://doi.org/10.3390/polym14081511>

About the Authors

Olga V. Slatinskaia, Cand. Sci. (Biol.), Researcher, Materia Medica Holding (47-1, Trifonovskaya ul., Moscow, 129272, Russia). E-mail: slatinskayaov@materiamedica.ru. Scopus Author ID 57197721882, ResearcherID ACK-0180-2022, RSCI SPIN-code 8576-8913, <https://orcid.org/0000-0002-9908-2637>

German O. Stepanov, Cand. Sci. (Biol.), Leading Researcher, Materia Medica Holding (47-1, Trifonovskaya ul., Moscow, 129272, Russia). E-mail: stepanovgo@materiamedica.ru. Scopus Author ID 15046034100, <https://orcid.org/0000-0002-8576-9745>

Olga V. Fartushnaya, Senior Researcher, Materia Medica Holding (47-1, Trifonovskaya ul., Moscow, 129272, Russia). E-mail: fartushnayaov@materiamedica.ru. <https://orcid.org/0009-0008-8704-4845>

Evgenii V. Zubkov, Senior Researcher, Materia Medica Holding (47-1, Trifonovskaya ul., Moscow, 129272, Russia). E-mail: zubkovev@materiamedica.ru. Scopus Author ID 59304858200, <https://orcid.org/0009-0001-8198-5942>

Anastasia D. Zatykina, Junior Researcher, Materia Medica Holding (47-1, Trifonovskaya ul., Moscow, 129272, Russia). E-mail: ZatykinaAD@materiamedica.ru. <https://orcid.org/0009-0001-8731-4293>

Olesya M. Gizitdinova, Senior Researcher, Materia Medica Holding (47-1, Trifonovskaya ul., Moscow, 129272, Russia). E-mail: GizitdinovaOM@materiamedica.ru. <https://orcid.org/0009-0002-2357-7542>

Nikita S. Karpov, Laboratory Assistant, Materia Medica Holding (47-1, Trifonovskaya ul., Moscow, 129272, Russia). E-mail: karpovns@materiamedica.ru. <https://orcid.org/0009-0004-5457-8614>

Alexey V. Smirnov, Junior Researcher, Materia Medica Holding (47-1, Trifonovskaya ul., Moscow, 129272, Russia). E-mail: SmirnovAlVI@materiamedica.ru. <https://orcid.org/0009-0002-7872-2866>

Vladimir S. Boriskin, Junior Researcher, Materia Medica Holding (47-1, Trifonovskaya ul., Moscow, 129272, Russia). E-mail: boriskinvs@materiamedica.ru. Scopus Author ID 57851926600, <https://orcid.org/0000-0001-6474-7005>

Natalia N. Rodionova, Cand. Sci. (Biol.), Head of Physicochemical Research, Materia Medica Holding (47-1, Trifonovskaya ul., Moscow, 129272, Russia). E-mail: rodionovann@materiamedica.ru. Scopus Author ID 57225350982, <https://orcid.org/0009-0001-7138-9063>

Anastasia O. Petrova, Cand. Sci. (Biol.), Head of the Scientific Research Laboratory, Materia Medica Holding (47-1, Trifonovskaya ul., Moscow, 129272, Russia). E-mail: petrovaao@materiamedica.ru. Scopus Author ID 57208625485, <https://orcid.org/0000-0002-6625-9061>

Об авторах

Слатинская Ольга Вадимовна, к.б.н., научный сотрудник, ООО «НПФ «Материя Медика Холдинг» (129272, Россия, Москва, ул. Трифононская, д. 47, стр. 1). E-mail: slatinskayaov@materiamedica.ru. Scopus Author ID 57197721882, ResearcherID ACK-0180-2022, SPIN-код РИНЦ 8576-8913, <https://orcid.org/0000-0002-9908-2637>

Степанов Герман Олегович, к.б.н., ведущий научный сотрудник, ООО «НПФ «Материя Медика Холдинг» (129272, Россия, Москва, ул. Трифононская, д. 47, стр. 1). E-mail: stepanovgo@materiamedica.ru. Scopus Author ID 15046034100, <https://orcid.org/0000-0002-8576-9745>

Фартушная Ольга Васильевна, ведущий научный сотрудник, ООО «НПФ «Материя Медика Холдинг» (129272, Россия, Москва, ул. Трифононская, д. 47, стр. 1). E-mail: fartushnayaov@materiamedica.ru. <https://orcid.org/0009-0008-8704-4845>

Зубков Евгений Владимирович, ведущий научный сотрудник, ООО «НПФ «Материя Медика Холдинг» (129272, Россия, Москва, ул. Трифононская, д. 47, стр. 1). E-mail: zubkovev@materiamedica.ru. Scopus Author ID 59304858200, <https://orcid.org/0009-0001-8198-5942>

Затыкина Анастасия Дмитриевна, младший научный сотрудник, ООО «НПФ «Материя Медика Холдинг» (129272, Россия, Москва, ул. Трифононская, д. 47, стр. 1). E-mail: ZatykinaAD@materiamedica.ru. <https://orcid.org/0009-0001-8731-4293>

Гизитдинова Олеся Маратовна, старший научный сотрудник, ООО «НПФ «Материя Медика Холдинг» (129272, Россия, Москва, ул. Трифононская, д. 47, стр. 1). E-mail: GizitdinovaOM@materiamedica.ru. <https://orcid.org/0009-0002-2357-7542>

Карпов Никита Станиславович, лаборант, ООО «НПФ «Материя Медика Холдинг» (129272, Россия, Москва, ул. Трифононская, д. 47, стр. 1). E-mail: karpovns@materiamedica.ru. <https://orcid.org/0009-0004-5457-8614>

Смирнов Алексей Владимирович, младший научный сотрудник, ООО «НПФ «Материя Медика Холдинг» (129272, Россия, Москва, ул. Трифононская, д. 47, стр. 1). E-mail: SmirnovAlVI@materiamedica.ru. <https://orcid.org/0009-0002-7872-2866>

Борискин Владимир Сергеевич, младший научный сотрудник, ООО «НПФ «Материя Медика Холдинг» (129272, Россия, Москва, ул. Трифононская, д. 47, стр. 1). E-mail: boriskinvs@materiamedica.ru. Scopus Author ID 57851926600, <https://orcid.org/0000-0001-6474-7005>

Родионова Наталья Николаевна, к.б.н., руководитель физико-химических исследований, ООО «НПФ «Материя Медика Холдинг» (129272, Россия, Москва, ул. Трифононская, д. 47, стр. 1). E-mail: rodionovann@materiamedica.ru. Scopus Author ID 57225350982, <https://orcid.org/0009-0001-7138-9063>

Петрова Анастасия Олеговна, к.б.н., заведующий научно-исследовательской лабораторией, ООО «НПФ «Материа Медика Холдинг» (129272, Россия, Москва, ул. Трифоновская, д. 47, стр. 1). E-mail: petrovaao@materiamedica.ru. Scopus Author ID 57208625485, <https://orcid.org/0000-0002-6625-9061>

Translated from Russian into English by the Authors

Edited for English language and spelling by Thomas A. Beavitt

Erratum
Исправления

<https://doi.org/10.32362/2410-6593-2025-20-2-185>
EDN OZFTTW



Erratum to the article “Study into optimizing the temperature regime for the reduction of Fischer–Tropsch synthesis catalysts”

Igor G. Solomonik, Vladimir Z. Mordkovich, Andrei S. Gorshkov

Tonkie Khimicheskie Tekhnologii = Fine Chemical Technologies. 2025;20(1):27–36. <https://doi.org/10.32362/2410-6593-2025-20-1-27-36>

Page 28, instead of:

Для цитирования

Соломоник И.Г., Мордкович В.З., Горшков А.С. Исследование возможности оптимизации температурного режима восстановления катализаторов синтеза Фишера–Тропша. *Тонкие химические технологии.* 2025;20(1):27–36. <https://doi.org/10.32362/2410-6593-2025-20-1-18-26>

should read:

Для цитирования

Соломоник И.Г., Мордкович В.З., Горшков А.С. Исследование возможности оптимизации температурного режима восстановления катализаторов синтеза Фишера–Тропша. *Тонкие химические технологии.* 2025;20(1):27–36. <https://doi.org/10.32362/2410-6593-2025-20-1-27-36>

The original article can be found under <https://doi.org/10.32362/2410-6593-2025-20-1-27-36>

MIREA – Russian Technological University
78, Vernadskogo pr., Moscow, 119454, Russian Federation.
Publication date *April 29, 2025*.
Not for sale

МИРЭА – Российский технологический университет
119454, РФ, Москва, пр-т Вернадского, д. 78.
Дата опубликования *29.04.2025*.
Не для продажи

www.finechem-mirea.ru

